TUNGSTEN MINERALISATION AT THE OTJUA PROSPECT : A GEOLOGICAL AND GEOCHEMICAL INVESTIGATION

by

NICHOLAS MACRAE STEVEN

Thesis submitted in fulfilment of the requirements for the degree of Master of Science at the University of Cape Town.

ABSTRACT

Two styles of tungsten mineralisation have been identified at the Otjua prospect. Firstly, fine-grained scheelite mineralisation is hosted by calc-silicate hornfels rocks of the Khan and Oberwasser Formations. These hornfels represent metamorphosed marls and are developed in an alternating sequence of biotite schist and minor carbonate units. Secondly, scheelite and fluorite mineralisation is developed in replacement bodies in carbonate units, the most economically significant mineralisation being hosted by the Rössing Formation marble. Three types or facies of skarn assemblage which represent varying degrees of replacment of the Rössing Formation have been identified. The garnet facies of skarn hosts the majority of the tungsten mineralisation.

The Otjua prospect is situated on the southern side of a major F_3 domal structure that has been intruded by a late stage Damaran granite (the Otjua granite) and associated pegmatites. The granite is geochemically specialised and possesses anomalously high $\delta^{18}O$ and $(^{87}Sr/^{86}Sr)_I$ values of 15.1 and 0.7196 respectively. Whole rock, mineral chemistry and stable isotope studies show that the skarn-hosted scheelite mineralisation has been derived from the Otjua granite. The skarn facies development and variations in mineral chemistry within the skarn system are similar to those present in skarns in the North American cordillera, though the absence of accompanying molybdenum, sulphide mineralisation and hydrous silicate assemblages make the deposit unusual.

The tungsten mineralisation hosted by the hornfels is considered to result from syn-sedimentary concentrations of the metal in the marls. It is postulated that the tungsten was derived from a deep-seated fracture such as the Omaruru lineament in Nosib and Lower Swakop times. This study suggests that geochemically specialised granites such as the Otjua granite were produced as the result of large scale anatexis of scheelite-rich metasediments during the final stages of the Damaran orogeny. A striking similarity between the distribution and development of granite-related uranium and tungsten mineralisation in central SWA/Namibia is noted.

LIST OF ABBREVIATIONS USED IN THESIS

$a_{Ca^{2+}}$ - activity of calcium ions

a_{F} - activity of fluoride

a_{H_2O} - activity of water

a_{Halide} - activity of halide

$a_{Introduced\ elements}$ - activity of introduced elements

AMSL - above mean sea level

An - anorthite

$\sim$ - approximately

B and O - B and O Mineral Exploration Company (Pty) Limited

Cc - calcite

cm - centimetre

$\delta^{13}C$ - carbon isotopic composition

$\delta^{18}O$ - oxygen isotopic composition

Δ^{13} C (CO_2 - Cc) - fractionation of ^{13}C between CO_2 and calcite

Δ^{18} O (CO_2 - Cc) - fractionation of ^{18}O between CO_2 and calcite

Eh - oxidation-reduction potential

F_n - folding phase

Gr - graphite

Gt - garnet

kb - kilobar

K_D - partition coefficient

Km - kilometre

LLD - lower limit of detection

ln - natural logarithm

LOI - loss on ignition

μ - micron

LIST OF ABBREVIATIONS USED IN THESIS (contd)

Ma -million years

Michel Lévy method - a method of determining plagioclase feldspar composition from albite twinning

mm - millimetre

n - number of samples

N.D. - not detected

PDB - Belemnitella americana from the Cretaceous Peedee Formation, South Carolina

‰ - per mil

pH - measure of acidity

ppm - parts per million

P/T - pressure and temperature

qtz - quartz

REE - rare earth elements

RSA - Republic of South Africa

S.Dev. - standard deviation

SMOW - standard mean ocean water

$(^{87}Sr/^{86}Sr)_I$ - initial $^{87}Sr/^{86}Sr$ ratio

S.W.A. - South West Africa

UCT - University of Cape Town

U.S.A. - United States of America

U.V. - ultraviolet

$\bar{x}$ - average

X.R.F. - X-ray fluorescence

X_{CO_2} - partial pressure of CO_2

X_{H_2O} - partial pressure of H_2O

TABLE OF CONTENTS

SKARN

The word "skarn" comes from Sweden, where it was originally used as a term of abuse and was subsequently adopted by miners to refer to calc-silicate gangue associated with iron ore (Geijer and Magnusson, 1952). More recently skarn has been used to describe calc-silicate rocks derived by a number of different processes as listed below (after Einaudi et al., 1981).

1) Metamorphic recrystallisation of a marl or shaly limestone, i.e. essentially isochemical metamorphism, resulting in the formation of a calc-silicate hornfels.

2) Local exchange of components by diffusion processes (usually over distances of less than a few tens of centimetres) between two dissimilar lithologies e.g. a marble and a shale during high grade metamorphism, resulting in the formation of a "reaction skarn" (Magnusson, 1960) or a "bimetasomatic diffusion skarn" (Korzhinskii, 1964, 1965) or "calc-silicate bands" (Vidale, 1969).

3) Local exchange of components at high temperatures between magmas and carbonate rocks referred to as "skarns of the magmatic stage" (Pertsev, 1974).

4) Large scale introduction of exotic material by a hydrothermal fluid, presumed to be of magmatic origin, into carbonate rocks, i.e. metasomatic replacement. These skarns are formed by "infiltrational metasomatism" (Korzhinskii, 1936, 1965, 1966).

In this thesis the use of the word skarn (sensu stricto) is confined to those rocks produced by metasomatic replacement of a carbonate unit, unless specifically stated.

1. INTRODUCTION

Scheelite mineralisation was first discovered on the farm Otjua 37, Omaruru district, central SWA/Namibia by B. and O. Mineral Exploration Company Pty. Ltd. during a regional stream sediment sampling programme (see Fig. 1). More detailed soil and drainage sampling, as well as U.V. traverse work conducted at night, helped to delineate several areas of tungsten mineralisation, including the Otjua prospect, the object of this study (see Maps 1 and 2). Intensive exploration at the Otjua prospect started in 1981 and in the following year the B. and O./Rössing Uranium Joint Venture (Joint Venture) was formed to evaluate the prospect. Extensive percussion drilling, conducted in several phases, was followed by the drilling of twenty-nine diamond boreholes in conjunction with geophysical surveys. The author of this thesis was involved in exploration in the Omaruru area from January 1983 until January 1985 with specific responsibility for the Otjua prospect from March 1983 onwards.

During the exploration programme, it readily became apparent that there are two different styles of scheelite mineralisation at the Otjua prospect. Firstly, there is fine to coarse grained scheelite (up to three centimetres diameter) mineralisation hosted by a characteristic coarse grained, inequigranular calc-silicate gangue comprised of scapolite, pyroxene and garnet or idocrase that appear to replace, or are at least hosted by carbonate units. These silicate assemblages are referred to as replacement (or metasomatic) skarns. The second style of mineralisation consists of fine grained scheelite (usually $<$ 1mm in diameter) hosted by fine grained, equigranular quartz + plagioclase + scapolite + diopside calc-silicate rocks that are unrelated to carbonate units. These calc-silicate rocks were loosely referred to during the exploration programme as calc-silicate skarns or regional skarns, but in this thesis, to avoid confusion with the calc-silicate gangue of the skarn proper, are referred to as scheelite-bearing hornfels.

These two types of mineralisation would probably be exploited in a different manner. The discontinuous, though volumetrically abundant nature of the scheelite mineralisation in the hornfels indicates that

it may be considered as a low grade - large tonnage resource. The skarn, possessing more evenly distributed tungsten within smaller orebodies is a high grade - low tonnage resource. However, it was felt that a better understanding of the relationship, if any, between the two styles of mineralisation and the enclosing metasediments and associated intrusives would facilitate further exploration both locally and regionally. Thus the aims of this thesis arose directly from problems encountered during the exploration programme and are summarised below:

1) to document the two styles of mineralisation, the enclosing metasediments and the associated intrusives
2) to establish whether a genetic link exists between the two styles of mineralisation
3) to establish whether the mineralisation at the Otjua prospect is related to the pegmatitic intrusives or to the granitic intrusions in the vicinity
4) to try and determine controls on mineralisation deposition i.e. petrogenetic processes of ore genesis

It was decided that these aims would be best achieved by an integrated study of the field relations and petrography of the lithologies concerned, whole rock geochemistry, mineral chemistry studies and stable isotope work.

The Otjua prospect was chosen for study for several other pertinent reasons. Firstly, very few skarns of economic interest in southern Africa have been described in the literature; indeed Einaudi et al. (1981), in their extensive review of skarn deposits, only mention one skarn example from the entire African continent. Secondly, the majority of replacement skarn deposits are of Phanerozoic (especially Mesozoic) age and thus the presence of a tungsten skarn in Precambrian rocks is of particular interest. Thirdly, several authors have described significant scheelite mineralisation within a variety of Precambrian rocks other than replacement skarns and the scheelite-bearing hornfels at the Otjua prospect appeared to be another example of an unusual style of tungsten mineralisation. Fourthly, tungsten is one of the few economic elements not found in abundance in southern

Africa and since skarns are the world's major sources of tungsten (Einaudi et al., 1981) an assessment of the Otjua prospect is of considerable economic and strategic significance. Finally, the diamond drilling programme has ensured the availability of unweathered rock samples and an unusually good opportunity to obtain a three-dimensional view of a tungsten prospect.

2. A REVIEW OF TUNGSTEN SKARNS

Skarns are the world's major source of tungsten (Einaudi et al., 1981) and the largest and best documented tungsten bearing skarns in the world are Pine Creek, California, U.S.A. (Newberry, 1982); Mactung, North West Territories, Canada (Dick and Hodgson, 1982); Cantung, North West Territories, Canada (Mathieson and Clark, 1984); King Island, Australia (Edwards et al., 1956; Kwak, 1978) and Sandong, Korea (Farrar et al., 1978).

There is a marked clustering of tungsten-bearing skarns in the continental margin orogenic belts of the Circum Pacific region (Einaudi and Burt, 1982). The majority of the world's tungsten skarns are associated with subduction-related, calc-alkali plutons of granodiorite and quartz monzonite composition. Because most of these mid-Palaeozoic to late Cretaceous age, I-type intrusions are emplaced at relatively great depths in the earth's crust, they exhibit few signs of forceful emplacement into country rocks and possess very little low temperature alteration. These coarse grained plutons are, however, intimately associated with aplitic and pegmatitic dykes (Kerr, 1946) and the presence of abundant quartz-feldspar myrmekite in these intrusives is very common (Bateman, 1945; Dick, 1976; Newberry, 1982).

The majority of tungsten skarns are hosted by relatively thin carbonate horizons within intercalated pelite-carbonate, hornfels-carbonate or volcanic-carbonate sequences of late Precambrian to Triassic age. Skarns may be produced by: 1) the contact metamorphic effects of the intrusive e.g. formation of calc-silicate minerals in marbles and marls; 2) heat induced diffusion of elements between unlike lithologies i.e. bimetasomatic diffusion; 3) purely metasomatic processes i.e. where a hydrothermal fluid derived from an intrusive replaces carbonate and/or hornfels. Indeed, metasomatic events often overprint earlier metamorphic events. Although all types of skarn may host scheelite mineralisation, ore grade mineralisation is normally restricted to metasomatised marble. Tungsten skarns formed by purely metasomatic processes are usually developed in the lowest carbonate bed of a stratigraphic sequence. Skarns formed from

impure or dolomitic marble tend to be coarse grained, vuggy and possess erratic distributions of scheelite in comparison to those formed from calcitic marble, which are medium grained, compact and have more even distributions of tungsten (Newberry, 1979a).

A characteristic feature of tungsten replacement skarns is a marked across-deposit zonation of the silicate gangue assemblages. Peripheral zones or facies of skarn in metasomatised marble distal to the intrusive are dominated by idocrase and wollastonite, while zones closer to the intrusive contain garnet and pyroxene (Dick, 1976; Nokleberg, 1981 and Newberry, 1982). These anhydrous silicate assemblages are invariably crosscut, replaced or overprinted by zones of hydrous silicates dominated by biotite and hornblende closer to the intrusive contact (Dick and Hodgson, 1982; Mathieson and Clark, 1984). Zoning of mineral composition across a deposit and within mineral grains is extremely common (Nockleberg, 1931; Kwak & Tan, 1981; Dick and Hodgson, 1982) and disequilibrium mineral assemblages in metasomatic skarns are widespread as a result.

Scheelite distribution in the anhydrous silicate facies is normally uniform in marked contrast to the hydrous silicate facies where it is erratic, but locally very high grade (Krauskopf, 1953; Bateman, 1956; Dick, 1980). Scheelite commonly has a considerable molybdenum content, scheelite ($CaWO_4$) and powellite ($CaMO_4$) forming a solid solution series. Wolframite is rare in skarns (Dick and Hodgson, 1982) but sulphides, notably molybdenite, chalcopyrite, sphalerite, pyrite and pyrrhotite are commonly associated with the hydrous facies of skarn, frequently in economic quantities.

Fluid inclusion studies indicate that tungsten-bearing skarns that are unequivocally replacement bodies after a relatively pure carbonate unit are formed by a hydrothermal, saline fluid ascending from a hot crystallising magma (Kerrick, 1977; Kwak, 1978). Temperatures of formation of anhydrous skarn silicate assemblages are in the range 500° to 600°C, while figures of 300° to 450°C are recorded for hydrous assemblages (Zaw, 1976; Farrar et al., 1978; Tan and Kwak, 1979). Stable isotope studies on calcites from marble and skarn in the Osgood Mountains (Taylor, 1976) and at Pine Creek (Brown et al.,

1985) show mixing trends between fluids in equilibrium with a magmatic source and unaltered marble.

However, in recent years there has been considerable dispute as to the origin of the hydrous silicate assemblages. For example, at Cantung, the initial interpretations proposed that the amphibole and biotite dominated skarns were formed as the result of retrograde alteration of the anhydrous garnet-pyroxene and pyroxene facies by meteoric waters (Zaw and Clark, 1977 and 1978). Einaudi et al. (1981) and Newberry and Einaudi (1981) broadly favoured this interpretation for skarns in the North American cordillera. In contrast, Dick and Hodgson (1982) in their regional study of tungsten skarns in north-west Canada concluded that the anhydrous and hydrous skarn facies developed simultaneously from a magmatically derived fluid and that the zonation reflected progressively decreasing fluid/rock ratios (and thus decreasing intensity of metasomatism) away from the main fluid pathway, (i.e. outwards from the granite), a conclusion supported by Mathieson and Clark (1984).

A classification scheme for tungsten skarns has been proposed by Newberry (1979b) based on the degree of oxidation of the skarn. "Reduced skarns" such as Cantung and Mactung have silicate assemblages dominated by ferrous iron including hedenbergitic pyroxene, almandine-grossular garnet, hornblende and biotite. These skarns are formed in carbonaceous host rocks or at great depth. In contrast, the "oxidised" skarns, e.g. King Island, contain abundant ferric iron assemblages dominated by epidote and andraditic garnet and are formed in noncarbonaceous or haematitic host rocks or at shallow depths. A broad continuum of skarn types exists between these two end members, but due to the diversity and complexity of processes involved in skarn formation, the classification scheme appears to be of limited use.

Tungsten skarns have a generally stratiform geometry, but their complexity and heterogeneity are notorious. The diversity of silicate assemblages, variety of ore minerals and the limited structural control on ore deposition and hence patchy distribution of mineralisation present numerous problems in research, sampling, exploration and mining. Although skarns are the world's primary

source of tungsten, few deposits exceed 10 million tonnes, the vast majority of orebodies being several orders of magnitude smaller.

3. TUNGSTEN MINERALISATION HOSTED BY ROCKS OTHER THAN SKARN

The aim of this section is to draw the reader's attention to the fact that, although the majority of tungsten orebodies and mines are restricted to replacement skarns and cassiterite-wolframite greisen deposits, there are considerable tonnages of tungsten present in a wide variety of Precambrian and Palaeozoic environments.The tungsten (usually scheelite) mineralisation within these mainly stratabound deposits is considered to result from syn-sedimentary or syn-diagenetic concentrations of the metal. Although in the majority of examples geochemical work, especially stable isotope studies, is lacking, the geological evidence strongly suggests that, to explain the tungsten mineralisation, recourse must be made to explanations other than epigenetic theories involving felsic intrusions.This has particular relevance to the Otjua prospect where granites are not exposed in the immediate vicinity of the tungsten mineralisation. Only a few examples of stratabound tungsten mineralisation are cited below:

a) Scheelite in Greenstone Belt Terrain

Stratabound tungsten mineralisation associated with submarine metavolcanics is found within the greenstone belts of Zimbabwe (Cunningham et al., 1973). The lower portion of the Bulawayan (2900 Ma) consists of ultramafic, basaltic and acidic lavas, lavas, tuffs and minor sediments that have been metamorphosed in the greenschist or amphibolite facies. Scheelite mineralisation is present at a number of localities: in skarns (sensu lato) accompanied by minor sulphide mineralisation in the Fort Victoria schist belt; associated with Cu-Au-Ag mineralisation hosted by metavolcanics, cherts and banded iron formation ores in the Uvuma schist belt; and within garnet-vesuvianite-epidote rocks hosted by ultramafic metavolcanic schists and in close proximity to Au-Ag-Sb-As mineralisation in the Umtali-Odzi schist belt. Cunningham et al. (1973) consider the scheelite mineralisation to be stratabound in all these cases and to be related to submarine volcanism.

b) Scheelite Hosted by Proterozoic Metasediments in Areas of Unusual Base Metal Concentrations

Scheelite mineralisation has been documented in close proximity to a number of the large Early-Middle Proterozoic stratabound Pb-Zn orebodies. At the Gamsberg Zn-Pb deposit in Namaqualand, South Africa, scheelite occurs as irregular aggregates within calc-silicate carbonates of the A3 bed in the Gams Formation (Rozendaal and Stumpfl, 1984). This bed, which lies in the immediate footwall of the sulphide ore zones, is an impersistent, finely banded horizon with gradational contacts into the underlying and overlying units. The A3 bed has a mineralogy dominated by ferroan calcite, manganoan calcite, rhodochrosite, K-feldspar and quartz with minor diopside and actinolite. Scheelite is present as aggregates interstitial to the silicates. The Gams Formation, which hosts the mineralisation, has undergone amphibolite facies metamorphism and has an extremely diverse, disequilibrium assemblage of silicates, oxides and sulphide minerals. This assemblage resulted from the metamorphism of unusual precursors produced as a result of interaction between chemical and sedimentological processes. These processes operated in a marine hydrothermal spring environment - similar to those operating during Red Sea-type incipient rifting (Rozendaal and Stumpfl, 1984).

In the Broken Hill Block, New South Wales, Australia, Barnes (1980, 1983) has described three types of stratiform tungsten occurrence, all developed in close proximity to, and at the same stratigraphic level as, the stratiform Pb-Ag-Zn mineralisation. The Broken Hill Block is composed of metasediments and minor amphibolites that have undergone upper amphibolite-granulite facies metamorphism. The majority of the base metal mineralisation is hosted by Suite 4 (Mine Sequence Suite), which is comprised of sulphide mineralisation, banded iron formation, magnetite-garnet-quartz-apatite rocks, amphibolites and quartz-feldspar-biotite-garnet gneiss. Tungsten mineralisation occurs within Suite 4 as: 1) scheelite disseminations and aggregates in finely bedded calc-silicate rocks; 2) scheelite disseminations in more massive calc-silicates associated with amphibolite and also within amphibolite (Corruga-type) and 3) in the Yanco Glen area as wolframite and scheelite in quartz veins in quartz-tourmaline rocks,

in quartz-muscovite-tourmaline pegmatites and as disseminations in quartz-feldspar-biotite gneiss. The calc-silicate and Corruga-type deposits are interpreted as chemical sediments formed from base-metal enriched fluids. The origin of the mineralisation at Yanco Glen is somewhat more complex, but is interpreted as being of an originally stratiform nature that has undergone remobilisation. It is concluded by Barnes (1983) that the primary concentrations of all metals result from the introduction of base metals from hot springs into an area of quiet sedimentation dominated by chemical sediments.

c) Scheelite Hosted by Regional Skarns Derived by Metamorphic Processes

Scheelite deposits have been described from late Precambrian (580-620 Ma) rocks from the San Luis and Cordoba provinces of Argentina (Brodtkorb and Brodtkorb, 1977). The metasedimentary sequence of quartz-oligoclase-biotite schists, marbles and both ortho- and para-amphibolites has undergone amphibolite facies metamorphism (Clayton, 1971) and been intruded by several post-metamorphic granites. Scheelite mineralisation is hosted both by the schists and various "tactised rocks" within the carbonate units. These tactites comprise calcite, epidote, actinolite, phlogopite, garnet, scheelite and sulphides. Reconcentration of scheelite into cross-cutting quartz veins and pegmatites occurred during regional metamorphism. The lack of intrusive bodies in the immediate vicinity of the tactites as well as the extensive mineralisation in lithologies other than tactite has led Brodtkorb and Brodtkorb (1977) to propose a regional metamorphic, not a metasomatic, origin for the tactites and, moreover, they suggest submarine volcanic rocks to have acted as the source of the tungsten.

Skaarup (1974) has described scheelite mineralisation hosted by Caledonian hornblende-diorite gneisses and skarns (sensu lato) that have undergone amphibolite facies metamorphism in the Bindal area of northern Norway. Scheelite occurs in skarn developed within marble layers at the contact between the calcareous lithology and the enclosing hornblende-biotite gneiss. The skarn assemblages are dominated by garnet, pyroxene, actinolite, tremolite and various Cu, Fe and Mo sulphides as well as scheelite and are best developed in

regions where the enclosing hornblende-biotite gneiss contain substantial disseminated sulphide mineralisation. Although the area has been extensively intruded by diorite sheets, granites, syenites and monzonites, Skaarup concludes that skarn formation is unrelated to felsic igneous activity and formed by the exchange of material between marble and schist during regional metamorphism, i.e. they are reaction skarns (Eskola, 1939). Moreover, Skaarup suggests that the scheelite has formed from tungsten concentrated in the volcanic precursor of the hornblende-biotite gneiss in a marine exhalative environment.

d) Scheelite Hosted by Calc-Silicate Rocks.

Beran et al. (1985) have described stratabound scheelite mineralisation hosted by calc-silicate hornfels in the Bohemian Massif of Austria. The fels are part of a metasedimentary sequence of marble, calc-silicates, amphibolites and sillimanite and graphite-bearing paragneisses of the Bunte Series, though, there is some dispute as to the age of these rocks; a late Archean to early Proterozoic age is favoured by Svoboda (1966) and Chalowpsky (1978), while Waldman (1951) and Thiele (1984) indicate a Silurian age. These metasediments that have undergone upper amphibolite facies metamorphism are interpreted as having originally been marine sediments with basic lava intercalations. The scheelite mineralisation is hosted by "dark calc-silicate" rocks, whose major constituents are ferrosalite pyroxene, meionitic scapolite and quartz. Accessory minerals include plagioclase, zoisite-clinozoisite, calcite, amphibole, sphene, apatite, scheelite and pyrrhotite with very minor pyrite and chalcopyrite. Whole rock analyses of calc-silicate indicate tungsten concentrations in the range 40 to 5000 ppm. The fact that no felsic intrusives are developed in the immediate area of scheelite mineralisation, the absence of skarn mineral assemblage and the lack of evidence for metasomatic replacement led Beran et al. (1985) to propose the presence of stratiform tungsten concentrations in the "dark calc-silicate" precursor, though a source for the metal was not specified.

e) Scheelite Hosted by Palaeozoic Volcanics

A large number of scheelite occurrences associated with tholeiitic, mafic and calc-alkaline metavolcanics are located within the Early Palaeozoic Habaschserie in Austria (Höll, 1977). At the Felbertal deposit, scheelite occurs in fine grained, conformable quartz lenses that are interpreted as metamorphosed exhalative cherts. Cross-cutting quartz-scheelite zones, which underly the stratiform bodies, are interpreted as fluid conduits. The highest grade scheelite mineralisation is accompanied by significant increases in the Mo, Cu, Bi, Au, Ag and Sn contents of the metamorphosed chert. The exhalative activity that formed the cherts is considered by Höll (1977) to be related to submarine mafic volcanism.

4. GEOLOGY OF THE OTJUA PROSPECT

4a Location of the Otjua Prospect

The Otjua prospect is located at 21°11'15"S, 16°00'25"E thirty kilometres north of the town of Omaruru, SWA/Namibia, 2.5 kilometres west of the Omaruru-Kalkfeld tar road and is easily accessible by farm tracks (see Fig.1 and Map 1). The prospect is situated at the eastern end of the twenty kilometre long Otjua Ridge, which comprises a series of low hills underlain by metasediments surrounded by plains of granite (see Photo 1). Geological exposure on the ridge is fairly good. The prospect is at an elevation of 1500 metres AMSL, 80 metres above the surrounding plain. Climatically, the area is semi-desert with high summer temperatures, often in excess of 35°C, and low annual rainfall. Night-time winter temperatures are seldom below 0°C. Grass and thorn bush form the sparse vegetation of the area.

4b Regional Setting of the Otjua Prospect

Central SWA/Namibia is almost entirely underlain by metasediments of the late Proterozoic Damaran sequence and rocks associated with the Pan-African Damaran orogeny. The Damara Orogen has been divided into several tectonostratigraphic zones which have undergone varying degrees of metamorphism and styles of pre-, syn- and post-tectonic plutonic intrusion (see Fig. 2). The Otjua prospect is situated in the Central Zone of the Damara Orogen , which is characterised by sillimanite-cordierite metamorphic assemblages, widespread granite intrusions and north-easterly trending F_3 domal structures. The Central Zone is subdivided into two portions by the Omaruru Lineament-Waterberg Fault. The Omaruru Lineament is "a fundamental line of crustal weakness" (Corner, 1981, p.56), which has been active during Damara and Karoo times and the Otjua prospect lies six kilometres to the north-west of this major fault zone.

Deposition of Damara sediments in the northern portion of the Central Zone occurred between 750 Ma and 650 Ma (Miller, 1983a). Feldspathic quartzites and arkoses of the basal Nosib Group were overlain by calcareous quartzites and marls of the Khan Formation (see Fig. 3).

The overlying Swakop Group sediments, from the base upwards, comprise carbonate units of the Rössing Formation, argillaceous rocks and marls of the Oberwasser Formation, the thick carbonate development of the Karibib Formation and argillites of the Kuiseb Formation.

These Damaran sediments were subsequently deformed during the Damaran Orogeny. In the northern Central Zone, the sediments underwent three phases of plastic deformation and regional metamorphism of amphibolite facies grade. The first folding phase, F_1 occurred in the region 570-560 Ma, while F_2, the recumbent phase, occurred between 530 Ma and 510Ma, coinciding with the metamorphic peak at about 520 Ma (Haack et al., 1980, see Fig. 4). F_3, which resulted in the formation of the broad, north-easterly trending, domal structures took place at 490-460 Ma (see Fig. 4).

The majority of igneous intrusives in the northern Central Zone are granitic in composition and are younger than 550 Ma (Haack et al., 1983). Minor igneous activity did occur prior to this time, but the intrusions are dioritic or syenetic in composition. The granites of the northern Central Zone, as elsewhere in the Damaran Orogen, are noticeably restricted to specific stratigraphic levels (Klein, 1980; Watson, 1982; Corner, 1983). Both syn-F_2 and syn-F_3 Salem-type granites with characteristic porphyritic K-feldspar are confined to the Kuiseb Formation, as are the syn-F_2 garnetiferous leucogranites. Late tectonic (490-460 Ma) leucogranites tend to intrude pre-Karibib formations, but there are some noticeable exceptions. In the light of petrogenetic investigations (Winkler, 1983) radiogenic and stable isotope data (Haack et al., 1983) the majority of granitic intrusions in the northern Central Zone are considered to have been produced during the widespread anatexis of Damaran metasediments that accompanied the Damaran orogen.

Post-Damaran activity in the northern Central Zone included subsequent movement on the Omaruru Lineament-Waterberg Fault and the intrusion of a considerable number of Karoo dykes.

4c District Setting of the Otjua Prospect

The Otjua prospect is situated on the southern side of a major anticlinal (possibly domal) structure in the northern Central Zone of the Damaran Orogen (see Fig. 2 and Map 1) hereafter called the Schönfeld dome. Metasediments of the Khan, Rössing, Oberwasser and Karibib Formations comprise this dome and have been intruded by a variety of felsic intrusives.

i)Metasediments:

The Khan and Oberwasser Formations are represented by a rapidly alternating sequence of quartz-biotite schists, calc-silicate rocks, scheelite-bearing hornfels and minor carbonate units. The proportion of the more carbonaceous units increases towards the contact with the Rössing Formation i.e. the top of the Khan Formation and the base of the Oberwasser Formation. Facies changes, both along and across strike are a feature of these two Formations. The schist is interpreted as representing metamorphosed muds, the calc-silicate rocks as marls and the marble as limestone. The fine intercalation of rocks composed of detrital material and chemical precipitates suggest that the sediments were formed in a quiet, marine(?) environment. Skarnification of the minor carbonate horizons has occurred locally, especially in the Khan Formation.

The Rössing Formation is represented by a single, very pure, continuous marble unit, varying in thickness from 0.7 to 6 metres, that is traceable for 22 kilometres on the southern side of the dome (see Map 1). This calcareous unit is a prominent marker horizon and probably marks a major unconformity between the underlying Khan and overlying Oberwasser Formations. The marble is interpreted to be a metamorphosed marine limestone. Replacement skarns within the Rössing Formation are developed at four localities within the domal structure: Tjirundo, Schönfeld, Roidina and Otjua (see Map 1). The latter hosts economic tungsten mineralisation. Skarnification appears to have occurred only where granite is proximal to the marble, though in none of the four examples is the contact between granite and marble exposed. Furthermore, at the Tjirundo, Schönfeld and Otjua

replacement skarns, pegmatite bodies, apparently derived from the granite, have extensively disrupted the stratigraphy.

The Karibib Formation is divided into three members: successively the Harmonie Member, composed of quartz-biotite schist, calc-silicates and minor marble, the Otjongeama Member with numerous calc-silicate and marble intercalations and the Arises Member, a distinctive coarse grained graphite-bearing, calcitic marble. The thickness of the Karibib Formation varies considerably, though this is thought to be for tectonic rather than sedimentological reasons.

ii) Metamorphism:

The granoblastic texture in the schists and calc-silicates of the Khan and Oberwasser Formations, the preferred orientation of biotite, amphibole and pyroxene and the presence of poikiloblastic pyroxene in the calc-silicates are all indicative of the sequence having undergone at least amphibolite facies metamorphism. The mineral assemblages appear to be in equilibrium and there is no evidence of more than one phase of metamorphism, though there may have been more than one stage of biotite growth. Garnet is notably absent in both biotite schist and calc-silicate rocks.

Regional mapping of the farms immediately surrounding the Otjua prospect by Kuyper (1984) indicated the presence of andalusite on the farm Tjirundo 91 in schists of the Oberwasser Formation. Sillimanite has not been identified in the immediate area surrounding the Otjua prospect, but is present on the farm Kassandara 40, 10 kilometres to the south-east (Thatcher, 1985). There is no evidence for in situ anatectic melting of the metasediments e.g. gneissose texture at the Otjua prospect and thus upper amphibolite conditions were probably not attained. These observations are consistent with the investigation into regional metamorphism in the Damaran conducted by Hoffer (1977): the andalusite-sillimanite isoreactiongrad passes almost exactly through the Otjua prospect (see Fig. 5).

Peak metamorphic temperatures were therefore in the range 500°C to 680°C (see Fig. 6). The lack of garnet in the calc-silicates at the

Otjua prospect indicates a peak metamorphic pressure of less than 4.8 kb since the reaction An + Cc + Qtz = Gt + CO_2 occurs above the andalusite stability field at higher pressures.

Although the contact between the Otjua granite and the metasediments is not exposed, contact metamorphic effects are likely to be insignificant or masked because, even at the time of crystallisation of the Otjua granite (478 $\pm$ 4 Ma), the metasediments of the Central Zone were still at a temperature of >300°C (Haack, 1983). Indeed no contact metamorphic (as distinct from metasomatic) effects have been noted in the vicinity of the Otjua prospect either associated with the Otjua granite or the pegmatites.

iii)Structure:

The metasedimentary sequence at the Otjua prospect strikes 103° and is overturned, dipping 75°-85° northwards (see Maps 1 and 2). Bedding is preserved in the Rössing Formation marble where graphite-rich zones are common and some of the calc-silicates are laminated on a fine scale, but way-up structures are inconclusive. Bedding is not preserved in the schist. There is therefore no proof in the immediate vicinity of the prospect that the metasedimentary sequence at Otjua youngs southward. Previous work conducted by the Geological Survey indicated the Schönfeld dome to be a basin (see present Geological Survey 1 : 1,000,000 map of SWA/Namibia, 1980). This is now known to be incorrect (Miller and Badenhorst, pers. comm.).

The quartz-biotite schist and calc-silicates of the Khan and Oberwasser Formations possess a well developed foliation, which is parallel to lithological contacts. This foliation is caused by the elongation and preferred orientation of minerals e.g. biotite and amphibole. No secondary foliation has been identified. Although the bedding-parallel foliation was almost certainly formed during F_1 and the metasedimentary sequence probably overturned during F_2 and slightly modified during F_3 to form the major domal structure, there is little direct evidence in the immediate vicinity of the Otjua prospect for three phases of ductile deformation. The calc-silicates and scheelite-bearing hornfels possess a prominent lineation that

plunges 68°-75° on a bearing 063° (See Map 2 and Fig. 7). This lineation is approximately parallel to minor, tight z-folds (see Map 2).

Approximately one kilometre east of the Otjua prospect, calc-silicates exhibit unusual, steeply eastward plunging, tube-like structures about ten centimetres in diameter and up to several metres long. These have been tentatively interpreted as boudins. The calc-silicate outcrops themselves pinch and swell over distances of 100 metres, in places being up to twenty metres thick and disappearing along strike. This variation is thought to be tectonic rather than sedimentological in origin. There is widespread evidence for boudinage of thin calc-silicate horizons within the more incompetent calcareous units of the Karibib Formation marbles in the western nose of the Schönfeld dome on the farm Etendero 85 (see Map 1).

The Otjua prospect has been disrupted by several faults that have limited surface expression, but have been intersected in drill core and detected by a "Turam" Electromagnetic Survey (Pferdekampfer, 1984). The faults can be grouped into two areas, the 16 West Fault Zone, oriented approximately 013° and the 29 West Fault Zone 020° (see Map 2). All faulting appears to be in the same sense i.e. minor sinistral horizontal displacements (1-20 metres) with considerable vertical downthrows to the west (see discussion on skarn and ore distribution).

iv)Intrusives:

The Schönfeld dome has been intruded by two types of granite. The Otjua granite has intruded the core of the Schönfeld dome, though the contact between the intrusive and the metasediments is obscured by scree. This granite has been dated by Haack (pers. comm.) and is referred to, by him, as the "leucocratic granite, 31 kilometres north of Omaruru" (Haack et al., 1983; see Map 1 for sample site). The granite has an Rb-Sr age of 478 $\pm$ 4 Ma, an initial $(^{87}Sr/^{86}Sr)_I$ value of 0.7196 and a high $\delta^{18}O$ value of 15.1‰. The closest exposure of the Otjua granite to the replacement skarn developed in the Rössing Formation marble at the Otjua prospect is 600 metres away. A similar

type of granite to the Otjua granite intrudes Lower Karibib Formation marbles on the farm Epako 38.

The second type of granite, a fine grained variety, is intrusive into Khan, Rössing and Oberwasser Formation metasediments and the closest exposure to the replacement bodies at the Otjua prospect is approximately 1.2 kilometres to the south (see Map 1). The fine grained variety has not been dated and the relationship between it and the Otjua leucogranite is unknown, but the two granites are thought to be cogenetic.

Of particular note is the fact that in the north-east corner of the farm Tjirundo 91 and the south-east corner of Schönfeld 92 (see Map 1) the fine grained granite is confined to a series of crosscutting dykes oriented 113° that transect the Khan, Rössing and Oberwasser Formations. In these dykes the fine grained granite exhibits a well developed foliation and most of the felsic minerals are fractured and show signs of having been strained. This locally developed foliation (the granite bodies to the north-west and south-east are unfoliated) is a result of post-crystallisation deformation and is possibly related to movement on the Omaruru Fault Zone (see discussion in chapter 8).

A particularly prominent feature of the core of the Schönfeld dome is the presence of a large amount of quartz-feldspar pegmatite (see Map 1). There are a considerable number of xenoliths of Khan Formation metasediments within these pegmatites, which was referred to as "Mixed Suite" during regional mapping (Kuyper, 1984). Quartz-feldspar-tourmaline pegmatites have extensively intruded the metasediments exposed on the Otjua Ridge in a passive or "lit par lit" manner. However, crosscutting pegmatites with a remarkably constant orientation of 113° are intimately associated with three areas on the Otjua Ridge where replacement bodies are developed within the calcareous units. Moreover, crosscutting pegmatites are virtually absent from those portions of the stratigraphy that are not skarned and the crosscutting pegmatites are confined (as are the skarns) to two areas where the metasediments strike between 090° and 105° (see Map 1). These points suggest that there is a strong structural

control on crosscutting pegmatite intrusion (and possibly skarn formation).

4d Detailed Geology and Petrography of the Otjua Prospect

i) Metasediments of the Khan and Oberwasser Formations:

1) Quartz-Biotite Schist

This schist comprises 60-70% of the metasediments within the vicinity of the Otjua prospect but is poorly exposed, due to weathering. It has a strong foliation which is parallel to bedding in the associated marble and calc-silicate horizons. In hand specimen the schist is brown grey and has a fine to medium grained (< 2mm) equigranular texture. Disseminated pyrite and chalcopyrite occur but are rare and sulphide stringers up to 2mm thick are locally developed.

In thin section the schist comprises biotite (15-40%), quartz and plagioclase feldspar (60-80%), clinopyroxene (2-3%) and minor apatite, chlorite, carbonate and sulphides. A granoblastic texture is present, but due to the small grain size (<150μ) of the mosaic of quartz and feldspar, it is difficult to estimate the proportion and composition of the feldspar since much of it is untwinned. However, the presence of clay minerals indicates that a considerable amount of feldspar is present. Biotite flakes (up to 1mm long) have a preferred orientation and the pyroxene exhibits a poikiloblastic texture indicating later crystallisation. Very occasional specks of scheelite within the schist have been noted when examined under U.V. light.

2) Calc-Silicate

This lithology comprises approximately a quarter of the metasediments at the Otjua prospect and occurs as rapidly alternating horizons and lenses within the schist (see Map 2). These lenses vary in thickness from 10cm to 20m. Facies changes into schist along and across strike are very common. The most continuous outcrop is a 10-20m thick marker unit of calc-silicate occurring in the structural footwall of the Rössing Formation (see Map 2). This marker contains minor thin biotite

bands and often has an orbicular appearance on the weathered surface. Calc-silicate exposures tend to be prominent due to their extreme hardness relative to the enclosing schist and on the weathered surface the calc-silicates often have a smooth, rounded, black appearance.

Varieties of calc-silicate include a brown-green, biotite-rich calc-silicate (20% biotite), an orbicular variety (0-5% biotite) and a pale green, massive, pure calc-silicate with almost no biotite. In thin section all types have a fine grained (< 1mm) equigranular texture. Quartz and plagioclase feldspar (An_{80-100}, determined by Michel Lévy method) comprise 80% of the rock type, but much of the plagioclase is untwinned making estimations of mineral proportions difficult. The remainder of this lithology is composed of biotite (0-20%), diopside (5-20%) and minor scapolite and sphene. A granoblastic texture with later, poikiloblastic diopside is ubiquitous. Very fine grained (<0.5mm) specks of scheelite can be seen in places with the aid of a U.V. lamp.

3) Scheelite-bearing Hornfels:

Scheelite-bearing hornfels comprise approximately 2-3% of the Khan and Oberwasser metasediments at the Otjua prospect and are developed as thin, discontinuous intercalations within the metasediments, especially the calc-silicate rocks. Horizons of scheelite-bearing hornfels vary in thickness from a few centimetres to several metres, but are more commonly in the 10-50cm range and are laterally discontinuous. The hornfels exhibits gradational contacts with enclosing calc-silicate lithologies, but where the hornfels is enclosed by biotite schist, an amphibole (probably hornblende) rich zone that varies between a few millimetres and one centimetre in thickness is developed at the contact between the two lithologies. This amphibole-rich zone is interpreted as a reaction skarn developed during regional metamorphism. Scheelite-bearing hornfels is light to dark green in colour and usually exhibits a fine to very fine grained massive texture (<1mm), though hornfels possessing amphibole may have a faint foliation. Scheelite-bearing hornfels is <u>not</u> associated with marble horizons. Two typical examples of scheelite-bearing hornfels are shown in Photo 2.

In thin section the hornfels is characterised by a diverse mineralogy. Mineral assemblages include: quartz (0-40%), plagioclase feldspar (0-40%), clinopyroxene (10-60%), scapolite (0-60%), hornblende (0-10%), clinozoisite (0-15%), sericite (0-10%), sphene (1-4%), biotite (0-2%), apatite (1-2%), carbonate (0-5%), scheelite (0-2%) and very minor pyrite and chalcopyrite. The grain size rarely exceeds 1.5mm and is usually finer than 1mm. The overall texture is xenoblastic-granoblastic, triple junctions being very common with scapolite and plagioclase locally exhibiting a poikiloblastic habit that encloses all other phases(see photos 3 and 4). However, in some sections the texture within the hornfels is very chaotic. Round pyroxene grains, xenoblastic quartz and scapolite are by far the most common minerals and all three frequently contain small round inclusions of sphene and euhedral apatite. Hornblende is usually found rimming pyroxene, though minor amounts of primary amphibole are also present. Clinozoisite is ubiquitously associated with altered scapolite and plagioclase, while the latter two minerals show considerable alteration to sericite. The minor carbonate is always interstitial to other minerals. The undulose extinction within the quartz indicates considerable post-crystallisation straining of the hornfels.

Two points are worthy of emphasis. Firstly, the fine grained ($<$0.5mm) scheelite is part of a stable metamorphic assemblage. It is in textural equilibrium with all other phases and is not a late stage mineral. Secondly, both plagioclase and scapolite are in textural equilibrium. Only occasionally does plagioclase rim scapolite or vice versa, therefore the scapolite is a primary metamorphic mineral, not an alteration product after feldspar.

Although mineral compositions are discussed in detail below, the pale green colour of the clinopyroxene in plane polarised light indicates that it is a member of the diopside-hedenbergite solid solution series, the highly birefringent nature of the scapolite testifies to its high meionite component and the plagioclase composition is An_{70-90} (determined by Michel Lévy method).

4) Marble:

Marble comprises a minor proportion of the Khan and Oberwasser metasediments at the Otjua prospect (see Map 2). The marble horizons vary in thickness, from a few centimetres to several tens of centimetres, though locally they are greater than 1 metre thick. Some of the thicker horizons are laterally continuous for hundreds of metres, but the thinner examples exhibit poorer continuity. Marble is invariably enclosed by calc-silicate rocks and gradational contacts, on both foot and hanging wall, between the two lithologies are common. The marble is grey-brown in appearance, fine - medium grained (<1.5mm) and locally graphitic. Although the mineralogy has not been fully investigated, the marble is a marly calcitic carbonate.

The more continuous marble horizons host scheelite-bearing skarn assemblages that are dominated by idocrase, garnet, scapolite, pyroxene and fluorite (see Map 2). Skarn development is more pronounced within marbles of the Khan Formation i.e. closer to the Otjua granite (see Maps 1 and 2). Skarn mineralogy and development are discussed in more detail in sub-section iv.

ii) Metaintrusive in the Khan and Oberwasser Formations:Sulphidic tonalite.

One lithology that is poorly exposed on surface, but has been intersected by several drillholes is a sulphidic tonalite. The dimensions of this lithology are difficult to establish due to its poor continuity (as indicated by the poor correlation between adjacent boreholes). The tonalite varies in thickness from a few tens of centimetres to several metres, the rock possessing a well defined foliation that is parallel to the contacts between the tonalite and the enclosing metasediments. Locally the tonalite interfingers (on a centimetre scale) with the schist. In hand specimen it is a fine grained, white quartz-feldspar rock with very minor, thin biotite stringers and finely disseminated pyrite and chalcopyrite. Thin (<1mm thick) stringers of quartz and occasional quartz eyes (<1mm) are also present. In thin section a granoblastic texture is readily apparent, the grain size being approximately 250µ. The tonalite is

dominated by a mosaic of anhedral quartz and plagioclase feldspar (An_{80}, determined by Michel Lévy method), but due to lack of twinning in the plagioclase, estimation of the modal composition is difficult. Up to 15% microcline is present, while biotite (0-5%), muscovite (0-2%), clinozoisite (0-2%) and sulphides (0-3%) comprise the remainder. The sulphide may be granoblastic or very ragged and interstitial. It is suggested that the rock, on account of its distribution and metamorphic characteristics was originally intrusive into the sequence and has been subsequently metamorphosed.

iii) Rössing Formation:

At the Otjua prospect the Rössing Formation is represented by a single marble horizon (see Map 2). This horizon varies in thickness from 0.7-4 metres and often exhibits a pinch and swell nature. The contact between the Rössing Formation marble and the enclosing metasediments is usually sharp, but there may be a transition zone in which thin (<5cm thick) bands of marble are developed in schist or calc-silicate (see Fig. 8). In hand specimen the marble is an extremely pure rock composed almost entirely of coarse grained (2-5mm) calcite. The marble is grey-white in colour and possesses finely disseminated pyrrhotite and fine grained graphite. The graphite lends a grey, often banded, colouring to the marble (see Photo 5).

In thin section a granoblastic texture is readily discernable(see photo 6).Calcite grains, varying in size from 1-5mm, form a polygonal mosaic that comprises approximately 95% of the rock. Very minor scapolite (0-2%), plagioclase feldspar (0-2%), clinopyroxene (0-2%), pyrrhotite (0-2%), graphite (0-2%) and trace amounts of apatite, sphene, sericite and clinozoisite comprise the remainder of the rock. Minerals other than calcite are very fine grained (<0.5mm) and fill the interstices between the carbonate grains. Pyroxene grains are round, while both scapolite and plagioclase may be xenoblastic and locally poikiloblastic. Graphite flakes are round or oval to very ragged.

iv) Skarn:

Metasomatic skarn is developed within several of the marble units at the Otjua prospect, but the most extensive and continuous skarn is hosted by the Rössing Formation marble (see Map 2). A strike length of approximately 700 metres of this marble has been skarned and has been investigated by diamond drilling to a depth of 370m below surface (see Long. Sect. 1). The continuity and thickness of the skarn hosted by the Rössing Formation combine to make it the most economically significant of all the skarns at the Otjua prospect. The description of skarn mineralogy and geochemistry that follows concentrates almost exclusively on the skarn types occurring in the Rössing Formation marble. Unless specifically stated, comments apply to skarns within that formation, though skarns hosted by marbles of the Khan and Oberwasser Formations exhibit similar characteristics.

The skarn replacing the Rössing Formation marble can be sub-divided into three zones or facies:

1) Idocrase facies skarn which hosts minor scheelite mineralisation
2) Garnet facies skarn which hosts the majority of scheelite mineralisation
3) Pyroxene facies skarn which is barren of scheelite mineralisation

These three facies of skarn appear to be related to varying degrees of replacement of the marble. Moreover, they appear to pass laterally into one another, but this cannot be proved due to poor exposure. However, transitional zones between the three facies have been recognised. There is no evidence that one facies of skarn replaces, overprints or crosscuts another facies.

From a mining point of view, the idocrase facies skarn is usually considered to be subeconomic: either the skarn is too thin or the tungsten grade is too low. Garnet facies skarn constitutes the major portion of the ore zone at the Otjua prospect while pyroxene facies skarn is essentially barren of tungsten.

1. Idocrase Facies Skarn:

This facies of skarn can be traced on surface for a distance of 325 metres west of the 27W fault (see Map 2) and drilling indicates that it extends at least 370m below surface (see Long. Sect. 1, Borehole OT24). Replacement of the Rössing Formation marble is always incomplete where idocrase facies skarn is developed. Skarn is especially well developed towards the structural footwall of the marble, with only minor development towards the structural hanging wall of the carbonate (see Fig. 9 and Photo 7). Normally the ratio of skarn thickness to combined marble and skarn thickness is less than 0.2, but the degree of replacement may be more extensive (e.g. borehole OT24, Table A). The skarn-marble contact is normally very sharp over a few millimetres.

In hand specimen idocrase facies skarn is dominated by pale brown to honey coloured prisms of strongly striated idocrase. These crystals, which vary in length from 1mm to 5cm, are randomly oriented within an equigranular fine to medium grained groundmass of the other minerals. In thin section the following minerals were noted: idocrase (30-70%), clinopyroxene (5-30%), scapolite (10-30%), calcite (5-40%), garnet (0-5%) as well as fluorite (0-2%), sphene (0-2%), plagioclase feldspar (0-2%), apatite (0-2%), clinozoisite (0-2%) and scheelite (0-1%). The idocrase contains numerous inclusions of very fine grained calcite and scapolite and can be seen overgrowing earlier coarser grained scapolite(see photos 8 and 9). Both the calcite (up to 3mm) and scapolite tend to be anhedral and the latter mineral is often extensively altered to clay minerals and clinozoisite. The scapolite, where fresh, exhibits high birefringence (second order colours) indicating that it has a high meionite content. Grains of pale green hedenbergitic pyroxene are seldom more than one millimetre in diameter and are present as individual, round or oval shaped grains or in clusters exhibiting triple point junctions. Rhombs of sphene are usually less than one millimetre long. The minor fluorite present is anhedral and appears to have developed slightly later in the crystallisaton sequence. Texturally the assemblage appears to be in equilibrium as all mineral phases are in contact with one another and there are no observable reaction relationships. However, the idocrase

prisms commonly exhibit a colour zoning that is concentric about the Z-axis.

2. Garnet Facies Skarn:

Garnet facies skarn can be sporadically traced on surface for a distance of 270 metres between the 16W and 27W faults (see Map 2) and has been intersected in drillcore at a depth of 350 metres below surface (see Long. Sect. 1, borehole OT26). However, within this area large zones of completely unreplaced marble exist (see Map 2). Where garnet facies skarn is developed, the degree of replacement of the marble is usually higher than in the idocrase facies and in many cases the carbonate unit has been entirely replaced (see Fig. 9 and Photos 10 and 11). However, the style of replacement in the idocrase and garnet facies is similar i.e. skarn is thicker on the structural footwall side of the marble (see Fig. 9). Contacts between the garnet facies and marble are sharp, although, in certain borehole intersections (e.g. borehole OT17) on the contact between the skarn and enclosing metasediments skarn is confined to thin ($<$5cm thick) bands and is intercalated with calc-silicate rock. This intercalation is thought to result from metasomatic replacement of thin bands of marble within a finely banded calc-silicate marble zone, which, in turn, reflects changing conditions of deposition during sediment formation (as discussed in the preceding section on the Rössing Formation marble). Therefore, the observed calc-silicate/skarn intercalation is interpreted not as metasomatic zoning resulting from diffusion of elements between marble and calc-silicate but to be due to the different compositional bands present in the original sediments (this is discussed in more detail in Chapter 8).

In hand specimen the skarn is distinctive due to the red brown garnet, the translucent colourless fluorite and the dark green pyroxene. The pyroxene exhibits one prominent cleavage and weathers to give a rusty, almost gossanous, appearance. Under U.V. light the skarn can be seen to contain finely disseminated scheelite which fluoresces a blue-white colour. The overall mineralogy of the garnet facies skarn as determined from thin section work is as follows: garnet (5-50%), hedenbergitic pyroxene (5-40%), scapolite (10-70%), fluorite (5-35%),

scheelite (0-3%), plagioclase feldspar (0-3%), clinozoisite (0-3%), apatite (0-3%), epidote (0-3%), hornblende (0-3%), chlorite (0-2%), carbonate (0-5%), pyrite (0-1%), pyrrhotite (0-2%) and chalcopyrite (0-2%). The garnet facies skarn has a granoblastic-poikiloblastic texture. A fine grained equigranular texture with numerous triple point junctions is locally developed, but elsewhere the texture is chaotic;some minerals, especially garnet, exhibit a poikiloblastic texture and the grain size varies considerably, often exceeding many centimetres.Garnet may be sub-idioblastic (see photo 12) or xenoblastic (see Photos 13 and 14) and is frequently associated with and appears to overgrow scapolite. The garnet frequently contains numerous, fine grained inclusions of calcite and scapolite and more rarely, clinopyroxene and sulphides. Garnet may form a skeletal network that encloses all other phases and occasionally is obviously a late stage mineral, for example it may rim scapolite.

Pale green, round or anhedral pyroxene crystals, which may be up to 1cm in diameter, though more often 1-2mm, often exhibit twinning and are usually found with scapolite or completely surrounded by a groundmass of fluorite (see photo 15). Scapolite is often present as granoblastic aggregates with clinopyroxene and is often considerably altered to clay minerals. Occasionally, very fine grained chlorite and more commonly, radiating aggregates of clinozoisite overgrow altered scapolite. Very fine grained aggregates of epidote may also be associated with scapolite. Round to almost rectangular scheelite crystals vary in size from 100-500μ in diameter, though they may be up to 4mm in diameter (see photos 16 and 17). The scheelite exhibits high relief and second order birefringence. Scheelite is present at triple points in equilibrium with pyroxene and scapolite, poikiloblastically enclosed by garnet and occasionally with fluorite. Anhedral calcite, usually less than 2mm in diameter, occurs as an interstitial mineral or as very fine grained inclusions in garnet. Fluorite is universally anhedral forming rounded embayments into pyroxene and scapolite and appears to be a late stage mineral. Plagioclase compositions are in the An_{50-60} range (determined by Michel Lévy method), though widespread alteration of the feldspar to clay minerals is common. The feldspar may contain irregular inclusions of calcite, apatite and scapolite. The very minor

hornblende exhibits strong pleochroism (dark green to blue green). The sulphides appear to be one of the last minerals to form either being interstitial to, or enclosing, garnet, fluorite and pyroxene.

Paragenetic summary: scheelite, scapolite and pyroxene all appear to have crystallised at about the same time but garnet, some of the fluorite and the sulphides, on account of their poikiloblastic and interstitial nature seem to have crystallised slightly later.

Unlike the other facies of skarn, garnet facies skarn is usually zoned across its width. This mineralogical zoning is by no means universally developed, but borehole intersections of garnet facies skarn exhibit many of the following characteristics which are summarised in Fig. 10:

1) a concentration of fluorite towards the structural hanging wall of the skarn
2) a sympathetic relationship between garnet and scheelite
3) a tendency for scheelite to be concentrated on the footwall side of the core of the skarn, but a decrease in scheelite immediately on the footwall contact
4) an antipathetic relationship between pyroxene and garnet
5) a concentration of pyroxene towards the hanging and footwall contacts of the skarn

No mineralogical zoning within the garnet facies skarn has been noted either down-dip or along strike.

3. Pyroxene Facies Skarn:

This facies can be traced on surface for a distance of approximately 90 metres on the eastern side of the 16W fault (see Map 2) and extends to at least 130 metres below surface (see Long. Sect. 1). Pyroxene facies skarn always replaces the entire width of the marble (see Fig. 9). Pyroxene facies skarn with minor fluorite mineralisation has been intersected in borehole OT14 on the western side of the orebody (see Long. Sect. 1). The skarn in borehole OT14 is interpreted as being

part of a transitional zone between the garnet and pyroxene facies (see Photo 18).

Pyroxene facies skarn is dominated by two minerals, scapolite and pyroxene. The mottled effect of the white scapolite and dark green pyroxene (the two principal minerals) lend the lithology a distinctive spotted appearance. In thin section the skarn comprises hedenbergitic pyroxene (20-80%), scapolite (20-80%), hornblende (0-5%) and minor clay minerals, calcite, clinozoisite and opaques. In thin section pale green, anhedral clinopyroxene and highly birefringent scapolite are usually developed in a polygonal mosaic. This mosaic is locally granoblastic (triple junctions are common), but elsewhere there is a considerable range in grain size from 100μ to many centimetres. The scapolite shows considerable alteration to clay minerals, while clinozoisite prisms up to one millimetre long are commonly associated with and occasionally may poikiloblastically enclose scapolite. The highly pleochroic hornblende occurs as rims on pyroxene and thus tends to be anhedral and ragged. Occasionally the amphibole may poikiloblastically enclose pyroxene. The fine grained opaques (<100μ) observed in thin section are thought to be magnetite. On surface, minor copper sulphide mineralisation has been oxidised to malachite, though sulphides have not been noted in thin section.

4. A summary of the essential petrographic differences between replacement skarns and scheelite-bearing hornfels is given in Table 1.

v)Intrusive Rocks

1. Otjua Granite:

In hand specimen the Otjua granite is a light grey, leucocratic, equigranular, medium to coarse grained rock. A slightly porphyritic texture is locally developed. The granite is homogenous and the lack of foliation indicates that it is of late tectonic age. The dominant mafic mineral is biotite. Minor garnet is present at sample locality OT128 (see Map 1), while coarse grained black schorl is well developed in quartz-tourmaline nests at sample locality OT112 (see Map 1 and Photo 19). These oval quartz-tourmaline nests vary in size from five

to fifteen centimetres in diameter. Locally, pegmatite and aplitic dykes can be seen to intrude the granite in a random fashion. The pegmatitic dykes are composed of quartz, feldspar, biotite, tourmaline and very minor garnet. Biotite xenoliths are locally present with the Otjua granite e.g. sample locality OT112 (see Map 1).

In thin section the Otjua granite has the typical granular, hypidiomorphic texture of an igneous rock and comprises quartz (30-40%), microcline feldspar (30-40%), plagioclase feldspar (10-25%), biotite (3-10%), muscovite (0-2%) and minor clay minerals zircon, tourmaline, carbonate and opaques. Small (<1mm), anhedral oligoclase, (determined by Michel Lévy method) feldspar crystals tend to be enclosed by large poikilitic microcline feldspars. The plagioclase is often considerably sericitised, though the alkali feldspar seldom exhibits signs of alteration. Quartz often has undulose extinction indicating minor post-crystallisation deformation. Minor, fine grained, ragged muscovite (not an alteration product after feldspar) is often associated with biotite. The mafic mica contains numerous tiny inclusions of zircon, which are surrounded by pleochroic haloes. This petrological data indicates that the intrusive is a true alkali granite.

A myrmekitic texture is well developed in the Otjua granite. A complicated intergrowth of quartz and plagioclase feldspar is developed in irregularly shaped projections of the latter mineral, only when in contact with microcline feldspar. These wart-like projections of the normally euhedral plagioclase appear to be replacing the alkali feldspar (see Photo 20).

2. Fine Grained Granite:

In outcrop the granite is light grey, fine grained and homogenous. In thin section an equigranular igneous texture is evident and the grain size only locally exceeds two millimetres. The major minerals present are: quartz (30-40%), orthoclase (30-40%) and plagioclase feldspar (15-25%) and the accessories comprise biotite (2-10%), muscovite (1-5%), apatite (1-2%), zircon (1-2%) and opaques (2-3%). Both the alkali and oligoclase feldspar (determined by Michel Lévy method) locally

contain quartz inclusions, while muscovite poikilitically envelopes quartz and apatite. The felsic minerals are present in a granular mosaic (<1.5mm) with randomly oriented coarser grained biotite.

A characteristic feature of this granite is the presence of a large number of randomly oriented needle-like crystals(see photo 21). They are especially well developed in quartz and to a lesser extent in the feldspars. Although up to 200μ long, the crystals are seldom more than a few microns thick. Some of the thickest examples have high relief, possess a slight greenish tinge in plane polarised light and straight extinction. The mineral is thought to be tourmaline.

3. Pegmatite:

Pegmatite comprises approximately half of all the lithologies present at the Otjua prospect (see Map 2). It is not possible to identify individual pegmatite bodies and the pegmatite can be more accurately described as a mass of apparently interconnected intrusive. A particularly prominent feature of the nature of pegmatite intrusion is the relative lack of disruption of the country rock. The strike of the majority of the pegmatite is conformable with that of the metasedimentary sequence and is only locally crosscutting, the transgressive portions of the pegmatite being consistently oriented 113°. This orientation is similar to that of crosscutting pegmatites developed at other skarn prospects on the Otjua Ridge suggesting that pegmatite intrusion was structurally controlled on a regional basis. However, there is no difference, mineralogically or chemically, between conformable and crosscutting portions of the pegmatite.

From drillcore it is apparent that contacts between the pegmatite and metasediments are very sharp and that contacts approximately parallel the schistosity of the countryrock (see Photo 22.) No chilled margin is present in the pegmatite, nor have the metasediments been baked. Only occasionally have metasedimentary xenoliths been incorporated into the intrusive. A biotite selvage on the schist-pegmatite contact is only locally developed.

All these points indicate that, firstly there was only a small temperature difference between the metasediments and the pegmatite magma at the time of intrusion and, secondly, that the pegmatite intruded in an relatively passive manner. In several instances, both on surface and in drillcore, skarn fragments can be seen within pegmatite, indicating that the intrusion of pegmatite postdates skarnification of the Rössing Formation marble.

A prominent textural feature of the pegmatite is a banding (not a foliation) parallel to lithological contacts. On outcrop scale, banding of tourmaline and biotite-rich zones is common, while banding may also be caused by alternating very coarse and very fine grained mineral assemblages (see Photo 23). In hand specimen the pegmatite is pink or white in colour and often exhibits a coarse grained micrographic quartz-feldspar (see Photo 24) or quartz-tourmaline intergrowth. The grain size varies from medium (2mm) to very coarse grained (15cm). Stumpy, black, prismatic schorl is ubiquitous, while pink-red euhedral garnet and biotite books are common. Muscovite is very rare. The pegmatites are very fresh (feldspar alteration is extremely minor) and essentially unmineralised-scheelite in pegmatite has been recorded very rarely in drillcore. In thin section pegmatite has an igneous texture and comprises the following minerals: microcline (20-60%), quartz (20-50%), plagioclase (20-40%), biotite (0-5%), garnet (0-10%), tourmaline (0-10%), muscovite (0-2%), chlorite (0-2%), zircon (0-1%), opaques (0-1%), clay minerals (0-2%) and carbonate (0-1%).

The plagioclase feldspar is oligoclase (determined by Michel Lévy method) and is mainly present as small crystals (<1mm) enclosed by microcline. Plagioclase that appears to have crystallised at the same time as the microcline tends to be coarser grained, but no compositional difference between the early and late plagioclase was noted. Subhedral to anhedral microcline tends to envelop all other phases. Quartz exhibits strained extinction. Although usually prismatic, tourmaline may be very ragged and exhibits a blue-brown-violet pleochroism. Garnet is universally euhedral and contains rings of inclusions, notably quartz, but also tourmaline. Muscovite is anhedral and usually very fine grained. Chlorite is an alteration

product after biotite or garnet, but tends to be very minor in content. Alteration of the feldspars is confined to minor sericitisation of the small plagioclase inclusions within the microcline.

The pegmatite exhibits two prominent textural features. Firstly, micrographic intergrowth of quartz and microcline is ubiquitous (see photo 24).The quartz "blobs" that are prominent in thin section are invariably in optical continuity. Similarly, the microcline feldspar crystals that form the intergrowth are often very large (many centimetres in size). This granophyric intergrowth is interpreted as being the result of the simultaneous crystallisation of quartz and K-feldspar at the eutectic temperature. The second prominent texture in the pegmatite is a myrmekitic intergrowth. As with the Otjua granite, a wormlike intergrowth of plagioclase feldspar and quartz is developed where projections of plagioclase extend into, and appear to replace, the alkali feldspar.

4. Karoo Dykes:

Minor dolerite dykes have disrupted the metasediments and intrusives at the Otjua prospect (see Map 2). Although poorly exposed, the two sets appear to be sub-vertical, though from drillcore it is apparent that they are locally conformable with the schistosity of the metasediments. Chilled margins of the dolerite and baked country rock attest to their post-Damaran age, i.e. they are most likely to be of Karoo age. The dykes vary in thickness from 0.5 to 10 metres and are traceable on surface for distances of up to 120 metres.

In hand specimen they are dark green, weathering to an olive brown colour. Outcrops are indistinct and exposures are usually marked by round weathered boulders and pebbles. The dolerite is very fine grained and in thin section comprises an equigranular mass of clinopyroxene and plagioclase feldspar. Several vessicles (up to 5mm in diameter) are filled with zeolites and crosscutting fractures filled with calcite and haematite are not uncommon. Irregular patches of chlorite alteration are widespread. Up to 5% opaques are present:

much of this is probably magnetite since the dolerite is highly magnetic.

4e Economic Geology

i) Sampling and Geochemical Analysis During Exploration:

During the exploration of the Otjua prospect routine analysis for Cu, Mo, WO_3, and F concentrations in the skarn, scheelite-bearing hornfels and other lithologies was conducted by a commercial laboratory, Scientific Services of Cape Town, RSA. Copper was determined by atomic absorption (LLD = 10ppm) and fluorine by specific ion electrode (LLD = 500ppm). Molybdenum and tungsten (LLD = 20ppm and 30ppm respectively) were both analysed for by XRF (10% wax pellet), but those samples containing in excess of 0.3% WO_3 were reanalysed by a fusion method. Tungsten concentrations are expressed as WO_3, not W, since this is standard practice in the mining industry when referring to tungsten ore. Fluorine concentrations in the skarn are expressed as wt.% fluorite since the element F is almost entirely present in this mineral. Analysis of many hundreds of scheelite-bearing rocks (both skarn and hornfels) revealed up to 312ppm molybdenum, but in the vast majority of samples analysed, the Mo concentration was below the detection limit. Therefore, the powellite component of the scheelite both in the skarn and the scheelite-bearing hornfels can be considered to be negligible. Similarly, copper contents of skarn and scheelite-bearing hornfels are of no economic interest.

Due to the possible complications caused by weathering and leaching effects, which incidentally seem to be minimal, only analyses from diamond core samples were used in the following study. The analyses quoted below are from 15-50 centimetre long lengths of core that were sampled on the basis of mineralogy and response under U.V. light during the exploration programme.

ii) Scheelite distribution in the various facies of skarn hosted by the Rössing Formation:

A particularly striking feature of scheelite distribution within skarn at the Otjua prospect is the virtual restriction of economic mineralisation to the garnet facies. Minor scheelite mineralisation is present in idocrase facies skarn, but is extremely uncommon in the pyroxene facies: WO_3 contents seldom exceed 200ppm in the latter. The style of scheelite mineralisation in the garnet and idocrase facies is similar: fine to medium grained and evenly distributed (except for a concentration of scheelite in the core of the garnet facies).

The low concentration of tungsten in idocrase facies skarn is evident from Fig. 11. 75% of the samples have WO_3 contents of less than 0.2 wt.% WO_3 with only one sample in twenty containing more than 2% WO_3 (see Fig. 12). The considerably higher tungsten content and almost lognormal distribution of tungsten in the garnet facies is evident from Fig. 13. The previously discussed zoning of garnet facies skarn across its width, with scheelite-poor peripheral zones and a scheelite-rich core (see Fig. 10), results in the WO_3 concentration of peripheral garnet facies skarn rarely exceeding 0.8 wt.% WO_3. Samples with WO_3 contents in excess of 0.8 wt.% WO_3 are almost exclusively confined to the garnet + scapolite dominated assemblages from the core of the skarn. 92% of all samples from garnet facies skarn have WO_3 contents of less than 1% WO_3 (see Fig. 14) indicating that in world-wide terms the skarn hosted by the Rössing Formation is relatively low grade.

iii) Fluorite distribution in the various facies of skarn hosted by the Rössing Formation:

Fluorite is noticeably concentrated in the garnet facies, while idocrase facies skarn hosts minor fluorite mineralisation and the pyroxene facies has none. Therefore fluorite distribution within the skarn system is similar to that of scheelite, but, as previously discussed, the former tends to be concentrated towards the structural hanging wall of the garnet facies skarn (see Fig. 10). The majority of idocrase facies samples have CaF_2 contents of less than 2% (see Fig. 15) while 95% of all samples contain less than 5% CaF_2 (see Fig. 16). The considerably higher concentrations of fluorite in garnet facies

skarn are evident from Fig. 17. The majority of samples containing in excess of 15% CaF_2 are from the (structural) hanging wall of the garnet facies skarn. The cumulative frequency diagram (see Fig. 18) emphasises the concentration of fluorite in the garnet facies; only 42% of all samples contain less than 5% CaF_2.

iv) Distribution of skarn and mineralisation within the Rössing Formation

1)Introduction:

The aim of this section is to discuss the inter-relationship between scheelite and fluorite distribution in the various facies of skarn, the thickness of the skarn, the original thickness of the Rössing Formation marble and the degree of replacement of the carbonate unit. For example, it would be of interest to know whether tungsten is concentrated in areas where fluorine contents are higher, whether tungsten and fluorine are concentrated in areas where the skarnification process has been more extensive or in those portions of the marble that have been structurally thickened. Exposure of the contacts between marble, skarn and the Khan and Oberwasser metasediments is poor, making direct measurements of parameters such as the skarn thickness and marble thickness difficult. Therefore the following investigation is based on information obtained from diamond drillhole intersections.

Definition of terms: At the Otjua prospect boreholes were drilled perpendicular to the strike of the metasediments (see Map 2), but at varying angles to the dip of the country rock (see Sect. 1). Therefore, borehole intersection of marble and skarn are apparent thicknesses dependent on the intersection angle, α , between the borehole and the inclined marble or skarn (see Fig. 19a). Table A lists the true thickness of the various facies of skarn hosted by the Rössing Formation intersected during drilling.

In Fig. 19b the Rössing Formation marble has been partially replaced by skarn. The combined true thickness of marble and skarn is therefore $\sin \alpha (a + b + c)$. The combined marble and skarn true

thicknesses for the borehole intersections are given in Table A. For the purpose of this investigation the process of skarn formation is assumed to have been a constant volume process. This is possibly an oversimplification and the validity of the argument is discussed in Chapter 8 but it would be interesting to know if the marble/skarn ratio shows any correlation with extent of mineralisation. Therefore the degree of replacement of the Rössing Formation marble is expressed as percentage skarnification. In Fig. 19b the percentage skarnification is:

$$\sin \alpha \frac{(a + c)}{(a + b + c)} \times 100$$

and the figures for the various boreholes are given in Table A.

The WO_3 and CaF_2 contents quoted for the borehole intersections in Table A are averages for the skarn intersections. During sampling of the drillcore unequal lengths of core were sampled on the basis of scheelite content and skarn mineralogy. Because of the differing specific gravities of the major skarn minerals, the unequal lengths of core have differing densities. Therefore corrections or "weighting" of the individual assay results have been made to arrive at average WO_3 and CaF_2 grades for the individual borehole intersections of skarn.

2)Longitudinal Descriptions:

The degree of skarnification of the Rössing Formation is shown in Long. Sect. 2. The incomplete metasomatic replacement of the carbonate is particularly apparent on the western side of the orebody where idocrase facies skarn is developed. The patchy nature of the replacement process, as shown by the large pods of unreplaced marble, is evident between the 16W and 29W faults, an area dominated by garnet facies skarn. East of the 16W fault, the pyroxene facies skarn, where developed, has completely replaced the marble. Of particular note is the fact that replacement of the Rössing Formation is most extensive nearest the major crosscutting pegmatites (see Long. Sect. 2 in conjunction with Map 2).

Long. Sect. 3 shows the distribution of WO_3 content within skarn hosted by the Rössing Formation. However, during percussion drilling

a considerable amount of scheelite was lost in drilling dust and therefore the concentrations of WO_3 quoted for the percussion drillholes are 20-30% lower than the in situ value. In spite of this, the diagram emphasises the fact that garnet facies skarn between the 16W and 27W faults comprises the bulk of the orebody; minor mineralisation is present west of the 29W fault, but the pyroxene facies skarn east of the 16W fault is barren. The skarn isopach (Long. Sect. 4) emphasises the thin development of idocrase facies skarn west of the 29W fault and indicates that the easterly pitching "shoot" between boreholes 27/35 and OT17 contains the bulk of the ore zone tonnage. This shoot roughly parallels the boudin structures in the calc-silicates 1 kilometre to the east of the prospect (see section on structure), but whether this is coincidental is not known. The combined marble and skarn isopach (Long. Sect. 5) indicates a similar shoot, suggesting that locally skarn formation is more extensive where the original carbonate was thicker. What is important is that this subtle trend, which is significant as far as planning of drilling is concerned, is not obvious from the statistical analyses (see subsequent section).

3)Relationship between mineralisation and skarn distribution in the garnet facies

The CaF_2 and WO_3 contents of the garnet facies skarn in sixteen borehole intersections are plotted in Fig. 20 and the correlation coefficient between CaF_2 and WO_3 concentration is +0.44. As discussed previously there is a tendency for garnet facies skarn to be zoned across its width and for there to be a generally antipathetic relationship between scheelite and fluorite distribution. However, Fig. 20 suggests that although concentrated in different portions of the skarn, scheelite and fluorite are possibly concentrated by similar processes.

CaF_2 and WO_3 concentrations of the garnet facies skarn are plotted versus skarn thickness in Fig. 21. Although there is considerable scatter, thicker skarn is generally associated with higher CaF_2 and WO_3 contents, the correlation coefficients being +0.41 and +0.55, respectively. Similarly, higher CaF_2 and WO_3 concentrations are

evident in portions of the skarn where the degree of replacement of the marble is higher (see Fig. 22). The correlation coefficients between CaF_2 and WO_3 contents and the percentage skarnification are +0.56 and +0.54 respectively. Both Figs. 21 and 22 strongly suggest that scheelite and fluorite formation was related to the skarn forming process and where this process was more extensive across strike higher concentrations of mineralisation resulted.

To test whether skarn is preferentially developed where the original Rössing Formation marble was notably thicker (or thinner), the combined marble and skarn thickness of the borehole intersections is plotted versus degree of skarnification. In Fig. 23 a wide scatter of points is evident and the correlation coefficient is +0.07. This lack of correlation on initial inspection is highly significant. However, if one examines the data from the previously mentioned easterly plunging shoot (between boreholes 27/35 and OT17) the correlation between the combined marble and skarn thickness and the degree of replacement of the carbonate unit for the five diamond drillholes (OT2, 3, 10, 16 and 17) and the three percussion drillholes (26/70, 27/35 and 27/60) is +0.76 and for the diamond drillholes alone is +0.98. This strongly suggests that within the seemingly disordered skarn development process, structurally (or sedimentologically?) thickened portions of the Rössing Formation <u>were</u> preferentially skarned and that skarn is best developed in linear shoots. Unfortunately the paucity of data points prevents a more detailed analysis.

Perhaps not surprisingly the correlation coefficients between combined marble and skarn thicknesses and WO_3 and CaF_2 contents of the skarn for all boreholes in garnet facies skarn are low: +0.31 and -0.03 respectively.

4)Conclusion:

It is apparent that, although chemical controls, intensity and type of skarnification played a dominant role in concentrating tungsten and fluorine and that both elements were concentrated by similar

processes, skarn-hosted tungsten ore as opposed to skarn-hosted tungsten mineralisation was probably localised by tectonic controls.

v) Fluorine and tungsten distribution in the metasediments of the Khan and Oberwasser Formations

1) Quartz-Biotite Schist:

Although specks of scheelite in schist have been detected with the aid of an U.V. lamp, routine analysis of this lithology during exploration indicates WO_3 concentrations to be below the LLD. However, fluorine contents of the schist are anomalous. No fluorite has been noted in hand specimen or thin section and the fluorine is presumed to be substituting for the hydroxyl ion in biotite. Twenty samples were selected from diamond drill core to investigate fluorine contents in the schist since surface samples of schist are severely weathered. Ten samples were selected from Otjua and ten from the Tjirundo prospect to investigate whether fluorine contents in the metasediments are particularly higher in the vicinity of significant skarn hosted scheelite-fluorite mineralisation as at Otjua relative to poorly mineralised skarn at Tjirund. The averages and standard deviations are as follows:

Prospect	Average F content (ppm)	One Standard Deviation
Otjua	2540	780
Tjirundo	2050	730

These data indicate that there is no significant enrichment of fluorine in the schist in the immediate vicinity of the Otjua prospect and suggests that the schist is regionally anomalous in fluorine. The significance of this is discussed more fully in Chapter 9.

2) Calc-silicate and Scheelite-bearing Hornfels:

Routine analysis by XRF of calc-silicate and hornfels has revealed that both lithologies contain highly anomalous concentrations of tungsten and fluorine. Concentrations of tungsten in the calc-

silicate seldom exceed 50ppm, while tungsten contents in the scheelite-bearing hornfels are frequently an order of magnitude higher, and up to 1.8 wt.% WO_3 has been recorded. One borehole, OT16, was chosen for a statistical study of the fifty scheelite-bearing hornfels intersected by drilling and compared with thirty-eight samples of hornfels from the Okakombo Horst (see Map 1) that were selected on the basis of U.V. response. The frequency distribution diagrams for the two sets of data are almost identical (see Figs. 24 and 25) and clearly show that, on average, tungsten contents in the hornfels are considerably lower than in the idocrase and garnet facies skarn (see Figs. 11 and 13). Fig. 26 shows the distribution of tungsten within all hornfels intersected by diamond drilling at the Otjua prospect that contain WO_3 concentrations in excess of 0.1 wt.%. This diagram emphasises that even those hornfels containing the highest concentrations of scheelite have tungsten contents considerably lower than garnet facies skarn (compare Fig. 26 with Fig. 13).

Fluorine contents of both the calc-silicate and hornfels are anomalous, though, apart from the presence of minor fluorite, it is not apparent as to exactly where the element is located. The concentrations of fluorite within the calc-silicate and hornfels are not of economic interest. The frequency distribution diagrams for fluorine hosted by scheelite-bearing hornfels at Otjua and within the Okakombo Horst show that fluorine contents at the former are considerably higher than in the latter area (see Figs. 27 and 28). Fluorine contents in both the calc-silicate and hornfels are an order of magnitude lower than those of the various skarn facies (compare Figs. 27 and 28 with Figs. 15 and 17). Unlike the various skarn facies there is a poor correlation between tungsten and fluorine concentration in the hornfels and, moreover, the WO_3/F ratio of the hornfels is distinctly different from that of the skarn:

	WO_3/F ratio
Okakombo: All scheelite-bearing hornfels	3.35
Okakombo: Scheelite-bearing hornfels with WO_3 concentrations in excess of 200ppm	6.89
Okakombo: Scheelite-bearing hornfels with WO_3 concentrations in excess of 1000ppm	13.82
Otjua: Scheelite-bearing hornfels from borehole OT16	.59
Otjua: Scheelite-bearing hornfels with WO_3 concentrations in excess of 1000ppm from borehole OT16	1.29
Otjua: All hornfels with WO_3 concentrations in excess of 1000ppm	1.16

These values are in marked contrast to the WO_3/F ratio of $\pm$0.1 for the idocrase and garnet facies skarns which suggests that either the mineralising fluids had markedly different composition in the skarn relative to the hornfels or that at least the mineralisation occurred under different physico-chemical conditions.

5. WHOLE ROCK GEOCHEMISTRY

a) Introduction:

One of the main aims of this investigation was to test the idea that the intrusives in the immediate vicinity of the Otjua prospect were responsible for skarn formation in the Rössing Formation and minor carbonate units of the Khan and Oberwasser Formations or, alternatively, whether skarn formation occurred as a result of a metamorphic reconcentration of elements from the enclosing metasediments into the marble horizons. Another main objective was to determine whether the fine grained scheelite mineralisation in the hornfels is related to the skarn-hosted scheelite or whether concentrations of tungsten existed in the metasediments prior to skarn formation. With these aims in mind a suite of granite, pegmatite, marble, skarn and scheelite-bearing hornfels samples were analysed for major and trace elements to provide data on their compositions. Samples of schist and calc-silicate were also analysed to help elucidate the sedimentary environment under which the precursors to these metamorphic rocks were formed. To gain an insight into the regional distribution of scheelite, scheelite-bearing calc-silicate rocks of the Khan and Oberwasser Formations from the core of two domal structures within the Okakombo Horst were also analysed (see Map 1). The Rössing Formation marble is traceable for forty kilometres within the core of these two domes, but is unskarned. No granites, nor pegmatites are developed within the core of these domal structures. Prospecting has confirmed the presence of widely distributed scheelite mineralisation within the calc-silicate rocks of the Khan and Oberwasser Formations in these domal structures suggesting that mineralisation in the calc-silicate rocks is unrelated to intrusive activity. A list of sample localities is given in Table 2 (see also Maps 1 and 2).

b) Biotite Schist:

The chemical composition of the biotite schist is given in Table 3-1. The two samples are similar in composition both containing higher alumina contents and lower SiO_2 concentrations than average shale and

are considerably less silicic than average greywackes (Pettijohn, 1975, pp.274 and 228). The high K_2O content of the schist indicates that the sedimentary precursor had a high argillaceous component and the significant carbonate component of the schist is reflected in the high CaO content. The ternary plot $CaO-Na_2O-K_2O$ (see Fig. 29) indicates that these three elements are present in similar proportions to average shale but are considerably different from average greywacke. Pettijohn (1975) has listed the following changes in chemical composition of a clastic sediment that occur with increasing maturity: an increase in the Al_2O_3 and K_2O contents as the clay component increases, while MgO, CaO and Na_2O concentrations tend to decrease. Concentrations of iron, silica and titanium are seemingly little affected by maturation processes. Thus, various inter oxide ratios can be used to assess the maturity of a sediment: for example, the average ratio $(Al_2O_3 + K_2O)/Na_2O$ for the biotite schist from Otjua is 10.85 which indicates a high degree of maturity. The ratio $(Al_2O_3 + Na_2O)/(MgO + CaO + Na_2O)$ is also suggested by Pettijohn to be a good maturity index, but due to the high carbonate component of the schist from Otjua this gives a misleadingly low value of 1.88.

One of the few published studies on sediment maturity in the Damaran has been completed by Miller et al. (1983). The authors conducted a geochemical traverse across the greywacke dominated Kuiseb Formation between Windhoek and Okahandja. Of particular interest is their discovery that pelites from the Vaalgras subgroup, which also contains lenses of marble and calcareous quartzite (indicating fluctuating chemical and detrital sedimentation) had similar proportions of CaO, Na_2O and K_2O as the schist of Otjua, both being quite distinct from the greywackes of the Kuiseb Formation (see Fig. 29). The average $(Al_2O_3 + K_2O)/Na_2O$ and $(Al_2O_3 + K_2O)/(MgO + CaO + Na_2O)$ ratios for the Vaalgras subgroup are very similar to those of the Otjua schist. The clastic component of the Vaalgras metasediments was considered to be the most mature of all Kuiseb sediments by Miller et al., (1983). Thus the schist from Otjua represents a metamorphosed highly mature argillaceous mud indicating a very low energy depositional environment. This is consistent with field observations which clearly indicate the fine intercalation and alternation of chemical and detrital sediments in the Khan and Oberwasser Formations.

c) Calc-Silicate and Scheelite-bearing Hornfels:

The chemical composition of samples of calc-silicate and scheelite-bearing hornfels are listed in Tables 3-1 and 3-2. There is considerable compositional variation of both lithologies, but the overall chemistry of the two lithotypes is remarkably similar. Biotite-rich varieties of calc-silicate are considerably more silicic and contain higher alkali contents than "purer" calc-silicate (sample OT118). However, concentrations of other elements are nearly identical. The ternary plot Al_2O_3-CaO-SiO_2 shows how differences in the mineralogy of the calc-silicate essentially result from variations in the CaO and SiO_2 contents and that mineral assemblages are dominated by quartz, scapolite and anorthite (see Fig. 30). The biotitic calc-silicate probably represents a calcareous quartzite with a minor argillaceous component, while the more calcic variety was probably a cleaner calcareous quartzite.

In the scheelite-bearing hornfels there is a strongly antipathetic relationship between SiO_2 and CaO content, those samples from the Okakombo Horst being considerably more silicic than those from the vicinity of Otjua. Fig. 30 clearly shows that there is little difference in the proportion of the elements Al_2O_3, CaO and SiO_2 in the hornfels and the calc-silicate and hence mineral assemblages are similar. The similarity in chemical composition of the two lithologies is further emphasised in the ternary plot Al_2O_3-FeO-MgO (see Fig. 31).

Tungsten concentrations in both the calc-silicate and scheelite-bearing hornfels are highly anomalous compared to average W contents of 1.8ppm in shales, 1.6ppm in sandstone and 0.6ppm in carbonate rocks (Turekian and Wedepohl, 1961). Concentrations of tungsten in the scheelite-bearing hornfels correlate positively with Al_2O_3,FeO, MnO, MgO, CaO and total alkali contents (see Table 4), but negatively with TiO_2 and SiO_2 indicating that scheelite is concentrated in the less silicic hornfels at Otjua. Fig. 32 shows how W contents of the hornfels increase with rising CaO content. Concentrations of fluorine in the calc-silicate and some of the hornfels are considerably in

excess of average contents of sedimentary rocks (average shale = 740ppm, average sandstone = 270ppm, average carbonate = 330ppm, from Turekian and Wedepohl, 1961).

The anomalous concentrations of tungsten and fluorine of the calc-silicate and hornfels are in contrast to those of the other trace elements whose contents are not unusual for sedimentary rocks. The behaviour of trace elements in sedimentary processes is not well understood due to the variety of competing processes, a point particularly relevant to a study of sediments of the Khan and Oberwasser Formations which possess sediments derived by chemical and detrital processes. However, a striking feature of the two lithologies is their almost identical trace element signature (see Fig. 33). This suggests that the two lithologies were derived by similar processes and that the hornfels represents an unusual type of metamorphosed marl.

d) Rössing Formation:

The highly calcitic nature of the Rössing Formation and its low proportion of impurities is evident from the compositions given in Table 3-3. The marble therefore represents a metamorphosed calcitic limestone with very small dolomite and siderite components. Chemical compositions of the various skarn facies are given in Table 3-5 and the average compositions are plotted in Figs. 34-38. The concentrations of elements within the skarn clearly indicate the large-scale introduction of material into the carbonate unit during metasomatism. The interpretation of the mechanism of skarn formation is discussed in detail in Chapter 8. Although the sampling of the various skarn facies at Otjua has not been very extensive when one considers the heterogenous nature of skarn deposits, the changes in major and minor element concentrations with progressive metasomatism of the Rössing Formation are systematic and can be accounted for by the presence or absence of certain minerals and by changes in mineral chemistry (see Chapter 6).

The decrease in total Ca content of the Rössing Formation with increasing metasomatism is matched by a corresponding increase in

SiO_2 concentration (see Fig. 34). This can be explained by an examination of the mineral assemblage in each facies: with progressive replacement of the carbonate unit the proportion of calcite in the mineral assemblages declines (idocrase facies: 5-40% calcite; garnet facies: 0-5% calcite; pyroxene: none) and less calcic silicates are developed. Where marble is replaced in the idocrase facies skarn, calcite is replaced by idocrase. Where replacement of the marble has been more extensive garnet, not idocrase, is present and where the carbonate unit has been entirely replaced, by pyroxene facies skarn, garnet is absent. However, the total Ca and SiO_2 contents of the idocrase and garnet facies skarn are similar suggesting that although metasomatism is usually more extensive across strike where garnet facies skarn is developed, the intensity of metasomatism in the garnet facies was not significantly different from the idocrase facies. This is an important point that will be discussed in detail in Chapter 8. The decrease in the LOI content of the marble with metasomatism is essentially a reflection of the loss of CO_2 resulting from calcite decomposition (see Fig. 34). However, since all facies of skarn contain considerable scapolite, the three facies have similar, but significant, LOI contents. The distribution of calcium between fluorite and other minerals is shown in Fig. 35.

The Rössing Formation marble contains very low concentrations of iron and aluminium (see Fig. 36), mainly present in pyroxene and plagioclase feldspar respectively. In the idocrase facies iron is a significant component of pyroxene and idocrase and with increasing replacement of the marble FeO concentrations rise to a maximum in the garnet facies. The inhomogeneity of the garnet facies is, however, evident from Table 3-5 which shows the large variation in Al_2O_3 content and the difficulties associated with sampling this facies. However, there is an overall trend towards higher aluminium contents with decreasing CaO content. Manganese is present in only one of the four marble samples analysed, but all skarn facies contain significant amounts of MnO (see Fig. 36), with the highest concentration in the garnet facies.

Magnesium concentrations are highest in the idocrase skarn, decline in the garnet facies and reach a minimum in the pyroxene facies. Titanium contents of the marble are very low while concentrations of TiO_2 in the various skarn facies follow MgO contents (see Fig. 37). The lack of Na_2O in the marble highlights the calcic nature of the plagioclase in the marble. Alkali contents of the idocrase and garnet facies skarns are similar, but increase dramatically in pyroxene facies skarn (see Fig. 38).

Trace element concentrations for the samples of Rössing Formation marble and skarns are listed in Tables 3-3 and 3-5 and average compositions are plotted in Fig. 39. Concentrations of trace elements within the Rössing Formation marble are similar to those of average carbonate (Turekian and Wedepohl, 1961) except for noticeably higher Sr and Mo and lower Zr and S contents (see Fig. 39). The absence of tungsten and fluorine in the marble indicates that the mineralisation in the Rössing Formation is related to skarn formation. The contrast in trace element signature of the marble and skarn clearly indicates that skarn formation involved the large scale introduction of elements (see Fig. 40). The distribution of trace elements within each skarn facies is systematic and can be divided into several groups:

1) Elements concentrated in the idocrase facies: Co, Cr, V, Ni, Zn, Y, Zr
2) Elements concentrated in the garnet facies: W, F, Mo
3) Elements concentrated in the pyroxene facies: Ba, Rb, Pb, Cu
4) Elements not concentrated in any particular facies, but present in amounts significantly above contents of the marble: Nb, Th, U, Sc
5) Elements depleted in the skarn facies relative to the Rössing Formation marble: Sr, S

1) Co, Cr, V, Ni, Zn, Zr, Y

The remarkably coherent behaviour of the elements Co, Cr, V, Ni, Zn, Zr, and Y in the three skarn facies is clearly evident from Fig. 41. Due to their similar ionic radii and electronegativities Co, Cr, V, Ni and Zn are concentrated in ferromagnesium minerals and particularly

in the first ferromagnesium minerals to form from a crystallising magma. The reason for this concentration in initial minerals is that the elements Ni, Co and Zn in particular have smaller ionic radii than the Mg^{2+} ion and are camouflaged in the magnesium-rich end members of a solid solution series. Magnesium concentrations for the various skarns are highest in the idocrase facies (see Table 3-5). Apart from pyroxene, idocrase can accommodate significant concentrations of Zn, Cu and Ni which are camouflaged by Mg^{2+} and Fe^{2+}, while the trivalent ions V^{3+} and Cr^{3+} will tend to substitute for Fe^{3+} within the idocrase structure (Deer et al., 1966; Hochella et al., 1982). The anomalous contents of yttrium in the idocrase facies are almost certainly accommodated within apatite or sphene, where Y can substitute for Ca (Goldschmidt, 1958). Idocrase skarn is the only facies to contain significant sphene. The coherence of these trace elements is of note because it suggests that an igneous or pseudo-igneous system was in operation.

2) W, F, Mo

The distribution of tungsten and fluorine within the individual skarn facies has already been discussed (see Section 4e). Mo concentrations broadly follow those of tungsten indicating coherent behaviour of the two elements, though the powellite component of the scheelite is clearly negligible.

3) Ba, Rb, Pb, Cu

The geochemical coherence of Ba, Rb and K is well known and can be attributed to their similar ionic radii and electronegativities. Fig. 42 shows that while concentrations of Rb rise steadily with increasing metasomatism, Ba contents of the skarn facies essentially mirror those of K (see Table 3-5). Due to the large ionic radius of the Pb^{2+} ion, lead is also a relatively incompatible element being diadochic with K^{+} and often concentrated in potassium rich minerals (Mason and Moore, 1982). Copper was only detected in one of the samples from the garnet and idocrase facies and the very low concentrations in the pyroxene facies are evident from Table 3-5.

4) Th, U, Nb, Sc

Although sporadically anomalous contents of Th and U are present in the various skarn facies no particular trends in their distribution, for example, in the Th/U ratio are evident. Niobium is evenly distributed throughout the skarn system. However, the presence of these three elements, which exhibit strongly lithophilic behaviour, within a replacement body suggests an acid igneous source for the skarn-forming fluid.

5) S, Sr

The extremely low concentrations of sulphur in the various skarn facies at Otjua are evident from Table 3-5 in contrast to other skarns worldwide. Sulphur concentrations in the marble are considerably higher than in the skarn suggesting volatilisation of pyrrhotite during skarn formation. The similar geochemical behaviour of Ca and Sr is well known and the anomalous concentrations of Sr in the marble result from substitution of Sr for Ca in the calcite lattice. The significant decrease in the Sr concentration of the skarn relative to the marble indicates removal of Sr and suggests that skarn formation did not occur within a closed system. The surprisingly constant concentration of Sr throughout the skarn system is evident from Fig. 42.

e) Calc-silicate, Scheelite-bearing Hornfels and Skarn : a Geochemical Comparison:

The aim of this section is to investigate the geochemical similarities and contrasts between the various skarn facies hosted by the Rössing Formation and the scheelite-bearing hornfels and calc-silicates of the Khan and Oberwasser Formations. In the preceding sections it was shown that the metasomatic replacement of the Rössing Formation marble has involved the removal of some elements and the addition of others, and that metasomatism of the carbonate has occurred in a very systematic manner. Therefore the specific question that this section aims to answer is whether the scheelite-bearing hornfels could also be a type of replacement body formed by metasomatism of calc-silicate and

hence whether mineralisation in the hornfels is not perhaps related to skarn formation and skarn-hosted mineralisation.

In all figures in this section total iron is expressed as FeO, since the majority of iron in all rock types under discussion (except idocrase and garnet facies skarn) is in the Fe^{2+} state, mainly in pyroxene. Because calcium is expressed as both CaF_2 and CaO in the idocrase and garnet skarns, for the purposes of this discussion the proportion of calcium in each has been calculated and added together to give "total Ca" concentrations. Concentrations of the various elements are plotted in Figs. 43-47. All curves in Figs. 43-47 have been fitted using the linear regression programme ΣLIN of Hewlett Packard (HP41C, STATISTICS APPLICATION PAC). The regression coefficients and curve equations for Figs. 43-47 are listed in Table 5. Although the validity of calculating regression lines on the basis of three samples of the calc-silicate lithology is perhaps questionable, the curves are shown for completeness.

The similarity in calcium and silica concentrations of the scheelite-bearing hornfels and the calc-silicates is evident from Fig. 43. The considerably higher SiO_2 and the lower total Ca contents of these two lithologies relative to the idocrase and garnet facies skarn can be explained by the presence of significant amounts of quartz and relatively minor carbonate in the hornfels and calc-silicates compared to the higher percentage of Ca-rich minerals in the skarn where quartz is absent. Concentrations of SiO_2 in pyroxene facies skarn are similar to those of the less silicic scheelite-bearing hornfels emphasising the overall similarity in mineralogy between the two rock types. However, the mizzonitic composition of scapolite in the pyroxene facies accounts for the lower total Ca contents relative to the hornfels (see Chapter 6). The relatively low scatter of skarn analyses about the regression line highlights the fact that the metasomatic process involves the systematic replacement of the carbonate by a silica-rich fluid, though the large garnet facies field indicates some of the problems associated with sampling this facies of skarn.

MgO contents of the scheelite-bearing hornfels and calc-silicates are similar (see Fig. 44). Because magnesium in the scheelite-bearing hornfels is only present in pyroxene and because this mineral is preferentially developed in the less silicic hornfels, the regression line for MgO versus total Ca concentration in the hornfels is positive, though there is considerable scatter of individual analyses about the curve. In contrast, the considerably lower MgO contents of the various skarn facies is evident from Fig. 44 with noticeably higher concentrations of magnesium in the idocrase facies.

The overall similarity in major element concentrations of the hornfels, calc-silicate and pyroxene facies skarn is evident from Fig. 45. Manganese, iron and magnesium behave coherently in these three lithologies, being essentially concentrated in pyroxene. Due to the concentration of this mineral in the more calcareous portions of the hornfels, the regression line for combined FeO + MnO + MgO versus total Ca concentration is steeply positive for this lithology. The calc-silicates plot considerably off the hornfels regression line and the lower contents of FeO, MnO and MgO in the calc-silicates are reflected in the smaller amounts of pyroxene and greater proportion of feldspar in this lithology. In contrast the relationship between combined FeO, MnO and MgO and total Ca contents in the idocrase and garnet facies skarn is more complex - a reflection of the more diverse distribution of these elements in minerals other than pyroxene and the presence of mineral zoning e.g. in garnet (see Chapter 6).

The total Ca contents of the various lithologies are plotted versus TiO_2 concentration in Fig. 46. The presence of significant sphene in the calc-silicates and hornfels accounts for the high concentrations of titanium in these two lithologies and their low total Ca content separates them from idocrase facies skarn, which, in turn, also contains significant sphene and titanium-bearing idocrase (see Chapter 6). Very low TiO_2 concentrations and different total Ca contents separate the garnet and pyroxene facies skarn from each other and other lithologies.

Total alkalis are plotted versus total Ca concentrations in Fig. 47. The scheelite-bearing hornfels cluster tightly around the regression

curve which has a shallow positive slope. Alkalis are confined to scapolite and plagioclase in this lithology and these two minerals are more extensively developed in the more calcareous, i.e. less siliceous, portions of the hornfels. The presence of biotite explains the high potassium contents in the two biotitic calc-silicates and the increased Na_2O concentrations result in (probably) more sodic plagioclase. Thus the negative slope of the regression line for the calc-silicates in Fig. 47 results from an increase in the proportion of detrital minerals, e.g. muds and clays in the biotitic calc-silicate precursor relative to the more calcareous marl where chemical processes predominated. Alkalis in the skarns are almost entirely present in scapolite and hence changes in total alkali content are reflected in the scapolite chemistry - unlike the scheelite-bearing hornfels where scapolite composition does not change (see Chapter 6). Total alkali contents for the individual idocrase and garnet facies skarn analyses do not vary significantly, in fact the average for each facies is the same. Due to the presence of significant alkali concentrations in the pyroxene facies, the regression line for combined alkalis versus total Ca content in the skarns has a negative slope.

Conclusion: The chemical composition of the scheelite-bearing hornfels is in many aspects indistinguishable from the calc-silicate strongly suggesting that the two lithologies were derived by the same process. A sedimentary origin for both rocks types is indicated. Scheelite-bearing hornfels has a chemical composition clearly distinct from the two skarn facies that host scheelite mineralisation. Indeed, the only unusual feature of the hornfels is the possession of anomalous tungsten and fluorine contents. It is therefore concluded that the scheelite-bearing hornfels is not a type of replacement body and that mineralisation in the hornfels is unrelated to skarnification of the Rössing Formation and skarn – hosted mineralisation. Moreover, mineralisation in the hornfels is not spatially associated with late stage granite or pegmatite activity and a syn-sedimentary (or at least pre-peak metamorphism) origin for the scheelite within the hornfels is indicated.

f) Intrusives:

i) Otjua and fine grained granite

1. Chemical composition:

The chemical composition of samples from the Otjua granite and the fine grained granite are listed in Table 3-6 and compared with the composition of average granite compiled by Taylor (1968) and average low-calcium granite (Turekian and Wedepohl, 1961; see Table 3-7). Although the number of samples analysed is small a few general comments can be made. The chemical composition of the Otjua granite is very uniform and almost identical to the fine grained variety and, in the light of previously discussed relationships to pegmatites and structure, the two types may well be cogenetic. The granites from the vicinity of the Otjua prospect have chemical compositions midway between average granite and average low-calcium granite except for higher K_2O and lower Na_2O contents. The average Otjua granite possesses the following distinguishing characteristics:

1) a high SiO_2 content with a restricted range : 71.66-73.44%
2) a high K_2O content : Average = 5.78%
3) a very high K_2O/Na_2O ratio : Average = 2.3
4) a high Rb content : Average = 340ppm
5) a high Rb/Sr ratio : Average = 4.66

A plot of K_2O versus Na_2O for the five granite samples is shown in Fig. 48. The points lie unequivocably in the granite field in good agreement with petrological studies which indicated that both the Otjua granite and the fine grained granite are true alkali granites. The evolved nature of the granite is also evident from the two binary plots, Ba versus Rb (Fig. 49) and Sr versus Rb (Fig. 50). Both the Otjua granite and the fine grained variety have higher tungsten contents than specialised granites (W content of specialised granites is 7ppm W; Tischendorf, 1977), though in the sample of the Otjua granite taken furthest away from the Otjua prospect tungsten was not detected. Similarly, fluorine was only detected in those samples of the Otjua granite from closest to the Otjua prospect, albeit in

surprisingly low concentrations (F content of specialised granites is 3,180ppm; Tischendorf, 1977). Although more detailed sampling would be required to prove that volatiles are concentrated in portions of the granite closest to the Otjua prospect, the observation that the quartz-tourmaline nests are particularly concentrated at sample point OT112 (see Map 1) suggests that this is so. A point of particular note is the lack of Mo in the Otjua granite.

2. Classification of the Otjua and fine grained granites:

A number of classification schemes for granites have been devised by various authors. Chappell and White (1974) distinguished between two granite series in Australia, those thought to have been derived from anatexis of sedimentary units (S-type granite) and those originating from igneous source materials (I-type granite). S-type granites exhibit the following characteristics: restricted range of SiO_2 contents (66-75%), high K_2O/Na_2O ratios, high $Al_2O_3/(K_2O + Na_2O + \frac{1}{2}CaO)$ ratios and are enriched in Rb relative to Sr. The granites from Otjua satisfy all of these four criteria. Beckinsale (1979) suggests that the Na_2O content of a granite should be less than 3.2% for granites with approximately 5% K_2O for it to be classified as S-type. The granites from the vicinity of the Otjua prospect also satisfy this condition.

Classification of granites on mineralogical grounds by Hine et al. (1978) indicate that I-type granites generally contain hornblende, while S-type intrusives may contain cordierite and/or muscovite and/or garnet as well as biotite. Both the Otjua granite and the fine grained variety contain biotite and very minor muscovite, while garnet is sporadically developed at sample locality OT128 and therefore all the granites can be considered to be S-type under this classification scheme as well.

Much use has been made in the literature of the elements Rb, Ba and Sr as indicators of magmatic fractionation, alteration and accompanying mineralisation (Nockolds and Allen, 1953; Taylor, 1964; Exley, 1957; McCarthy and Hasty, 1976; Plimer and Elliot, 1979). During late magmatic differentiation Rb is concentrated in residual melts while

both Ba and Sr tend to be depleted since they have been removed by feldspar crystallisation. The high Rb, low K/Rb ratio and relatively low Ba contents of the granites surrounding the Otjua prospect indicate that they are fractionated granites. A ternary plot of Rb-Ba-Sr (see Fig. 51) after El Bouseily and El Sokkary (1975) indicates that the Otjua granites plot in or on the edge of the field marked "strongly differentiated granites".

However, when compared to highly fractionated granites associated with cassiterite mineralisation in Nigeria (Imeokparia, 1981) and Queensland, Australia (Sheraton and Black, 1973) the K/Rb value of the Otjua granite is relatively high. Similarly, although the Rb/Sr ratio for the Otjua granites is higher than that of average granite, when compared to greisenised granite associated with W-Mo-Bi mineralisation at Wolfram Camp (Plimer and Elliot, 1979) where fresh or slightly altered granite has an average Rb/Sr ratio of 17, the Rb/Sr ratio from Otjua is not particularly anomalous. Likewise, the Ca/Sr and Ba/Rb ratios of the Otjua granite are not particularly unusual when compared to late stage granites associated with mineralisation elsewhere in the world. Highly fractionated granites associated with cassiterite-wolframite deposits would plot in the Rb apex of Fig. 51. The fundamental difference between the Otjua granites and granites that host cassiterite-wolframite mineralisation is that the latter universally show extensive alteration and greisenisation as well as high muscovite and water contents and mineralisation within the intrusive. These features are absent from the Otjua granite, which can be classified as a highly fractionated, anhydrous, S-type alkali granite. This is consistent with other studies which indicate that the late Damaran (530-460 Ma) is particularly dominated by S-type granites (Miller, 1983a).

3. Comparison between the Otjua granite and other Damaran granitoids:

One of the main problems encountered when comparing granite geochemistry in the northern Central Zone of the Damaran is the paucity of data, especially in the Omaruru area. In his investigation into uranium genesis in the Damaran, Marlow (1981) has compiled some

of the data available for the Damaran granitoids, while Winkler (1983) has conducted a more extensive survey of Damaran granitoid geochemistry, but he does not quote trace element analyses. The geochemical data from the Otjua intrusives has been plotted onto diagrams modified from the first author's work.

The plot ln $CaO/(Na_2O + K_2O)$ versus SiO_2 can be used to distinguish between calc-alkaline and alkaline granitoid series (Brown, 1979). Both the fine grained granite and the Otjua granite plot with the leucogranites in the area between granites and pegmatites (see Fig. 52). Moreover, the leucogranites possess $(^{87}Sr/^{86}Sr)_I$ values in excess of 0.710 suggesting that they have a crustal origin. The acidic nature of both types of granite from the vicinity of the Otjua prospect is highlighted in Figs. 53 and 54. The positive correlation between K_2O and Rb for Damaran granitoids is shown in Fig.55 which also indicates the relative enrichment of these two elements and, more importantly, the low K/Rb ratio for the granites from Otjua. Fig. 52, in particular, emphasises the point that granites from the vicinity of the Otjua prospect have considerable affinity with Damaran leucogranites and alaskites and, that in the Damaran context, can be regarded as highly fractionated granites.

4. Petrogenesis of the Otjua granite

The ratio $(^{87}Sr/^{86}Sr)_I$ has particular application to problems concerning the origins of granites since I-type granites tend to have low $(^{87}Sr/^{86}Sr)_I$ ratios (usually less than 0.708) while S-type granites derived from anatexis of sedimentary or metasedimentary precursors have values exceeding 0.708. Miller (1983a) has suggested a lower limit of 0.711 for the initial $^{87}Sr/^{86}Sr$ ratio of S-type Damaran granites. Therefore the $(^{87}Sr/^{87}Sr)_I$ of 0.7196 for the Otjua granite (Haack et al., 1983) is highly anomalous and strongly suggests that the Otjua granite is derived from upper crustal source rocks. Although there is some dispute as to the significance of high initial Sr-isotope ratios (Simpson et al., 1979; Plant et al., 1980) it seems unlikely that the high $(^{87}Sr/^{86}Sr)_I$ value of the Otjua granite can be attributed to re-equilibration of the Sr-isotope system during extensive high temperature meteoric water-magma

interaction because of the lack of alteration within the Otjua granite. Of all the felsic intrusives analysed in the central Damaran to date only red granites associated with uranium mineralisation, uraniferous alaskites, pegmatites and some leucogranites possess $(^{87}Sr/^{86}Sr)_I$ values in excess of the Otjua granite (see Haack et al., 1983; Marlow, 1981).

The Otjua granite has an unusually high $\delta^{18}O$ value, the highest of all intrusives and sediments analysed in the central Damaran to date (Haack et al., 1983). On the basis of oxygen isotope composition granitic rocks have been subdivided into three main groups (Taylor, 1977): normal granitic rocks with $\delta^{18}O$ values between +6‰ and +10‰ high $\delta^{16}O$ granitic rocks with $\delta^{18}O$ values in excess of +10‰ and granitic rocks with $\delta^{16}O$ values less than 6‰ .

Granitoids with $\delta^{18}O$ values in excess of +10‰ tend to be S-type (O'Neil and Chappell, 1977) since the fractionation of oxygen in metamorphic rocks and sediments is more extensive than in the precursors of I-type magmas. It can therefore be inferred that the source rock for the Otjua granite had a high component of sedimentary material. Indeed, Haack et al. (1983) suggest that the positive trend of $^{87}Sr/^{86}Sr$ versus $\delta^{18}O$ of the younger isotopically heavy granites from the northern Central Zone is best explained by a source material that included "alternating layers of arkoses and metavolcanics" (op. cit. p.865). One point of particular note discovered by Haack et al. (1983) during their regional investigation is that oxygen isotopic fractionations between minerals in the granites were normal, "especially no quartz-feldspar reversals were noted", indicating very little secondary interaction between meteoric water and felsic intrusives in the Damaran.

The late tectonic age of the Otjua granite is regarded as highly significant. The geochemical and isotopic data clearly indicate that the intrusive is a residual melt enriched in incompatible elements formed during the final phases of Damaran granite intrusion. It is suggested that the Otjua granite was derived from the products of the widespread anatexis of metasediments that accompanied the Damaran orogeny.

ii) Pegmatite

The pegmatite was analysed for two principal reasons: firstly, to determine whether it could be a source of tungsten mineralisation and secondly, to test whether the pegmatite is related to the granite bodies in the vicinity of the prospect or whether pegmatite has been derived by metamorphism of the metasediments. The chemical composition of four pegmatite samples from the Otjua prospect is listed in Table 3-8. Because of the concentration of incompatible elements within pegmatites, considerable chemical inhomogeneity in this rock type is common and it is therefore somewhat surprising to note that the four samples from Otjua have very similar chemical compositions. The pegmatite contains higher SiO_2,Al_2O_3 and total alkali contents than the granites in the vicinity of the Otjua prospect with correspondingly lower ferromagnesium and calcium concentrations. The more evolved nature of the pegmatite relative to the granites is well illustrated on the AFM plot (see Fig. 56). However, the K_2O/Na_2O ratio of the pegmatite is lower than that of the granite (see Fig. 48) with the result that the former can be classified as an adamellite.

A comparison of the trace element compositions of the granite and pegmatite was conducted to test for a genetic link between the two lithologies. Ba and Sr contents of the pegmatite are considerably lower in the pegmatite than in the granites. As a result the various interelement ratios Rb/Sr, Ba/Rb, K/Rb and Ca/Sr, which are all commonly used fractionation factors, clearly indicate the more highly evolved nature of the pegmatite (see Table 3-8 and Figs. 49 and 50). Niobium's incompatibility and subsequent concentration in the liquid phase of a crystallising magma and concentration in highly fractionated pegmatite is very common throughout the Damaran. At Otjua Nb concentrations in the pegmatite are two and a half times those of the granites. The conclusion of Drake and Weill (1975) that trivalent REE and yttrium are depleted in crystallising plagioclase and concentrated in residual phases of a granite melt could explain enrichment of yttrium in the pegmatites of Otjua relative to the granites. The significant depletion of Zr as well as lower concentrations of Zn, Co, Cr, V and S in the pegmatite are also

indications that the pegmatites are fractionated derivatives of the granites in the vicinity.

The other most significant features of the pegmatite are its anhydrous nature (LOI = 0.34% compared to 0.62% in the Otjua granite), the lack of Mo, the very low concentrations of fluorine and the elevated tungsten content relative to the Otjua and fine grained granites. The importance of this is discussed more fully in Chapter 8, but suffice to say at this stage that the enrichment of tungsten, a highly incompatible element in an anhydrous granitic melt, within the pegmatite relative to the granite is deemed to be highly significant. Moreover, the development of skarn within the metasedimentary sequence, only where crosscutting pegmatite is developed suggests a genetic link between the two lithologies.

The igneous texture of the pegmatite, the very sharp pegmatite/country rock contacts, the widespread development of graphic intergrowth indicating eutectic crystallisation of quartz and feldspar, the similar mineralogy of the pegmatites at the prospect and those in the Otjua granite and the presence of extensive myrmekite in both types of intrusives all indicate that the pegmatites at the Otjua prospect are derived from the nearby granite. Moreover, the lack of contact metamorphic effects in the metasediments indicates that pegmatite intrusion was a late Damaran event and it is suggested that the most likely source of the magma is the Otjua granite. The highly acidic chemistry of the pegmatites and enrichment in the incompatible elements also strongly suggests that the pegmatites are fractionated derivatives of the Otjua granite. The mineralogical and textural banding of the pegmatite can be best explained as growth bands or crystallisation fronts that developed as the intruding magma crystallised. It is suggested that the schistosity in the metasediments represented the line of least resistance for an intruding magma resulting in intrusion of magma parallel to lithological contacts. This tendency for pegmatite dykes to be developed conformable with the strike of the country rock is common elsewhere in the central Damaran (Gevers and Frommurze, 1929). Therefore an intrusive origin for the pegmatite is preferred over models of pegmatite formation invoking alkali metasomatism of

metasediments, derivation by partial melting of metasediments or by metamorphic differentiation.

g) Conclusion

The salient features of this geochemical study are as follows:

i) The biotite schist represents a metamorphosed mature mud, the calc-silicate and sheelite-bearing hornfels types of marl and the marble is a metamorphosed calcitic limestone.

ii) Replacement of the marble has occurred in a systematic manner and there is evidence that the skarn formation process occurred within an open system. The trace element data in particular suggests an acid igneous source for the skarn-forming fluid.

iii) Scheelite mineralisation is hosted both by metasediments and found within replacement bodies within marble. The mineralisation in the calc-silicate and hornfels is thought to result from pre-metamorphic/syn-sedimentary concentrations of tungsten. The mineralisation in the replacement body is clearly related to the skarn formation process.

iv) The Otjua granite is a highly fractionated (in Damaran terms) anhydrous S-type granite. The fine grained granite and Otjua granite have similar chemistries and are presumed to be co-genetic, both having been derived from sedimentary precursors.

v) The pegmatite at the Otjua prospect prospect is unmineralised. The suggested source of the pegmatite is the Otjua granite.

6. MINERAL CHEMISTRY

a) Introduction:

It was decided that an investigation into the mineral chemistry of the three skarn facies would help elucidate the nature of the metasomatic process as well as possibly provide data for determination of the P/T conditions under which the skarn system developed. For example, several garnet-pyroxene geothermometers have been described in the literature (Finnerty and Boyd, 1984). Therefore, electron microprobe analyses of scapolite and pyroxene from the three skarn facies (and suspected transitional assemblages) as well as determinations of idocrase and garnet compositions were undertaken. Analyses of pyroxene and scapolite from the scheelite-bearing hornfels and calc-silicate were determined for comparison with those from the skarn. A list of all sample localities is given in Tables 6-1 and 6-2.

b) Skarn:

i) Minerals present in all three skarn facies:

1) Scapolite:

Scapolite compositions for the various skarn facies as well as for two intermediate assemblages (from boreholes OT14 and OT15) are given in Table 7-1. Scapolites form a solid solution series between the two end members chloride marialite, $Na_4(Al_3Si_9O_{24})Cl$, and carbonate meionite, $Ca_4(Al_6Si_6O_{24})CO_3$, the main substitution in the series being $K + Na + Si \rightleftharpoons Ca + Al$ (Deer *et al.*, 1966). Atomic proportions for the analyses in Table 7-1 have been calculated on the basis of Al + Si atoms = 12.0 following the methods of Evans *et al.* (1969) and meionite components (%Me) have been determined from the ratio (Ca + Mg + Fe + Mn + Ti)/(Ca + Na + K + Mg + Fe + Mn + Ti) as suggested by Deer *et al.* (1966).

In all three facies of skarn considerable compositional variations were noted both between scapolite grains within the same microprobe section and even within single grains. Although numerous analytical

traverses across scapolite grains were completed, no systematic variations from the core to rim of crystals were discovered. In the few examples where differences in chemical composition between the cores and edges of grains were noted, the scapolite grains possess a meionite-rich core (see analyses 14 and 15, Table 7-1). The compositional limits of scapolite recorded in the literature are between 17.4 and 87.3% of the meionite component (Deer et al., 1966) but some analyses from Otjua exceed this upper limit (see Table 7-1).

A substitution index, $(SiO_2 + Na_2O + K_2O)/(CaO + Al_2O_3)$ is plotted versus CaO content for all skarn scapolite analyses (see Fig. 57). The diagram illustrates several important points. Firstly, scapolites from the garnet facies tend to be the most calcic of all facies, although there is a considerable overlap in chemical composition with those from the idocrase facies. CaO contents of scapolites from the garnet facies range from 17.5 to 21.0wt%, compared to between 16.8 and 18.9wt% in the idocrase facies.

Secondly, scapolites from pyroxene facies skarn have a different composition from the other two facies, possessing higher alkali contents and CaO concentrations in the range 12.3-13.5wt%. The transitional nature of the OT14 borehole mineral assemblage (slide 24649) between garnet and pyroxene facies skarn is readily apparent from Fig. 57. The large compositional variations of scapolites within individual microprobe sections is exemplified by the analyses from slide 24649 where CaO contents of the scapolite vary between 12.9 and 22.1wt%. These large variations in scapolite chemistry either indicate disequilibrium at the time of scapolite formation or that the scapolite crystallised from a fluid of rapidly changing composition.

A most interesting discovery of the investigation into scapolite chemistry is the fact that variations in scapolite composition are closely related to scheelite distribution in both the idocrase and garnet facies. Scapolites from the idocrase facies that contain more than 18.5wt% CaO are associated with scheelite mineralisation (slide 24472), while those portions of idocrase skarn containing less calcic scapolites are essentially devoid of scheelite (slides 24475 and 24476). Similarly, scapolites from the garnet facies intimately

associated with tungsten mineralisation are considerably more meionitic than those from barren skarn. This noteworthy discovery is highlighted in Fig. 58 where the average CaO contents of all scapolites analysed from each thin section have been plotted against the WO_3 content of the particular 15-25cm length of core from which the thin section was cut. Scapolites with CaO concentrations in excess of 18.5wt% are associated with ore grade scheelite mineralisation regardless of facies.

This suggests that scheelite formation and scapolite chemistry, throughout the skarn system, were controlled by the availability of calcium ions. The occasional development of scapolite with Ca-rich cores and the textural evidence indicating early crystallisation of scheelite and scapolite suggests that $a_{Ca^{2+}}$ was greatest during the earliest stage of skarn formation (see discussion in Chapter 8).

One borehole, OT5, (see Map 2) was selected to test whether scapolite chemistry varies across the garnet facies in relation to tungsten distribution (see Fig.59 for mineralogical variations across borehole OT5 intersection). Scapolites from the scheelite-barren hanging wall (slides 24626 and 24627) have average CaO contents of 17.5wt% and 17.7wt% respectively, while those scapolites associated with scheelite mineralisation on the footwall side of the skarn (slides 24628 and 24630) possess average CaO concentrations of 20.3 and 19.9wt% (see Fig. 60). This implies that the activity of calcium ions during skarn formation was highest on the (structural) footwall side of the Rössing Formation.

2) Pyroxene:

Representative analyses of pyroxene from the various skarn facies are listed in Table 7-2, while a comprehensive summary of pyroxene composition within the skarn system is given in Fig. 61. None of the pyroxenes from any of the skarn facies exhibit systematic compositional zoning from rim to core although minor compositional variations within grains were recorded.

Pyroxenes from the idocrase facies are the most magnesium-rich of all skarn pyroxenes at Otjua, ranging in composition from 58.5mol%Hd to 67mol%Hd and from 6.2 to 9.3mol%Jo (see Fig. 61). Concentrations of manganese in pyroxene are highest in the garnet facies where compositions range from 71.3mol%Hd to 83.1molHd while the Jo content varies between 6.0mol% and 12.5mol% (see Fig. 61). Pyroxenes from the pyroxene facies are the most ferrous of all skarn pyroxene and range in composition from 80.8 to 88.1mol%Hd and from 3.2 to 4.6mol%Jo. Magnesium concentrations in pyroxenes from the garnet and pyroxene facies skarns are similar (see Fig. 61). Pyroxenes therefore exhibit considerable compositional variation within each facies but each facies possesses pyroxene of characteristic composition.

From Figs. 61 and 62 an evolutionary trend towards Fe enrichment with progressive replacement of the marble is apparent. The presence of pyroxene of intermediate composition in the transitional facies (boreholes OT14 and OT15) clearly demonstrates a genetic link between the facies. This tendency towards ferrous and manganese enriched pyroxene in the later stages of prograde growth of calcic tungsten-bearing skarn is very common worldwide (Einaudi et al., 1981)

Because of the mineralogical zoning across the width of the garnet facies (see Fig.10), it was decided to test for variations in pyroxene composition across the skarn. Two boreholes, OT5 and 17 (see Map 2), were selected for this study, skarnification of the Rössing Formation being complete in OT5 and incomplete in OT17 . Visual estimates of garnet and pyroxene percentages as well as WO_3 and fluorite distribution across the width of the skarn are given in Figs. 59 and 63. Note how the distribution of mineralisation and silicate minerals across the OT5 skarn intersection closely follow the observations discussed in Fig.10, while although the systematic zonation is not so well developed in the skarn intersection of borehole OT17, a garnet and scheelite-rich core zone is clearly identifiable.

Compositions of pyroxene from a traverse across the OT5 borehole skarn intersection are shown in Fig. 64. Pyroxenes from the hanging and footwall peripheral zones are magnesium-rich (76.4-79.5mol%Hd, 6.0-9.3mol%Jo) while those from the garnet and scheelite-rich core zone

(slides 24628 and 24629) on average have higher Hd and Jo components (79.5-83.0mol%Hd and6.5-11.0mol%Jo). However, although the core of the garnet facies skarn is obviously enriched in manganese and iron, the Mn/Fe ratio of the pyroxene is relatively constant across the skarn. In contrast, no such systematic variation in pyroxene composition was noted in the traverse across the OT17 skarn intersection (see Fig. 65). All pyroxenes, with the exception of those from sample 24637, comprise between 78.9 and 82.6mol%Hd and between 8.0 and 12.5mol%Jo. Pyroxenes from slide 24637 are anomalously rich in magnesium. The reason for the less systematic variation in pyroxene composition across the OT17 skarn is almost certainly related to the less systematic mineralogical zonation.

This study has served to highlight several mineralogical and chemical features of the skarn. On the deposit scale the skarn system has developed in a broadly systematic manner. However, on the local scale considerable chemical disequilibrium during skarn formation is indicated.

ii) Minerals specific to a particular facies:

1) Idocrase from idocrase facies skarn:

The ideal formula of idocrase has been reported by Deer et al. (1982) as $Ca_{19}(Al,Fe)_{10}(Mg,Fe)_3(Si_2O_7)_4(SiO_4)_{10}(O,OH,F)_{10}$, but there has been considerable dispute as to the exact structure of idocrase because of its complex and variable composition (see Deer et al., 1982 for discussion). In spite of the uncertainty over the true formula of idocrase, early investigators discovered that the structure of idocrase is very similar to that of grossular garnet (Warren and Modell, 1931). Partial analyses of idocrase from idocrase facies skarn are given in Table 7-3, cation proportions having been calculated on the basis of 78 oxygens.

No systematic variations in chemistry were noted between the cores and rims of idocrase grains, although it must be emphasised that, due to the very large size of the crystals, considerably more analytical work is necessary to prove or disprove the presence of zonation. The

concentric colour rings developed around the z-axis of idocrase prisms suggest that trace elements, at least, are unevenly distributed within the mineral. Idocrase composition is surprisingly uniform throughout the idocrase facies at Otjua, no major differences being noted between idocrase from the three borehole intersections (see Table 7-3). This homogeneity is unexpected when it is considered that the volatile fraction was not analysed and there is, therefore, some uncertainty as to the precision of the data. Certain unaccountable chemical inhomogeneities do exist, for example, in both slides 24625 and 24472, while concentrations of CaO, FeO, MgO and MnO are remarkably constant, local sharp increases in TiO_2 content with a corresponding decline in Al_2O_3 concentration and vice versa were noted.

TiO_2 contents in the idocrase are normally in the range 0.9-1.2wt% (see Table 7-3) although locally may vary from 0.2-1.8wt%, while Al_2O_3 contents may be as low as 15.1wt%. MnO contents of the Otjua idocrase (0.58-0.71wt%), while not highly unusual, are above average concentrations for idocrase (see Deer et al., 1982) and the low MgO contents (1.1-1.7wt%) mean that the idocrase from Otjua can be classified as magnesium-poor. It is probable that F is substituting for OH in the anion position.

Although there is uncertainty as to the true distribution of elements within idocrase, the ternary plot Fe-Mg-(Al + Ti) has been used by several authors to summarise idocrase chemistry. For example, Newberry (1982) used a Fe-Mg-(Al + Ti) plot to distinguish between iron-rich idocrase developed in metasomatic tungsten skarn at the Pine Creek mine and iron-poor idocrase derived during metamorphism of calc-silicate marble in the metasediments that enclose the skarn at Pine Creek. The data from Otjua and the two compositional fields of Newberry (1982) are plotted in Fig.66, the idocrase from Otjua falling squarely in the "metasomatic" idocrase field.

2) Garnet from garnet facies skarn:

Representative analyses of garnet from the Otjua skarn are listed in Table 7-4 and can be broadly classified as grossular garnets. Atomic proportions and mole percentages of end members for the garnets from

Otjua were calculated on the basis of 12 oxygens following the methods of Shimazaki (1977). Since Fe^{2+}/Fe^{3+} ratios of the garnet were not determined, a proportion of iron is assumed to be in the ferrous state and therefore some Fe is subtracted from the total Fe content so that atomic $Al + Fe^{3+} = 2.00$. The trivalent site is essentially occupied by Al and minor Fe, the divalent sites by Ca, Mn and Fe.

Unlike the other silicate minerals developed in the Otjua skarn, garnet occurs as anhedral grains or intergrown, anastomosing masses, making it almost impossible to distinguish between early and late crystallising phases of the garnet. This presented serious problems in deciding what portions of the garnet to analyse. Large compositional variations within individual garnet grains over very short distances (<50 microns) as well as between garnet grains within an individual polished section were noted. These variations are not systematic, i.e. garnets from the Otjua skarn do not have Ca-rich cores with Fe and Mn enriched rims, which is common in some scheelite skarns (Dick and Hodgson, 1982). However, not all garnet grains from the Otjua skarn are zoned. Several analytical traverses were conducted over grains which possess uniform composition and garnets that show no compositional variations are often in contact with grains showing marked oscillatory zoning. A good example of a garnet grain exhibiting non-systematic, but substantial variations in composition is a grain that poikiloblastically encloses a scheelite crystal in slide 24659. Traverses were conducted as shown in Fig. 67, variations in composition are summarised in a ternary plot (see Fig. 68) and three representative analyses are given in Table 7-4.

Although an extensive amount of electron microprobe analysis was completed specifically to understand the zoning within garnet at Otjua, no systematic patterns were detected and it can only be concluded that the garnet crystallised from a fluid of constantly changing composition. The late stage nature of the garnet suggests that the garnet formed from residual fluid. Substantial variations in skarn garnet chemistry have, however, been noted by several workers, e.g. Burton et al. (1982) and Mathieson and Clark (1984) and thus the situation at Otjua is not atypical of skarn deposits.

The most significant features of garnet chemistry at Otjua are the very low MgO contents (ND - 0.16wt%), substantial FeO and MnO concentrations (6.12-14.56wt% and 3.28-9.29wt% respectively) and the high proportions of calcium and aluminium (19.61-32.18wt% and 19.42-20.74wt% respectively) which result in the mol% grossular component seldom being less than 68%. A summary of garnet chemistry at Otjua is given in Fig. 69. Garnets from the transitional idocrase/garnet facies (borehole OT15) have the highest Ca contents of all analyses, while Fig. 69 emphasises the broad trend of increasing Fe and Mn substitution for Ca within the garnet facies. However, garnet composition does not appear to be related to its spatial position within the orebody: garnets from the OT26 borehole intersection (see Long. Sect. 1) are indistinguishable from samples taken on surface. Similarly, although low-calcium garnets are present in the OT12 borehole intersection (which lies closest to the transitional garnet/pyroxene facies), some of the garnets analysed from surface samples have a similar chemistry.

iii) Conclusion:

Several important conclusions can be drawn from this study of the mineral chemistry of the Otjua skarn:

1) A genetic link between the three facies of skarn has been clearly demonstrated. The variations in pyroxene composition throughout the Otjua skarn are very similar to those observed at several other metasomatic tungsten skarns, for example, the Strawberry Mine, California (Nokleberg, 1981, p.122).

2) The first skarn minerals to form exhibit considerably more homogeneity than is common in skarns. However, on the local scale the skarn system possesses disequilibrium mineral assemblages, with garnet exhibiting extensive compositional variation.

3) The few scapolite grains that possess mineral zonation have calcium-rich cores and scapolite chemistry and scheelite distribution are closely linked in the skarn system.

4) Unfortunately, because of the high variances of the skarn mineral assemblages and the large solid solution ranges of the pyroxene and garnet, it is not possible to determine the P/T conditions under which the skarn has formed. However, a model for the skarn formation process is discussed fully in Chapter 8.

5) In terms of the mineralogical guidelines suggested by Newberry (1979b) and listed by Einaudi et al. (1981, p.337) the Otjua skarn can be classified as a reduced tungsten skarn because:

   i) The pyroxene-garnet ratio at Otjua is approximately 2 : 1
   ii) The pyroxene composition at Otjua is in the range 58.5-88.1mol%Hd, 3.2-12.5mol%Jo
   iii) The garnet at Otjua is andradite-poor
   iv) The diagnostic opaques at Otjua are pyrrhotite and chalcopyrite

c) Metasediments:

i) Scapolite in scheelite-bearing hornfels:

Representative analyses of scapolite from one sample of scheelite-bearing hornfels are given in Table 7-1. Atomic proportions and meionite components have been calculated as previously discussed. Scapolites in the hornfels do not possess chemical zoning and are highly calcic, meionite components ranging between 79.7% and 82.7%. Although the study of scapolite chemistry in the metasediments is by no means extensive, the association of highly calcic scapolites with scheelite mineralisation and interstitial carbonate, marl formation and carbonate development is highly significant. The importance of this is discussed more fully in Chapter 9.

ii) Pyroxene in scheelite-bearing hornfels:

Several analyses of pyroxene from scheelite-bearing hornfels were completed and are listed in Table 7-2. Traverses across individual grains indicate that the hornfels pyroxenes are unzoned - consistent with petrographic studies which indicate the presence of a stable

metamorphic assemblage. The composition of pyroxenes from scheelite-bearing hornfels varies considerably, pyroxenes tending to possess higher diopside components ($Di_{33.5-45-5}$) than pyroxenes from the various skarn facies, although some examples have the same composition as the most Mg-rich pyroxenes of the idocrase facies (see Fig. 61). Manganese contents of hornfels pyroxene ($Jo_{3.4-7.5}$) tend to be lower than idocrase and garnet facies pyroxenes (see Fig. 61). Fig. 62 shows that skarn pyroxenes tend to be more calcic than pyroxenes from hornfels as well as indicating that, in general, pyroxene chemistry is markedly different in the two lithologies.

iii) Pyroxene in calc-silicate:

Representative analyses of pyroxene from calc-silicate are listed in Table 7-2 and plotted in Fig. 62. Calc-silicate pyroxenes possess a higher diopside component than scheelite-bearing hornfels and skarn pyroxenes.

iv) Conclusion:

The following conclusions can be drawn from this study:

1) Skarn minerals are enriched in Fe and Mn and depleted in Mg relative to those minerals produced by metamorphism of the metasediments. This finding is similar to that of Newberry (1982), who noted that pyroxene, garnet and idocrase derived by essentially isochemical metamorphism of sediments in the vicinity of the Pine Creek Mine are iron-poor relative to metasomatic silicates.

2) Scheelite mineralisation in both the skarn and the hornfels is associated with highly calcic scapolite, the relevance of which is discussed more fully in Chapters 8 and 9.

7. STABLE ISOTOPE INVESTIGATION

a) Carbonate

i) Introduction:

From the petrological, geochemical and mineralogical investigations discussed in the preceding chapters it is apparent that a large quantity of elements has been introduced into the Rössing Formation marble to form the replacement skarn. Investigations into metasomatic replacement bodies elsewhere indicate the involvement of an essentially hydrous fluid in the skarn forming process (e.g. Kerrick, 1977). Brown et al. (1985) have used the stable isotope composition of minerals within tungsten skarns at Pine Creek to elucidate the origin and history of ore-forming fluids, while Taylor and O'Neil (1977) have conducted an extensive study on skarn formation in the Osgood Mountains with the aid of stable isotopes.

It was therefore decided to look at the isotopic composition of the carbonate within the Rössing Formation marble and skarn to discern: 1) the origin of the skarn forming fluid, and 2) to compare the isotopic composition of skarn calcite with interstitial calcite from the scheelite-bearing hornfels. This might reveal genetic differences in the two styles of mineralisation. Furthermore, it would be interesting to know whether there is an isotopic alteration halo surrounding the skarn in visibly unaltered marble. This would have relevance in exploration for concealed skarn deposits.

The systematic fractionation of isotopes between minerals (Taylor and Epstein, 1962a, 1962b; Taylor, 1967) and the temperature dependence of these fractionations mean that isotopes have many applications in geothermometry. Furthermore, isotope fractionations are independent of pressure (Clayton et al., 1975). Several authors (Valley and O'Neil, 1981 and Kreulen and van Beek, 1983) have discussed the possibility of using the isotopic composition of coexisting calcite and graphite as a geothermometer to determine peak metamorphic conditions and since these minerals coexist in the Rössing Formation marble an attempt to use this geothermometer was made.

Finally, minor interstitial calcite from an unusual pegmatite was analysed isotopically for use in a quartz-calcite geothermometer to establish the temperature of formation of the pegmatite (see section 7c).

ii) Analytical Procedure:

Calcite crystals were handpicked from rock samples crushed and dried in the oven overnight at 110°C. Whole rock samples were ground for twelve minutes in the carbon steel mill. Twenty milligram samples of the carbonate (or 500 milligrams of the whole rock) were then reacted overnight with 100% H_3PO_4 at 25°C (McCrea, 1950; Sharma and Clayton, 1965). The CO_2 was extracted and analysed on a VG Micromass 602E mass spectrometer in the Department of Archaeology, UCT. All samples were run in duplicate. Repeat samples run on the same day had an average error of less than 0.1‰, though reproductibility over a longer period is more like 0.15‰. All $\delta^{18}O$ values are reported in the standard delta notation relative to SMOW and all $\delta^{13}C$ values are reported relative to PDB. Isotopic fractionation between two compounds A and B is defined as follows: $\Delta(A - B) = 10^3 \ln(1000 + \delta A/1000 + \delta B)$ which is approximately $\delta A - \delta B$.

iii) Rössing Formation:

1) Results:

Isotopic composition of the marble calcite

Table 8 lists isotopic analyses of calcite from the Rössing Formation (see also Fig.70) from: a) in the immediate vicinity of the Otjua replacement skarn, b) at various localities up to 2km along strike from the replacement body, and c) at two localities within the Okakombo horst structure on the farm Tjirundo Süd. The average isotopic composition of the calcite from the Rössing Formation marble is as follows: $\delta^{18}O$ = 15.5‰ (standard deviation = 0.3) and $\delta^{13}C$ = +0.1‰ (standard deviation = 0.6). Although there is a small compositional variation, notably in the $\delta^{13}C$ value, no systematic spatial differences are apparent. In the immediate vicinity of the Otjua prospect, the isotopic composition of the marble is very

uniform. Of particular interest is the fact that there is little compositional difference between samples taken within as little as five centimetres of the skarn (e.g. sample OTS-26-0008) and samples taken up to 2km away from the replacement body e.g. OTS-00-01. This indicates that the skarn-forming fluid has not formed an isotopic alteration halo in the enclosing marble and that isotopic analysis of marble to locate blind skarn deposits would be of no use. Furthermore, the similarity in isotopic composition of the Rössing Formation on Tjirundo Süd supports the stratigraphic correlation between the domal structure within the Okakombo horst and the sequence at Otjua and, moreover, indicates that the Otjua granite has had no modifying influence on the isotopic composition of the Rössing Formation marble on a regional scale.

Isotopic composition of the skarn calcite

Table 9 lists isotopic analyses of interstitial calcite from the idocrase and garnet facies skarn developed at the Otjua prospect. Calcite is not present in the pyroxene facies. The average $\delta^{18}O$ composition of the skarn calcite is 15.3‰ (standard deviation = 0.1) and the average $\delta^{13}C$ value is -5.1‰ (standard deviation = 0.6). The data are plotted in Fig. 70. The most important features of note are: the similarity of the $\delta^{18}O$ value of the skarn calcite and the marble calcite; the depletion of the $\delta^{13}C$ composition to values exhibiting a large range from -4.2‰ to -5.9‰ ; there is no systematic variation in isotopic composition between idocrase and garnet facies calcite.

2) Discussion:

The essential features to be explained are a significant reduction in the $\delta^{13}C$ value of the skarn calcite and the similarity of the $\delta^{18}O$ values of the skarn and marble calcite.

Carbon: Hoefs (1980) has summarised the three major sources of carbon within a hydrothermal system:

1) marine limestones with average $\delta^{13}C$ values near zero
2) juvenile carbon with a range of $\delta^{13}C$ values between -5‰ and -8‰

3) organic carbon from sedimentary rocks with $\delta^{13}C$ lighter than -20‰ .

Hoefs' $\delta^{13}C$ value of ∿ zero for marine limestones has been well established (see Veizer and Hoefs, 1976). The Rössing Formation marble is interpreted as a shallow marine carbonate and therefore its $\delta^{13}C$ value of +0.1‰ is consistent with this interpretation. Hoefs' range of $\delta^{13}C$ values for juvenile carbon is based on investigations into kimberlites and carbonatites (Baertschi, 1957 and Taylor et al., 1967). More recently Taylor and O'Neil (1977) interpreted $\delta^{13}C$ values of -8.0 ± 1.0‰ for skarn calcite from the Osgood Mountains, Nevada as having a magmatic source. Brown et al. (1985) came to a similar conclusion when interpreting skarn calcite values of between -5.6‰ and -10.2‰ from Pine Creek, California. Thus, the simplest interpretation of the $\delta^{13}C$ value of -5.1‰ for the Otjua skarn calcite is that it has a significant magmatic component.

However, although the majority of hydrothermal deposits have carbonate with $\delta^{13}C$ values in the range -5‰ to -8‰ , it must be remembered that since calcite was not one of the first minerals to crystallise within the skarn, skarn calcite may have been in equilibrium with a fluid whose composition was different from the initial fluid. The fluid that formed the skarn at Otjua was presumably CO_2 rich (see discussion in Chapter 8) and there would have been a fractionation of ^{13}C between the CO_2 in the fluid and calcite in equilibrium with it. At a temperature of 500°C (an approximate estimate of temperature of skarn formation) $\Delta^{13}C(CO_2 - Cc) = 2.8$, (Bottinga, 1968), i.e. skarn calcite with a $\delta^{13}C$ value of -5.1‰ would be in equilibrium with a CO_2 rich fluid with a $\delta^{13}C$ value of -2.3 ‰ . Furthermore, low $\delta^{13}C$ values are not proof of an igneous origin for a hydrothermal fluid. Interaction between a hydrothermal fluid and graphite at the Bluebell deposit, British Columbia and at Panasqueira, Portugal lowered the $\delta^{13}C$ value to -7‰ and -14‰ respectively (Rye and Ohmoto, 1974). At Otjua, $\Delta^{13}C(Cc - Gr)$ averages 4.3 (see section on calcite-graphite geothermometry), but the small volume of graphite (< 2%) in the marble indicates that this mechanism cannot fully account for the reduction in the $\delta^{13}C$ value. However, the

concentration of graphite within certain layers within the marble may account for the range of $\delta^{13}C$ values in the skarn calcite.

Oxygen:

Marine limestones have $\delta^{18}O$ values in the range +20‰ to +28‰ (Keith and Weber, 1964), though Precambrian limestones tend to have lower $\delta^{18}O$ values (Veizer and Hoefs, 1976). However, volatilisation of carbonate during prograde metamorphism at temperatures in excess of 192°C evolves CO_2 that is enriched in ^{13}C and ^{18}O relative to the remaining calcite (Bottinga, 1968) causing a depletion in the $\delta^{18}O$ and $\delta^{13}C$ values of the marble (Taylor and O'Neil, 1977). Reduction of $\delta^{18}O$ values of carbonate rocks due to isotopic exchange with the enclosing country rocks during peak metamorphic conditions is also a well known phenomenon. Therefore, the $\delta^{18}O$ value of 15.5‰ for the Rössing Formation marble is not unusual for a metamorphosed marine limestone. If the $\delta^{18}O$ value of the carbonate was reduced during metamorphism, the pre-metamorphic $\delta^{13}C$ value of the Rössing Formation marble was probably in excess of 0.1‰ .

The fact that the $\delta^{18}O$ composition of the skarn calcite is so high implies that the fluid in equilibrium with the skarn calcite was also enriched in ^{18}O. At a temperature of 500°C (suggested temperature of skarn formation) $\Delta^{18}O(CaCO_3 - H_2O) = 1.8$ (O'Neil et al., 1969) i.e. skarn calcite with a $\delta^{18}O$ value of 15.3‰ would be in equilibrium with water with a $\delta^{18}O$ value of 13.5‰. A fluid with such a high $\delta^{18}O$ value is almost certainly not meteoric in origin. Although the $\delta^{18}O$ isotopic composition of Precambrian meteoric waters is unknown, present day meteoric waters range in composition from -55‰ in the polar regions to approximately 0‰ in equatorial regions (Taylor, 1974). Water with a $\delta^{18}O$ value of 0‰ would be in equilibrium with calcite with a $\delta^{18}O$ value of 15.3‰ at a temperature of 120°C (O'Neil et al., 1969), a rather improbable skarn formation temperature. The restricted range of $\delta^{18}O$ values of the skarn calcite indicates a fluid of constant composition and a juvenile source is far more likely. The isotopic composition of a juvenile fluid will not only be controlled by the $\delta^{18}O$ value of the igneous magma since temperature will control the fractionation of ^{18}O between water and magma. However, since isotopic fractionations tend

to be minimal at temperatures of 600-700°C (most likely temperature of hydrothermal fluid at time of release from granite), the isotopic composition of a fluid will approximate the composition of the parent igneous body. The isotopic composition of the Otjua granite is remarkably similar to the skarn calcite (15.3‰ for skarn calcite versus 15.1‰ for Otjua granite: Haack et al., 1983). Due to the similarities in oxygen isotope composition of the reservoirs, the "mixing line" (see Fig.70) has a vertical gradient. Thus a preliminary interpretation of the isotope data suggests that the source of the skarn-forming fluid is the Otjua granite.

However, as discussed previously, simple volatilisation of calcite during metamorphism results in a depletion of $\delta^{13}C$ in the residual calcite. During skarnification of the Rössing Formation marble considerable CO_2 was evolved during calcite dissolution and thus the possibility cannot be excluded that the reduction in the $\delta^{13}C$ value of the skarn calcite was due to decarbonation and not the involvement of an igneous fluid. Depletion of ^{18}O would almost certainly not be as extensive due to the large reservoir of oxygen that is in the rock or fluids from which the silicates crystallised. Moreover, a skarn-forming fluid with a high $\delta^{18}O$ value would essentially buffer against any tendency towards depletion of the $\delta^{18}O$ value of skarn calcite.

Two extreme cases are considered here: firstly, where evolved CO_2 remains in contact with and is able to isotopically exchange with the remaining calcite and subsequently evolved CO_2, i.e. a closed system in which fractionation would be small. Secondly, in an open system, evolved CO_2 which is removed from the rock cannot exchange with calcite or late CO_2. This would result in the maximum depletion of the carbon value and can be treated by a Rayleigh fractionation model.

Volatilisation of the marble: $\delta^{13}C$ depletion within a closed system:

During decarbonation the depletion of ^{13}C in calcite depends on the amount of calcite that is dissociated and the fractionation of ^{13}C between the two compounds CO_2 and calcite. The latter has been

calculated for various temperatures by Bottinga (1968). The degree of depletion is therefore given by the following equation:

$$\delta^{13}C_{Cc} = \delta^{13}C_{system} - \alpha(X_{CO_2})$$

where $\delta^{13}C_{Cc}$ is the ^{13}C composition of the remaining calcite, $\delta^{13}C_{system}$ is the value of the marble (in this case $\delta^{13}C$ will be +0.1‰ - the average $\delta^{13}C$ value of the Rössing Formation marble, see Table 8), α is the fractionation factor for ^{13}C between CO_2 and calcite and X_{CO_2} is the percentage of carbon that has been removed as CO_2.

Although there is some uncertainty regarding the skarn formation temperature, 500-550°C seems a reasonable estimate for those portions of skarn that contain signifiant calcite. The fractionation of ^{13}C between carbon dioxide and calcite is at a maximum at 470°C (see Bottinga, 1968). Depletions of ^{13}C in the calcite have been calculated for various temperatures (see Table 10) and are plotted in Fig. 71. Fig. 71 indicates that at 550°C a system with only 5% calcite (modal average for the idocrase facies) should show a $\delta^{13}C$ depletion from 0.1‰ to -2.5‰. Garnet facies skarn (1-2‰ calcite) should show a $\delta^{13}C$ depletion to -2.6‰. Both these values are considerably heavier than the observed average value of -5.1‰ for the two facies (see Table 9). Therefore, simple single stage volatilisation of CO_2 from within a completely closed system is unlikely to have been responsible for the reduction in the $\delta^{13}C$ value.

Volatilisation of the marble: $\delta^{13}C$ depletion within an open system

In this case, all the CO_2 that is released by the decomposition of calcite is assumed to have been removed from the marble and has not exchanged with the remaining calcite or subsequently evolved CO_2. Modelling of the volatilisation process is given by Rayleigh fractionation (Matthews and Kolodny, 1978) $R^f/R^i = F^{(\alpha-1)}$; where R^i and R^f are the initial and final ^{13}C values respectively, F is the fraction of carbonate remaining in the rock and α is the fractionation factor for the relevant temperature. As discussed previously, it has

not been possible to obtain an estimate of the temperature of formation for the Otjua skarn, although a temperature in the region of 500-550°C is considered reasonable. Table 11 lists the calculated $\delta^{13}C$ depletions at 200°C, 300°C and 500°C within an open system and the values are plotted in Fig. 72. The rate of depletion in the $\delta^{13}C$ value for the initial 60% of the calcite is similar to that evaluated in the closed system model, thereafter it decreases at a much faster rate. The calculated depletions in the $\delta^{13}C$ value at 500°C indicate a $\delta^{13}C$ value of -8.3‰ for the idocrase facies and approximately -11‰ for the garnet facies. Both values are much lighter than the average observed figure of -5.1‰ for skarn calcite (see Table 9). Even at lower temperatures, e.g. 300°C and 350°C, the calculated depletions in the $\delta^{13}C$ value of the remaining calcite are significantly lower than the observed values. However, both the closed and open systems modelled here are ideal systems and the possiblity that decarbonation occurred in a partially open system cannot be discounted.

The main problem with accepting that decarbonation alone can account for the reduction in the $\delta^{13}C$ value is the lack of distinction in $\delta^{13}C$ composition between the idocrase and garnet facies. Calcite is a very minor component in the latter (1-2‰) while it is fairly extensive in the former (up to 15‰). Furthermore, the modal average of 5% for the idocrase facies has been calculated on the basis of two whole rock analyses - 10‰ would be a more reasonable estimate. Decarbonation in a partially open system would almost certainly have resulted in major differences in isotopic composition between the two facies because of the very rapid increase in rate of depletion in $\delta^{13}C$ with such small quantities of residual calcite (see Fig.72).

3) Conclusion:

The most plausible explanation of the carbon and oxygen isotope data is the interaction of a magmatic fluid with a marine carbonate. The very limited range of high $\delta^{18}O$ values in the skarn calcite indicates the presence of a fluid with a constant isotopic composition and the suggested source of this fluid is the Otjua granite. Fluctuations in the $\delta^{13}C$ values of the skarn calcite which has an essentially juvenile

signature may be accounted for by local concentrations of graphite in the Rössing Formation marble which has a $\delta^{13}C$ value considerably lighter than coexisting calcite. Simple decarbonation of the calcite in a partially closed system would result in depletion of $\delta^{13}C$ to values similar to those that are observed in the skarn. However, the idocrase facies and garnet facies calcites are indistinguishable isotopically - according to the volatilisation model they should be different due to the different amounts of calcite within the facies. Furthermore, volatilisation of the marble would be unlikely to produce skarn calcite with such a uniform $\delta^{18}O$ value. Moreover, petrological evidence indicates that the majority of the calcite is interstitial to other minerals, i.e. crystallised late in the paragenetic sequence.

iv) Scheelite-bearing Hornfels:

1) Introduction:

Several of the scheelite-bearing hornfels that enclose the Rössing Formation marble/skarn contain small, but significant amounts of calcite (up to 5%). As discussed previously, these hornfels are considered to represent metamorphised marls. However, the presence of scheelite within these hornfels begs the questions of whether the scheelite could have been introduced into the hornfels at the same time as the skarn was formed, or whether the marls provided the tungsten now hosted by the skarn. The carbon and oxygen isotope composition of the calcite within the hornfels was investigated to try and discern the origin of the carbonate. Eight samples of scheelite-bearing hornfels with high tungsten contents (up to 1.4%W) were selected for analysis: four from the hornfels that enclose the skarn at Otjua and four from the hornfels that enclose the Rössing Formation marble on Tjirundo Süd (see Map1).

2) Results:

The results are listed in Table 12 and plotted in Fig. 70. A large spread in both $\delta^{13}C$ and $\delta^{18}O$ values for the calcite from the scheelite-bearing hornfels is apparent. $\delta^{13}C$ values range from -2.5‰ to -5.8‰ and $\delta^{18}O$ values vary between 16.0‰ and

18.5‰ . The $\delta^{13}C$ values for the hornfels calcite ($\bar{x}$ = -3.9‰) tend to be heavier than those from the skarn calcite ($\bar{x}$ = -5.1‰). $\delta^{18}O$ values for the hornfels calcite ($\bar{x}$ = 17.0‰) are also heavier than the skarn calcite ($\bar{x}$ = 15.3‰) and have a wide range in values in contrast to the compositionally uniform skarn calcite. Significantly, no distinction can be made between the hornfels calcite in the vicinity of the Otjua replacement skarn and that on Tjirundo Süd.

3) Discussion:

It is clear from Fig.70 that the calcite from the replacement skarn and the calcite from the scheelite-bearing hornfels are isotopically quite different. The large spread in $\delta^{18}O$ and $\delta^{13}C$ values of the hornfels calcite suggests a considerable range in composition of fluid in equilibrium with the calcite. This indicates that the two types of calcite are not genetically related, unless the isotopic composition of the hornfels calcite has been subsequently modified by meteoric water. However, it seems unlikely that meteoric water would selectively affect the hornfels calcite and not the skarn calcite. Moreover, interaction between silicates and carbonates and substantial volumes of meteoric water invariably leads to a significant drop in the $\delta^{18}O$ value of the minerals in equilibrium with meteoric water (Taylor, 1974, 1977).

A more plausible explanation for the different isotopic compositions of the calcite is that the calcite in the hornfels was formed during prograde metamorphism of a slightly calcareous marl. Decarbonation reactions that occur during metamorphism evolve CO_2 that is heavier than the remaining calcite since both $\Delta^{18}O(CO_2 - Cc)$ and $\Delta^{13}C(CO_2 - Cc)$ are positive at temperatures in excess of 192°C (Bottinga, 1968). This results in a depletion of both $\delta^{18}O$ and $\delta^{13}C$ in the residual calcite of a metamorphic rock relative to unmetamorphosed limestone (Taylor and O'Neil, 1977). Thus the wide range of values of $\delta^{13}C$ and $\delta^{18}O$ could be attributed to varying degrees of devolatilisation of minor calcite within the marl. However, since the initial isotopic composition of the calcareous material within the marl is unknown and the fact that there is no

correlation between $\delta^{13}C$ and $\delta^{18}O$ values for the hornfels calcite and the amount of calcite within the hornfels means that the suspected depletions cannot be quantified.

As an alternative to the above theory, the presence of organic material within the original marl cannot be excluded. Organic carbon in sedimentary rocks normally has $\delta^{13}C$ values lighter than -20‰. Under metamorphic conditions this carbonaceous material would be converted to graphite. Although no graphite is present within the hornfels today, it is possible that at some stage during metamorphism this graphite was oxidised to form CO_2 with a very light $\delta^{13}C$ value. If trapped in the rock this CO_2 would isotopically exchange with any calcite in the rock, consequently lowering the $\delta^{13}C$ of the carbonate.

4) Conclusion:

The hornfels calcite and skarn calcite are isotopically distinct. Hornfels calcite shows a large range in $\delta^{13}C$ and $\delta^{18}O$ values either as a result of varying degrees of volatilisation of the carbonate during prograde metamorphism or possibly due to exchange with isotopically light CO or CO_2 derived from oxidation of organic material. In contrast, the small range in $\delta^{13}C$ and $\delta^{18}O$ values of the skarn calcite is indicative of an igneous origin for the skarn-forming fluid. These two populations of calcite are considered good supporting evidence for the suggestion of two stages of scheelite mineralisation, i.e. a pre-metamorphic syn-sedimentary event and a late tectonic one associated with granite intrusion.

v) Calcite-Graphite Isotope Geothermometer:

1) Introduction:

Graphite and calcite commonly coexist in a wide variety of limestones and marbles. The fractionation of ^{13}C between coexisting calcite and graphite as a function of temperature has been investigated by a number of authors (Pineau et al., 1976; Kreulen, 1977; Valley and O'Neil, 1981). Organic carbon in recent marine rocks usually has

a $\delta^{13}C$ value lighter than -20‰ and there is a large fractionation of ^{13}C between calcite and graphite, i.e. $\Delta^{13}C$ (Cc - Gr) >15. In contrast, graphite in marbles has a considerably heavier $\delta^{13}C$ value (> - 10‰) and $\Delta^{13}C$(Cc - Gr) is usually smaller. Valley and O'Neil (1981) have proposed that the fractionation of ^{13}C between calcite and graphite can be used as a geothermometer. During their investigation of calcite-graphite pairs from the Adirondack Mountains, New York, temperatures obtained agreed well with those gained from studies of metamorphic assemblages.

However, they emphasise that isotopic equilibrium is usually attained when peak metamorphic temperatures are in excess of 500-600°C and therefore this geothermometer can only be used for marbles that have undergone metamorphism in excess of 550°C. Moreover, Valley and O'Neil concluded that the theoretically calculated fractionation factors for the calcite-graphite pair given by Bottinga (1969) were 2‰ too large. This discrepancy between observed and theoretical values was highlighted by an investigation by Kreulen and van Beek (1983) into calcite-graphite isotope fractionations in marbles from Naxos, Greece. They concluded that their data agreed better with Bottinga's theoretical work than the empirical fractionation curve of Valley and O'Neil. They also concluded that the calcite-graphite geothermometer was not particularly sensitive. In spite of these contradictory conclusions, it was decided that calcite-graphite isotope fractionations might give a peak metamorphic temperature for the Rössing Formation marble.

2) Sample selection and analysis:

Four samples of the Rössing Formation marble were selected for analysis: two from 500m and 800m west of the Otjua skarn and two from the domal structure on Tjirundo Süd. As discussed by Valley and O'Neil (1981), it is essential that the graphite and calcite pairs to be used as a geothermometer were in equilibrium at the peak of metamorphism and did not exchange carbon at lower temperatures. Petrographic analysis of the Rössing Formation marble indicates that equilibrium has been attained: triple junctions between equidimensional calcite grains are very common and no retrogressive

features are present. Graphite flakes, seldom larger than 1mm do not comprise more than 2% volumetrically of the rock and are unevenly distributed throughout the marble. Graphite and calcite were separated from the same $30cm^3$ large hand specimens. Graphite separates were obtained by hand picking of coarser grains and dissolution of the remaining carbonate in dilute HCl. Graphite flakes were then separated from residual material with the aid of a binocular microscope and were then reacted at 800°C with CuO to form CO_2 in evacuated silica tubing. The CO_2 was then extracted and isotopically analysed. Yields of CO_2 varied between 94 and 103% of the theoretical values.

3) Results:

The isotopic compositions of calcite and graphite pairs are listed in Table 13. $\delta^{13}C$ values for the calcite range from -0.7‰ to +1.3‰, $\delta^{13}C$ values of graphite range from -4.8‰ to -3.5‰ and $\Delta^{13}C$(Cc - Gr) from 4.0 to 4.8 (average = 4.3). That isotopic equilibrium has probably been attained is suggested by the high $\delta^{13}C$ values of the graphite and the small range in $\Delta^{13}C$(Cc - Gr) values. Furthermore, the fractionation of ^{13}C between calcite and graphite is independent of the ^{13}C composition of calcite. Both Valley and O'Neil (1981) and Kreulen and van Beek (1983) suggest that isotopic equilibrium between calcite and graphite is not attained below 550°C and the latter's data even above this temperature show considerably more scatter than the Rössing Formation marble. Overall, the $\Delta^{13}C$(Cr - Gr) values of the Rössing Formation marble are smaller than Kreulen and van Beek's data, but similar to Valley and O'Neil's.

4) Discussion:

Due to the highly calcic nature of the Rössing Formation marble, a diagnostic mineral assemblage characteristic of certain metamorphic conditions is not present. However, petrographic study of the enclosing metasediments indicates that peak metamorphic temperatures were in the range 500-680°C (see section on metamorphism). These temperatures are characteristic of amphibolite facies metamorphism.

Valley and O'Neil (1981) have conducted a study of $\Delta^{13}C$(Cc -Gr) from a number of carbonates from different metamorphic facies. The $\Delta^{13}C$(Cc-Gr) value of 4.3 obtained for the Rössing Formation marble is consistent with their data from amphibolite (and possibly granulite) terrains (Valley and O'Neil, 1981, Fig. 3). For the temperature range 500°C to 680°C a fractionation of 4.3 between calcite and graphite is more consistent with the data of Valley and O'Neil than that of Bottinga (see Kreulen and van Beek, 1983). Substituting the average $\Delta^{13}C$(Cc - Gr) value of 4.3 for the Rössing Formation marble into the fractionation curve of Valley and O'Neil gives a peak metamorphic temperature of 590°C. This is in excess of 550°C, suggesting that isotopic equilibrium was attained and is consistent with the temperature obtained by petrographic analysis of the enclosing metasediments. In contrast, substitution of $\Delta^{13}C$(Cc - Gr) values of the Rössing Formation marble into Bottinga's fractionation curve indicate peak metamorphic conditions in excess of 700°C which is obviously too high. This is the same conclusion that Valley and O'Neil came to regarding their data from the Adirondack Mountains, i.e. Bottinga's predicted fractionations are 2‰ larger than those shown by natural assemblages. Wada (1977) also concluded that $\Delta^{13}C$(Cc - Gr) in marbles from high temperature assemblages are consistently lower than those predicted by Bottinga.

Of particular interest is the fact that Valley and O'Neil applied their fractionation curve to four marble analyses taken from elsewhere in the Damara by Pineau (1976) and found good agreement with temperatures determined by Puhan (1976): 598°C by calcite-graphite isotope geothermometry as against 620°C by calcite-dolomite thermometry.

Thus, although only four samples have been analysed and a larger population of samples would have been preferable, it is suggested that Valley and O'Neil's fractionation curve has given meaningful temperature ranges, although it is hard to escape the conclusion of Kreulen and van Beek that, used in isolation, the graphite-calcite isotope geothermometer is not particularly sensitive.

5) Conclusions:

Although the following conclusions are based on only four sets of data, they are considered to be valid:

i) On petrological grounds and from isotopic investigations, isotopic equilibrium between calcite and graphite within the Rössing Formation marble has been attained.

ii) Fractionations between graphite and calcite in the Rössing Formation marble are more consistent with the empirically derived fractionation curve of Valley and O'Neil than the theoretical curve of Bottinga.

iii) Substitution of the $\Delta^{13}C$(Cc - Gr) values obtained for the Rössing Formation marble into the fractionation curve proposed by Valley and O'Neil indicates temperatures for the peak of metamorphism of between 519°C and 626°C and an average of 586°C. These temperatures are consistent with those derived by petrographic study of the metamorphic assemblages in the enclosing metasediments. This good agreement may be coincidental, but is consistent with studies from elsewhere in the Damaran.

iv) The calcite-graphite isotope geothermometer used is isolation has low sensitivity, but when used in conjunction with other studies may help to confine peak metamorphic temperatures.

b) Silicate:

i) Introduction:

The systematic fractionation of ^{18}O between coexisting minerals noticed by many early workers in stable isotope geochemistry resulted in Taylor (1967) listing minerals in decreasing order of affinity for ^{18}O. However, although the order of fractionation of ^{18}O between minerals is a result of chemical properties, the degree of fractionation between minerals is dependent on temperature. As a result, O'Neil and Clayton (1964) and O'Neil and Taylor (1967) were the first to experimentally determine fractionations of ^{18}O between quartz and water and between quartz and feldspar respectively with the aim of producing a quartz-feldspar geothermometer. Direct measurements of the ^{18}O fractionation between quartz and K-feldspar at

600°C were subsequently made by Blattner and Bird (1974) and more experimental work was completed by Bottinga and Javoy (1973 and 1975). Considerable discrepancies between fractionation curves suggested by the different authors were reviewed by Matsuhisa et al. (1979) who proposed the use of a new quartz-feldspar fractionation curve which has found wide acceptance.

The aim of this study was therefore twofold:

1) to investigate the ^{18}O composition of quartz and K-feldspar from the pegmatite and test the suspected co-genesis of the Otjua granite and the pegmatite developed in the vicinity of the skarn. Quartz and K-feldspar comprise 70% of the pegmatite and because the plagioclase feldspar is relatively sodic (oligoclase), the weighted average ^{18}O composition of these two minerals will approximate the whole rock value.

2) by determining the fractionation of ^{18}O between quartz and K-feldspar and using experimentally derived fractionation factors to obtain a temperature of formation for the pegmatite

ii) Analysis:

Oxygen was extracted from quartz and K-feldspar by fluorination of the minerals with ClF_3 at temperatures of between 600°C and 650°C (Borthwick and Harmon, 1982). The oxygen was then converted to CO_2 by reaction with a hot carbon rod and was then isotopically analysed in the same manner as the CO_2 produced from the carbonate (see preceding section). $\delta^{18}O$ values are reported in the standard notation relative to SMOW.

iii) Results:

The $\delta^{18}O$ compositions of quartz and K-feldspar from the pegmatite are listed in Table 14. The fractionation of ^{18}O between the two minerals are fairly substantial. That they are positive indicates no "reversals" have occurred and that the pegmatites have not exchanged oxygen with significant amounts of meteoric water (Taylor,

1974, 1977). The $\delta^{18}O$ compositions of the quartz and feldspar bracket the $\delta^{18}O$ value of 15.1 for the Otjua granite determined by Haack et al. (1983), suggesting that the Otjua granite could well be the source of the pegmatite or at least that the pegmatite was derived from the same source material.

Using the fractionation curve of Matsuhisa et al. (1979), the fractionation of ^{18}O between quartz and feldspar indicates temperatures of crystallisation for the pegmatite ranging from between 240°C and 300°C (average = 280°C).

iv) Discussion:

The oxygen isotope investigation of silicate minerals in the pegmatite clarifies several important points:

Firstly, as previously stated, the close spatial relationship between highly fractionated late stage granites, unaltered tourmaline pegmatites and replacement skarns suggests a genetic relationship. Petrological, textural and geochemical evidence for cogenesis of the pegmatite and granite is supported by the oxygen isotope data.

Secondly, the normal isotopic fractionation of ^{18}O between quartz and feldspar in the pegmatite at Otjua indicates that no secondary interaction with other oxygen reservoirs has occurred. This is in agreement with the observations of Haack et al. (1983) who noted no quartz-feldspar reversals in their regional survey of the Damaran granitoids. This has implications for the genesis of the scheelite within the hornfels, i.e. it seems unlikely that Damaran intrusives formed large scale convective hydrothermal cells and that large scale leaching of metals from rocks surrounding the intrusions did not occur (see discussion in Chapter 9).

Thirdly, the low temperature of formation of the pegmatites (average = 280°C) explains the lack of contact metamorphic effects between the pegmatite and enclosing country rock. It is suggested that the presence of considerable boron within the pegmatitic melt (as evidenced by the schorl) lowered the solidus resulting in this low

temperature of formation. Haack (1983) has reconstructed the cooling history of the Central Zone of the Damaran orogen using Rb/Sr, K/Ar and fission track ages. At 478 Ma (age of Otjua granite and consequently approximate age of Otjua pegmatites), Haack indicates that the metasediments within the Central Zone of the Damaran were at temperatures of between 300° and 400°C (Haack , 1983, Fig. 9).

c) Calcite-bearing Pegmatite

i) Introduction

Several boreholes intersected an unusual calcite-bearing pegmatite. These vuggy pegmatites are seldom more than a few metres thick, have caused minor potassic alteration of the enclosing country rock and may grade into normal pegmatites. This lateral gradation into normal pegmatite with no sharp mineralogical or textural boundaries suggests that the two types of pegmatite are cogenetic. It is therefore assumed that the isotopic composition of silicate minerals in the two lithologies is similar. The only significant mineralogical differences are the presence of calcite, chlorite and pyrite and absence of tourmaline in the calcitic pegmatite. Calcitic pegmatites comprise a very small component of the total pegmatite at Otjua - less than one percent.

The isotopic composition of interstitial calcite from the calcitic pegmatite was measured:

1) to determine whether the calcite has an igneous signature
2) by using the average $\delta^{18}O$ composition of the calcite and the average $\delta^{18}O$ composition of the pegmatite quartz, an approximate temperature of formation of the calcitic pegmatite could be obtained from quartz-calcite fractionation data.

ii) Analysis and Results:

Calcite was analysed as previously described. The results are listed in Table 15 and plotted in Fig. 70. Large differences in $\delta^{13}C$ and $\delta^{18}O$ values for these samples are readily apparent. This isotopic inhomogeneity indicates that either isotopic equilibrium was

not attained during crystallisation or that possibly due to the vuggy nature of the rock, meteoric groundwaters have exchanged oxygen with the calcite. However, the average $\delta^{13}C$ composition of -4.8‰is only slightly heavier than the suggested range of -5‰ to -8‰ for "igneous" carbon of Hoefs (1980). Moreover, the fact that the calcite is depleted in ^{18}O relative to the quartz and feldspar (see Table 14) is consistent with Taylor's observations on ^{18}O fractionations between coexisting minerals (Taylor, 1967) and therefore it is doubtful whether significant adjustments to the isotopic composition of the calcite have been made by meteoric waters. It is therefore assumed that isotopic equilibrium in the calcitic pegmatite was not attained during crystallisation. However, the fractionation of 4.3 between the <u>average</u> $\delta^{18}O$ value of the calcite and the <u>average</u> $\delta^{18}O$ value of the quartz (see preceding section) indicates a temperature of formation of 240°C - not too dissimilar from the normal pegmatites developed at the Otjua prospect.

iii)Conclusion:

Significant differences in the isotopic composition of calcite indicate that isotopic equilibrium has not been fully attained. This is perhaps not to be unexpected in a vuggy late stage intrusive. However, $\delta^{13}C$ values are consistent with an igneous source for the calcite and, secondly, although not particularly suitable for temperature determinations, the average fractionation of ^{18}O between quartz and calcite indicates a temperature of formation for the calcitic pegmatite only slightly cooler than the normal pegmatite.

8) SKARN FORMATION

a) Timing of Skarn Formation:

At the Otjua prospect the metasediments of the Khan and Oberwasser Formations all exhibit a fine grained equigranular texture indicating that these minerals were brought to equilibrium during peak metamorphic conditions at 520Ma. In contrast, the skarns hosted by the Rössing Formation exhibit a diverse range of textures. Garnet exhibits a considerable range in composition over short distances indicating chemical disequilibrium. These petrological and mineralogical features clearly indicate that the skarn formation process postdates the peak of metamorphism. However, one fact suggests that there was only a small difference in temperature between the skarn-forming fluid and the carbonate - there is no contact metamorphic effect between skarn and marble. Moreover, the skarn and metasediments are transected by pegmatitic dykes which possess an unequivocal igneous texture, but no contact metamorphic effects are developed in the rocks that they intrude. Mineralogical, textural, geochemical and isotopic evidence indicates that the pegmatite is derived from the Otjua granite. Similarly, isotopic investigations suggest an igneous source for the skarn-forming fluid. Therefore the skarn formation process must have occurred between the peak of regional metamorphism (520Ma) and the final crystallisation of the Otjua granite (478 $\pm$ 4Ma).

b) Skarn Formation - the Mechanism:

Several possibilities as to the mode of formation of the skarns hosted by the Rössing Formation are discussed below:

i) Metamorphism of a mineralised dolomite:

Although it is impossible to determine the composition of the carbonate that has been skarned, there are no significant variations in the composition of the Rössing Formation marble on a regional basis. Four analyses of the carbonate from the Otjua prospect show the carbonate to be virtually pure calcite and three samples taken of

the Rössing Formation at the Tjirundo prospect, 8km west of Otjua (see Map 1), indicate that the marble there is also very pure (see Table 3-4). Whole rock analysis of major and trace element concentrations within the skarn clearly show that a large proportion of the elements in the skarn are exotic compared to the surrounding marble. Moreover, the diverse textural features of the various skarn facies and the compositional variations in the garnet indicate that the skarn assemblages have not attained equilibrium under peak regional metamorphic conditions. Therefore it is extremely improbable that the skarns hosted by the Rössing Formation formed "in situ" from a mineralised dolomitic precursor and this possibility is thus rejected as a mechanism for skarn formation at Otjua.

ii) Metasomatic exchange between the marble and enclosing metasediments:

Some or all of the elements required to form the silicate minerals in the skarn could have been provided by the wall rocks. It is therefore necessary to examine the evidence for an exchange of elements between the carbonate and the metasediments to test the theory that the various skarn facies formed as a result of "bimetasomatic exchange". Thompson (1959) was one of the first people to note that marble-schist contacts frequently contain simple mineral assemblages whose chemical compositions do not suggest that they were originally derived from sediments. These types of calc-silicate bands were the object of a study by Vidale (1969) who experimentally produced zonation patterns similar to those observed in kyanite and sillimanite grade calc-silicate bands. However, although diffusion models can explain a number of thin reaction zones, it is widely accepted that they cannot explain the large thicknesses of skarn in most metasomatic deposits (Einaudi et al., 1981).

On first examination the idocrase facies skarn, which is a thin development of silicates at the contact between the Rössing Formation marble and the enclosing metasediments, could be interpreted as a reaction skarn. Garnet facies skarn is locally intercalated with calc-silicate rocks (on a 1-5 centimetre scale) at the contact between the Rössing Formation and the country rocks. However, nearly all

reaction skarns exhibit a well defined, fine grained mineralogical banding that probably reflects diffusion fronts of the various ions. This fine grained mineralogical banding is absent from all the facies of skarn at Otjua. Furthermore, both the idocrase facies and garnet facies skarn exhibit coarse grained mineral assemblages.

Several features argue against an exchange of elements between the carbonate and the wall rocks. Firstly, drillhole intersections of marble indicate that there has been no reaction between the marble and the enclosing country rocks in areas away from the skarn. This is in contrast to the scheelite-bearing hornfels, which usually has a thin amphibole-rich zone where in contact with biotite schist. Secondly, for the skarn to have been derived from an exchange of elements between marble and the enclosing wall rock it would seem logical that, if the marble was in contact with schist, then a different mineral assemblage would be developed from where the marble was in contact with calc-silicate rocks. This is quite clearly not the case : all three facies of skarn are in contact with both lithologies. Thirdly, an examination of the whole rock analyses of calc-silicates and biotite schist indicates that concentrations of certain elements in these lithologies (which were sampled at some distance from the skarn) e.g. Mn, Fe, Na are present in very low concentrations compared to the skarn. It would thus seem logical that the biotite schist and calc-silicate directly in contact with skarn would be considerably depleted in these elements, a depletion accompanied by considerable alteration or at least visual modification of the wall rock. Presumably Ca and CO_2 would migrate out of the marble into the enclosing country rock resulting in alteration or calcitisation of the enclosing wall rock. None of the features expected from this model have been observed. Fourthly, although there are small but significant concentrations of tungsten and fluorine in the scheelite-bearing hornfels and the calc-silicates of the Khan and Oberwasser Formations, to concentrate these elements to the amounts present in the idocrase and garnet facies skarn requires a model invoking the migration of tungsten and fluorine for distances of many tens of metres across strike. Kwak (1978), in his investigation of the King Island scheelite deposit, showed that hornfels even one centimetre thick was probably impermeable to skarn-forming solutions (op. cit.

p.953). Fifthly, the systematic variations in mineralogy, mineral chemistry and whole rock compositions of the three facies of skarn along strike suggest an evolutionary trend in a system that has developed over many hundreds of metres, which is essentially incompatible with a model involving local bimetasomatic exchange between the carbonate unit and the enclosing country rocks.This model is therefore rejected.

iii) Infiltrational Metasomatism:

The geochemical evidence indicates that the Rössing Formation marble acted as a reactive conduit for mineralising fluids that progressively metasomatised the carbonate. It is suggested that the various skarn facies developed simultaneously and that the facies development is a result of variations in the $a_{Ca^{2+}}$ /a $_{\text{Introduced elements}}$ ratio, fluid/rock ratio and temperature. This is the most plausible explanation for the petrographic evidence which precludes the possibility of one facies of skarn crosscutting or replacing another facies. Where transitional skarn assemblages have been identified, investigations into the mineral chemistry of these areas have shown mineral compositions to be transitional. This indicates that one pulse of magmatically derived skarn-forming fluid can account for the facies development.

Before considering a model of skarn formation , the following must be addressed. Was the metasomatic event a constant volume process or not? The density of the skarn is considerably greater than that of the marble (idocrase and garnet facies = 3.26; pyroxene facies = 3.2; marble = 2.75). Accommodation of the large volume of introduced material within the former Rössing Formation cannot be accounted for by these relatively small increases in density and it must therefore be established whether the components of the marble have been removed during skarn formation or whether the CaO and CO_2 have been retained within the system.

Relatively few studies have been published on the volume changes during skarn formation. Nokleberg (1981) reported an extensive investigation at the Strawberry mine, California, in which he made

hundreds of layer thickness measurements on either side of the contacts between marble and skarn and between the various skarn facies, both on surface and underground. Nokleberg conducted a statistical study of the data, from which he concluded that skarn formation was essentially a constant volume process. At Otjua, due to the poor surface exposure of the contacts of marble and skarn between each other and the enclosing metasediments, as well as the lack of underground workings, no investigation of the possible volume changes during skarn formation has been completed. However, because of the many similarities of skarn mineralogy, geochemistry and orebody geometry between Otjua and the Strawberry mine, it is considered that skarn formation at Otjua was essentially a constant volume process (see discussion on wollastonite, X_{H_2O} and X_{CO_2} during skarn development).

This is an important conclusion because this implies that at least some of the CaO and a major proportion of the CO_2 produced by the dissociation of calcite during skarn formation has been removed from the system.

c) Composition of the Skarn-forming Fluid:

Before commencing this discussion it is important to reiterate that the size of the skarn sample population is small and therefore some caution should be exercised when interpreting inter-element ratios. For this reason only the inter-element ratios for average skarn facies compositions have been calculated and are listed in Table 16.

The changes in mineral assemblages and mineral composition as the Rössing Formation was progressively metasomatised can be best shown using a modified ACF plot (see Fig. 73). Only the major minerals present in the skarn are shown on this diagram. The introduction of aluminium, magnesium, iron and manganese that accompanied metasomatism results in the idocrase and garnet facies skarns plotting well away from the marble. Although the garnet facies skarn exhibits considerable compositional variation, the garnet facies field includes the idocrase facies samples emphasising the similar bulk compositions of the two facies. Moreover, the average garnet facies skarn has only

a slightly lower Ca content than the idocrase facies. The wide range in composition of the garnet is also clearly evident. The pyroxene facies skarn plots in a distinct field furthest from the Ca apex, the three whole rock analyses lying on the relevant scapolite-pyroxene tie line.

The three major elements that have been introduced into the Rössing Formation marble by the hydrothermal fluid are Si, Al and Fe. Whether calcium also formed part of the fluid is not known. The proportions of Si, Al and Fe in the skarns are plotted on a ternary diagram (see Fig. 74). Garnet facies skarn, especially, exhibits considerable variation in the proportion of Si, Al and Fe in individual samples. However, the average compositions of the various facies of skarn are surprisingly similar (idocrase and pyroxene facies skarn have identical proportions of Si, Al and Fe) indicating that the overall concentration of these three major elements within the fluid was constant. This is considered to be good evidence for only one pulse of skarn-forming fluid having passed through the Rössing Formation.

In marked contrast, the content of the minor elements, Ti, Mg, Mn, Na and K are highly variable within the system (see Fig. 75). The variations observed in this diagram are readily accounted for by differences in mineralogy and mineral chemistry of the three skarn facies. Due to the high concentrations of Ti and Mg near the fluid front idocrase and more Mg-rich pyroxene formed . With progressively more intense metasomatism higher manganese concentrations resulted in the formation of garnet and more Mn-rich pyroxene. Alkali concentrations and hence scapolite compositions in the idocrase and garnet facies are essentially the same. Marked enrichments in alkalis in the area of increased fluid/rock ratios resulted in the formation of less meionitic scapolite and low concentrations of manganese and magnesium resulted in the formation of more hedenbergitic pyroxene .

Thus the skarn facies development can be directly attributed to the different behaviour of the major elements (Si, Al, Fe) and the minor (Ti,Mg, Mn, Na and K) and trace elements within the skarn-forming fluid.It is suggested that this partitioning of minor and trace elements within the system was temperature controlled.

d) Wollastonite : The Significance of its Absence and a Discussion of X_{H_2O} and X_{CO_2} during Skarn Formation:

A particularly unusual feature of the various skarn mineral assemblages at Otjua is the absence of wollastonite. Wollastonite is a common component of metamorphic assemblages derived from the contact metamorphism (and metasomatism) of calcitic marbles. At many other replacement skarn deposits the furthermost skarn facies from the granite contains considerable wollastonite and idocrase. At Pine Creek, wollastonite is a prominent mineral in the outermost zone of skarn (Newberry, 1982), while at Mactung wollastonite facies skarn is "generally in contact with unaltered marble" and at Cantung wollastonite skarn "only occurs in weakly altered limestone pods" (Dick and Hodgson, 1982).

As carbonate rocks are metamorphosed considerable CO_2 is evolved during decarbonation reactions. The result of this decarbonation is that the pressure of the fluid phase (P_{fluid}) of metamorphosed carbonate rocks consists of the not inconsiderable partial pressures of CO_2 as well as H_2O (and other volatile phases). Therefore, when considering the stability fields of minerals in metamorphosed carbonate rocks, the mole fraction of CO_2 (X_{CO_2}) must be taken into consideration, since this variation in composition of the fluid phase results in the system possessing another degree of freedom. For example, the reaction calcite + quartz = wollastonite + CO_2 moves to the right at high temperatures, but calcite and quartz also tend to react when either the CO_2-rich fluid phase has been diluted by H_2O or the pressure of the CO_2-rich fluid has been low as in shallow contact metamorphism (Winkler, 1976,see Figs.76 and 77).

Investigations of the metamorphic assemblages developed in the metasediments at Otjua indicate that confining pressures at the peak of regional metamorphism did not exceed 4.8kb. Skarn formation occurred after the peak of regional metamorphism (520Ma), but before crystallisation of the Otjua granite (478 $\pm$ 4Ma) and thus the confining pressure during metasomatism of the Rössing Formation is somewhat arbitarily estimated to have been in the region of 3kb.

However, the following question must be asked: did load pressure (P_{load}) equal fluid pressure (P_{fluid}) in the Rössing Formation at the time of skarn formation? Winkler discusses the importance of H_2O and CO_2 produced by dehydration and decarbonation reactions and that in certain cases P_{fluid} exceeds P_{load}. At Otjua the large volumes of CO_2 evolved from decarbonation of the Rössing Formation indicate that $P_{fluid} >> P_{load}$ during replacement of the carbonate. This is supported by two pieces of evidence. Firstly, a surprising feature of the skarns developed at Otjua is that no evidence has yet been found for escape of CO_2 evolved from decarbonation reactions into the metasediments. The country rock enclosing the marble is not brecciated in any way, nor does visual examination of the country rock indicate that any metasomatism or carbonation has occurred. Secondly, investigations clearly demonstrate that there has been no isotopic exchange between CO_2 evolved during decarbonation reactions and calcite within marble from as little as two centimetres away from the skarn, i.e. evolved CO_2 has not been dispersed throughout the marble. Therefore, what happened to the evolved CO_2? Dissociation of the calcite released large volumes of CO_2 resulting in (temporarily) very high P_{fluid}. It is suggested that this increase in P_{fluid} in the skarn-forming fluid increased the tendency of the skarn-forming fluid to move up the vertical, reactive sheet of marble and that, once initiated, the replacement process was self-propagating. This implies that the replacement of the marble by the fluid happened extremely quickly and that the metasomatic event was almost certainly a constant volume process. This also indicates that the majority of CO_2 was removed from the system prior to skarn formation, i.e. that an open system was in operation (see Chapter 7). It is therefore proposed that the CO_2 generated by decarbonation of calcite drove the fluid (or at least the gaseous-rich portion of the fluid) up many thousands of metres of marble and was then dispersed into the atmosphere via deep-seated fractures. Dissociation of CO_2 may have provided oxygen to form the silicates and carbon and carbon monoxide (as well as the presence of graphite) in the system ensured a reducing environment during skarn formation.

If $P_{fluid} >> P_{load}$ in the marble during skarn formation, this has profound implications for the mineral assemblages developed in the

various skarn facies. For example, examination of Fig. 77 indicates that when P_{fluid} = 3kb wollastonite is only stable at temperatures in excess of 625°C when X_{CO_2} = 0.25. If P_{fluid} exceeded 3kb then wollastonite is only stable at even higher temperatures - almost certainly higher than the temperature of the skarn-forming fluid at Otjua.

The confining pressure at the time of skarn formation at Otjua was considerably higher than at skarns in the North American cordillera. At Cantung a confining pressure of 1 ± 0.3kb for the formation of the E zone orebody was accepted by Mathieson and Clark (1984) on the basis of sphalerite geobarometry carried out by Hutchison and Scott (1981). The maximum confining pressure in the metasediments of the Pine Creek septum prior to skarn formation was in the region of 1.5-2kb (Brown, 1980) and a pressure of 1.5kb was used by Brown et al. (1985) in calculating fO_2 - fF_2 diagrams for the skarn assemblages. Moreover, Brown et al. (1985) conclude that "the fluid composition at the time of skarn growth was water dominated; X_{CO_2} was usually less than 0.25. It is apparent that despite the prevalence of decarbonation reactions accompanying replacement of marble by skarn, high X_{CO_2} values were prevented in the skarn-forming fluid by the great influx of water carrying the Si, Al and Fe and W necessary for skarn formation". In the following discussion it will be shown that, on account of the relatively anhydrous nature of the Otjua granite, the skarn-forming fluid at Otjua is thought to have been considerably more saline with lower H_2O contents than at the previously discussed examples in North America.

The small temperature difference between the skarn-forming fluid and the metasediments at Otjua suggests that, if anything, temperatures of skarn formation at Otjua were higher than in the North American cordillera, favouring the development of wollastonite. However, at Otjua the skarn formation process occurred under considerably higher confining pressures than at Cantung or Pine Creek, hence P_{load} and (therefore P_{fluid}) was very high inhibiting wollastonite development. High X_{CO_2} values as evidenced by the anhydrous nature of the skarn in the Rössing Formation (probably in excess of 0.25) decreased the likelihood of wollastonite formation even further. At

Pf = 3kb, when X_{CO_2} = 0.5, wollastonite is only stable at temperatures in excess of 700°C (see Fig. 77). However, the presence of very minor hornblende in pyroxene facies skarn suggests an increase in X_{H_2O} in the skarn-forming fluid with progressive metasomatism. From the foregoing discussion it is apparent that the skarn-forming fluid was essentially anhydrous and therefore the term "hydrothermal fluid" has been avoided throughout this thesis.

e) Tungsten Partitioning within the Ot;ua Granite and a Review of the Possible Complexes involved in the Transport of Tungsten within the Skarn-forming Fluid:

Experimental data is of particular relevance in understanding the behaviour of tungsten in the Ot;ua granite, pegmatites and the subsequent transport of tungsten in the skarn-forming fluid and a review is given below.

Some of the initial experimental work on the behaviour of tungsten in aqueous granitic environments was conducted by Foster (1973) who showed that for the system granite-H_2O up to 6000ppm W can enter a water saturated melt at P_{H_2O} = 1-2kb at 800°C-850°C. Moreover, Foster indicated that the W content of a granite melt is probably a function of a_{H_2O} in the melt. Foster also demonstrated that tungsten is strongly partitioned into aqueous chloride solutions that are in equilibrium with granitic melts, indicating that tungsten is readily removed from a crystallising magma by chloride ions.

In their study of the Richardsons Kop wolframite deposit, Zimbabwe, Foster et al. (1978) have combined experimental and theoretical data on the stability of H_2WO_4, polytungstates and other molecular and ionic species of tungsten and concluded that polytungstates (e.g. $[H_3W_6O_{21}]^{3-}$) and simple tungstate ions (WO_4^{2-}) are dominant at low temperatures, whereas the molecular hexahalides (WCl_6 and WF_6) are present at magmatic temperatures within a halide-rich hydrothermal fluid. Moreover, Foster et al. (1978) mention that the four main controls on the transport and deposition of tungsten are f_{O_2}/f_{S_2}, $a_{Ca^{2+}}/(a_{Fe^{2+}}+a_{Mn^{2+}})$, temperature and pH. The authors placed

particular emphasis on the activities of Ca^{2+}, Fe^{2+} and Mn^{2+}, noting that scheelite is thought to form under slightly alkaline conditions.

The most recent experimental investigations into the behaviour of tungsten in granitic melt vapour systems have been conducted by Manning and Henderson (1984) and Manning (1984). The authors calculated partition coefficients for tungsten between melt and vapour for the different volatile species types at various concentrations. Manning and Henderson's data show that in the presence of chloride, tungsten partitioned strongly into the aqueous phase, the partition coefficient (K_D = molality $W_{(vapour)}$ /molality $W_{(melt)}$) increasing with increasing chloride concentration in agreement with Foster (1973). In contrast, with water and fluoride, tungsten was concentrated in the melt, though K_D values were in the range 0.53-0.84 for fluoride as opposed to 0.11 with water. At low concentrations of carbonate (CO_3^{2-}) K_D was 1.9, at high concentrations 0.36, indicating a change in behaviour of tungsten with increasing carbonate concentration. In the presence of phosphate, tungsten partitioned strongly into the fluid, showing little variation with increasing concentration, while investigations into tungsten behaviour in borate solutions suggest that tungsten partitions roughly equally between melt and fluid phases. On the basis of this experimental data combined with knowledge of theoretical tungsten complexes, Manning concluded that complexes between tungsten and fluoride, carbonate and borate anions are relatively unimportant in the transport of tungsten, but that phosphate, and chloride species in particular, are most relevant in tungsten transport. This, to a certain extent, contradicted the findings of Higgins (1980) who considered carbonate-bicarbonate complexes to be important in the transport of tungsten, especially at high fluid pressures.For the chloride species Manning suggests that at low chloride concentrations species with high W/Cl ratios (such as $H(WO_3)_2Cl$) are present whereas at high chloride concentrations complexes with low W/Cl ratios (such as WCl_6) predominate. The stabilities of tungsten complexes are particularly sensitive to changes in pH, but little data is available on the temperature dependence of tungsten complex stability.

Average tungsten concentrations in the Otjua granite are 10ppm and 14ppm in the pegmatite (see Tables 3-6 and 3-8). Granites associated with tungsten deposits often do not show abnormal concentrations of tungsten, except in greisen zones (Wedepohl, 1970) which are absent at Otjua. For example, investigations at the McDame tungsten prospect in Canada (Cooke and Godwin, 1984), where mineralisation is associated with an S-type granite with high initial $^{87}Sr/^{86}Sr$ ratios (like Otjua), show that the intrusion only contains 4ppm W which is less than the world average of 7ppm W for specialised granites (Tischendorf, 1977). The reason for these low concentrations of tungsten in relatively anhydrous granites is that the large difference between the ionic radius of W^{6+} and major ions of silicate minerals indicates that tungsten will be concentrated in the vapour phase and thus excluded from crystals until the end of magmatic crystallisation (Wedepohl, 1970; Foster et al., 1978). The presence of only minor muscovite in the Otjua granite and associated pegmatites and the lack of alteration of feldspar indicates that concentrations of water were low in the intrusives and hence tungsten did not partition into the melt. Therefore, the potential for a hidden greisen zone at Otjua is considered to be low. That Damaran granitoids of the northern Central Zone are essentially anhydrous is evident from the lack of greisen hosted tin-tungsten mineralisation throughout the orogen. It is therefore concluded that water played a minor role in controlling tungsten distribution between melt and vapour phases in the Otjua granite.

Fluorine: Fluorine concentrations in the Otjua granite are very low and was not detected in the pegmatite. Fluorite is abundant in both the idocrase and garnet facies skarns and the low content of fluorine in the intrusives is on first examination somewhat surprising. However, this is consistent with the McDame tungsten prospect where the intrusive responsible for the mineralisation has an F content of 583ppm, but some of the skarn facies contain up to 5% fluorite. Granites with extensive greisen zones almost universally have anomalous fluorine contents, but this is not the case with anhydrous granites. In the light of Manning's conclusion that fluorine complexes are not important in the transport of tungsten and the strong coherence of tungsten and fluorine behaviour in the skarn-

forming fluid at Otjua, it is suggested that the two elements were excluded from the melt phase of the granite and concentrated in the vapour phase.

Boron: Although boron concentrations in the intrusives have not been determined, the development of quartz-tourmaline nests in the Otjua granite and the abundance of tourmaline in the pegmatite indicates the presence of significant quantities of boron in the intrusives. Manning's data suggests that boron complexes are of limited significance in the transport of tungsten, though the association of tungsten mineralisation with intrusions enriched in boron is deemed to be highly significant.

Phosphorous: Concentrations of phosphorous in the Otjua granite (average = 720ppm) are just below the world average of 870ppm for granitic rocks (Goldschmidt, 1958, p.457) and phosphorous contents in the Rössing Formation marble (491ppm) are significantly higher than the world average for marine calcite sediments (150-200ppm; Goldschmidt, 1958, p.464) and may partly account for the higher concentrations in the various skarn facies (idocrase facies = 808ppm; garnet facies = 410ppm; pyroxene = 611ppm). The only phosphorous mineral to be noted in the various skarn facies and intrusives is minor apatite and it is therefore considered that phosphorous only played a minor role in the transport of tungsten in the skarn-forming fluid at Otjua.

Arsenic: Based on the observation that tungsten ores are commonly associated with arsenopyrite (FeAsS) and löllingite $(Fe\ As)_2$, Manning (1984) has suggested that arsenic is involved in the transport of tungsten. However, the absence of arsenic minerals and sulphide mineralisation in the various skarn facies indicates that arsenic was not involved in the transport of tungsten in the skarn-forming fluid.

Carbon dioxide: The possibility that CO_2 played a role in the transport of tungsten from the Otjua granite cannot be excluded. If the Otjua granite is indeed derived from the anatectic products of the calc-silicate - carbonate -rich sediments of the Lower Swakop Group as has been suggested, then CO_2 would comprise a significant proportion

of the fluid phase of the granite melt. Moreover, the skarn-forming fluid was undoubtedly released from the Otjua granite under a high confining pressure (see Higgins, 1980 for discussion on tungsten transport under high pressure).

Chloride: Fluid inclusion studies at King Island (Kwak and Tan, 1981) and at Cantung (Mathieson and Clark, 1984) indicate that chloride species are of particular relevance in the formation of tungsten skarns. In the absence of any geochemical evidence it is inferred that very low concentrations of water and the presence of significant chloride species resulted in a strong partitioning of tungsten into the fluid phase of the Otjua granite and that halide species predominated over all others within the skarn-forming fluid. On account of the anhydrous nature of the Otjua granite and associated intrusives, it is suggested that the salinity of the skarn-forming fluid at Otjua was considerably higher than at skarn deposits elsewhere in the world. Stormer and Carmichael (1971) have shown that the concentration of Cl^- in the aqueous phase of a granite melt is enhanced by high magmatic a_{SiO_2}: the Otjua granite is highly silicic. These high concentrations of chloride ions resulted in the transport of tungsten as hexahalide species (WCl_6 , WF_6) which explains the coherence of tungsten and fluorine within the skarn-forming fluid.

Although under equilibrium conditions fluoride complexes of tungsten are preferentially concentrated in the melt, it is suggested that, with the explosive release of the aqueous (chloride-rich) phase all volatile components escaped essentially simultaneously from the Otjua granite.

The economic relevance of the foregoing discussion is that due to the anhydrous nature of Damaran granitoids associated with tungsten skarn mineralisation, tungsten concentrations in Damaran granites are low (compared to greisen zones hosting wolframite mineralisation). Therefore little importance should be attached to the tungsten content of a granite when assessing its relationship to (or its potential to have been responsible for) skarn mineralisation. Moreover, it is strongly suggested that, in the Damaran, the type and concentration of volatiles (especially water and fluorine) within the granite magma are

the main controls on how far a skarn deposit may form from the granite body.

The following four reactions are considered to describe scheelite and fluorite formation within the Rössing Formation:

i) $WF_6 + 4CaCO_3 \longrightarrow 4CO_2 + 3CaF_2 + CaWO_4$

ii) $WCl_6 + 4CaCO_3 \longrightarrow 4CO_2 + 3CaCl_2 + CaWO_4$

iii) $(WO_3)_{12}.4H_2O + 12CaCO_3 \rightarrow 12CaWO_4 + 12CO_2 + 4H_2O$

and possibly

iv) $H_3PO_4(WO_3)_{12} + 12CaCO_3 \rightarrow 12CaWO_4 + 12CO_2 + H_3PO_4$

$(3H_3PO_4 + 5CaCO_3 \longrightarrow Ca_5(PO_4)_3OH + 4H_2O + 5CO_2)$

The high ratio of $CaF_2/CaWO_4$ in the skarns suggests that $a_{WF_6} >> a_{WCl_6}$.

f) Model of Skarn Formation at the Otjua Prospect:

i) Introduction:

Before discussing a model of skarn formation it must be clearly stated that this is an attempt to explain a complex process from borehole information alone. Not all borehole intersections exhibit all of the mineralogical features discussed. A model of skarn formation must account for the skarn facies development, the changes in mineral chemistry, the petrographic features of the skarn facies as well as the distribution of scheelite and fluorite and a brief summary of these is given below. A diagramatic cross-section of the Rössing Formation marble is given to help explain the metasomatic process (see Fig. 78). It is especially important to visualise the three-dimensional geometry of the marble pods (C) in the garnet facies skarn.

The ACF diagram (Fig. 73) clearly shows the similarity in overall composition between the idocrase and garnet facies. Both facies contain the most meionitic scapolite and the highest concentrations of scheelite within a garnet-rich core zone suggesting an increase

in Ca^{2+} availability in the centre of the skarn (see Figs. 79, 80 and 81). The similarity in overall chemistry of the idocrase and garnet facies is also evident from the inter-element ratio data (see Table 16). The ratio Ca/(Si + Al + Fe) gives perhaps the best indication of the intensity of the metasomatic process since these four elements comprise the bulk of the skarn assemblages. In contrast, the ACF diagram and inter-element ratios clearly distinguish the pyroxene facies skarn from other facies indicating the significantly lower proportion of Ca in the zone of increased fluid/ rock ratios.

Several clues as to the manner of the skarn-formation process are provided by the textural features of the skarn facies. In the idocrase facies skarn the coarse grained, prismatic nature of the idocrase is unique amongst all the skarn minerals developed at Otjua. It is suggested that this is because of the extensive recrystallisation of calcite in an area of low fluid/rock ratios. Because of the small amounts of fluid present at the fluid front, crystallisation of minerals had a significant effect on the composition of the remaining fluid, resulting in concentric compositional zoning in the idocrase crystals.

The garnet facies possesses a predominantly granoblastic texture in the footwall and hanging wall peripheral zones and a poikiloblastic-granoblastic texture in the garnet- dominated core. In the peripheral zones which are dominated by pyroxene and scapolite (and fluorite on the handing wall side) the minerals are commonly found at triple junctions in equigranular aggregates. This relationship between scapolite and pyroxene is also present in the idocrase facies and indicates contemporaneous crystallisation of the two minerals. In contrast, in the core of the garnet facies skarn, the late stage nature of the garnet is clearly evident: a xenoblastic-poikiloblastic habit enclosing all other phases. The large compositional variations of the garnet over distances of less than 50 microns are in contrast to all other minerals indicating that garnet in particular was crystalling from a fluid of fluctuating composition. This suggests that garnet formed from residual fluid in the core of the skarn - the last portion of the garnet facies to crystallise.

The textural feature of the pyroxene facies is an inequigranular, coarse grained polygonal mosaic which indicates a relatively high temperature of formation. It is suggested that the lack of textural zoning across the skarn results from high fluid/rock ratios which maintained similar temperatures across the width of the Rössing Formation. Furthermore, the lack of mineralogical zonation indicates that pyroxene facies skarn crystallised from a fluid of relatively constant composition unlike the garnet facies.

ii) Presentation of model of skarn formation:

It was decided that in the absence of any better criteria, the best way of describing the fluid/rock ratio during metasomatism of the Rössing Formation would be to plot the amount of calcite in the various skarn facies, since the skarn formation process essentially involves the dissolution of calcite. The calcite contour diagram is shown in Fig. 82 showing a progressive decrease in the amount of calcite in the various facies which is interpreted as an increasing fluid/rock ratio with increasing metasomatism.

In the area now represented by idocrase facies skarn the preferential development of skarn on the hanging and footwall contacts suggests that the country rock - marble contact acted as a channel of higher permeability for the skarn-forming fluid (see fluid front in Fig. 78). In the area now represented by garnet facies skarn, where the marble was incompletely replaced, fluid/rock ratios were high on the country rock - marble contacts as well, but where the Rössing Formation has been completely replaced across strike, fluid/rock ratios were higher on the footwall side. The absence of calcite in those portions of the Rössing Formation replaced by pyroxene facies skarn indicates that fluid/rock ratios were highest where metasomatism was most intense.

Data on the temperature of formation of the various skarn facies at Otjua is unfortunately not available. However, temperatures of formation of anhydrous skarn silicate assemblages at other skarn deposits are in the range 500°C to 600°C (Einaudi et al., 1981). It is suggested that the skarn-forming fluid was released from the Otjua granite at a temperature of 650°C. In the preceding discussion it

was concluded that the skarn formation event occurred considerably after 520Ma and before 478Ma. Therefore the metasediments at Otjua were at a temperature of 300-400°C at the time of skarn formation (Haack, 1983, p.881, Fig. 9).

Although a thermodynamic study of the skarn formation process is not possible due to a lack of experimental data a few general statements can be made. The reaction $CaCO_3 \longrightarrow CaO + CO_2$ is endothermic. This means that calcite dissolution occurred fastest in those areas where the skarn-forming fluid was hottest. However, the majority of reactions involving the crystallisation of skarn minerals were almost certainly exothermic so that the heat budget (and therefore temperature of the fluid) was probably not decreased by calcite dissolution. The late stage nature of the garnet indicates that the temperature of the fluid was highest in the core zone throughout skarn formation.

In trying to understand the thermal structure during skarn formation the following model is proposed. As the hydrothermal fluid progressively moved through the reactive marble, the temperature difference between the carbonate and the skarn-forming fluid would result in loss of heat from the latter into the marble and the country rocks. Temperatures at the "fluid front" (see Fig. 78) would consequently drop substantially. Where the fluid only replaced 25% of the thickness of the marble (distance t_1), the surface area to volume ratio of fluid in contact with the metasediments would be considerably higher than where the fluid completely replaced the marble (distance t_2 ,). Therefore fluid temperatures would drop at a faster rate and to a lower value at point A than at point B. Moreover, because the fluid/rock ratio is higher at B_1, than at B_2 (see Fig. 82) the temperature of the fluid would drop at a faster rate at B_2 than at B_1 : the higher flowthrough of fluid would essentially maintain higher temperatures on the footwall side of the Rössing Formation. In areas of highest fluid/rock ratios (point D) the increased flow of fluid maintained an even temperature across the Rössing Formation. The above model is the basis for the theoretical isotherm diagram (Fig. 83).

There are several points worthy of emphasis in Fig. 83. Note that the hottest part of the fluid in the portion represented by garnet facies skarn is not in the centre of the Rössing Formation but is "footwall shifted" (point B). At point E the temperature is below 550°C, but the fluid/rock ratio is relatively high at this point (see Fig. 82) in comparison with point F at the fluid front where the temperature is similarly low, but the fluid/rock ratio is at a minimum. At point D due to the higher fluid/rock ratio fluid temperatures remain above 625°C across the whole width of the Rössing Formation.

iii) Summary of skarn-formation model:

The major controlling factors on the skarn formation process were the fluid/rock ratio and the fluid activity across strike within the Rössing Formation. These two factors dictated the rate of dissipation of heat from the skarn-forming fluid into the metasediments and consequently the temperature of formation of the skarn assemblages. The fluid/rock also controlled the $a_{Ca^{2+}}/a_{\text{Introduced elements}}$ ratio (essentially the intensity of metasomatism) which, in turn, controlled the mineral assemblages of each facies, but a strong (temperature dependent?) partitioning of minor elements within the system was responsible for the variations in mineral chemistry.

iv) An explanation of scheelite crystallisation:

Fluid inclusion studies of hydrothermal tungsten deposits frequently indicate the presence of high temperature, moderately saline (NaCl) aqueous fluids or fluids possessing high carbon dioxide contents or fluids with both these properties (Kwak and Tan, 1981; Mathieson and Clark, 1984; Manning, 1984). This is inferred to have been the case with the skarn-forming fluid at Otjua. The presence and relevance of the CO_2 -rich inclusions is discussed by Manning (1984): "No evidence was produced by the experimental work that carbonate solutions will transport tungsten effectively at 800°C and increasing carbonate concentration appears to have a negative effect on the solubility of tungsten in the fluid. This observation suggests three possibilities: that a change takes place in the behaviour of tungsten in CO_2-bearing solutions with a reduction in temperature; that the presence of CO_2-

rich inclusions in association with tungsten ores is coincidental; or that the presence of CO_2 affects the stability of tungsten and other elements, an augmentation in CO_2 reducing the solubility of tungsten in the fluid".

Because dissolution of calcite at the fluid front (idocrase facies) was not very extensive it is suggested that significantly less CO_2 was available to reduce the solubility of tungsten in the skarn-forming fluid than where the garnet facies subsequently formed, i.e. the higher fluid/rock ratio in the garnet facies resulted in greater dissolution of calcite and hence increased availability of Ca^{2+} ions for scheelite formation. Moreover, because the reaction $CaCO_3 \rightarrow CaO + CO_2$ is endothermic, dissolution of calcite occurred at a faster rate in the hottest portion of the skarn-forming fluid, i.e. the footwall shifted core of the garnet facies skarn (see Fig. 83). Thus the main control on scheelite formation was the temperature dependent dissolution of calcite which: (1) produced large volumes of CO_2 which decreased the solubility of tungsten (by increasing pH?) within the skarn-forming fluid and (2) simultaneously ensured the availability of Ca^{2+} ions for scheelite (and fluorite) formation. This model explains why scheelite distribution and scapolite chemistry are so closely related-both were controlled by the availability of Ca^{2+}.

This model also explains why scheelite concentrations in the garnet facies correlate positively with skarn thickness (+0.55) and with percentage skarnification of the Rössing Formation (+0.54): where replacement of the marble across strike was more extensive the fluid was hotter and calcite dissolution occurred at a faster rate. This also explains the scheelite distribution in the idocrase facies - scheelite is only present in the thickest portions of the facies. Overall tungsten grades in the idocrase facies are significantly lower, because idocrase facies skarn formed from a cooler part of the fluid than the garnet facies.

The absence of scheelite in pyroxene facies skarn can be directly attributed to the increased fluid/rock ratio and the fact that the calcite had already been dissolved: hence no or very little CO_2 was available to precipitate tungsten. The increase

in the $a_{Ca^{2+}}$ / $a_{\text{Introduced elements}}$ ratio caused a decrease in Ca^{2+} activity resulting in the cessation of scheelite formation, though paradoxically, temperatures were favourable for extensive dissolution of calcite. The decline in Ca^{2+} activity in this area of increased fluid/rock ratio also terminated fluorite formation and the drop in the Ca/(Na + K) ratio to 12.7% of the value at the fluid front resulted in the change in scapolite composition.

v) An explanation of fluorite distribution:

Examination of borehole intersections of garnet facies skarn show that there is a positive correlation between overall concentrations of WO_3 and CaF_2 (+0.44) as well as positive correlations between concentrations of fluorite and skarn thickness (+0.41) and percentage skarnification (+0.56). This distribution of scheelite and fluorite suggests that tungsten and fluorine were concentrated for similar reasons - essentially the availability of Ca^{2+}. It has already been suggested that the availability of Ca^{2+} was essentially temperature controlled and was highest in the core of that portion of the fluid from which garnet facies skarn formed. Petrological investigations indicate that fluorite is universally anhedral and frequently envelops all other minerals suggesting crystallisation late in the paragenetic sequence. However, fluorite is especially concentrated towards the hanging wall of the Rössing Formation in those portions of the skarn where the carbonate has been most extensively replaced across strike. Examination of Fig. 83 shows that this was the coolest part of the fluid from which garnet facies skarn formed. This suggests a migration of $Ca^{2+}(F^-)_2$ from the core zone towards the periphery of the skarn. This is considered to be the most likely explanation for the positive correlation between fluorine and tungsten concentrations in those portions of the garnet facies where metasomatism across the width of the Rössing Formation was most extensive, but also the strongly antipathetic nature of scheelite and fluorite distribution across garnet facies skarn (see Fig. 10).

g) Skarn Formation at Other Prospects in the Schönfeld Dome:

A review of skarn formation at the Tjirundo, Schönfeld and Roidina prospects is given below and a general model for skarn formation within the Schönfeld dome is proposed. A longitudinal section in the plane of the Rössing Formation is shown in Fig. 84 which summarises the geometry of the skarn systems.

i) Skarn formation at the Tjirundo prospect:

The skarn facies developed at the Tjirundo prospect are somewhat different from Otjua and are summarised below:

1) Idocrase facies : this facies is poorly developed in contrast to Otjua and contains very minor scheelite. Minor wollastonite is locally present.

2a) Garnet facies: unlike Otjua, this is an extremely inequigranular assemblage of minerals ranging in size from hundreds of microns to 30 centimetres. This facies has a wider variety of minerals than the garnet facies at Otjua: idocrase, garnet, pyroxene and scapolite all frequently exhibiting subhedral to euhedral crystal forms with interstitial fine to very fine grained quartz, scapolite, epidote, minor fluorite, clinozoisite, amphibole and considerable calcite. The skarn is vuggy in nature with calcite frequently found in vugs between euhedral silicate crystals. Reaction rims in garnet are locally developed and the hydrous mineral assemblages frequently rim or crosscut anhydrous minerals. Finely disseminated scheelite is present, the average WO_3 concentration being 600ppm.

2b) Amphibole-scapolite-scheelite facies: this facies is sporadically developed within the garnet facies. The amphibole is not a retrograde mineral or an alteration product. It is a primary mineral, though locally poikilitic and the mineralogy of this facies is fairly simple: scapolite (40-55%), hornblende (45-55%), calcite (0-15%), epidote (0-2%), opaques (0-2%), scheelite (0-2%) and minor fluorite. A particularly noteworthy fact about

this facies of skarn is that where it is fine grained and equigranular it hosts considerable scheelite mineralisation (up to 0.88% WO_3), but, where the scapolite and hornblende are coarse grained, euhedral and prismatic, the skarn is essentially barren of tungsten.

3) Pyroxene Facies: the overall appearance, mineralogy and texture are indistinguishable from the pyroxene facies at Otjua. WO_3 contents are in the range 0-200ppm.

The skarn formation process at the Tjirundo prospect is thought to have operated in essentially the same manner as it did at Otjua: progressive replacement of the Rössing Formation marble by a fluid that emanated from a granite. However, the presence of a number of hydrous minerals (epidote and amphibole) in the skarn assemblages at Tjirundo indicates that X_{H_2O} during the skarn formation process was considerably higher than at Otjua. The presence of minor wollastonite in the peripheral facies of the skarn also indicates that X_{CO_2} was considerably lower than at Otjua. Muscovite is well developed in the pegmatites and intrusive rocks at Tjirundo (in contrast to Otjua), though alteration of feldspar is minimal. This strongly suggests that a_{H_2O} was considerably higher in the intrusives at Tjirundo than at Otjua. Furthermore, the very minor fluorite within the skarn facies assemblages at Tjirundo indicates that a_{H_2O}/a_F was considerably higher in the Tjirundo granite than in the Otjua granite.

Although the regional metamorphic conditions at the Tjirundo prospect are considered to have been similar to those at Otjua through time (similar P_{load} and temperature), the higher fluorine content and the lower a_{H_2O}/a_F within the Otjua granite magma resulted in both a higher P_{fluid} within the Otjua granite and a more complete segregation of volatiles into the fluid phase of the magma than in the Tjirundo granite. As a result P_{fluid} exceeded P_{load} in the Otjua granite at a greater depth within the earth's crust resulting in volatile release under higher confining pressures at Otjua than at Tjirundo. The higher a_{H_2O}/a_F in the Tjirundo granite magma possibly resulted in the retention of many of the volatile components within

the magma so that the skarn-forming fluid was considerably more viscous at Tjirundo than at Otjua.

This model explains a number of features:

1) Fluid/Rock ratio at Tjirundo:

Fluid/rock ratios in the portion of the fluid from which garnet facies skarned formed at Tjirundo were considerably lower than at Otjua. This is indicated by the large percentage of interstitial calcite in the vuggy garnet facies . Garnet facies skarn from Tjirundo would plot at point A on the calcite contour plan of Otjua (Fig. 82).

2) Temperature of formation of Tjirundo skarn:

Petrographic studies of the garnet facies at Otjua indicate the presence of curved grain boundaries and an overall metamorphic texture suggesting a high temperature of formation (and rapid crystallisation?) compared to the very coarse grained, prismatic, inequigranular garnet facies of Tjirundo which suggests a much slower process of crystallisation at lower temperatures. The textural features of the garnet facies at Tjirundo are somewhat similar to those of the idocrase facies at Otjua, which crystallised from an area of low fluid/rock ratios.

3) Scheelite formation:

It was concluded that the main controlling factor on scheelite formation in the garnet facies at Otjua was the availability of Ca^{2+}, which, in turn, was dependent on the rate of dissolution of calcite. Because of lower fluid/rock ratios at Tjirundo the rate of calcite dissolution and temperature of skarn formation, were significantly lower than at Otjua. Therefore, scheelite is not particularly concentrated within any portion of the garnet facies skarn at Tjirundo. Moreover, the higher a_{H_2O} within the Tjirundo granite probably resulted in retention of significant amounts of tungsten within the pluton.

The possibility that a volatile-rich (especially fluorine) portion of fluid was released from the Tjirundo granite, from which an Otjua-type idocrase and garnet facies orebody formed considerably above the present day erosion level cannot be precluded (see Fig. 84). However, because the roots of the skarn system (pyroxene facies) are preserved at a higher altitude it is strongly suggested that higher a_{H_2O}/a_F ratios within the Tjirundo granite ensured the release of volatiles at a lower confining pressure (and a less explosive release) than at Otjua.

Due to poor exposure, the relationship between garnet facies skarn and amphibole facies skarn cannot be determined. However, the fine grained scheelite-bearing amphibole skarn does not appear to replace or crosscut the garnet facies and it suggested that this facies formed from localised "pockets" of high X_{H_2O} within the skarn-forming fluid. The presence of several hydrous minerals within the garnet facies indicates a higher overall X_{H_2O} than at Otjua. That the fine grained equigranular type of amphibole skarn hosts the scheelite mineralisation rather than the coarse grained variety also suggests that scheelite is concentrated in areas where skarn formed at higher temperatures (where calcite dissolution was most rapid and extensive). Fluorite is also particularly concentrated within the fine grained amphibole facies skarn relative to garnet facies skarn.

ii) Skarn formation at the Schönfeld prospect:

The mineralogy of the skarn facies is summarised below.

1) Idocrase facies skarn is poorly developed and contains minor hornblende, epidote and pyroxene.

2) There are two types of garnet facies skarn at the Schönfeld prospect. Type I is similar to garnet facies skarn at Otjua, though contains less fluorite. Type II is similar to the garnet facies skarn at Tjirundo, but does not contain amphibole-scapolite-scheelite facies. There is no evidence that one type of garnet facies skarn crosscuts, replaces or overprints the other. They are considered to be contemporaneous.

3) The pyroxene facies is similar to Otjua but contains considerable epidote and amphibole and minor pyrrhotite.

The skarn system appears to be intermediate between the Otjua and Tjirundo systems. The pockets of Type I garnet facies within Type II skarn indicate local areas of high X_{CO_2} and high W and F concentrations within a fluid with higher X_{H_2O} than Otjua. The fact that the roots of the skarn system are exposed at a higher altitude than at Tjirundo suggests that P_{fluid} in the granite was much less than at Otjua while the relative absence of pegmatite at the Schönfeld prospect suggests that the granite had a lower volatile content in general. However, the possibility that an Otjua-type orebody existed above the present day erosion level cannot be excluded.

iii) Skarn formation at the Roidina prospect:

The Roidina skarn is developed over a distance of 500m but is poorly exposed. No marble is visible on surface, thus it has only been assumed that the calc-silicate assemblage has replaced the Rössing Formation. However, stratigraphic correlations indicate that the skarn is in the zone where the Rössing Formation marble should be, is of similar thickness and that the mineral assemblage shows some of the features of the Otjua skarn. Only one skarn facies is present, an extremely hard, fine to medium grained rock comprising approximately equal proportions of grossular garnet and hedenbergitic pyroxene. The skarn is not zoned across its width.

In thin section the overall texture is very similar to the Otjua skarn, i.e. granoblastic-poikiloblastic. Triple point junctions between pyroxene grains are common, while xenoblastic garnet may be interstitial to other minerals, poikiloblastic or even skeletal. Minor scheelite occurs as round (100-500 µ) grains occurring in clusters, associated with garnet and pyroxene . Very minor calcite, sphene, chlorite, quartz and opaques are also present. Electron microprobe analysis has shown the chemistry of garnet and pyroxene from Roidina and Otjua to be similar.

However, several significant differences between the Otjua and Roidina skarns are apparent. The Roidina skarn:

1) contains no fluorite. This is in contrast to Otjua where the garnet facies contains approximately 8% CaF_2.

2) contains very minor scheelite: the Roidina skarn is anomalous in tungsten in the order of tens to hundreds of ppm, but this is significantly below WO_3 contents in the garnet facies at Otjua. Geochemical analysis of samples and percussion borehole dust indicate the Roidina skarn to be of no economic interest.

3) possesses very minor scapolite - < 5%. This is in contrast to the Otjua occurrence where scapolite comprises 30-40% of the mineral assemblage.

4) has a high clinozoisite content (5-10%). This mineral is universally in contact with scapolite and garnet, the latter often enveloping it. Clinozoisite is virtually absent at Otjua, indicating that X_{H_2O} during skarn formation was higher at Roidina than at Otjua.

5) is developed very close to a granite. Granite is exposed within 100m of the skarn.

It is thought that the Roidina skarn represents complete skarnification of a marble unit by SiO_2-dominated, slightly hydrous residual fluids. Potential for tungsten mineralisation at depth towards the granite contact is very low.

iv) Conclusion:

From the preceding discussion it is apparent that the amount of volatiles within the skarn-forming fluid and the proportions of X_{H_2O} and X_{CO_2} were of critical importance in determining the mineralogy and mineralisation developed in the four skarn prospects. It is also clear that tungsten is concentrated within portions of a skarn system and when assessing a skarn's potential to contain tungsten the

individual facies must be treated as a part of a system. The three types of skarn system developed within the Schönfeld dome are therefore:

1) Anhydrous volatile-rich system - Otjua
2) Hydrous volatile-rich system - Tjirundo/Schönfeld
3) Anhydrous volatile-poor system - Roidina

h) The Relationship between Structure, Skarn Formation and Pegmatite Intrusion - a Possible Explanation:

The Otjua prospect lies within 6km of the Omaruru Fault Zone (see Map 1) which is the surface expression of the Omaruru Lineament oriented 053°. This fault zone was active in Damaran times and movement on this structure may account for the consistent orientation of cross-cutting pegmatites at the Tjirundo, Schönfeld and Otjua prospects. It is suggested that dextral movement on the Omaruru Fault Zone was reponsible for the formation of a series of regional stress zones in a shear couple (the ductile equivalent of tension gashes) oriented at 60° to the major fracture (see Fig. 85). The word tension gash is used to describe these zones for want of a better word.

As late Damaran granites progressively intruded the metasediments, volatile fluids from the magma were expelled into the carbonates of the Lower Swakop Group. Contact metasomatic skarns developed on the granite/marble contact, while tungsten and fluorine-rich fluids under high pressure preferentially migrated into low pressure zones, for example areas where the carbonate was cross-cut by these regional tension gashes. Skarn-forming fluids moved hundreds (maybe thousands) of metres away from the intrusive. Subsequently the pegmatitic phase of the granites intruded the metasediments parallel to the regional schistosity, but also locally, taking advantage of pre-existing tension gashes (and possibly new ones set up by further movement on the Omaruru Fault Zone). This model helps explain the following features:

1) The consistent regional orientation of the cross-cutting pegmatite.

2) The close association of skarn and cross-cutting pegmatite and more specifically the consistent angle of 10-15° between the strike of the metasediments and the strike of the cross-cutting pegmatite at the Tjirundo, Schönfeld and Otjua prospects.

3) Why pyroxene facies skarn when located near a major cross-cutting pegmatite (an original tension gash) can be situated above garnet facies skarn (compare boreholes OT14 and OT26, Long. Sect. 1)

Chemical controls are often cited as being of overwhelming importance in the location and formation of skarn deposits, but this study of four skarn systems within the Schönfeld dome has shown that structural features maybe of great importance when fluids have been released from a granite under high pressure. P_{load} during skarn formation in the Damaran was considerably higher than confining pressures in the Circum Pacific.

i) Conclusions:

This model has hopefully made an advance in the understanding of how skarn systems develop. The following list summarises the most fundamental discoveries of this investigation into skarn formation at the four prospects.

1) At Otjua, the three facies of skarn, the pegmatite and the Otjua granite are regarded as a continuum that crystallised from an anhydrous granite magma. The magma possessed a significant non-hydrous volatile component that locally reacted with and subsequently replaced carbonate metasediments.

2) Tungsten and fluorine are concentrated in the volatile-rich part of the skarn system which is usually situated farthest from the granite.

3) When assessing the potential of a skarn to host tungsten mineralisation, each facies must be treated as a part of a skarn system. Within the Schönfeld dome the root zone of a skarn system (pyroxene facies) contains very minor tungsten.

4) Calculations of the total tonnage of skarn in the Rössing Formation at the four prospects indicate the presence of 5.4mn tons of skarn. Allowing for skarn hosted by other carbonate units, and considerable post-Damaran erosion, the total amount of skarn within the four systems would have exceeded 10 million tonnes. These skarn systems are therefore of a considerable size by world standards.

5) The proportions of X_{H_2O} and X_{CO_2} were of critical importance in determining the skarn mineral assemblage that developed and is indeed the key to understanding the differences between the four prospects.

6) It seems unlikely that the water within the skarn systems (for example amphibole in pyroxene facies skarn) is derived from meteoric sources. The anhydrous nature of the Otjua granite can account for the very low X_{H_2O} during skarn formation at Otjua. Even at Tjirundo, where X_{H_2O} was considerably higher during skarn formation, it seems more likely that the water within the skarn is derived from magmatic sources.

7) Because the skarn-forming fluid was released under such high confining pressures the fluid streamed up the marble from a focal discharge point - the apex of the granite. The resultant skarn system therefore has two large dimensions and one very small one (thickness).

8) The tungsten content of a granite is a factor that must be treated with some caution when assessing a granite's potential to have been responsible for tungsten skarn development. A granite possessing high muscovite contents had high a_{H_2O} in the magma, hence tungsten tended to partition into the melt phase and is therefore concentrated in the granite. Thus a muscovite-rich granite may have a high tungsten content, but have a lower potential to form tungsten skarn deposits (or at least the skarn will be developed close to the pluton). Low tungsten concentrations in a granite possessing no muscovite (therefore low a_{H_2O} in magma) indicate a partitioning of tungsten into the volatile phase of the magma and tungsten-bearing skarns may be present, albeit at some considerable distance from the pluton.

9) Where a skarn develops in relation to the granite is controlled by a number of factors:

i) The amount of water in the melt. High a_{H_2O} will tend to retain tungsten in the melt. It is suggested that a_{H_2O}/a_{Halide} is the most fundamental control on the partitioning of tungsten between melt and vapour phases of a magma.

ii) A high volatile content plus low a_{H_2O}/a_{Halide} will ensure that P_{fluid} exceeds P_{load} at great depth resulting in an explosive release of the volatile phase as at Otjua.

iii) P_{load} is obviously critical since P_{fluid} must exceed P_{load} for release of volatiles.

iv) Because a_{H_2O}/a_{Halide} is (generally) low in the Damaran (due to the anhydrous nature of the intrusives) endoskarn development in minimal.

10) Although the skarn-forming fluid probably did react with the scheelite-bearing hornfels where the granite was in immediate contact with the metasediments, extensive interaction between the volatile-rich fluid and the hornfels did not occur (see discussion in Chapter 9).

9. THE ORIGIN OF THE SCHEELITE IN THE METASEDIMENTS

a) Introduction:

The extensive areal distribution of scheelite within hornfels and calc-silicates of Precambrian age in the vicinity of the Otjua prospect is a discovery of particular note. The stratabound nature of the tungsten mineralisation bears similarities to some of the styles of mineralisation discussed in Chapter 3, especially that described by Beran et al. (1985). Possible mechanisms that could account for the anomalous concentrations of tungsten and fluorine within the calc-silicates and scheelite-bearing hornfels of the Khan and Oberwasser Formations are reviewed below.

b) Introduction of Metals Contemporaneous with Infiltrational Metasomatism of the Rössing Formation:

In comparison to the Rössing Formation marble, where a vertical layer of calcite has been skarned by a metasomatic fluid, the calc-silicates and scheelite-bearing hornfels do not represent good channelways for migrating hydrothermal fluids. These two lithologies are laterally discontinuous and contain very minor carbonate. No feeder zones, breccia pipes or crosscutting fractures that could have acted as channelways for mineralising fluids have been recognised within the metasediments. Petrological studies indicate that the scheelite in the hornfels is part of a stable metamorphic assemblage and geochemical investigations clearly show that the major and trace element geochemistry of the scheelite-bearing hornfels is very similar to that of the calc-silicates (for which a sedimentary origin is indicated). The various skarn facies have geochemical characteristics distinct from the scheelite-bearing hornfels and calc-silicates; for example, the WO_3 : F ratio of the metasediments is greater than 0.5 while in the skarn it is ± 0.1 indicating that tungsten and fluorine were introduced into the metasediments and the skarn under different physico-chemical conditions. Isotopic studies show that the interstitial calcite in the skarn has a restricted range of $\delta^{18}O$ values in marked contrast to the calcite within the scheelite-bearing hornfels.

The lack of evidence for large-scale metasomatism of the metasediments and the absence of significant hydrothermal alteration within the Otjua granite and pegmatites precludes the possibility that a hydrothermal convection cell (where large volumes of tungsten were leached from the granite by meteoric waters and deposited in the metasediments) was in operation. Taylor (1977) has shown that epizonal granitic intrusions that have been emplaced at shallow levels within the earth's crust have acted as "heat engines" to form hydrothermal convection cells. These intrusions are characterised by sub-volcanic ring complexes associated with explosion breccias, extensive alteration of feldspar and miarolitic cavities within the intrusives, highly fractured country rocks and, because of the extensive interaction with meteoric waters, unusually low $\delta^{18}O$ values. All these features are absent from the Otjua granite which contains very minor muscovite, is relatively anhydrous and possesses an anomalously high $\delta^{18}O$ value. The possibility that the magma from which the Otjua granite crystallised interacted with meteoric water with an isotopically light composition cannot be excluded. This does seem unlikely though, since at the time of skarn formation, the metasediments at the Otjua prospect were undergoing regional metamorphism at a pressure of 3kb. Winkler (1976) has suggested that load pressure increases at a rate of about 250-300 bars/kilometre which means that the Otjua granite intruded at a depth of 10-12 kilometers - almost certainly below the depths of circulating ground water. The very low concentrations of tungsten and fluorine in the pegmatites do not indicate that these intrusives were responsible for the introduction of mineralisation either. Moreover, the presence of significant scheelite mineralisation within the Lower Swakop metasediments preserved within the Okakombo horst structure, where late stage Damaran granitic intrusives are conspicuously absent, indicates that this style of mineralisation is not related to or derived from granitic intrusives.

It is therefore concluded that the more calcareous metasediments of the Khan and Oberwasser Formations contained anomalous concentrations of tungsten and fluorine prior to the intrusion of the Otjua granite and associated intrusives and that the scheelite mineralisation in the hornfels is unrelated to infiltrational metasomatism of the Rössing

Formation marble and other carbonate units. An epigenetic origin for the scheelite mineralisation in the metasediments in thus rejected.

c) Syngenetic:

i) Detrital origin:

Several features argue against a detrital source for the tungsten in the metasediments. Scheelite is only present in calc-silicate and hornfels, which are interpreted as having been chemical sediments prior to metamorphic recrystalisation, while the schist, a metamorphosed mud, contains almost no tungsten. This restriction of mineralisation to the two most calcic lithologies suggests a chemical control on the localisation of scheelite. The rather brittle nature of scheelite and its hardness (4.5-5) do not suggest that scheelite would survive transportation as detrital grains over significant distances. Scheelite is not concentrated along sedimentary structures (e.g. bedding planes) in the calc-silicates or hornfels as detrital gold or magnetite would be, but is present as very finely disseminated grains throughout the host rock. There is no evidence to suggest that scheelite is pseudomorphing detrital wolframite either. Therefore a detrital origin for the scheelite within the metasediments of the Khan and Oberwasser Formations is rejected.

ii) Chemical Precipitation:

The confinement of scheelite to the calc-silicate and hornfels lithologies and the widespread regional distribution of scheelite suggests that scheelite formation occurred during interrupted periods of marl development, the tungsten either being provided from seawater or possibly exhalative brines. During essentially isochemical metamorphism the marls were converted to calc-silicates and scheelite-bearing hornfels. No evidence of remobilisation or concentration of scheelite by regional metamorphic processes has been noted and it is thought that the present day distribution of the scheelite corresponds to the original distribution of tungsten within the sediments.

The calc-silicates of the Khan and Oberwasser Formations represent metamorphosed marls and their intercalation with the discontinuous calcareous lithologies and close stratigraphic association with the highly calcitic Rössing Formation suggest that shallow marine, calcareous, sedimentary processes were in operation. The development of muds, now represented by biotite schist, indicates the presence of mature argillaceous detritus distal from its provenance area. This intercalation of chemical and detrital sediments indicates a low energy, shallow water environment. Furthermore, the extensive areal distribution of the relatively thin Rössing Formation points to considerable crustal stability (at least locally) at the time of sedimentation.

In Nosib times shallow water sediments were deposited both within and marginal to a series of rifts or graben structures within continental crust (Tankard et al., 1982). The Nosib sediments (Khan Formation) at Otjua were deposited close to the southern boundary of the northern graben (see Fig. 86). The southern boundary of this graben is marked by the Omaruru lineament (see Fig. 87) which is considered by Corner (1983) to have played a significant role in controlling sedimentation (op.cit. p.353). The absence of mass flow and conglomeratic alluvial fan deposits in the Khan and Oberwasser Formations at Otjua and the presence of mature detritus and chemical sediments suggests low relief to the south-east in Nosib and lower Swakop times and an even, slow rate of subsidence within the graben (compare with mass flow deposits in the Chuos Formation, the stratigraphic equivalent of the Oberwasser Formation, in the southern Central Zone; see Miller, 1983a). The presence of minor pyrrhotite in the Rössing Formation and sulphide mineralisation in the biotite schist and scheelite-bearing hornfels suggest a poorly oxygenated (low Eh) environment at the time of sedimentation unless the sulphides were formed from the reduction of sulphates (Hall, 1982). The presence of marble units and the considerable amounts of interstitial carbonate within the calc-silicate and hornfels indicate that the pH at the time of marl formation exceeded 7.8 (see Pettijohn, 1975, p.423, Fig. 11-27). The absence of scheelite mineralisation in the marble horizons suggests that scheelite precipitation occurred when the pH of the seawater exceeded 7.8, but before the onset of major carbonate deposition, i.e.

scheelite crystallised within a "pH window". The controlling factors on scheelite formation were therefore the availability of Ca^{2+} under the relevant Eh-pH conditions.

The Khan Formation is the stratigraphic equivalent of the Duruchaus Formation developed in the Southern Margin Zone (see Figs.2 and 86, also Behr et al., 1983). Behr et al. have shown the presence of a continental evaporitic playa-lake deposit within the Duruchaus Formation similar to others developed in continental rifts elsewhere in the world (for example the Adelaide geosyncline, Rowlands et al., 1980). These evaporitic sediments are developed within graben zones in close proximity to major fault zones and their potential to host mineralisation has been recognised by many authors (see Miller, 1983b for discussion on the possible presence of evaporites in the Khan Formation and the potential of the Duruchaus and Khan Formations to host copper and gold mineralisation).

It must be emphasised that the Khan and Oberwasser metasediments at Otjua are not interpreted as sabhka deposits. There is no evidence to suggest that any subaerial deposition occurred. Indeed the highly calcic nature of the scapolite in the scheelite-bearing hornfels (see Chapter 6) indicates that the precursor to the hornfels was rich in calcium, strongly suggesting that scheelite formation occurred in a non-emergent, Ca-rich environment. This is in contrast to the Duruchaus Formation where considerable alkali and sulphate-rich horizons have been identified in sabhka sediments. However, some of the textures identified by Behr et al. (1983) in the Duruchaus Formation are similar to those developed within the Khan and Oberwasser Formations at Otjua: for example the scapolite in Fig. 4, Behr et al. (1983, p.6).

The presence of anomalous fluorine contents (and occasional fluorite mineralisation) in the scheelite-bearing hornfels of the Khan and Oberwasser Formations at Otjua is of particular interest. Smith (1965) noted minor fluorite in quartzites of the "Upper Stage Nosib Formation" (Khan Formation equivalent) in the vicinity of the Rössing Uranium Mine, suggesting that anomalous fluorine contents may be a characteristic feature of Nosib and lower Swakop Group calc-silicates

and calcareous quartzites on a regional scale. The association of tungsten and fluorine mineralisation in the metasediments may indicate the involvement of fluoro complexes in tungsten transport.

d) Speculations on the Source of the Tungsten:

With the exception of the relatively thin Matchless Member, there are only minor occurrences of basic volcanics within the central Damaran (Miller, 1983a). No mafic volcanic rocks of Damaran age have been noted in the immediate vicinity of the Schönfeld dome. It therefore seems unlikely that the concentrations of tungsten in the lower Swakop sediments are related to submarine mafic volcanism.

In recent years mapping throughout the Damaran orogen has led to the identification of several evaporitic sequences and exhalite horizons. These sequences are usually marginal to major fractures and it has been suggested that these fractures controlled sedimentation (Corner, 1981 and 1983). For example, on the farm Ohere (see Map 1), tin, tungsten, fluorine and minor sulphide mineralisation is associated with tourmalinites, idocrase exhalites and scheelite-bearing calc-silicates of Kuiseb age which are very similar to those described from the vicinity of the Broken Hill Pb-Zn deposits (Barnes, 1983). These exhalites are thought to mark the position of syn-sedimentary growth faults, the fractures having acted as feeder zones for mineralising fluids emanating from rifted continental crust. This resulted in the development of syn-sedimentary tungsten mineralisation in the calc-silicates of the Kuiseb Formation.

A similar origin for the tungsten, fluorine and minor sulphide mineralisation within the sediments of the Khan and Oberwasser Formations is proposed. It is suggested that the Omaruru Lineament was the deep-seated fracture zone up which mineralising fluids migrated. This is important because it suggests that not only did major fractures control sedimentation, but that these faults also define metallogenic provinces. Tungsten and fluorine mineralisation within Khan Formation metasediments is therefore best developed close to the Omaruru Lineament (in low energy, restricted basins).

e) Conclusion:

It is postulated that during Nosib and low Swakop times considerable quantities of tungsten were exhaled onto the sea floor from a number of north-east trending deep-seated faults. These faults controlled sedimentation and the subsequent development of linear metallogenic provinces. Tungsten was possibly transported from the upper crust by fluorocomplexes resulting in a high concentration of tungsten and fluorine within the sea water or brines. During periods of interrupted marl formation tungsten was precipitated from seawater. The presence of a "pH window" during which scheelite formed is invoked to explain the lack of tungsten in the marble horizons.

10. SUMMARY AND CONCLUSIONS

The Otjua skarn occurrence has many similarities, though several important contrasts, with other tungsten-bearing skarns formed by infiltrational metasomatism. The similarities are summarised below:

1) The Otjua skarn is developed within a thin carbonaceous marble horizon in an intercalated pelite/calc-silicate /marble sequence.
2) A sequence of skarn facies with an idocrase periphery is developed. These facies represent progressive replacement of the marble. Mineral chemistry studies indicate that certain of the skarn facies minerals crystallised from a fluid of fluctuating composition and hence evidence of chemical disequilibrium in the skarn system is widespread.
3) The garnet facies hosts the majority of the scheelite mineralisation.
4) The silicate minerals in the later skarn facies show a tendency towards Fe and Mn enrichment.
5) Pegmatite dykes are associated with the granite that was responsible for the tungsten mineralisation and both intrusives exhibit a myrmekitic texture.
6) There are few indications of forceful emplacement of the felsic intrusives or the mineralisation and alteration of the country rock is minimal.

The major differences between the Otjua skarn and replacement skarns developed elsewhere are:

1) The granite responsible for the mineralisation is highly fractionated (in Damaran terms), exhibiting S-type characteristics and is relatively anhydrous.
2) The absence of Mo in the scheelite, skarn and intrusives is unusual.
3) The skarn system is relatively Fe-poor and the absence of notable sulphide mineralisation is uncommon.
4) The absence of a retrogressive/hydrated skarn facies containing biotite/hornblende makes the deposit very unusual.

5) There is considerable evidence for a strong structural control on the localisation of skarn deposits within the Schönfeld dome.
6) Due to the high confining pressure at the time of release of the skarn-forming fluid from the granite, the skarn is developed at a considerable distance from the intrusive (more than 400 metres).

The similarities between the Otjua skarn and other tungsten skarns suggest that skarn development as a result of infiltrational metasomatism at Otjua occurred in a similar manner to other replacement skarns. This study has also shown that the skarn formation processes that are so well documented from the Circum Pacific region (associated with mainly Cretaceous intrusions) were already in operation in the early Phanerozoic. Not only is the Otjua skarn one of the oldest examples of a tungsten replacement body, it is also one of the few documented tungsten skarns to have been formed synorogenically (albeit in the late stages) when the country rocks were undergoing relatively high grade regional metamorphism. The important differences between the Otjua skarn and other Phanerozoic tungsten skarns are thought to be a result of the different source areas of the tungsten and the intrusives. If, as has been suggested, the Otjua granite is an anatectic melt derived from Damaran metasediments, then the low sulphide and low Mo contents of the skarn are a reflection of the geochemistry of lower Swakop Group sediments.

The fact that tungsten skarn development within the Schönfeld dome has been caused by a late tectonic Damaran granite is of particular interest. Marlow (1981) concluded in his investigation of uraniferous felsic intrusives that uranium mineralisation in the Damaran is restricted to late/post-tectonic granites and pegmatites. The alaskites at Rössing Uranium Mine, at present the only economic uranium body in SWA/Namibia, are dated at 458±8Ma, the youngest age of Damaran intrusive recorded in the literature. The youngest uraniferous leucogranite investigated by Marlow (1981) was the Stinkbank leucogranite which, not only has an age similar to that of the Otjua granite (484±25Ma, Marlow, 1981), as well as a high $(^{87}Sr/^{86}Sr)_I$ value of 0.7390 (Haack et al., 1983), but has recently been discovered to be associated with tungsten-bearing skarn mineralisation. Tin mineralisation is also notably hosted by the

youngest Damaran granitoids (480-460Ma, Miller, 1983b). Thus, the discovery that tungsten skarn mineralisation in the northern Central Zone of the Damaran is associated with the later tectonic granites is consistent with other types of granite-related mineralisation throughout the orogen.

This study has also shown that there was a subtle, though important, regional tectonic control on the development of tungsten skarn mineralisation, as there is with tin and uranium in central SWA/Namibia. Corner (1981) recognised several lineament zones which he interpreted as fault controlled geanticlinal ridges (see Fig. 87, also Corner, 1983). Corner noted that most of the uraniferous granite and pegmatite occurrences in the central Damaran appear to be related to a north-north-easterly-trending structural phase ($F_{..}$- approximately 470Ma) that parallels the Welwitschia Lineament. Cores of domal structures, notably Khan Formation sediments, are more likely to be exposed along this geanticlinal ridge (Corner, 1983). Regional mapping of the Omaruru area has indicated the presence of several north-east trending F_3 domal structures in the cores of which scheelite-bearing lower Swakop Group metasediments are exposed (see Map 1). These domal structures are only developed on the north-west side of (and close to) the Omaruru lineament. Mapping has also shown that, both within the Schönfeld dome and elsewhere within the vicinity of Omaruru, tungsten skarn mineralisation is associated with leucogranites developed on the north-west side of the Omaruru lineament. This indicates that the F_3 (north-east) structural phase was of particular importance to the emplacement of late tectonic granites ($\pm$480Ma) responsible for tungsten mineralisation. Evidence for the existence of a regional shear couple within the Schönfeld dome at the time of skarn formation and pegmatite intrusion has already been discussed.

Martin (1978), amongst others, has commented on the paucity of contact metasomatic deposits in the central Damaran. Considering the widespread development of calcareous metasediments and the large number of granitic intrusions present in the orogen, this apparent lack of mineralised skarns is indeed surprising. Martin (1978) concluded that the styles of mineralisation and the predominance of granite over all

other intrusive rock types were more suggestive of widespread anatectic melting of the crust rather than the operation of plate tectonic processes during the Damaran orogenic phase. The lack of widespread hydrothermal deposits in the Damaran was attributed by Martin (1978) to the loss of permeability of the sediments during folding and perhaps more importantly the lack of syn-/post-tectonic fractures.

This study of Otjua has shown that, although not strictly hydrothermal, metasomatic deposits are developed near a major syn-tectonic fracture zone in the central Damaran. In spite of the extensive prospecting that has been conducted in central SWA/Namibia, skarn deposits have not been paid much attention due to the difficulty in identifying scheelite and the lack of sulphidic gangue in the skarn.

There has been considerable dispute over the origin of the Damaran orogeny and a number of models including an ensialic aulacogen model (Martin and Porada, 1977) and various plate tectonic models (Miller, 1983a) and subsequent modifications (Martin, 1983) have been proposed to explain the various geological features (see also Tankard et al., 1982, pp.320-326 for a review). On the basis of this study of tungsten mineralisation at the Otjua prospect it is postulated that the tungsten hosted within the lower Swakop Group sediments was derived from deep crustal sources, brought into sea water via deep-seated fractures and deposited within shallow marine marl sediments during the rifting stage of the Damara Province.

The formation of the Otjua granite and associated mineralisation is considered to have little to do with an intrusive formed in a magmatic arc at a destructive plate boundary as in the North American cordillera. Geochemical evidence (isotopic in particular) is cited to support this contention. The similarities between the styles of granite-related tungsten and uranium mineralisation in the Damaran are particularily striking. Corner (1983) concluded that the geophysical data for the central Damaran showed a stronger compatibility with the multiple aulacogen model for the Damaran of Martin and Porada (1977) than with a plate tectonic model.

Perhaps the most fundamental discovery of this investigation has been the recognition of a style of mineralisation characteristic of the Proterozoic developed in close proximity to (and suggested as the precursor for) a type of mineralisation more characteristic of the Phanerozoic. This emphasises the rather unique and transitional nature of the Damaran orogeny which spans the Precambrian-Cambrian boundary (see Fig. 88).

ACKNOWLEDGEMENTS

An investigation of this nature would not have been possible without the cooperation and support of a large number of people both in the mining industry and at the University of Cape Town. It is my sincere hope that further research work of this nature will be encouraged by all concerned.

Thank you to:

1) John Gurney for initially suggesting that an investigation of the Otjua prospect be undertaken.

2) The management of the parent companies of the Joint Venture, Rössing Uranium Limited and Johannesburg Consolidated Investment (JCI) for allowing this M.Sc. study to go ahead. Project managers Stuart Comline and Ken Hart are particularly thanked for allowing extensive sampling of drill core. Special thanks to the management of Rössing Uranium Limited and JCI for arranging study leave and paying for laboratory costs and travelling expenses to Cape Town.

3) Jurgen Hoffman and Joss Purbrick for interesting discussions during the "handover" period in early 1983.

4) Jonathan Kuyper for much advice, support, encouragement and many stimulating talks in Omaruru.

5) Derrick Pretorius and Nina Carelse for some outstanding drafting.

6) Clive Parsons for petrographic help.

7) Roger Cousins, Ralph Freese and Tony Strauss of Scientific Services for completing the tungsten and fluorine analyses for samples OT101-139.

8) Andy Duncan and James Willis for helping me understand the various XRF procedures.

9) Dick Rickard for explaining the intricacies of the microprobe.

10) Stuart Smith for advice, guidance and damage control in the isotope laboratory.

11) Nick Ikin for assistance in the isotope laboratory and especially for completing the oxygen isotope analyses of the silicates discussed in Chapter 7.

12) John Lanham for help on the mass spectrometer.

13) Nadimir Ebrahim, Shereen Abrahams, Shereen Davids and Shaamielah Davids for guiding me through various computer programmes as well as "running" XRF samples in my absence.

14) Dave Wilson for slide-cutting, Charlie Basson for photographic advice and taking pictures of sections for microprobe study, and Patrick Seass for printing maps and sections.

15) Lynnette and Stuart Smith, Dot and John Gurney, Belinda and Graham White and Torsten Vennemann for providing me with accommodation on my visits to Cape Town.

16) Anne Grant for her patience, efficiency and effort with the typing.

17) A big thank you is directed to my supervisors, John Gurney and Stuart Smith. Stuart Smith, in particular, is thanked for his advice, discussions, criticisms and proof-reading.

18) Very special thanks to my wife, Möve for her understanding and support over the last few years. An extra big thank you for drafting the diagrams.

Thank you all very much.

APPENDIX

1) Whole Rock Analyses:

Whole rock samples were analysed by X-ray fluorescence (XRF) in the Department of Geochemistry, University of Cape Town (for operating conditions, see Willis *et al.*, 1971 and 1972). All major elements, except Na, were determined using the lithium tetraborate fusion methods of Norish and Hutton (1969). Na and trace elements were analysed by XRF using pressed powder briquettes, prepared using the method of Baird (1961). Tungsten concentrations were determined by X-ray fluorescence at Scientific Services, Cape Town. Samples of idocrase and garnet facies skarn as well as scheelite-bearing hornfels containing high tungsten ($> 0.1\% WO_3$) contents as determined using pressed powder briquettes were reanalysed using lithium tetraborate fusion discs. For those samples containing high tungsten contents, the concentration determined by the fusion method is quoted in the thesis. Fluorine determinations were completed by the specific ion electrode method by Scientific Services, Windhoek.

XRF Detection Limits:

Detection limits and errors for trace elements for samples of marble (OT101) and granite (OT112) are given below in ppm:

	OT101		OT112	
	LLD	Error	LLD	Error
W	5.6	-	5.6	-
F	(487)	-	(487)	-
Rb	2.0	.7	1.5	.9
Ba	1.8	.7	2.6	1.5
Sr	2.0	1.9	1.4	.6
Th	5.2	1.7	3.9	1.4
U	4.3	1.4	3.1	1.1
Zr	2.9	1.0	1.5	.7
Nb	1.9	.7	1.4	.5
Mo	1.6	.6	1.2	.4
Cr	2.7	.9	1.6	.6
V	2.9	1.0	1.8	.7
Sc	3.4	1.3	.8	.3
Co	1.9	.6	1.6	.6
Pb	5.8	2.0	4.4	1.5
Zn	1.2	.4	0.9	.3
Cu	1.7	.6	1.2	.4
Ni	1.7	.6	1.2	.4
S	6.0	2.2	7.3	2.7
Y	2.1	.7	2.0	.7

APPENDIX

2) Electron Microprobe Analyses:

Mineral grains were analysed using a Cameca Microprobe electron microprobe in the Department of Geochemistry, University of Cape Town. The size of each polished section was approximately 2cm by 3cm. The operating conditions were as follows:

Beam Current : 40nA

Accelerating Voltage : 15kV

Analysing Crystals : TLAP for the elements Si, Al, Mg, Na
PET for the elements Ca, K, Ti, Cr
LiF (200) for the elements Fe and Mn

Detection : Flow counters with Ar/CH_4 gas mixture

The electron microprobe was calibrated using the following standards:

Si, Mg, Ca	: Synthetic Standard - Pure Dopside glass
Ti	: Synthetic Standard - Rutile
Mn	: Synthetic Standard - Rhodonite
Al, Fe	: Natural Standard - Kakanui Pyrope
Cr	: Natural Standard - Stillwater Chromite
Na, K	: Natural Standard - Kakanui Hornblende

Nominal concentrations were corrected using the methods of Bence and Albee (1968).

REFERENCES

Baertschi, P., 1957, Messung und deutung relativer Häufigkeits variationen von O^{18} and C^{13} in Karbonatgesteinen und Mineralen: Schweiz. Min. Petr. Mitt., Bd., 37, 73-152

Baird, A.K., 1961, A pressed specimen die for the Norelco vacuum-path X-ray spectrograph: Norelco Rep., 8, 108-109

Barnes, R.G., 1980, Types of mineralisation in the Broken Hill Block and their relationship to stratigraphy, 33-70. In: Stevens, B.P.J., Ed., A guide to the stratigraphy and mineralisation of the Broken Hill Block, New South Wales, N.S.W., Geol. Surv., Rec. 20

Barnes, R.G., 1983, Stratiform and stratabound tungsten mineralisation in the Broken Hill Block, N.S.W.: Jour. Geol. Soc. of Austral., 30, 225-239

Bateman, P.C., 1945, Pine Creek and Adamson tungsten mines, Inyo County, California: California Jour. Mines Geology, 41, 231-249

Bateman, P.C., 1956, Economic geology of the Bishop tungsten district, California: California Dept. Nat. Resources Div. Mines Spec. Rept., 47, 87p

Beckinsale, R.D., 1979, Granite magmatism in the tin belt of South-east Asia. In: Atherton,M.P. and Tarney, J., Eds., Origin of Granite Batholiths - Geochemical Evidence. Shiva Pub., Kent, 148p

Behr, H.J., Porada, H., Rohrs, J. and Weber, K., 1983, Upper proterozoic playa and sabkha deposits in the Damara Orogen, SWA/Namibia: Spec. Publ. Geol. Soc. S. Afr., 11, 1-20

Bence, A.E. and Albee, A.L., 1968, Empirical correction factors for the electron microanalysis of silicates and oxides: J. Geology, 76, 382-403

Beran, A., Gtod, R., Gotzinger, M. and Zemann, J., 1985, A scheelite mineralisation in calc-silicate rocks of the Moldanubicum (Bohemian Massif) in Austria: Mineral. Deposita, 20, 16-22

Blattner, P. and Bird, G.W., 1974, Oxygen isotope fractionation between quartz and K-feldspar at 600°C: Earth Planet. Sci. Lett., 23, 21-27

Borthwick, J. and Harmon, R.S., 1982, A note regarding ClF_3 as an alternative to BrF_3 for oxygen isotope analysis: Geochim. et Cosmochim. Acta, 46, 1665-1668

Bottinga, Y., 1968, Calculation of fractionation factors for carbon and oxygen isotopic exchange in the system calcite-carbon dioxide-water: Jour. Physics and Chemistry, 72, 800-808

Bottinga, Y., 1969, Calculated factionation factors for carbon and hydrogen isotope exchange in the system calcite-carbon dioxide-graphite-methane-hydrogen-water vapour: Geochim. et Cosmochim. Acta, 33, 49-64

Bottinga, Y. and Javoy, M., 1973, Comments on oxygen isotope geothermometry: Earth Planet. Sci. Lett., 20, 250-265

Bottinga, Y. and Javoy, M., 1975, Oxygen isotope partitioning among the minerals in igneous and metamorphic rocks: Rev. Geophys. Space Phys., 13, 401-418

El Bouseily, A.M. and El Sokkary, A.A., 1975, The relation between Rb, Ba and Sr in granite rocks: Chem. Geol., 16, 207-219

de Brodtkorb, M.K. and Brodtkorb, A., 1977, Stratabound scheelite deposits in the Precambrian basement of San Luis, Argentina, 141-149. In: Klemm, D.D. and Schneider, H.H.,Eds., Time and Stratabound Ore Deposits, Springer Verlag, Berlin, 444p

Brown, G.C., 1979, The changing pattern of batholith emplacement during earth history, 106-115. In: Atherton, M.P. and Tarney, J., Origin of Granite Batholiths - Geochemical Evidence. Shiva Pub., Kent, 148p

Brown, P.E., 1980, A petrologic and stable isotopic study of skarn formation and mineralisation at the Pine Creek, California tungsten mine: Unpub. PhD thesis, Ann Arbor, Univ. Michigan, 240p

Brown, P.E., Bowman, J.R. and Kelly, W.C., 1985, Petrologic and stable isotope constraints on the source and evolution of skarn-forming fluids at Pine Creek, California: Econ. Geol., 80, 72-95

Burton, J.C., Taylor, L.A., Chou, I-M., 1982, The f_{O_2}-T and f_{S_2}-T stability relations of hedenbergite and of hedenbergite-johannsenite solid solutions: Econ. Geol., 77, 764-783

Chalowpsky, J., 1978, The Precambrian tectogenesis in the Bohemian Massif: Geol. Rundsch., 67, 72-90

Chappell, B.W. and White, A.J.R., 1974, Two contrasting granite types: Pacific Geology, 8, 173-174

Clayton, R., 1971, Estudio petrologico de algunos yacimientos de tungsteno en la Sierra del Morro y la Sierrita del Yulta, prov. de San Luis, Argentina: Contr. Cient. y Tecn. Univ. del Estado, No. 2, Chile

Clayton, R.N., Goldsmith, J.R., Karel, K.J., Mayeda, T.K. and Newton, R.C., 1975, Limits on the effects of pressure on isotope fractionations: Geochim. et Cosmochim. Acta, 39, 1197-1201

Cooke, B.J. and Godwin, C.I., 1984, Geology, mineral equilibria and isotopic studies of the McDame tungsten skarn prospect, North-Central British Columbia: Econ. Geol., 79, 826-847

Corner, B., 1981, An interpretation of the aeromagnetic data covering a portion of the Damara Orogenic Belt, with special reference to occurrence of uraniferous granite: Unpub. Ph.D. thesis, Univ. of Witwatersrand, S. Africa, 100p

Corner, B., 1983, An interpretation of the aeromagnetic data covering the western portion of Damara Orogen in South West Africa/Namibia: Spec. Publ. Geol. Soc. S. Afr., 11, 339-354

Cunningham, W.B., Höll, R. and Taupitz, K.C., 1973, Two new tungsten bearing horizons in the older Precambrian of Rhodesia: Mineral. Deposita, 8, 200-203

Deer, W.A., Howie, R.A. and Zussman, J., 1966, An introduction to the rock-forming minerals. Longmans, London, 528p

Deer, W.A., Howie, R.A. and Zussman, J., 1982, Rock-forming Minerals, Volume 1A, Orthosilicates. Longmans, London, 919p

Dick, L.A., 1976, Metamorphism and metasomatism at the Macmillan Pass tungsten deposit, Yukon and District of Mackenzie, Canada: M.Sc. thesis, Queen's Univ., Kingston, 226p

Dick, L.A., 1980, A comparative study of the geology, mineralogy and conditions of formation of contact metasomatic mineral deposits in the NE Canadian Cordillera: Ph.D. thesis, Queen's Univ., Kingston, 473p

Dick, L.A. and Hodgson, C.J., 1982, The Mactung W-Cu(Zn) contact metasomatic and related deposits of the Northeastern Canadian Cordillera: Econ. Geol., 77, 845-867

Drake, M.S. and Weill, D.F., 1975, Partition of Sr, Ba, Ca, Y, Eu^{2+}, Eu^{3+} and other REE between plagioclase, feldspar and magmatic liquid: an experimental study: Geochim. et Cosmochim. Acta, 39, 689-712

Edwards, A.B., Baker, G. and Callow, K.J., 1956, Metamorphism and metasomatism at King Island scheelite mine: Geol. Soc. Australia Jour., 3, 55-100

Einaudi, M.T., Meinert, L.D. and Newberry, R.J., 1981, Skarn deposits: Econ. Geol., 75th Anniversary Volume, 317-391

Einaudi, M.T. and Burt, D.M., 1982, A special issue devoted to skarn deposits: Introduction - terminology, classification and composition of skarn deposits: Econ. Geol., 77, 745-754

Eskola, P., 1939, Die metamorphen Gesteine, 263-407. In: Barth, T.F.W., Correns, C.W. and Eskola, P., Die Entstehung der Gesteine. Springer-Verlag, Berlin, 422p

Evans, B.W., Shaw, D.M. and Haughton, D.R., 1969, Scapolite stoichiometry: Contr. Mineral. and Petrol., 24, 293-305

Exley, C.S., 1957, Magmatic differentiation and alteration of the St. Austell Granite: Q.J. Geol., London, 114, 197-230

Farrar, E., Clark, A.H. and Kim, O.J., 1978, Age of the Sandong tungsten deposit, Republic of Korea and its bearing on the metallogeny of the southern Korean peninsula: Econ. Geol., 73, 547-552

Finnerty, A.A. and Boyd, F.R., 1984, Evaluation of thermobarometers for garnet peridotites: Geochim. et Cosmochim. Acta, 48, 15-27

Foster, R.P., 1973, Some aspects of the geochemistry of tungsten: Unpub. PhD thesis, Univ. Manchester

Foster, R.P., Mann, A.G., Armin, T. and Burmeister, B.B., 1978, Richardson's Kop wolframite deposit: a geochemical model for the hydrothermal behaviour of tungsten. In: Verwoerd, W.J., Ed., Mineralisation in metamorphic terranes: Spec. Publ. Geol. Soc. S. Africa, 4, 107-128

Geijer, P. and Magnusson, N.H., 1952, The iron ores of Sweden: Internat. Geol. Cong., 19th Algiers, 2, 477-499

Gevers, T.W. and Frommurze, H.T., 1929, The tin-bearing pegmatites of the Erongo area, S.W. Africa: Trans. Geol. Soc. S. Africa, 32, 11

Goldschmidt, V.M., 1958, Geochemistry. Oxford University Press, 730p

Haack, U., 1983, Reconstruction of the cooling history of the Damara Orogen by correlation of radiometric ages with geography and altitude, 873-884. In: Martin, H. and Eder, F.W., Eds., Intracontinental Fold Belts. Springer Verlag, Berlin, 945p.

Haack, U., Gohn, E. and Klein, J.A., 1980, Rb/Sr ages of granitic rocks along the middle reaches of the Omaruru River and the timing of orogenetic events in the Damaran Belt (Namibia): Contr. Mineral. Petrol., 94, 349-360

Haack, U., Hoefs, J. and Gohn, E., 1983, Genesis of Damaran granites in the light of Rb/Sr and $\delta^{18}O$ data, 848-872. In: Martin, H. and Eder, F.W., Eds., Intracontinental Fold Belts. Springer Verlag, Berlin, 945p

Hall, A.J., 1982, Gypsum as a precursor to pyrrhotite in metamorphic rocks: Mineral. Deposita, 17, 401-409

Higgins, N.C., 1980, Fluid inclusion evidence for the transport of tungsten by carbonate complexes in hydrothermal solutions: Can. J. Earth Sci., 17, 823-830

Hine, R., Williams, I.S., Chappell, B.W. and White, A.J.R., 1978, Contrasts between I- and S-type granitoids of the Koscuiska Batholith: Jour. Geol. Soc. Austral., 25, pt. 4, 219-234

Hochella, M.F., Liou, J.G., Keskinen, M.J. and Kim, H.S., 1982, Synthesis and stability relations of magnesium idocrase: Econ. Geol., 77, 798-808

Hoefs, J., 1980, Stable Isotope Geochemistry. Springer Verlag, Berlin, 208p

Hoffer, E., 1977, Petrologische Untersuchungen zur Regional-metamorphose Al-reicher Metapelite im südlichen Damaran Orogen (Südwest-Afrika): Habilitations-schrift, Univ. Gottingen, 150p

Höll, R., 1977, Early Palaeozoic ore deposits of the Sb-W-Hg formation in the Eastern Alps and their genetic interpretations, 169-198. In: Klemm, D.D. and Schneider, H.-J.,Eds., Time and Stratabound Ore Deposits, Springer Verlag, Berlin, 444p

Imeokparia, E.G., 1981, Ba/Rb and Rb/Sr ratios as indicators of magmatic fractionation, postmagmatic alteration and mineralisation - Afu Younger Granite Complex, Northern Nigeria: Geochem. Journal, 15, 209-219

Keith, M.L. and Weber, J.N., 1964, Carbon and oxygen isotopic composition of selected limestones and fossils: Geochim. et Cosmochim. Acta, 28, 1787-1816

Kerr, P.F., 1946, Tungsten mineralisation in the United States: Geol. Soc. America Mem. 15, 241p

Kerrick, D.M., 1977, The genesis of zoned skarns in the Sierra Nevada, California: Jour. Petrology, 18, 144-181

Klein, J.A., 1980, Geological report on area 2115A: Unpub. Rept. of the Geol. Surv. SWA/Namibia

Korzhinskii, D.S., 1936, Mobility and inertness of components in metasomatism: Akad. Nauk. SSSR, Izv., Ser. Geol,1, 58-61

Korzhinskii, D.S., 1964, An outline of metasomatic processes (trans. M.E. Bergunker): Internat. Geology Rev., 6, 1713-1734

Korzhinskii, D.S., 1965, The theory of systems with perfectly mobile components and processes of mineral formation: Am. Jour. Sci., 263, 193-205

Krauskopf, K.B., 1953, Tungsten deposits of Madera, Fresno and Tulare Counties, Calif.: California Div. Mines Spec. Rept., 35, 83p

Kreulen, R., 1977, CO_2 -rich fluids during regional metamorphism on Naxos, a study on fluid inclusions and stable isotopes: Ph.D. thesis, Univ. of Utrecht, 85p

Kreulen, R. and van Beek, P.C.J.M., 1983, The calcite-graphite thermometer; data on graphite bearing marbles from Naxos, Greece: Geochim. et Cosmochim. Acta, 47, 1527-1530

Kuyper, J.L., 1984, Report on the Regional 1 : 10 000 Mapping of the Omaruru Tungsten Prospect: Unpub. Co. Rept.

Kwak, T.A.P., 1978, Mass balance relationships and skarn-forming processes at the King Island Scheelite Deposit, King Island, Tasmania, Australia: Am. Jour. Sci., 278, 943-968

Kwak, T.A.P. and Tan, T.H., 1981, The geochemistry of zoning in skarn minerals at the King Island (Dolphin) Mine, Econ. Geol., 76, 468-497

Magnusson, N.H., 1960, Iron and sulfide ores of central Sweden: Internat. Geol. Cong., 21st, Copenhagen, Excursion Guides A26 and C21, 48p

Manning, D.A.C., 1984, Volatile control of tungsten partitioning in granitic melt-vapour systems: Trans. Inst. Min. Metall., 93, 185-189

Manning, D.A.C. and Henderson, P., 1984, The behaviour of tungsten in granitic melt-vapour systems: Contr. Mineral. Petrol., 86, 286-293

Marlow, A.G., 1981, Remobilisation and primary uranium genesis in the Damaran Orogenic Belt: Unpub. Ph. D. thesis, Leeds Univ., England, 277p

Martin, H., 1978, The mineralisation of the ensialic Damara orogenic belt, 405-415. In: Verwoerd, W.J., Ed., Mineralisation in Metamorphic Terranes: Geol. Soc. S. Afr. Spec. Pub., 4, 551p

Martin, H., 1983, Alternative geodynamic models for the Damara Orogeny. A critical discussion, 913-945. In: Martin, H. and Eder, F.W., Eds., Intracontinental Fold Belts. Springer Verlag, Berlin, 945p.

Martin, H. and Porada, H., 1977, The intracratonic branch of the Damaran Orogen in South West Africa. I. Discussion of geodynamic models: Precambrian Res., 5, 311-338

Mason, B. and Moore, C.B., 1982, Principles of Geochemistry. John Wiley, 344p

Mathieson, G.R., and Clark, A.H., 1984, The Cantung E Zone scheelite skarn orebody, Tungsten, Northwest Territories : A revised genetic model: Econ. Geol., 79, 883-901

Matsuhisa, Y., Goldsmith, J.R. and Clayton, R.N., 1979, Oxygen isotopic fractionation in the system quartz-albite-anorthite-water: Geochim. et Cosmochim. Acta, 43, 1131-1140

Matthews, A. and Kolodny, Y., 1978, Oxygen isotope fractionation in decarbonation metamorphism : The mottled zone event: Earth Planet. Sci. Letters, 39, 179-192

McCarthy, T.S. and Hasty, R.A., 1976, Trace element distribution patterns and their relationship to the crystallisation of granite melts: Geochim. et Cosmochim Acta, 40, 1351-1358

McCrea, J.M., 1950, On the isotopic chemistry of carbonate and a palaeotemperature scale: J. Chem. Phys., 18, 849-857

Miller, R. McG., 1983a , The Pan-African Damara Orogen of South West Africa/Namibia: Spec. Publ. Geol. Soc. S. Afr., 11, 431-515

Miller, R. McG., 1983b , Economic implications of plate tectonic models of the Damara Orogen: Spec. Publ. Geol. S. Afr., 11, 385-395

Miller, R. McG., Barnes, S-J., and Balkwill, G., 1983, Possible active margin deposits within the southern Damara Orogen : The Kuiseb Formation between Okahandja and Windhoek: Spec. Publ. Geol.Soc. S.Afr., 11, 73-88

Nanz, R.H., 1953, Chemical composition of Precambrian slates with notes on the geochemical evolution of lutites: Jour. Geol., 61, 51-64

Newberry, R.J., 1979a, The importance of stratigraphy and structure of Sierran metamorphic rocks in the development of economic tungsten deposits [abs.]: Geol. Soc. America, Abstracts with Programs, 11, 120

Newberry, R.J., 1979b, Systematics in W-Mo-Cu skarn formation in the Sierra Nevada : An overview [abs.]: Geol. Soc. America, Abstracts with Programs, 11, 486

Newberry, R.J., 1982, Tungsten-bearing skarns of the Sierra Nevada. I., The Pine Creek Mine, California: Econ. Geol., 77, 823-844

Newberry, R.J. and Einaudi, M.T., 1981, Tectonic and geochemical setting of tungsten skarn mineralisation in the Cordillera: Symposium on tectonics and ore deposits, Tucson, Proc., 99-111

Nokleberg, W.J., 1981, Geologic setting, petrology and geochemistry of zoned tungsten-bearing skarns at the Strawberry mine, Central Sierra Nevada, California: Econ. Geol., 76, 111-133

Nockolds, S.R. and Allen, R., 1953, The geochemistry of some igneous rock series. I., Calc-alkali igneous trends: Geochim. et Cosmochim. Acta, 4, 105-142

Norrish, K. and Hutton, J.T., 1969, An accurate X-ray spectrographic method for the analysis of a wide range of geological samples: Geochim. et Cosmochim. Acta, 33, 431-453

O'Neil, J.R. and Chappell, B.W., 1977, Oxygen and hydrogen isotope relations in the Berridale batholith, Southwestern Australia: J. Geol. Soc., 133, 559-571

O'Neil, J.R. and Clayton, R.N., 1964, Oxygen isotope geothermometry, 157-168. In: Craig, H., Miller, S.L. and Wasserburg, G. J., Eds., Isotopic and Cosmic Chemistry. North Holland Pub., Amsterdam

O'Neil, J.R. and Taylor, H.P., 1967, The oxygen isotope and cation exchange chemistry of feldspars: Am. Mineral., 52, 1414-1437

O'Neil, J.R., Clayton, R.N. and Mayeda, T.K., 1969, Oxygen isotope fractionation in divalent metal carbonates: Jour. Chem. Physics, 51, 5547-5558

Pertsev, N.N., 1974, Skarns as magmatic and postmagmatic formations: Internat. Geology Rev., 16, 572-582

Pettijohn, E.J., 1975, Sedimentary Rocks. Harper and Row, London, 628p

Pferdekampfer, H., 1984, Geophysical investigation of the Otjua prospect: Unpub. Co. Rept.

Pineau, F., Latouche, L. and Javoy, M., 1976, L'origine du graphite et les fractionnements isotopiques du carbon dans les marbres metamorphiques des Gours Oumelalen (Ahaggar, Algerie), des Adirondacks (New Jersey, U.S.A.) et du Damara (Namibie, Sud-Ouest africain): Bull. Soc. Geol. Fr., XVIII, 1713-1723

Plant, J., Brown, G.C., Simpson, P.R. and Smith, R.T., 1980, Signatures of metalliferous granites in the Scottish Caledonides: Trans. Instn. Min. Metall., 89, B198-B209

Plimer, I.R., and Elliot, S.M., 1979, The use of Rb/Sr ratios as a guide to mineralisation: Journal of Geochemical Exploration, 12, 21-34

Puhan, D., 1976, Metamorphic temperature determined by means of the dolomite-calcite solvus geothermometer - Examples from the central Damaran orogen (South West Africa): Contr. Mineral. Petrol., 58, 23-28

Rowlands, N.J., Blight, P.G., Jarvis, D.M. and Von Der Borch, C.C., 1980, Sabkhas and playa environments in late Proterozoic grabens, Willouran Ranges, South Australia: J. Geol. Soc. Austral., 27, 55-68

Rozendaal, A. and Stumpfl, E.F., 1984, Mineral chemistry and genesis of Gamsberg zinc deposit, South Africa: Trans. Instn. Min. Metall. , 93, B161-B175

Rye, R.O. and Ohmoto, H., 1974, Sulphur and carbon isotopes and ore genesis : a review: Econ. Geol., 69, 826-842

Sharma, T. and Clayton, R.N., 1965, Measurement of O^{18}/O^{16} ratios of total oxygen of carbonates: Geochim. et Cosmochim. Acta, 29, 1347-1353

Sheraton, J.W. and Black, L.P., 1973, Geochemistry of mineralised granitic rocks of northeast Queensland: Journal of Geochemical Exploration, 2, 331-348

Shimazaki, H., 1977, Grossular-spessartine-almandine garnets from some Japanese scheelite skarns: Canadian Mineralogist, 15, 74-80

Simpson, P.R., Brown, G.C., Plant, J. and Ostle, D., 1979, Uranium mineralisation and granite magmatism in the British Isles: Phil. Trans. R. Soc., London, A291, 385-412

Skaarup, P., 1974, Strata-bound scheelite mineralisation in skarns and gneisses from the Bindal area, northern Norway: Mineral. Deposita, 9, 299-308

Smith, D.A.M., 1965, The geology of the area around the Khan and Swakop rivers in South West Africa: Mem. Geol. Surv. S. Afr., South West Africa Series, 3, 113p

Stormer, J.C. and Carmichael, I.S.E., 1971, The free energy of sodalite and the behaviour of chloride, fluoride and sulphate in silicate magmas: Am. Mineral., 56, 292-306

Svoboda, J., 1966, Regional Geology of Czechoslovakia. Part I. The Bohemian Massif : Prague: Geol. Surv., Czeckoslovakia

Tan, T.H. and Kwak, T.A.P., 1979, The measurement of the thermal history around the Grassy granodiorite, King Island, Tasmania by the use of fluid inclusion data: Jour. Geology, 87, 43-54

Tankard, A.J., Jackson, M.P.A., Eriksson, K.A., Hobday, D.K., Hunter, D.R. and Minter, W.E.L., 1982, Crustal Evolution of Southern Africa. Springer Verlag, New York, 523p

Taylor, B.E., 1976, Origin and significance of C-O-H fluids in the formation of Ca-Fe-Si skarn, Osgood Mountains, Humboldt Co., Nevada: Unpub. Ph.D. thesis, Stanford Univ., 149p

Taylor, B.E. and O'Neil, J.R., 1977, Stable isotope studies of metasomatic Ca-Fe-Al-Si skarns and associated metamorphic and igneous rocks, Osgood Mountains, Nevada: Contr. Mineral. Petrol., 63, 1-49

Taylor, H.P., 1967, Oxygen isotope studies of hydrothermal mineral deposits. In: Barnes, H.L., Ed., Geochemistry of Hydrothermal Ore Deposits. Holt, Pinehart and Winston, Inc., New York

Taylor, H.P., 1974, The application of oxygen and hydrogen isotope studies to problems of hydrothermal alteration and ore deposition: Econ. Geol., 69, 843-883

Taylor, H.P., 1977, Water/rock interactions and the origin of H_2O in granitic batholiths: J. Geol. Soc. Lond., 133, 509-558

Taylor, H.P. and Epstein, S., 1962a, Relation between O^{18}/O^{16} ratios in coexisting minerals of igneous and metamorphic rocks, Part I : Principles and experimental results: Bull. Geol. Soc. Am., 73, 461-480

Taylor, H.P. and Epstein, S., 1962b, Relationship between O^{18}/O^{16} ratios in coexisting minerals of igneous and metamorphic rocks, Part II : Application to petrologic problems: Bull. Geol. Soc. Am., 73, 675-694

Taylor, H.P., Frechen, J. and Degens, E.T., 1967, Oxygen and carbon isotope studies of carbonatites from Laacher See District, West Germany and the Alno District, Sweden: Geochim. et Cosmochim. Acta, 31, 407-430

Taylor, S.R, 1964, Abundance of chemical elements in the continental crust: a new table: Geochim. et Cosmochim. Acta, 28, 1273-1285

Taylor, S.R., 1968, Geochemistry of Andesites, 559-583. In: Ahrens, L.H., Ed., Origin and Distribution of the Elements: Int. Ser. Monogr. Earth Sci., 30

Thatcher, E.C., 1985, Petrographic description of a slide from Kassandara 40, Unpubl. Rept. for Rössing Uranium

Thiele, O., 1984, Zum Deckenbau und Achsenplan des Moldanubikums der südlichen Böhmischen Masse (Österreich): Jb. Geol. B.-A., 126, 513-523

Thompson, J.B., 1959, Local equilibrium in metasomatic processes. In: Abelson, P.H., Ed., Researches in Geochemistry. John Wiley

Tischendorf, G., 1977, Geochemical and petrographic characteristics of silicic magmatic rocks associated with rare element mineralisation. In: Stemprok, M., Ed., Metallization associated with acid magmatism: Prague, Czechoslovakia, Geol. Survey, 3, 41-96

Turekian, K.K. and Wedepohl, K.H., 1961, Distribution of the elements in some major units of the earth's crust: Bull. Geol. Soc. Am., 72, 175-192

Valley, J.W. and O'Neil, J.R., 1981, $^{13}C/^{12}C$ exchange between calcite and graphite : a possible thermometer in Grenville marbles: Geochim. et Cosmochim. Acta, 45, 411-419

Veizer, J. and Hoefs, J., 1976, The nature of O^{18}/O^{16} and C^{13}/C^{12} secular trends in sedimentary carbonate rocks: Geochim. et Cosmochim. Acta, 40, 1387-1395

Vidale, R., 1969, Metasomatism in a chemical gradient and the formation of calc-silicate bands: Am. Jour. Sci., 267, 857-874

Wada, H., 1977, Isotopic studies of graphite in metamorphosed carbonate rocks of central Japan: Geochem. J., 11, 183-197

Waldmann, L., 1951, Das AuBeralpine Grundgebirge Österreichs, 10-104. Schaffer, F.X., Ed., Geologie von Österreich.

Warren, B.E. and Modell, D.I., 1931, The structure of vesuvianite $Ca_{19}Al_4(MgFe)_2Si_9O_{34}(OH)_4$: Z.Krist., 78, 422-432

Watson, N.I., 1982, The geology of area 2115C: Unpub. Rept. of the Geol. Surv. SWA/Namibia

Wedepohl, K.H., 1970, Handbook of Geochemistry. Springer Verlag, Berlin

Willis, J.P., Ahrens, L.H., Danchin, R.V., Erlank, A.J., Gurney, J.J., Hofmeyr, P.K., McCarthy, T.S. and Orren, M.J., 1971, Some interelement relationships between lunar rocks and fines and stoney meteroites: In: Proc. Second Lunar Sci. Conf., 1123-1138

Willis, J.P., Erlank, A.J., Gurney, J.J., Theil, R.H. and Ahrens, L.H., 1972, Major, minor and trace element data for some Apollo 11, 12, 14 and 15 samples: In: Proc. Third Lunar Sci. Conf., 1269-1273

Winkler, H.G.F., 1976, Petrogenesis of Metamorphic Rocks. Springer Verlag, New York, 334p

Winkler, H.G.F., 1983, A survey of granitic rocks of the Damara Orogen and considerations on their origin, 817-837. In: Martin, H. and Eder, F.W., Eds., Intracontinental Fold Belts. Springer Verlag, Berlin, 945p

Zaw, U.K., 1976, The Cantung E-zone ore body, Tungsten, Northwest Territories - A major scheelite skarn deposit: Unpub. M.Sc. thesis, Queen's Univ., Kingston, Ont., 327p

Zaw, U.K. and Clark, A.H., 1977, The E-zone scheelite skarn orebody, Canada tungsten mine, Tungsten, Northwest Territories : A petrological and fluid inclusion study [abs.]: Geol. Assoc. Canada-Mineralog. Assoc. Canada-Soc. Econ. Geologists-Canadian Geophys. Union, Programs with Abstracts, 2, 57

Zaw, U.K. and Clark, A.H., 1978, Fluoride-hydroxyl ratios of skarn silicates, Cantung E-zone scheelite orebody, Tungsten, Northwest Territories: Canadian Mineralogist, 16, 207-221

LIST OF FIGURES

LIST OF FIGURES (continued)

LIST OF FIGURES (continued)

LIST OF FIGURES (continued)

LIST OF FIGURES (continued)

LIST OF FIGURES (continued)

LIST OF TABLES

LIST OF PHOTOGRAPHS

LIST OF PHOTOGRAPHS (continued)

LIST OF MAPS

FIGURES

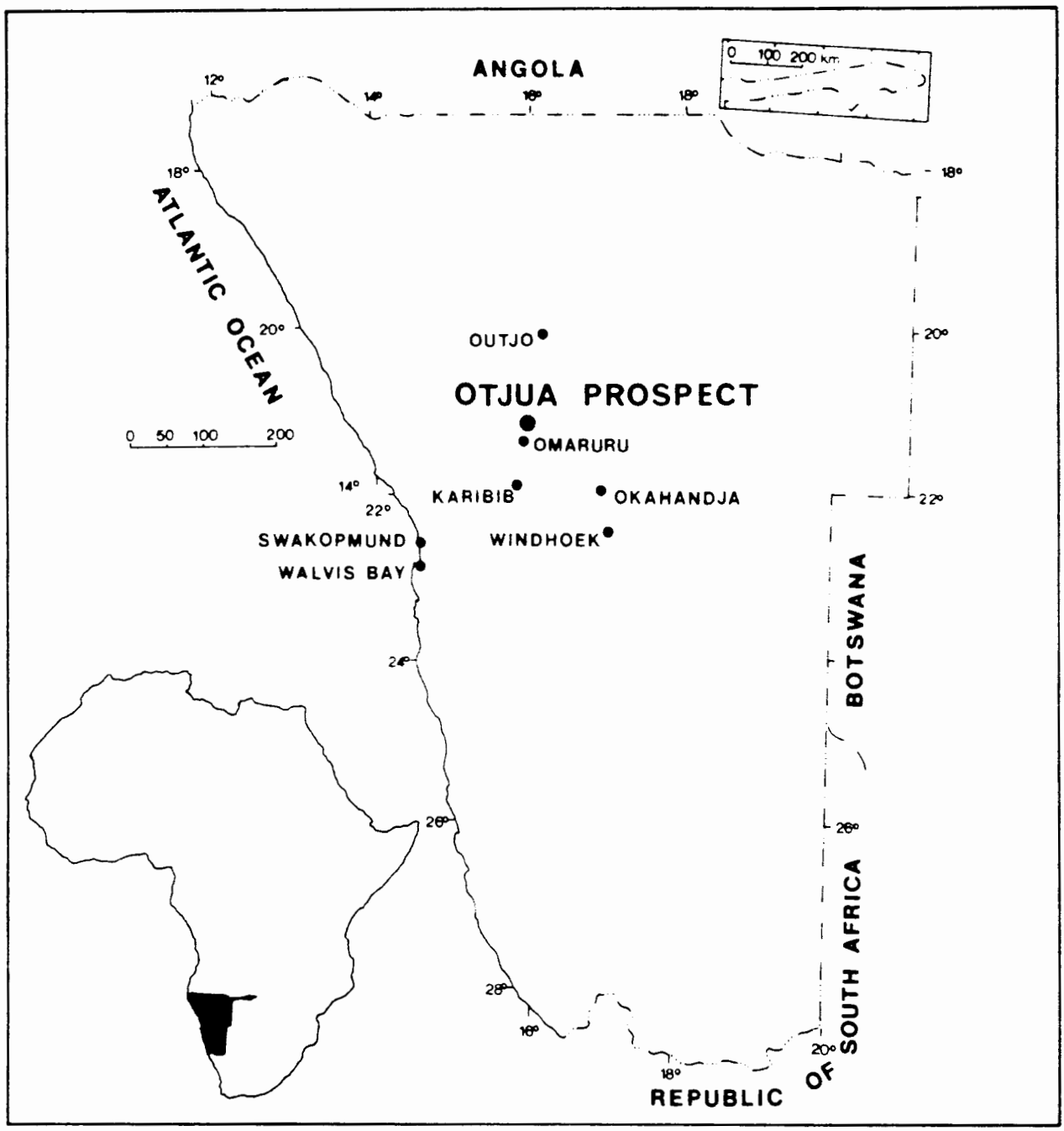

Fig. 1 : Location of the Otjua Prospect, central SWA/Namibia

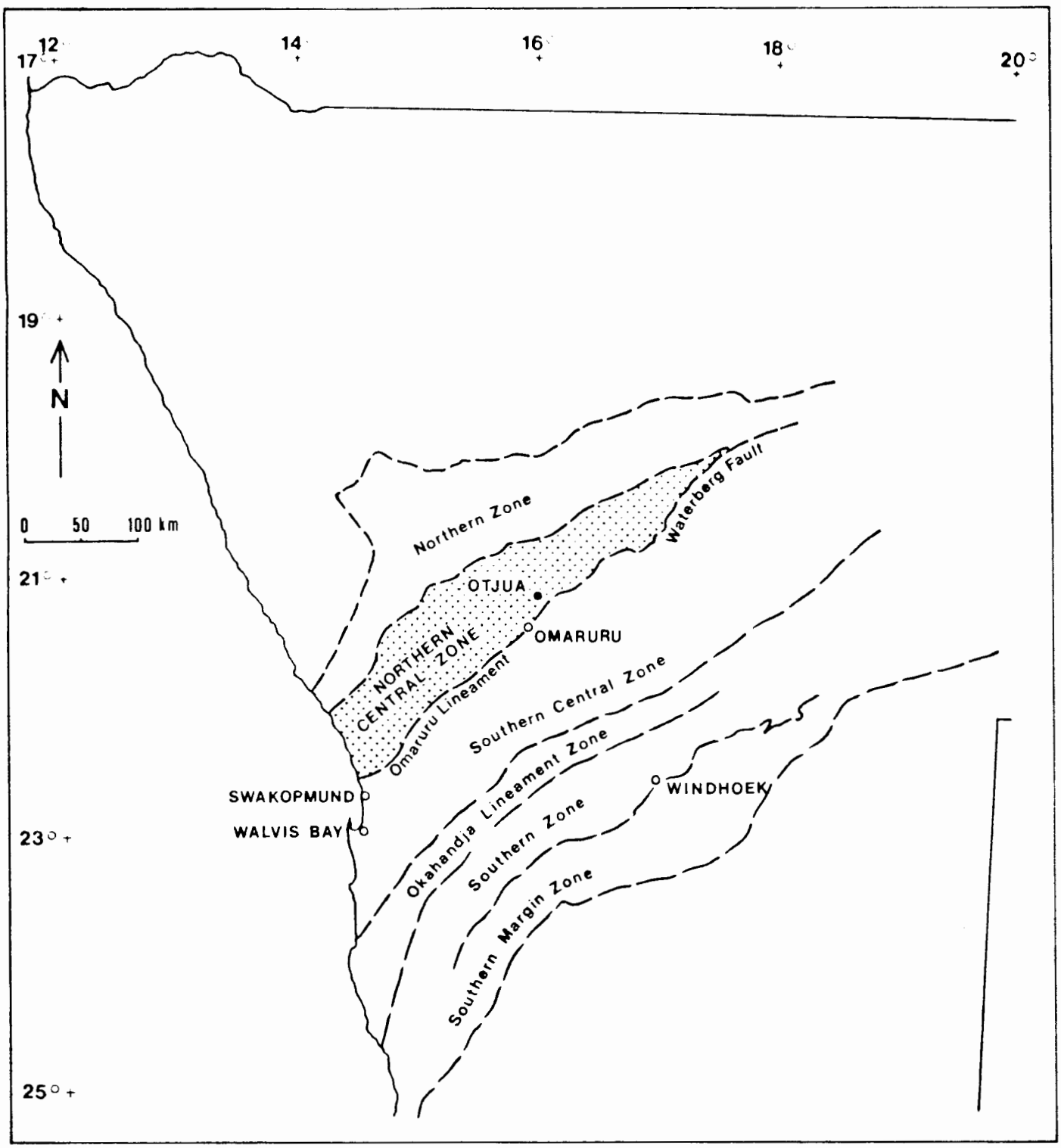

Fig. 2 : Tectonostratigraphic zones of the Damaran (after Miller, 1983a)

Swakop Group	- Kuiseb Formation - Karibib Formation - Oberwasser Formation - Rössing Formation
Nosib Group	- Khan Formation

Fig. 3 : Stratigraphy of the northern Central Zone (after Miller, 1983a)

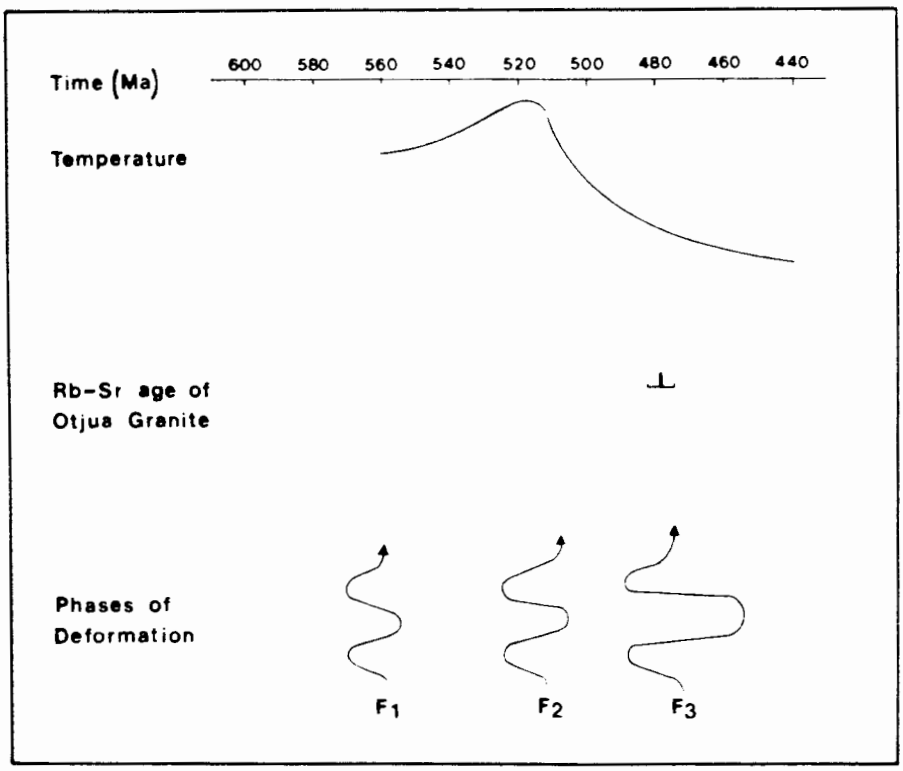

Fig. 4 : Relationship between deformation phases, metamorphism and intrusion of the Otjua granite in the northern Central Zone (after Haack et al., 1980)

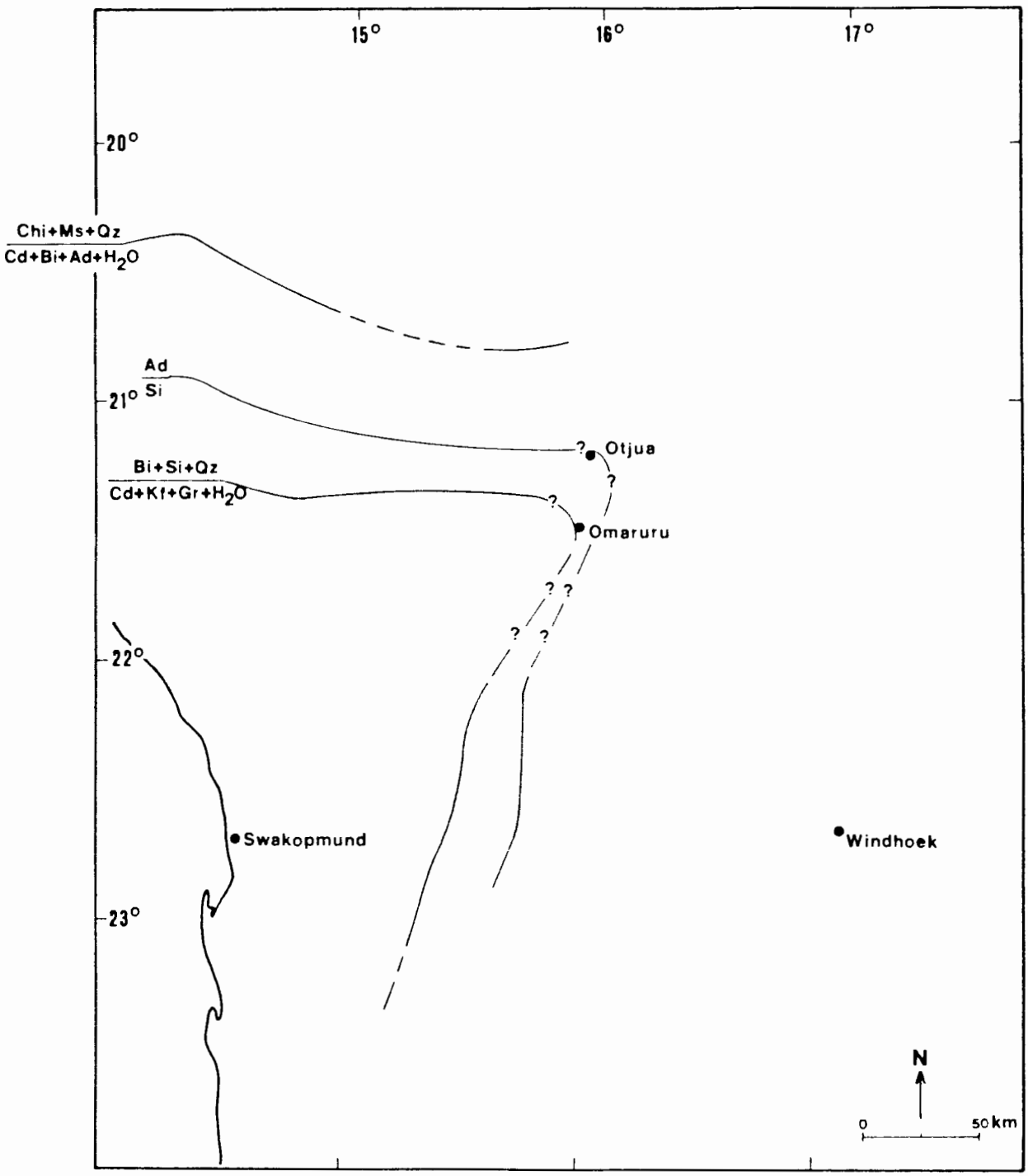

Fig. 5 : Isoreaction grads in the Central Zone (after Hoffer, 1977)

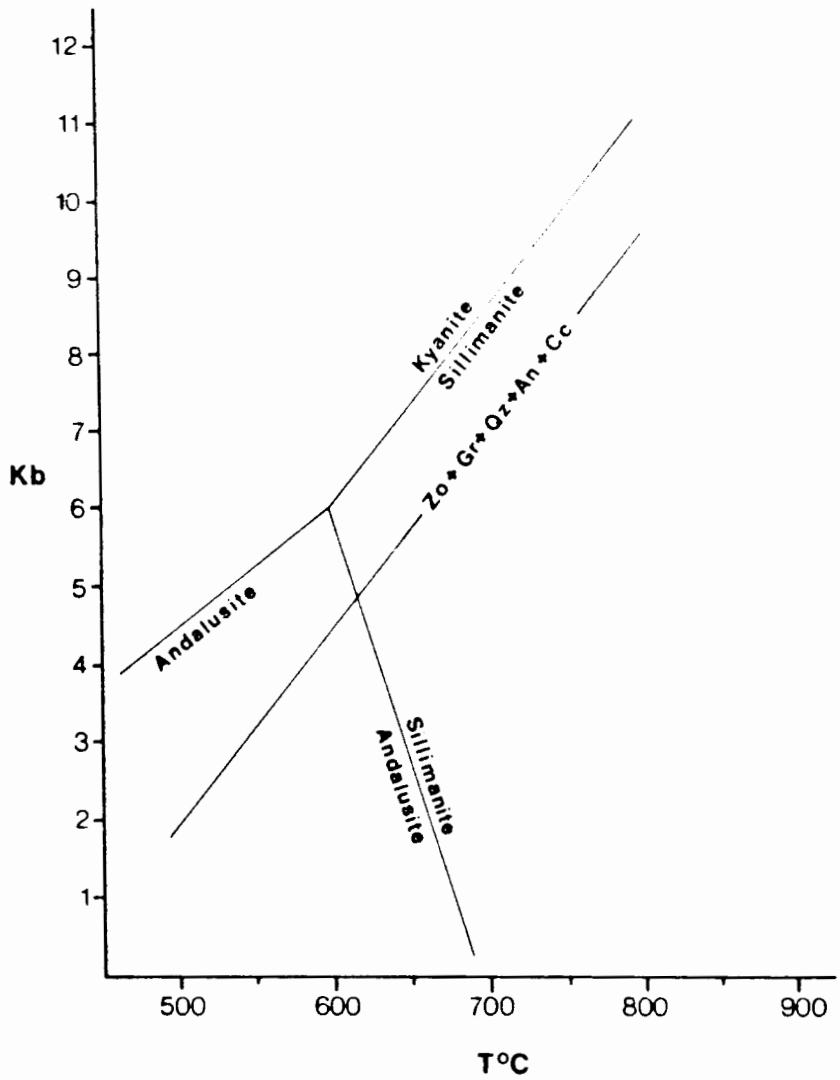

Fig. 6 : Medium and high grade metamorphism (after Winkler, 1976)

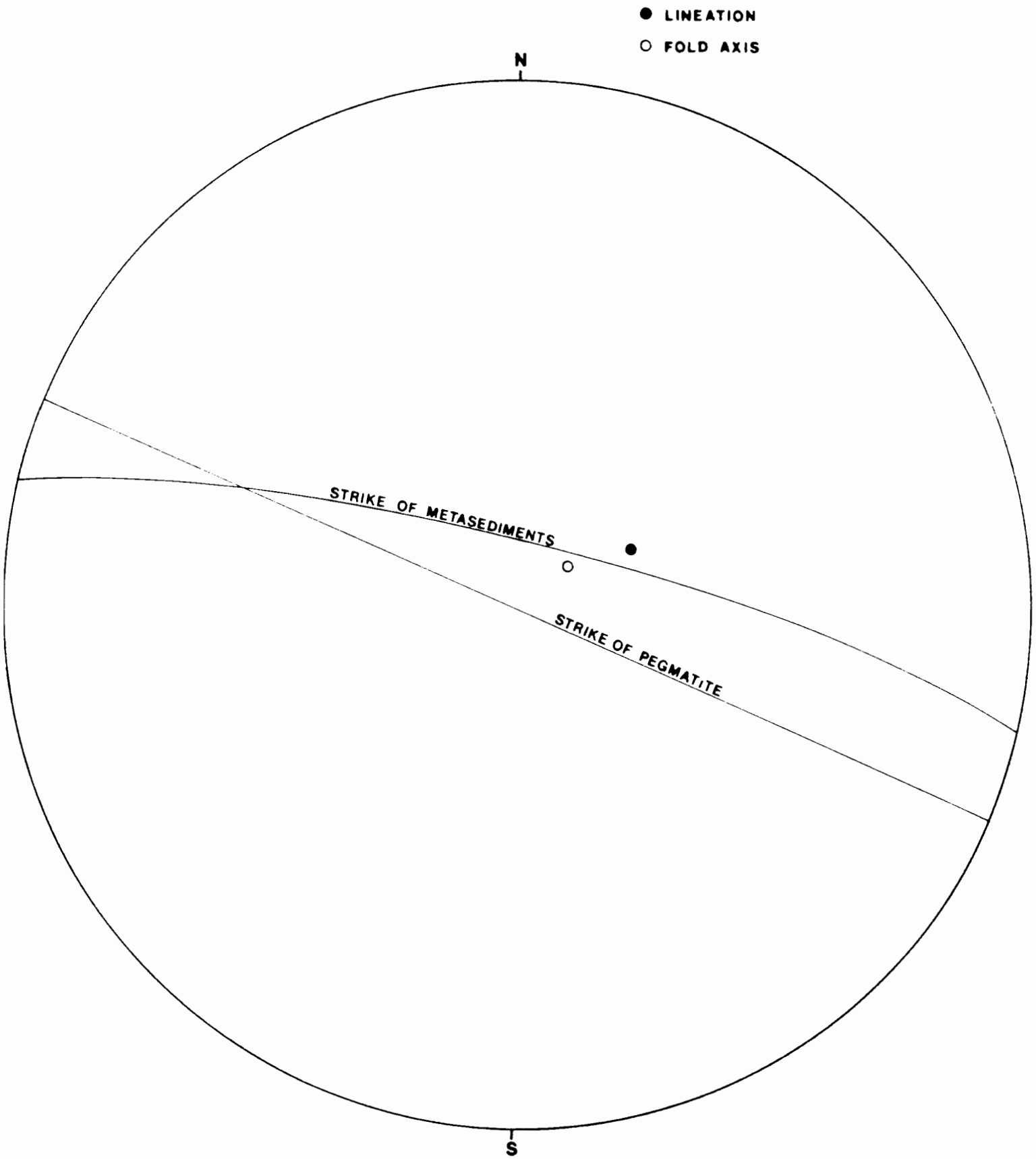

Fig. 7 : Equal area projection showing essential strucural features of the Otjua prospect

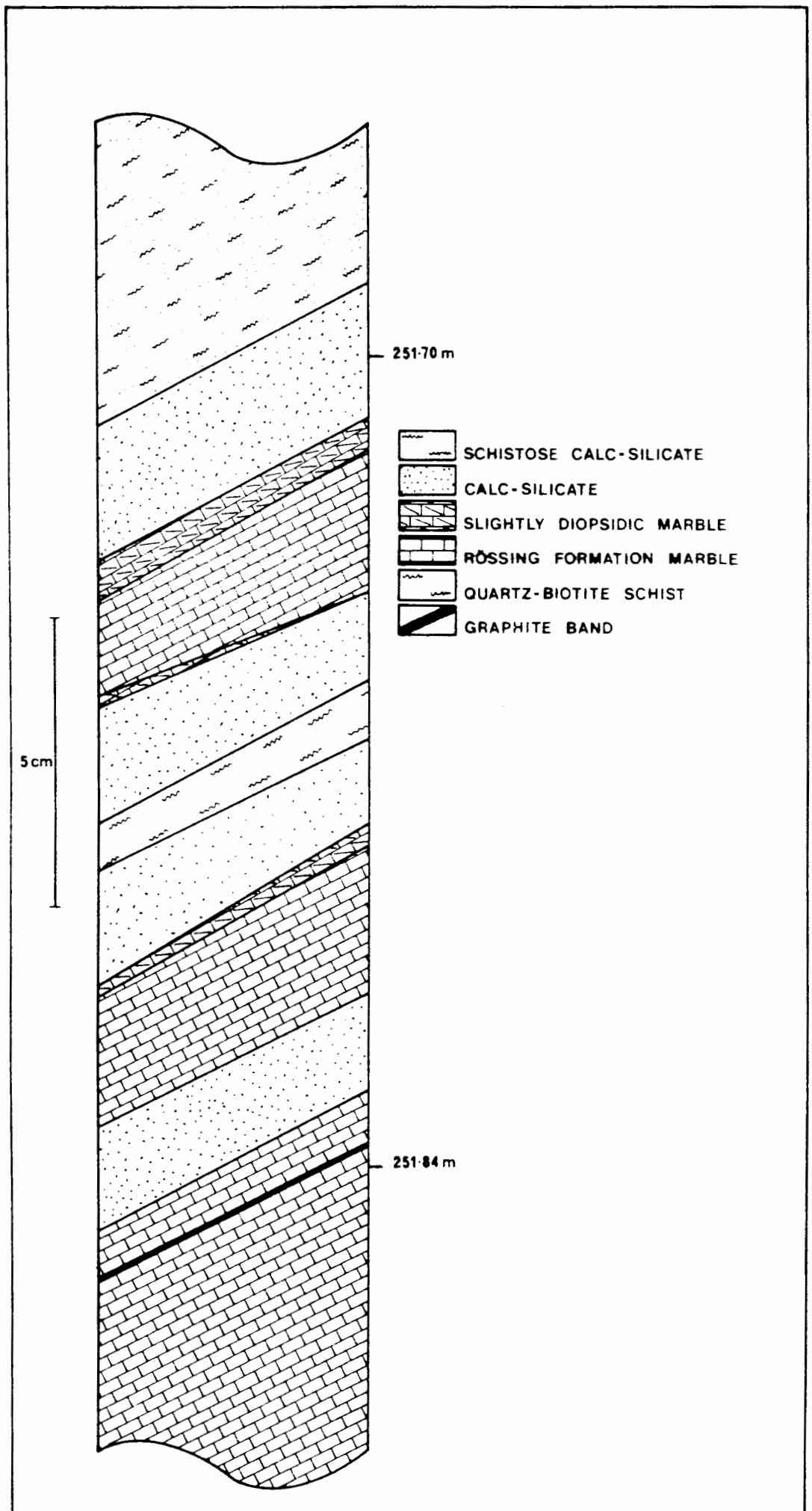

Fig. 8 : Upper contact of the Rössing Formation and enclosing metasediments in borehole OT22

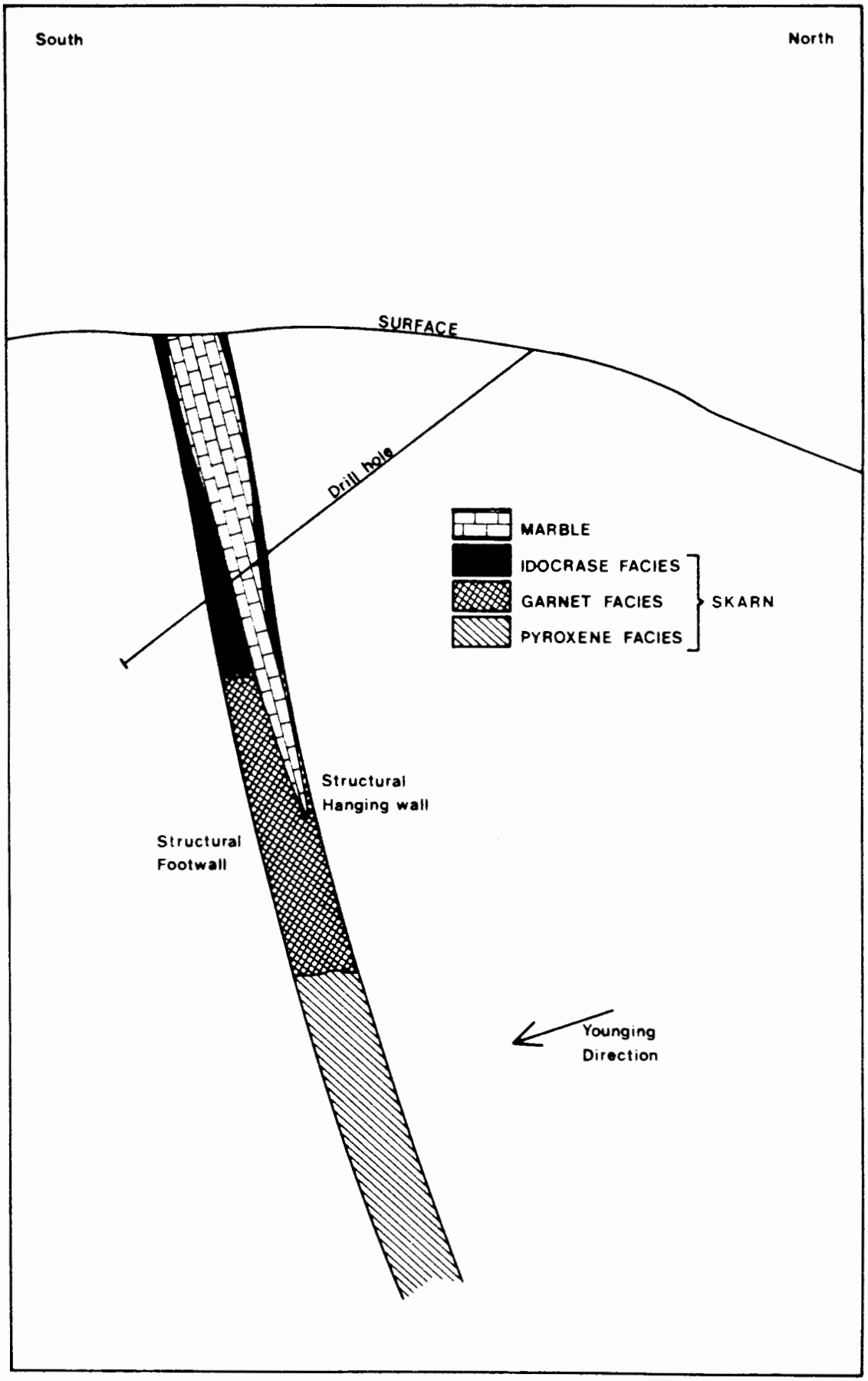

Fig. 9 : Schematic cross-section through the Otjua prospect to show direction of drillholes, overturning of sequence and varying degrees of replacement of the Rössing Formation by skarn

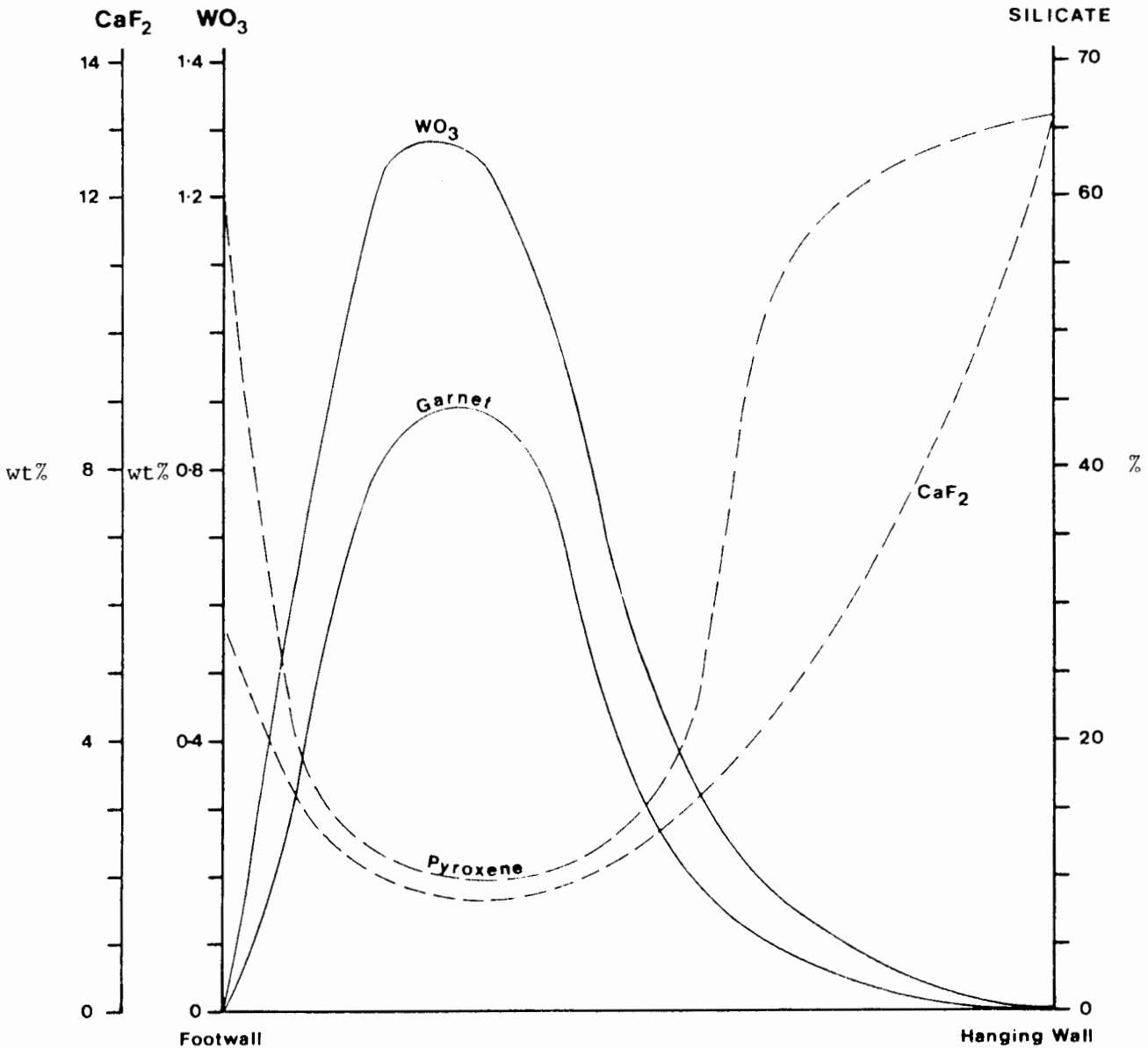

Fig. 10 : Schematic diagram to show mineralogical zoning and variations in wt% CaF_2 and wt% WO_3 contents across garnet facies skarn

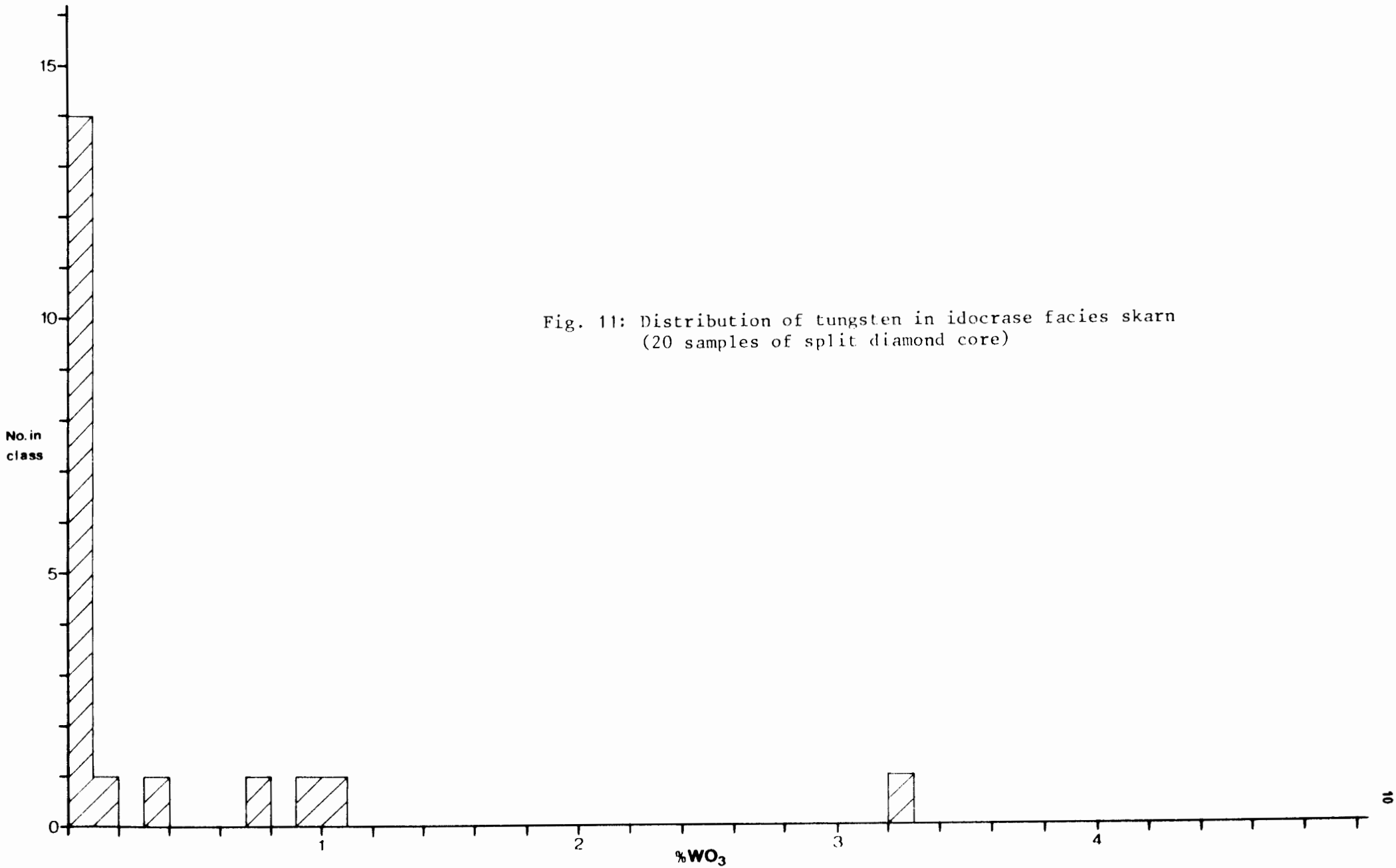

Fig. 11: Distribution of tungsten in idocrase facies skarn
(20 samples of split diamond core)

Fig. 12 : Cumulative frequency diagram of tungsten distribution in idocrase facies skarn (20 samples of split diamond core)

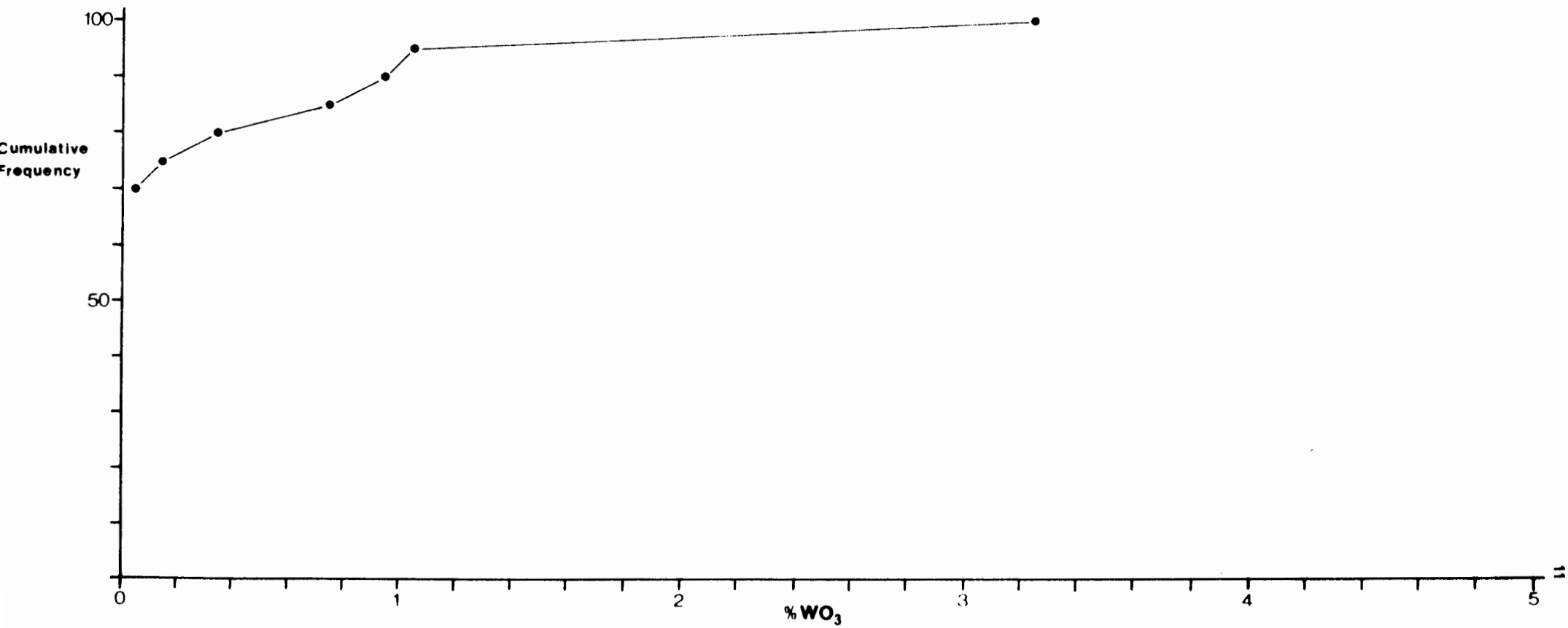

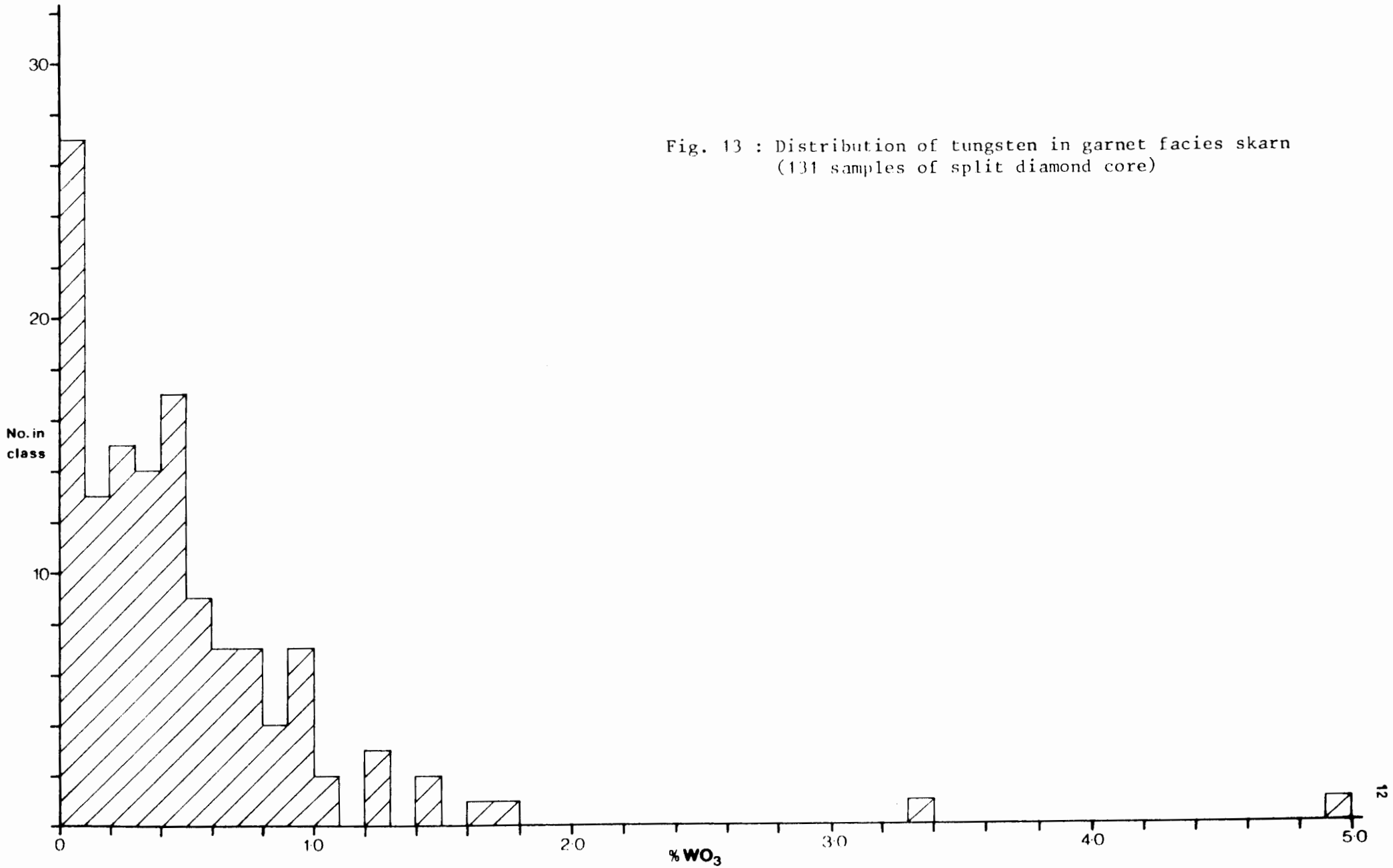

Fig. 13 : Distribution of tungsten in garnet facies skarn
(131 samples of split diamond core)

Fig. 14 : Cumulative frequency diagram of tungsten distribution in garnet facies skarn (131 samples of split diamond core)

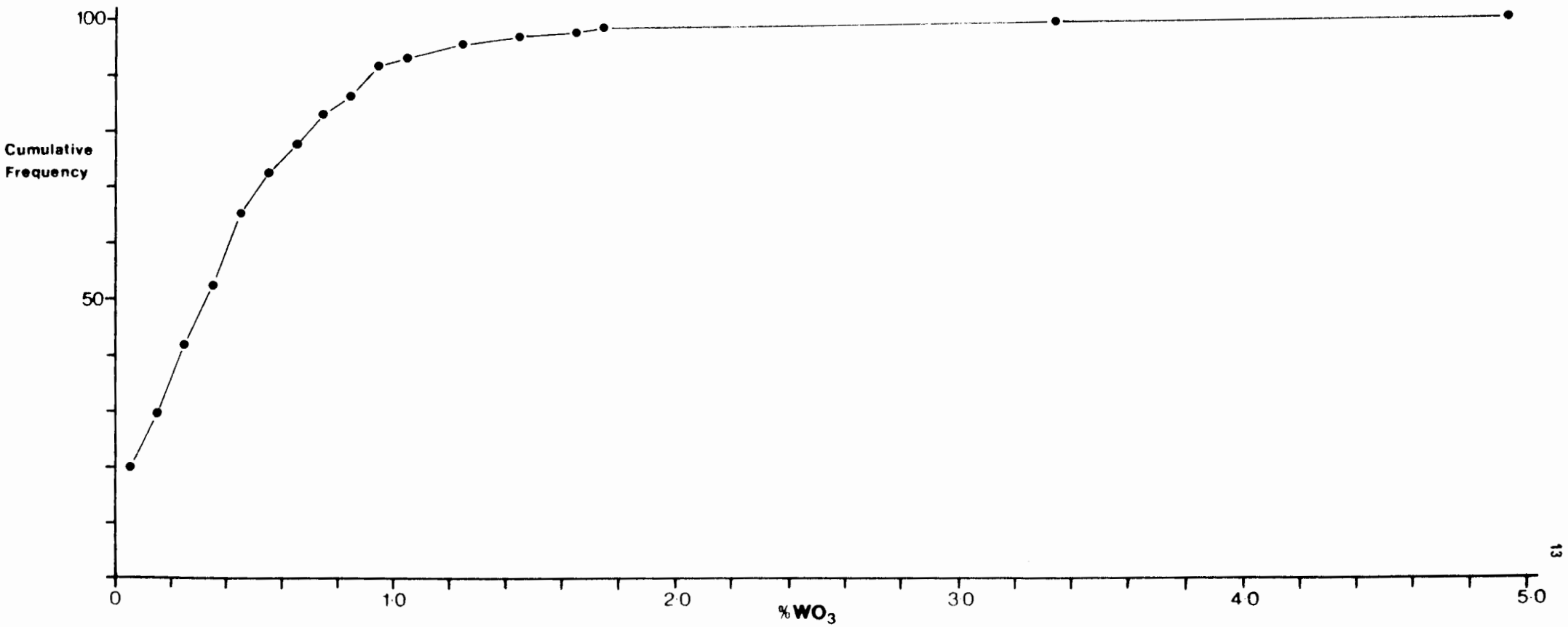

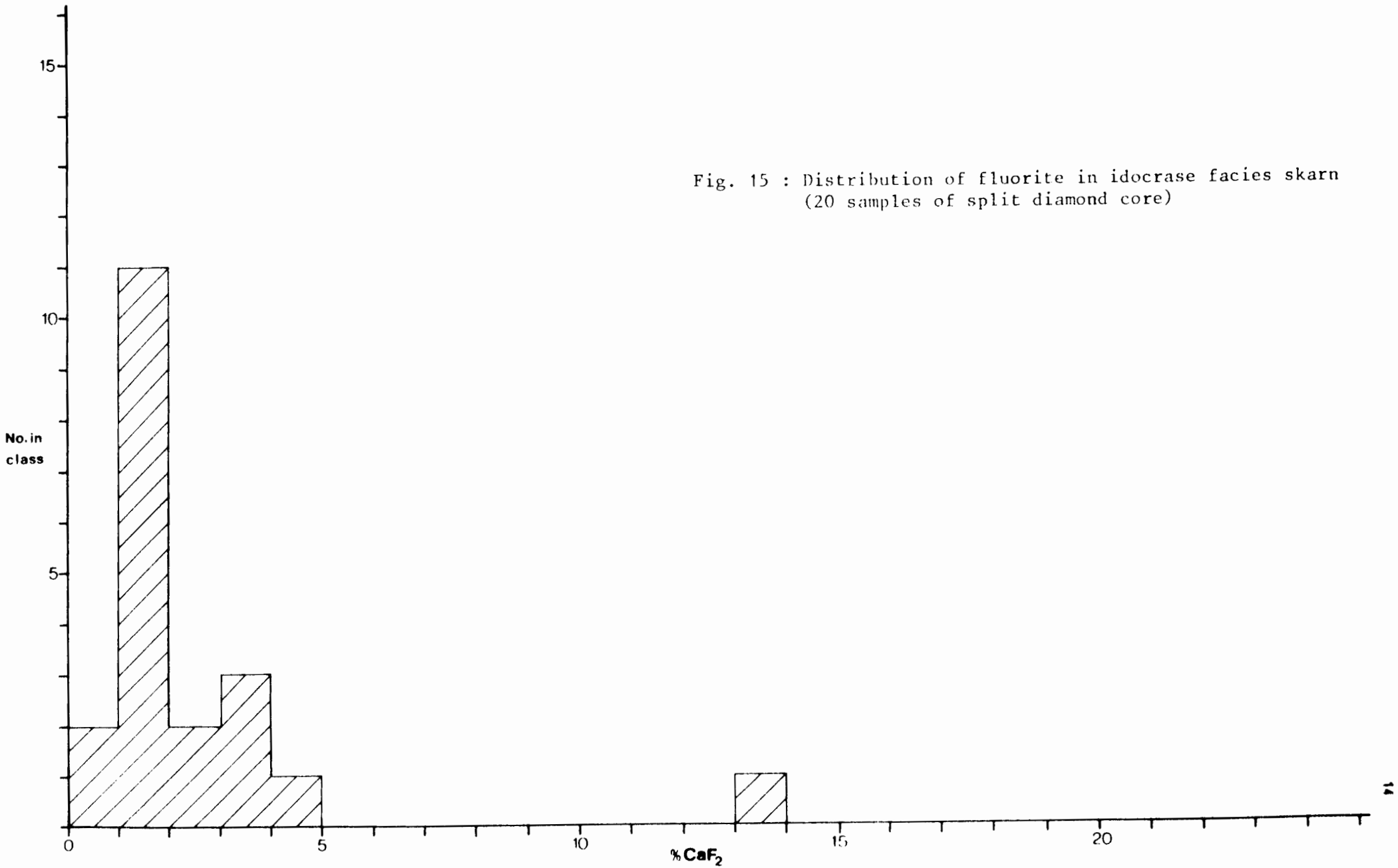

Fig. 15 : Distribution of fluorite in idocrase facies skarn
(20 samples of split diamond core)

Fig. 16 : Cumulative frequency diagram of fluorite distribution in idocrase facies skarn (20 samples of split diamond core)

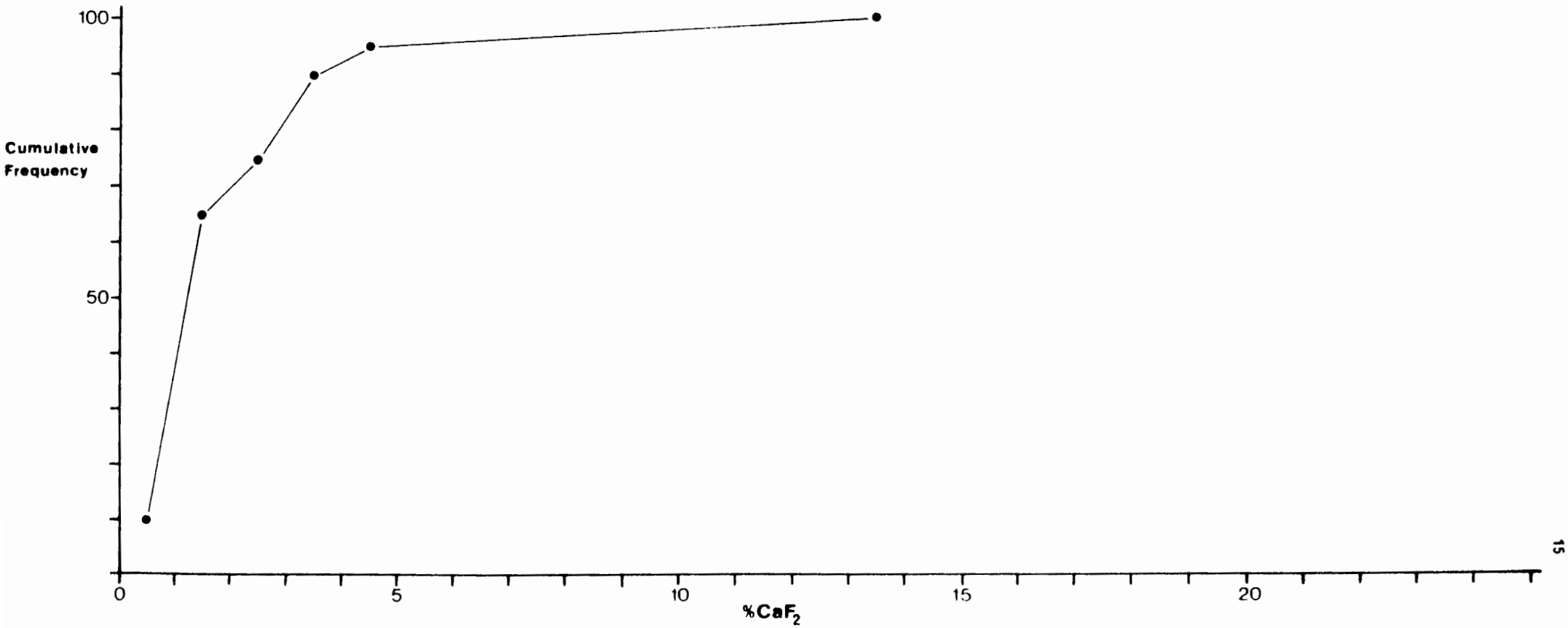

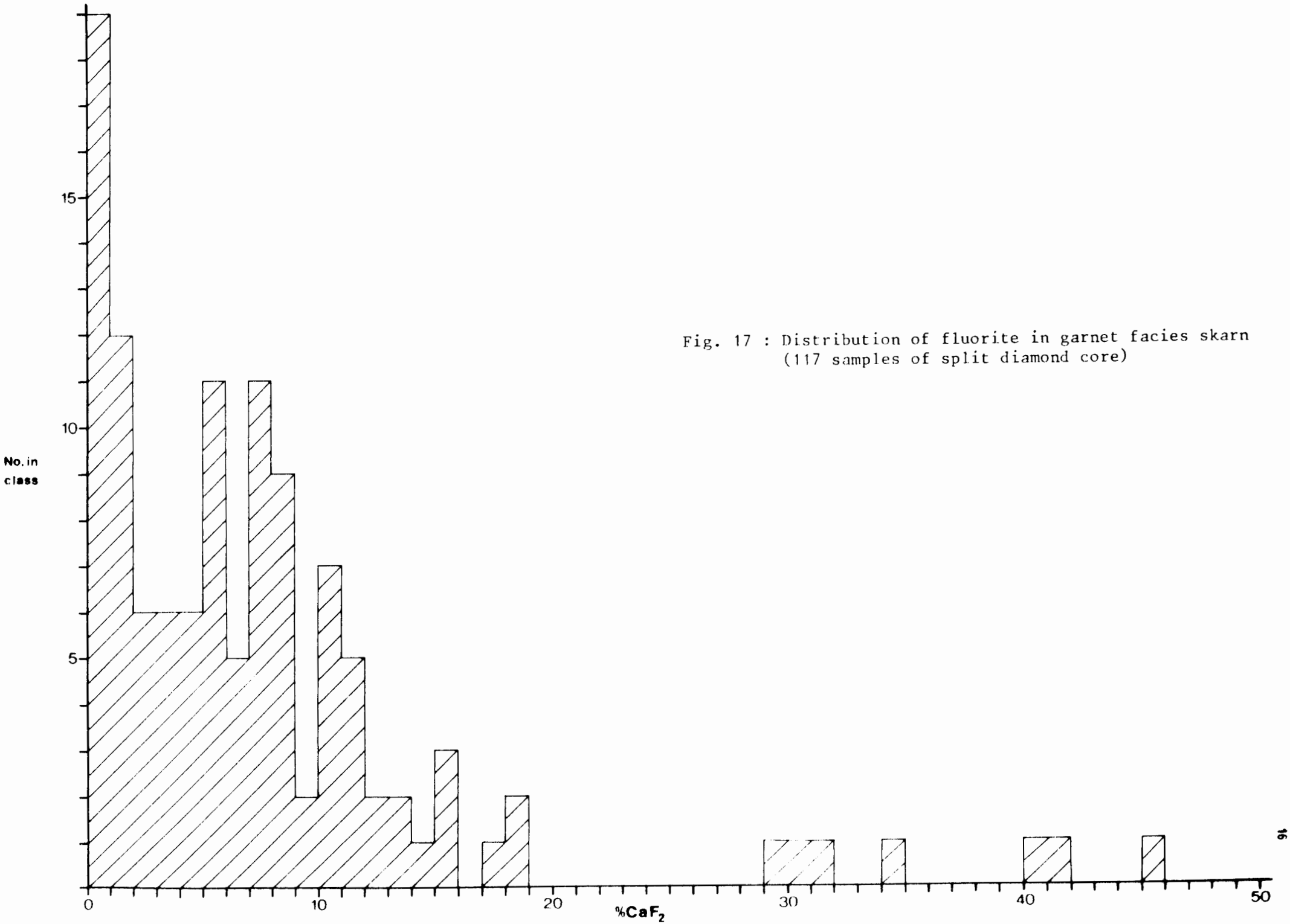

Fig. 17 : Distribution of fluorite in garnet facies skarn
(117 samples of split diamond core)

Fig. 18 : Cumulative frequency diagram of fluorite distribution in garnet facies skarn (117 samples of split diamond core)

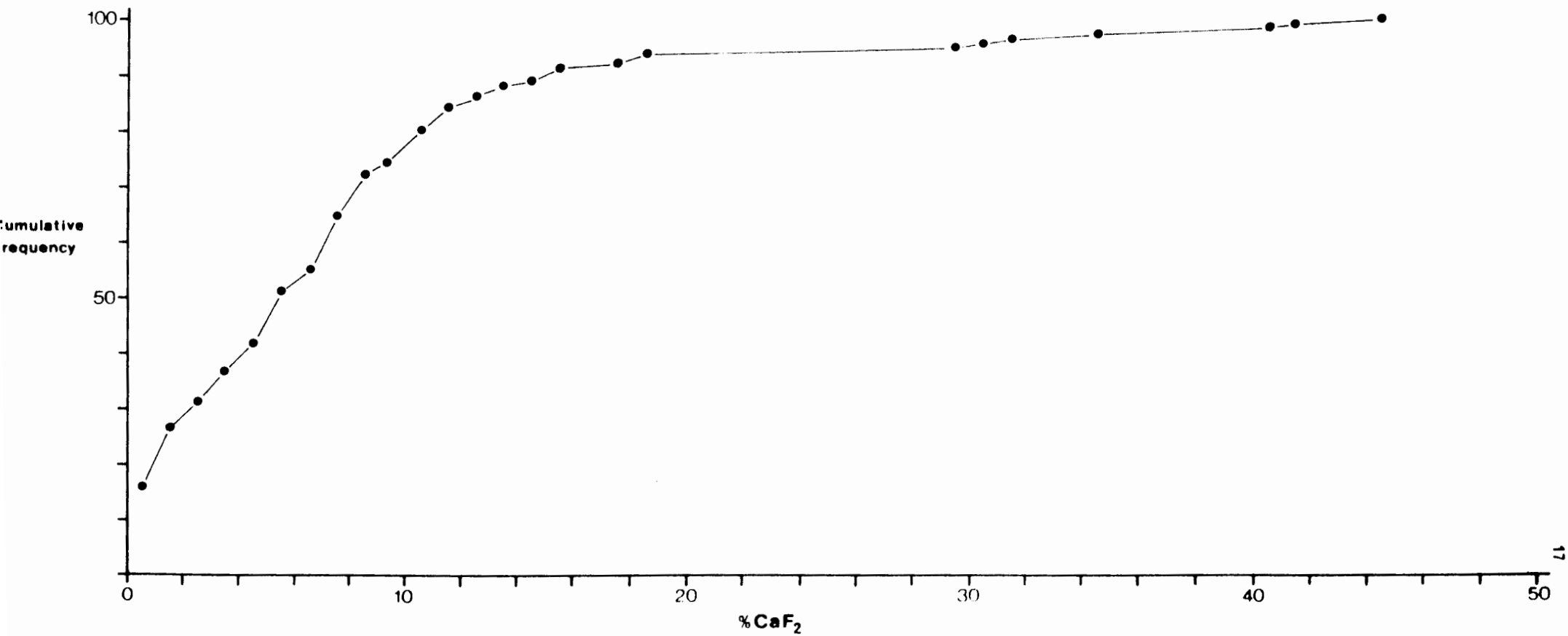

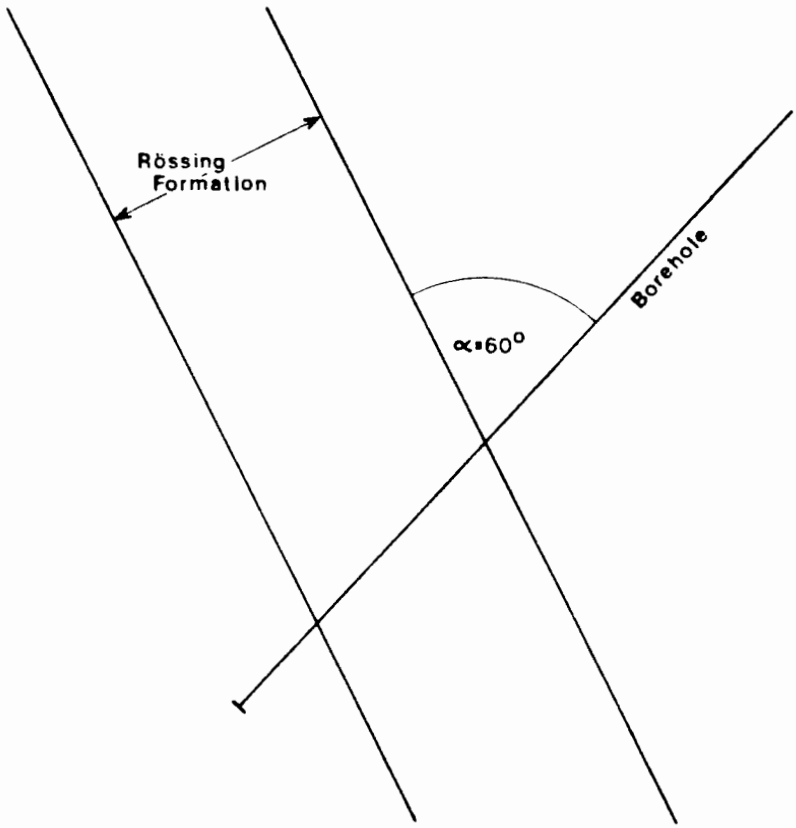

Fig. 19a : Explanation of apparent true thickness (see text)

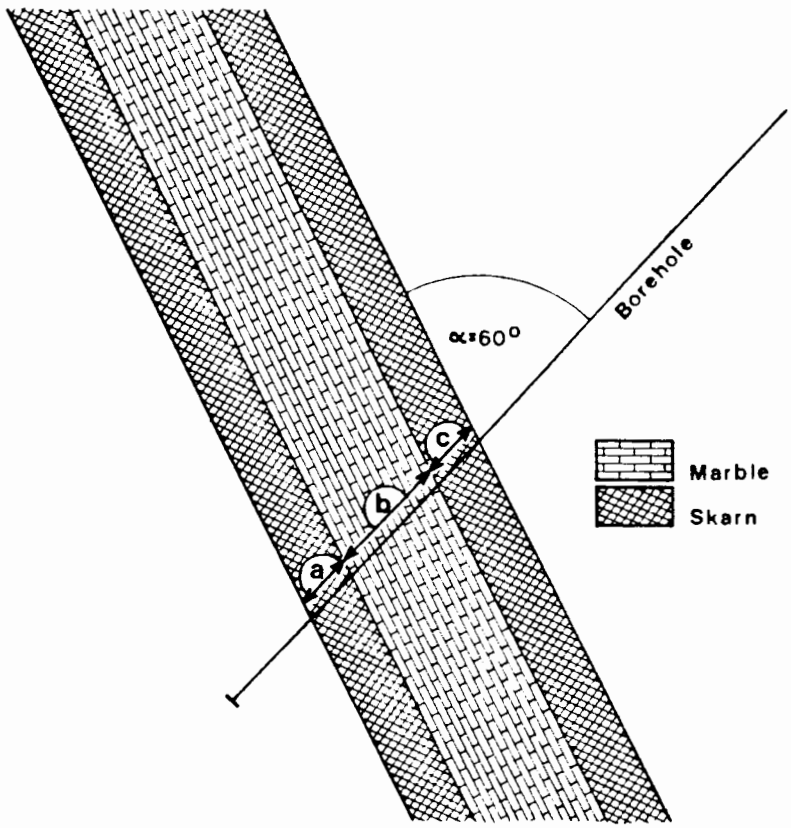

Fig. 19b : Explanation of percentage skarnification (see text)

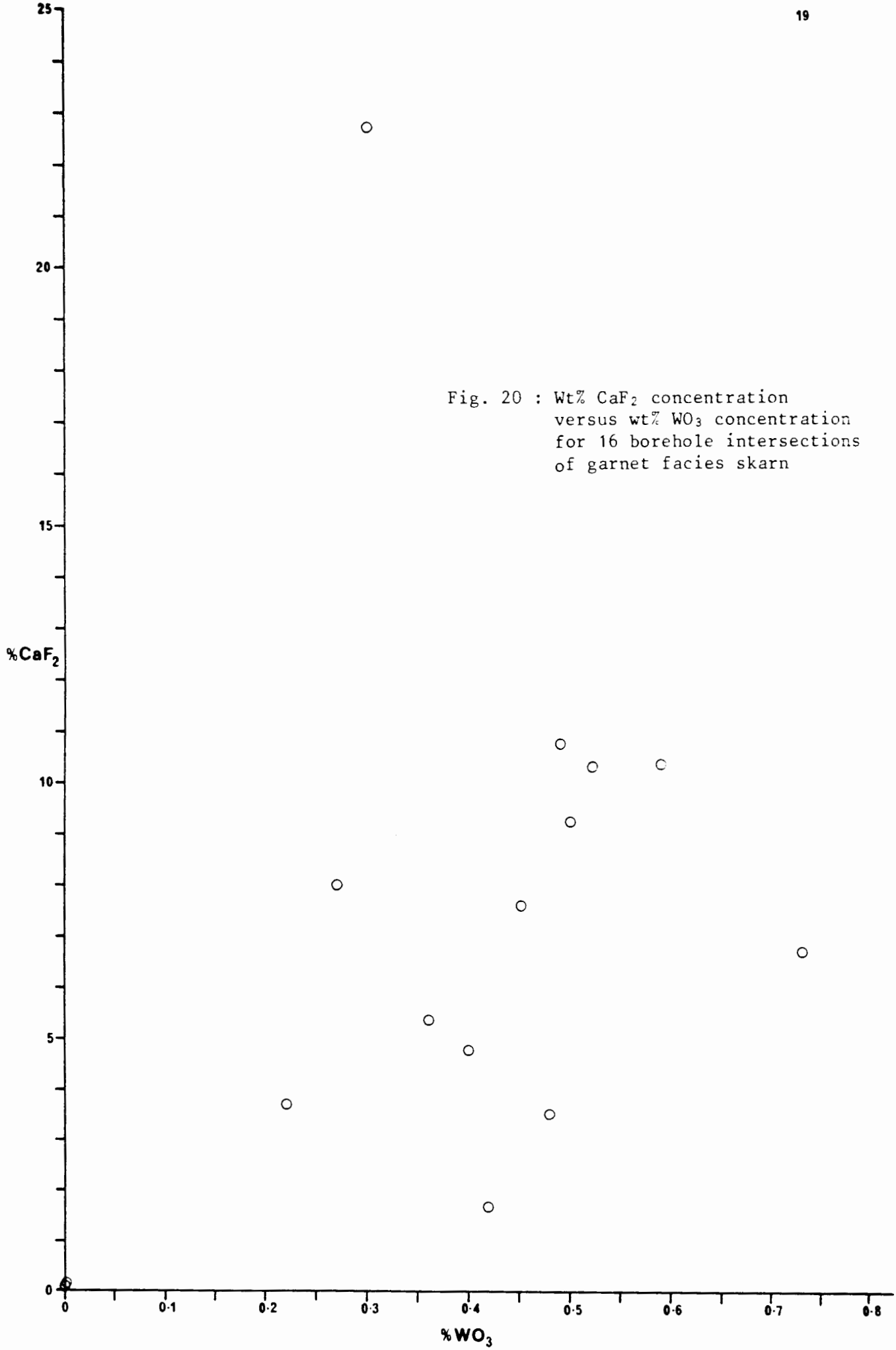

Fig. 20 : Wt% CaF_2 concentration versus wt% WO_3 concentration for 16 borehole intersections of garnet facies skarn

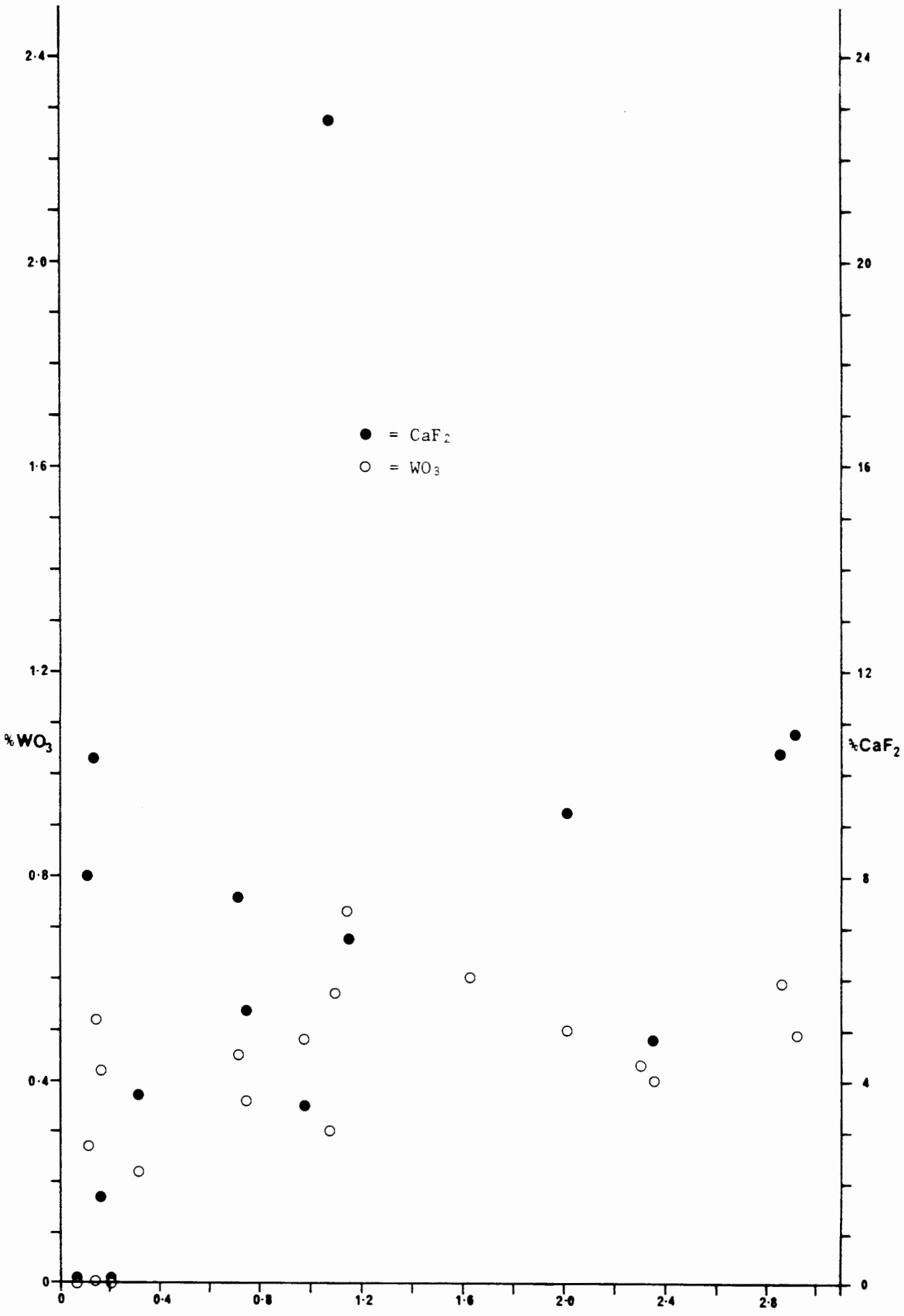

Fig. 21 : Wt% WO_3 and wt% CaF_2 concentrations versus skarn thickness (in metres) for borehole intersections of garnet facies skarn

Fig. 22 : Wt% WO_3 and wt% CaF_2 concentrations versus % skarnification for borehole intersections of garnet facies skarn

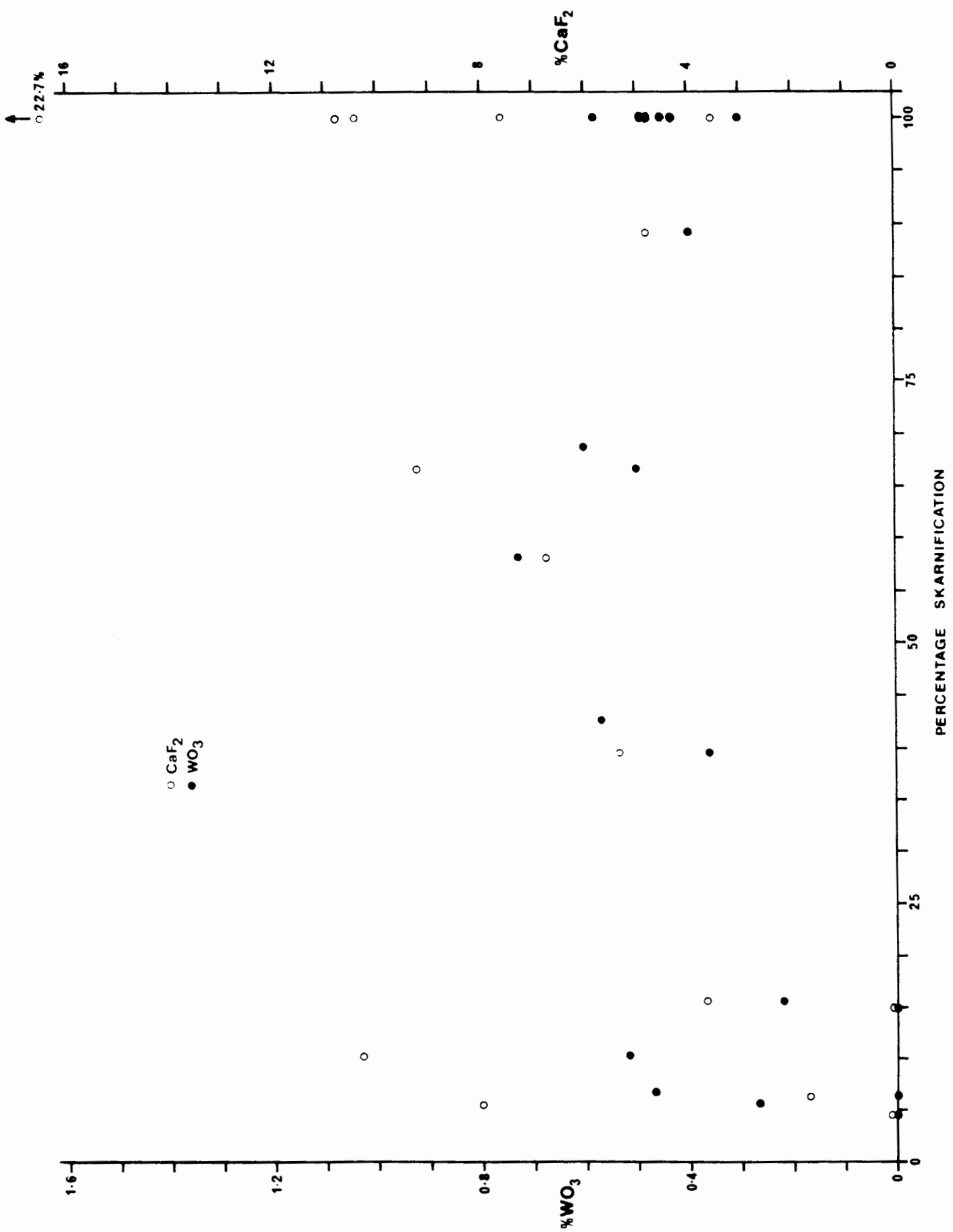

Fig. 23 : Combined marble and skarn thickness (in metres) versus % skarnification for borehole intersections of garnet facies skarn

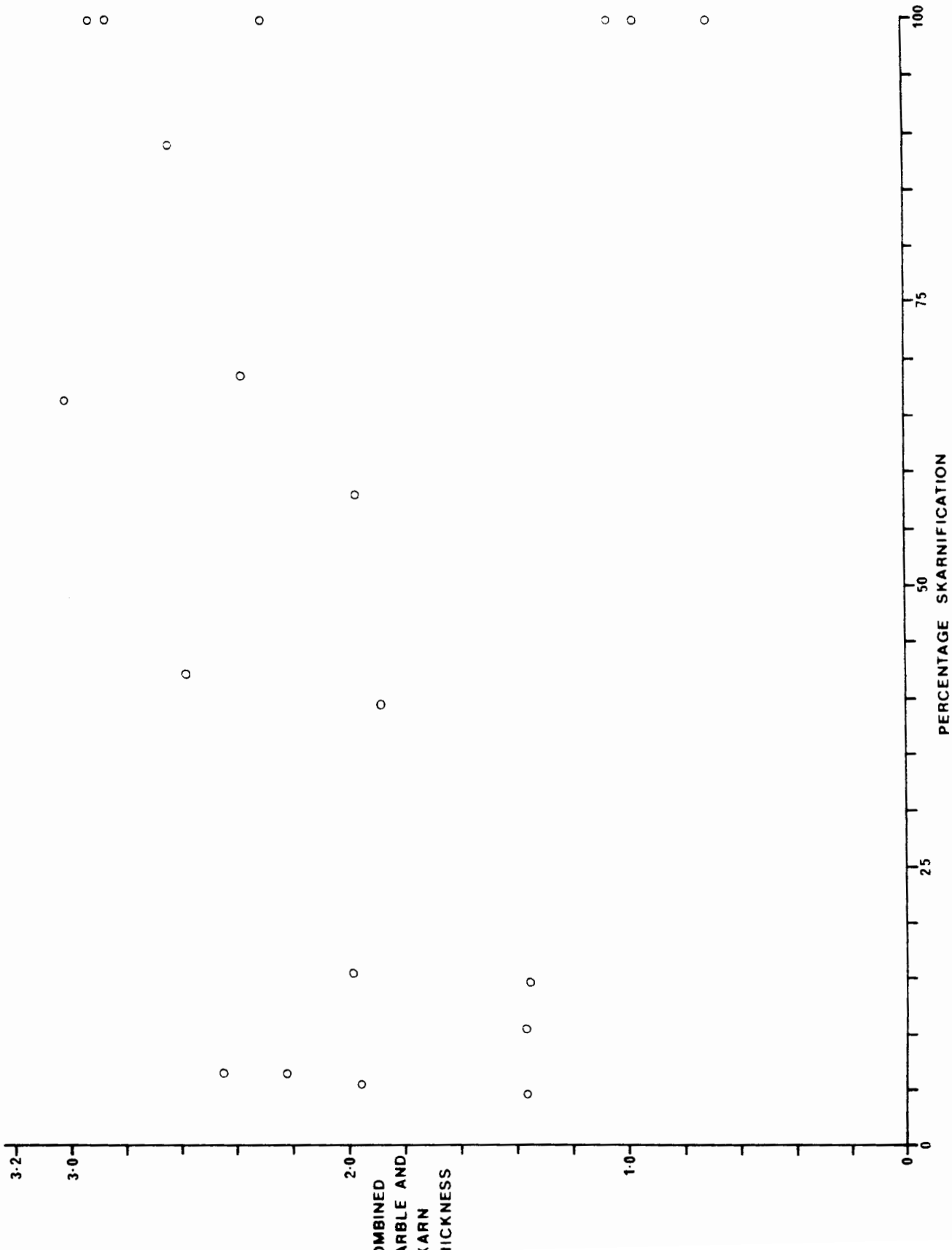

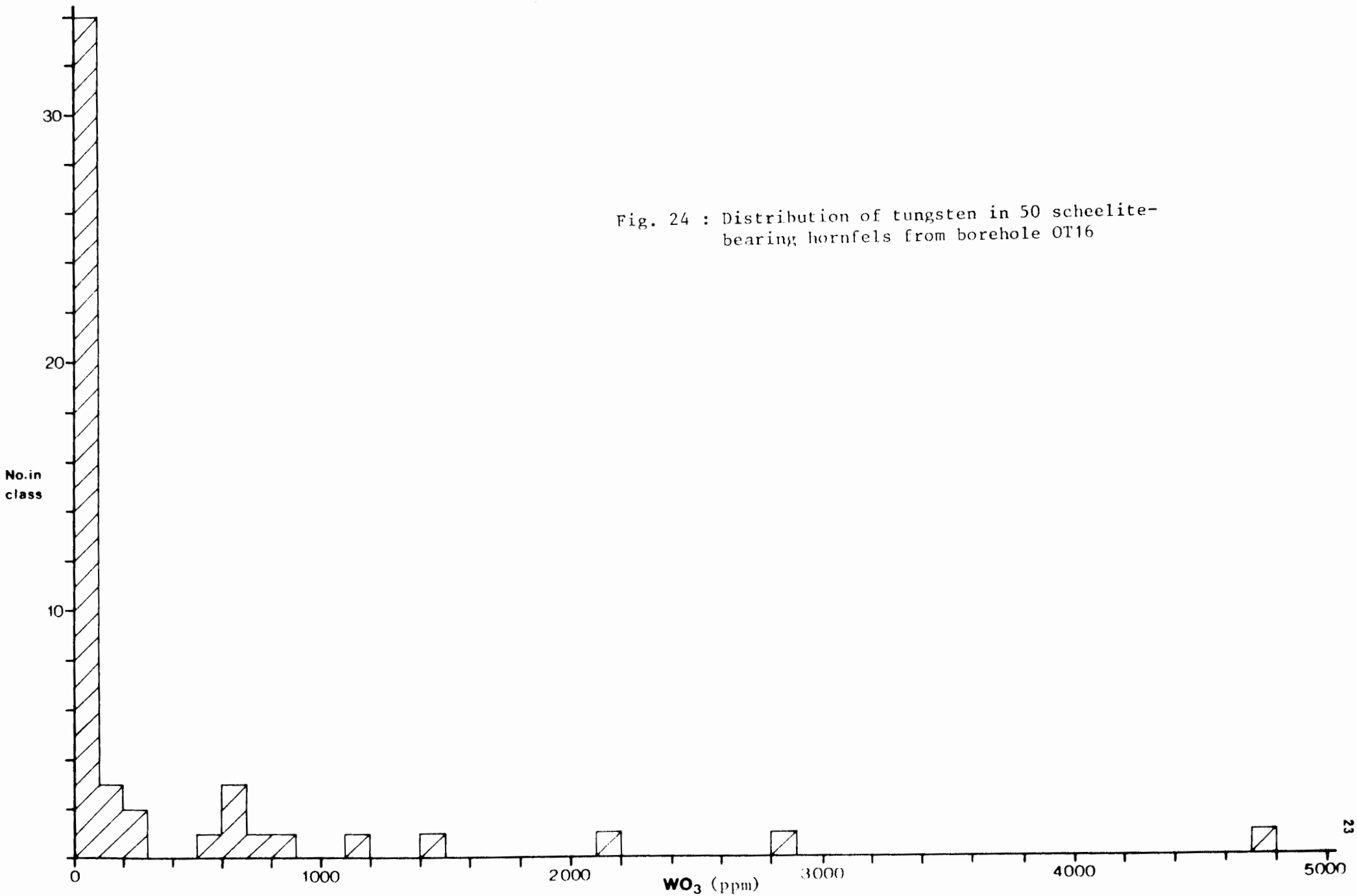

Fig. 24 : Distribution of tungsten in 50 scheelite-bearing hornfels from borehole OT16

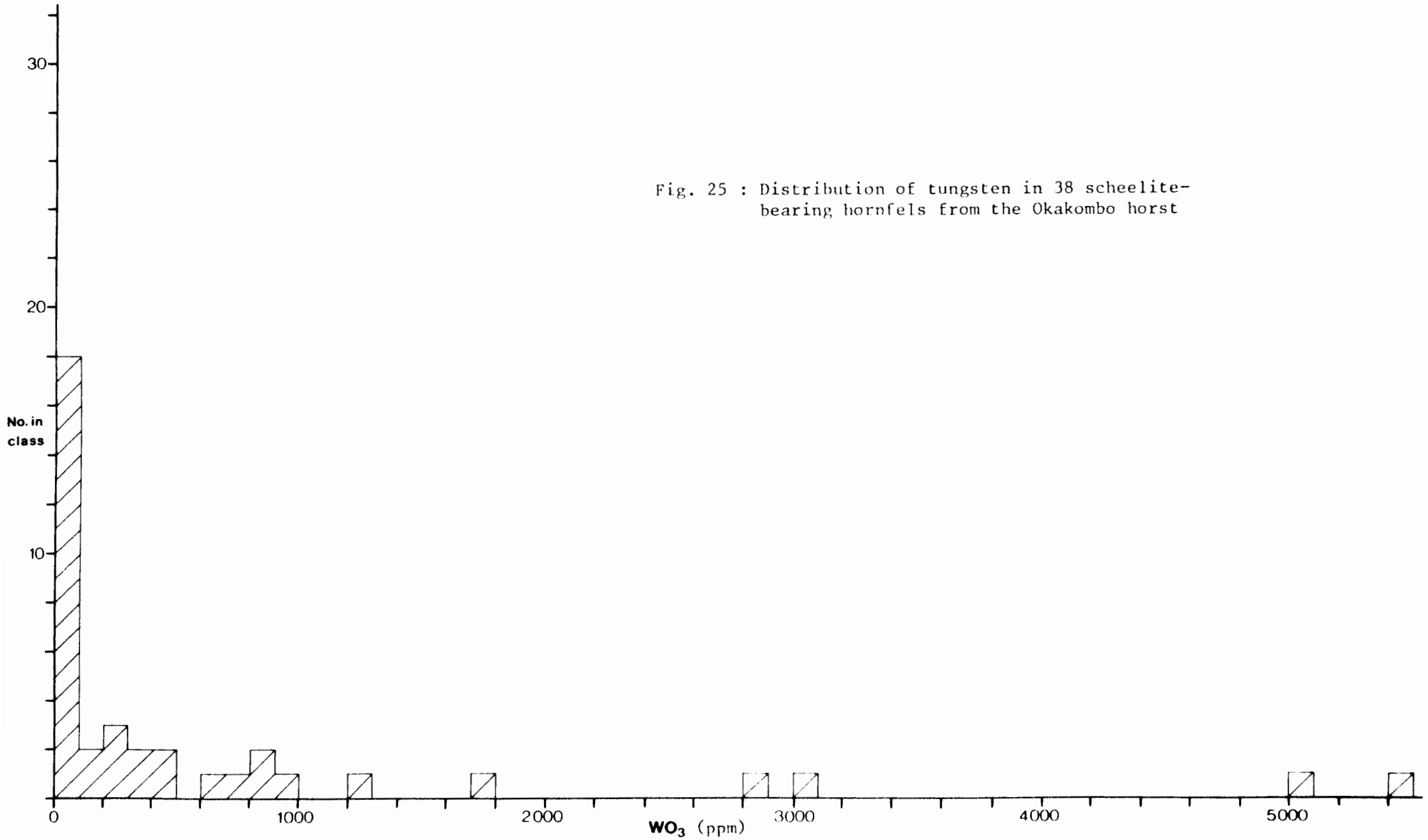

Fig. 25 : Distribution of tungsten in 38 scheelite-bearing hornfels from the Okakombo horst

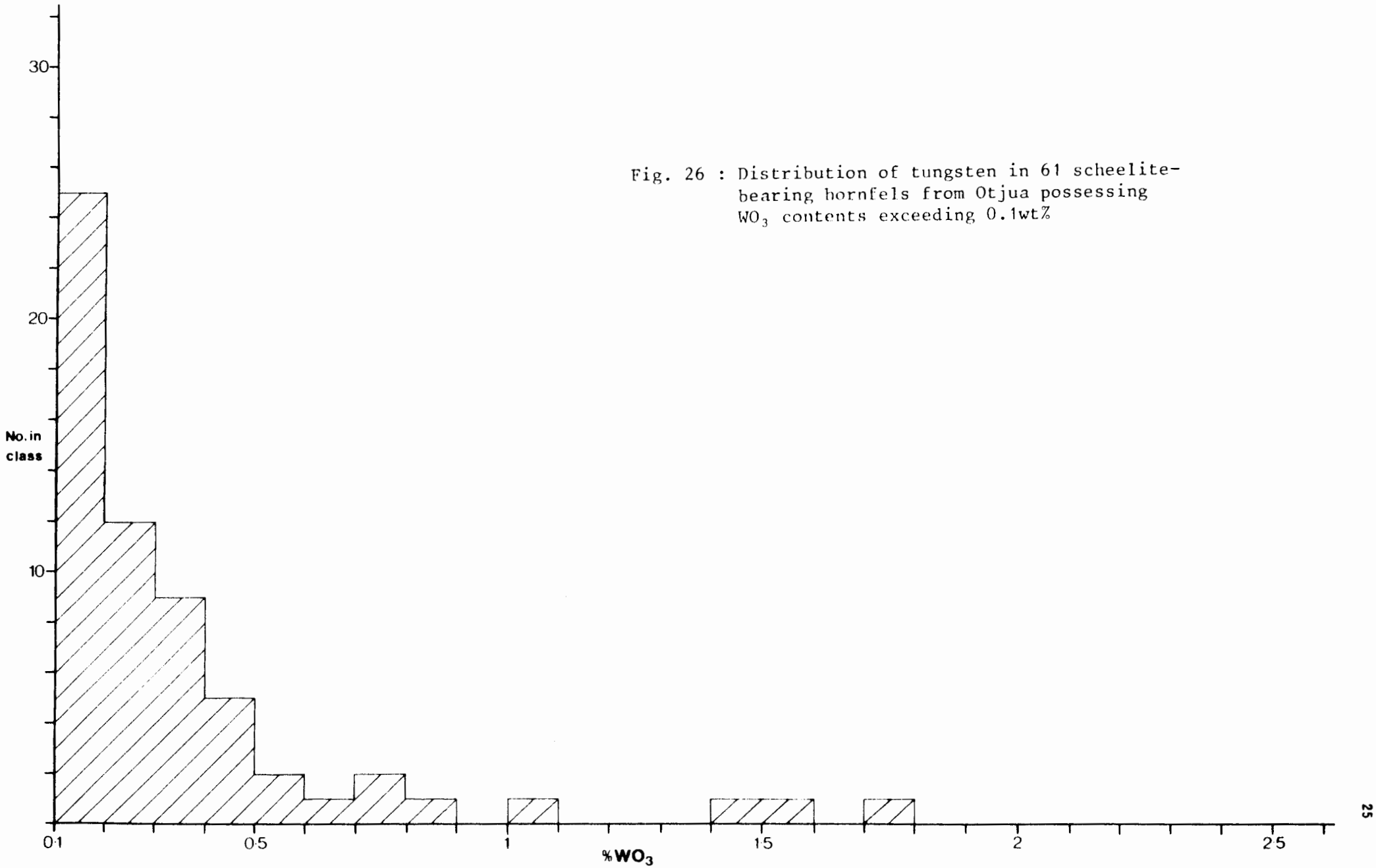

Fig. 26 : Distribution of tungsten in 61 scheelite-bearing hornfels from Otjua possessing WO_3 contents exceeding 0.1wt%

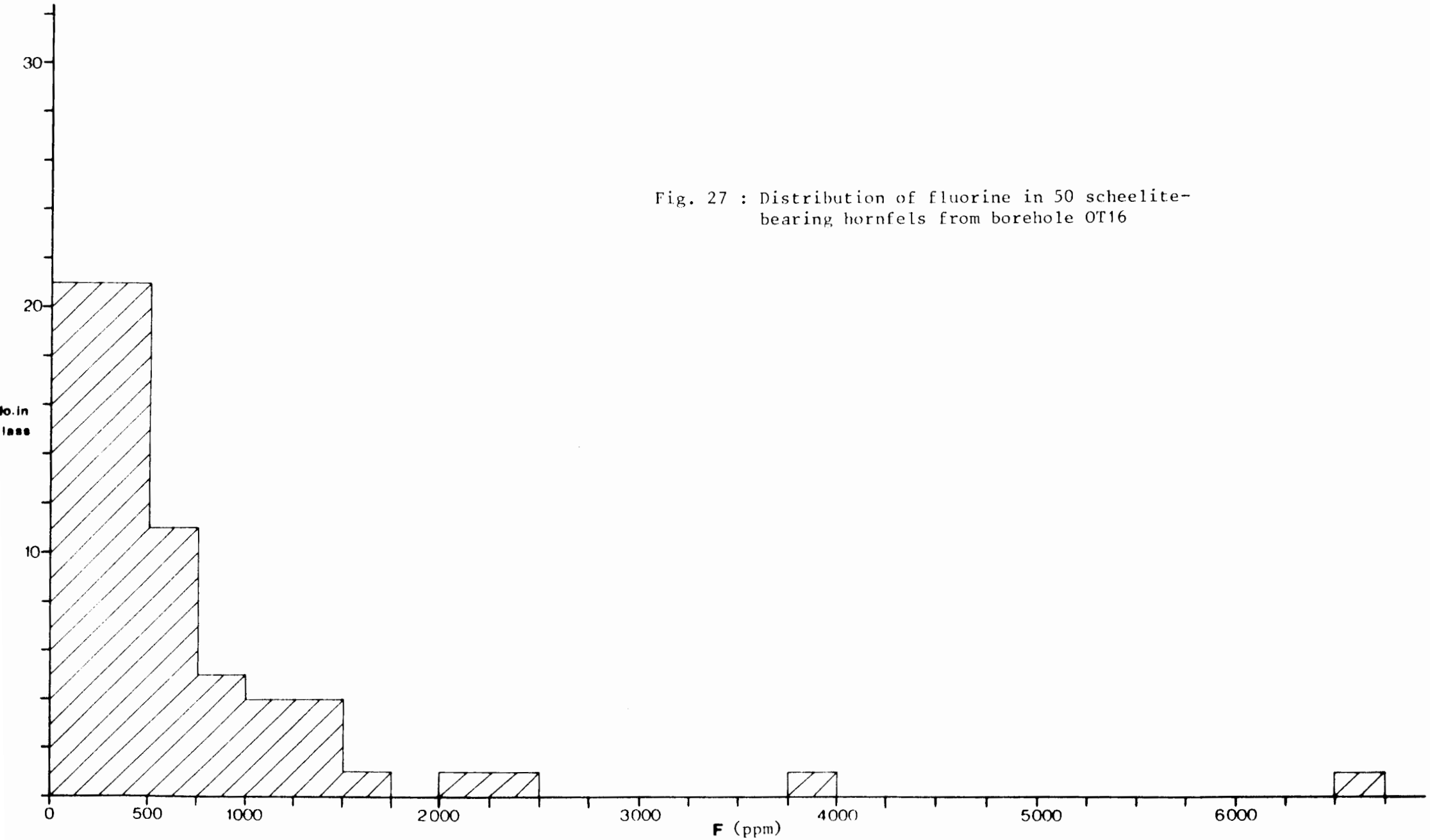

Fig. 27 : Distribution of fluorine in 50 scheelite-bearing hornfels from borehole OT16

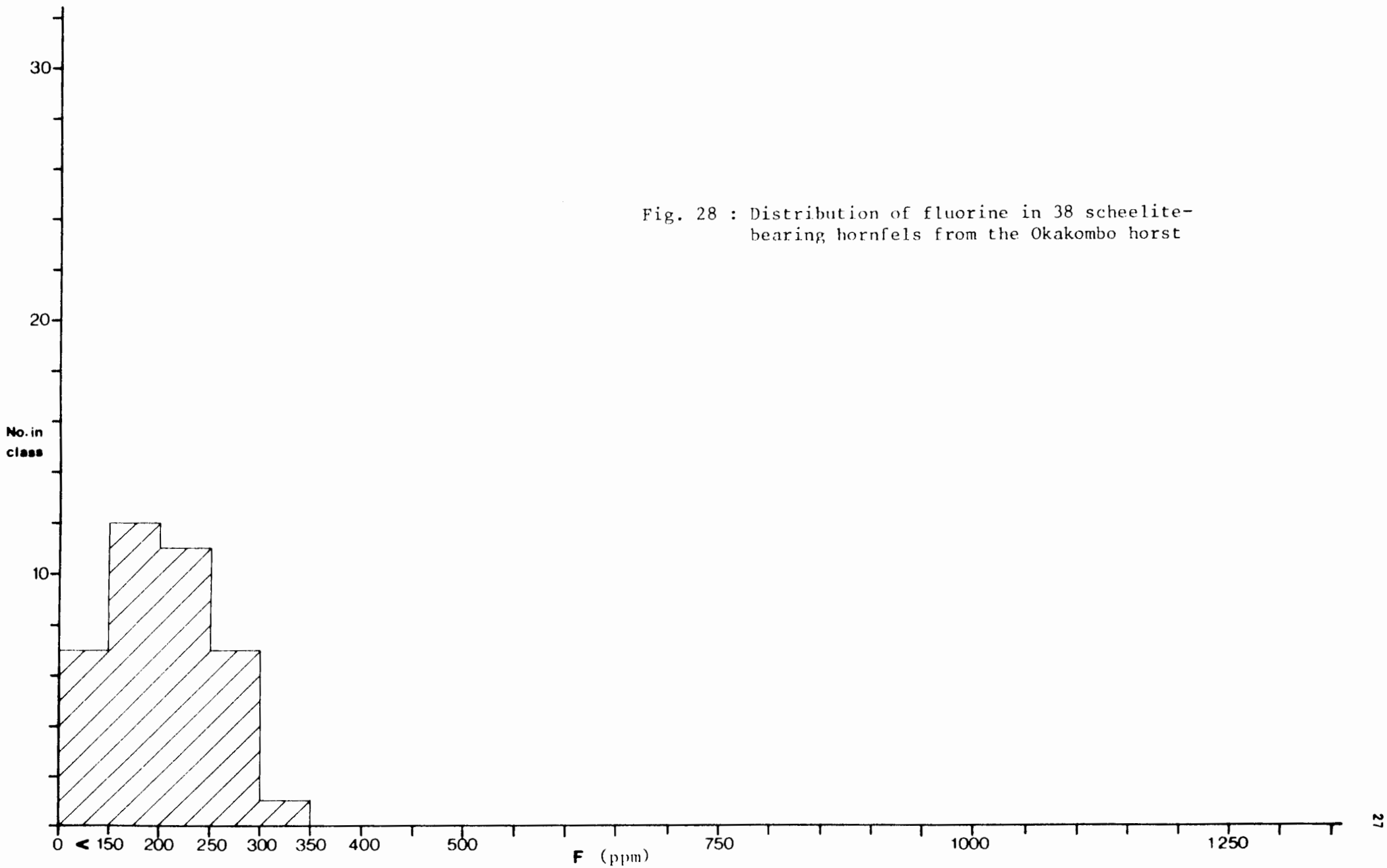

Fig. 28 : Distribution of fluorine in 38 scheelite-bearing hornfels from the Okakombo horst

Fig. 29 : Ternary plot $CaO-Na_2O-K_2O$ for biotite schist from Otjua and other pelites

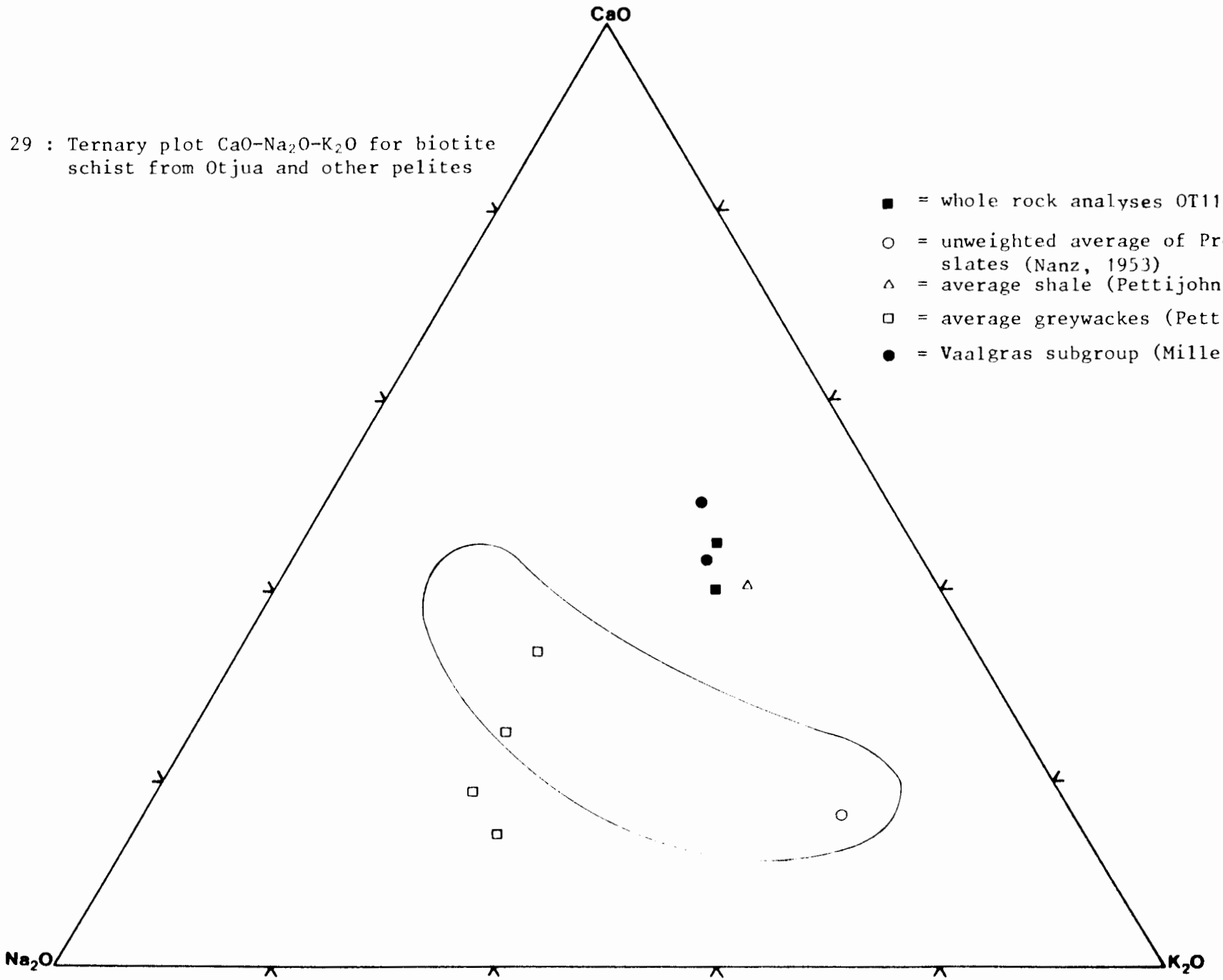

Fig. 30 : Ternary plot Al_2O_3-CaO-SiO_2 for calc-silicates and scheelite-bearing hornfels

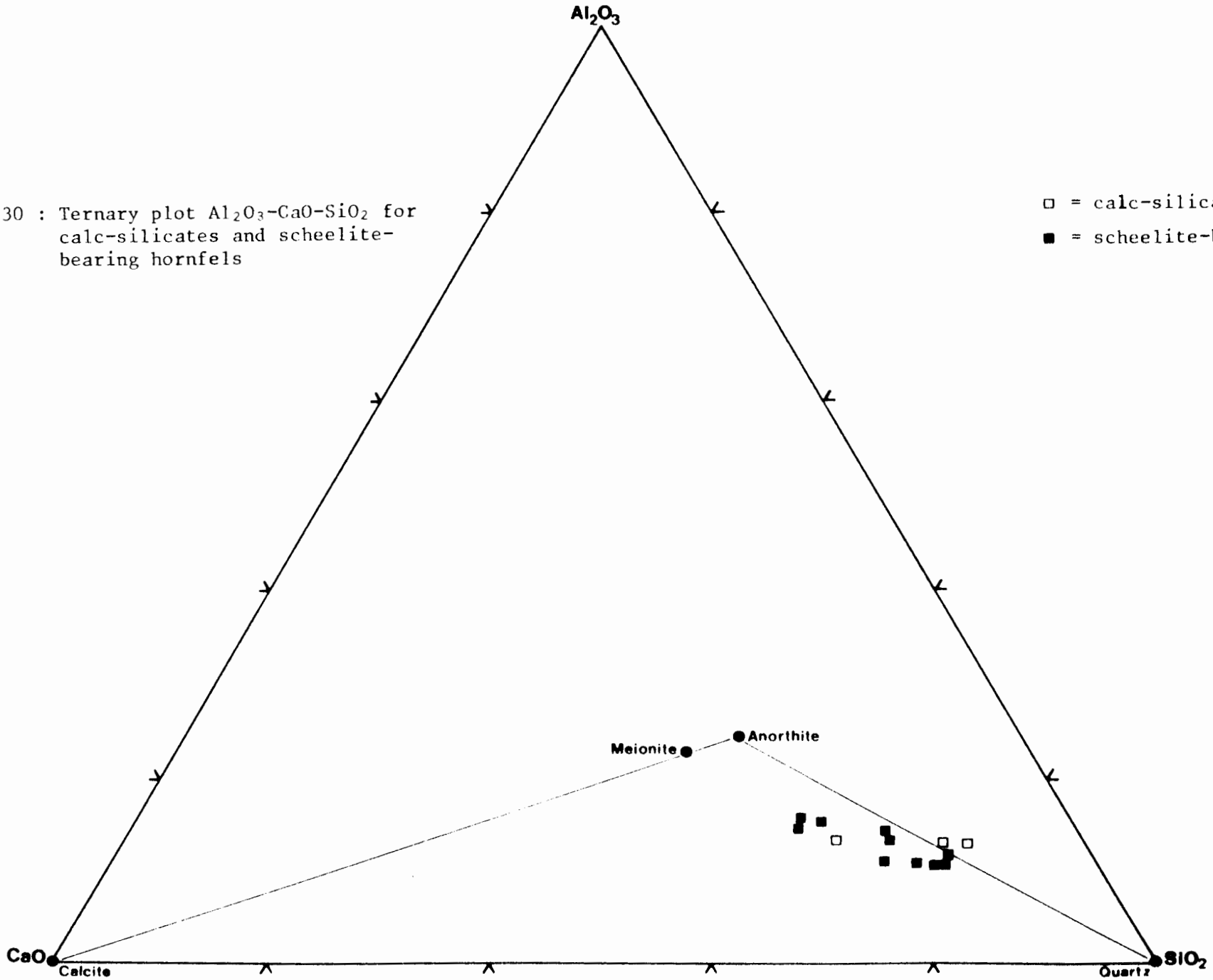

Fig. 31 : Ternary plot Al_2O_3-FeO-MgO for calc-silicates and scheelite-bearing hornfels

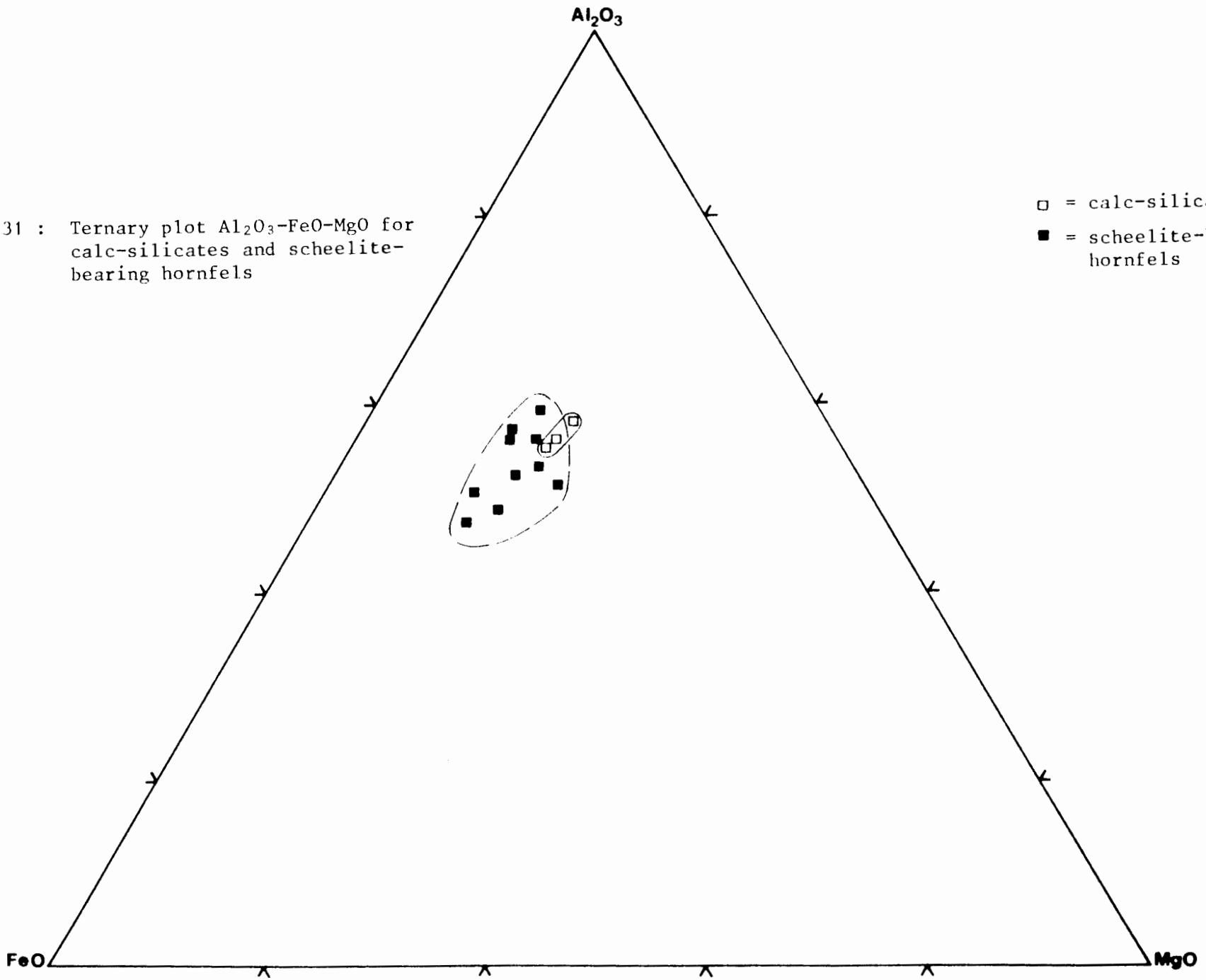

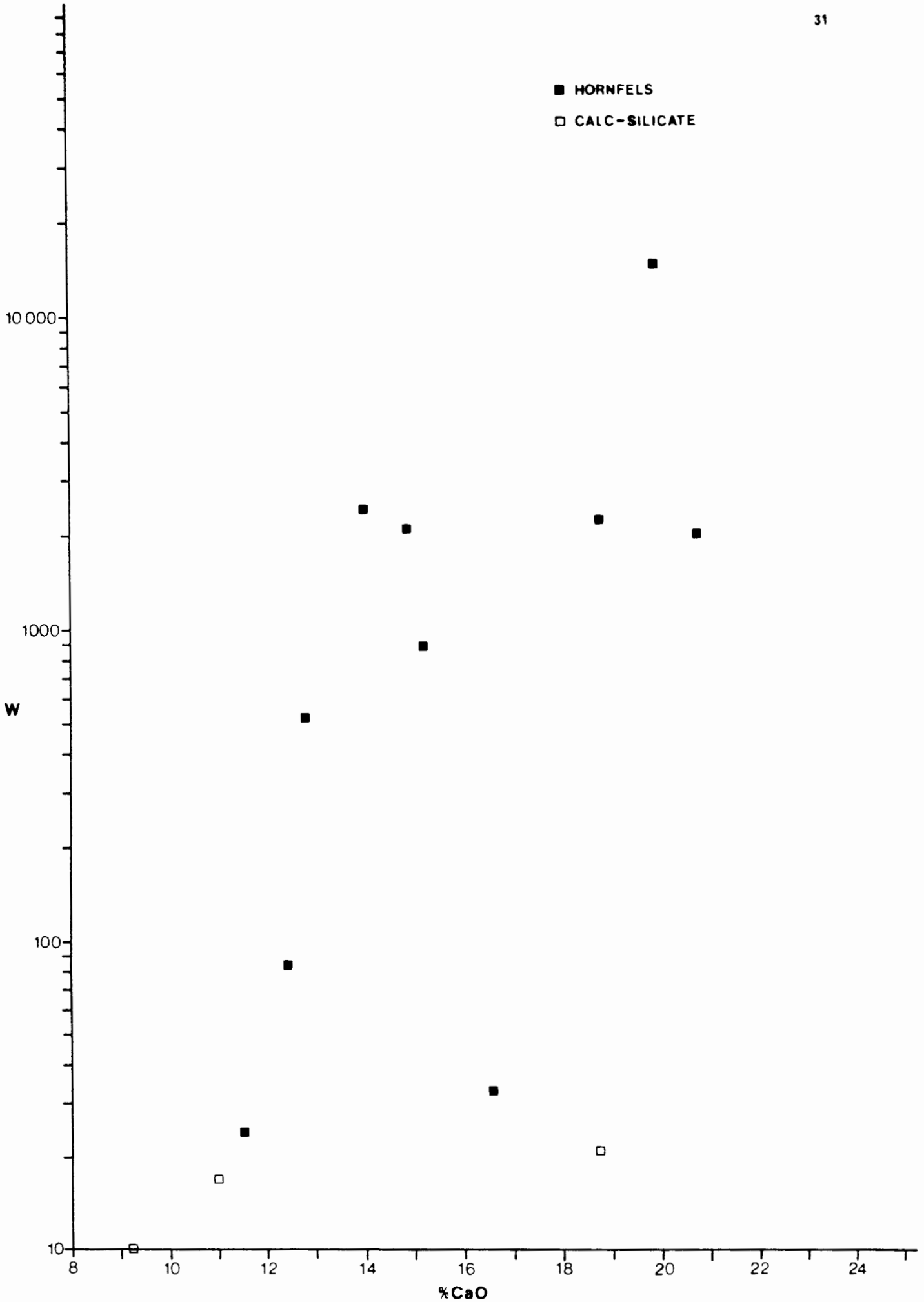

Fig. 32 : W concentration (in ppm) versus wt% CaO content of calc-silicate and scheelite-bearing hornfels

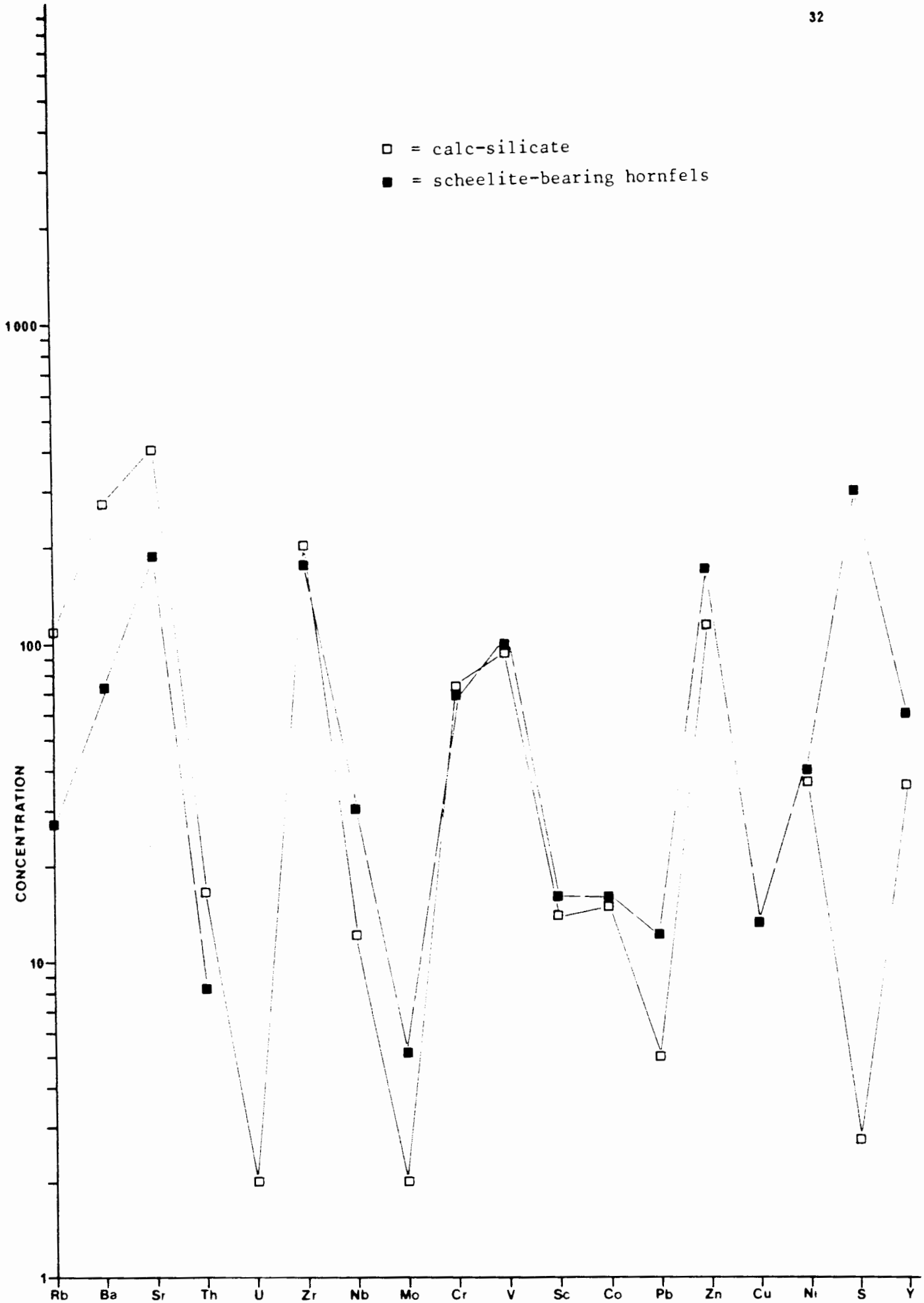

Fig. 33 : Average trace element concentrations (in ppm) of calc-silicate and scheelite-bearing hornfels

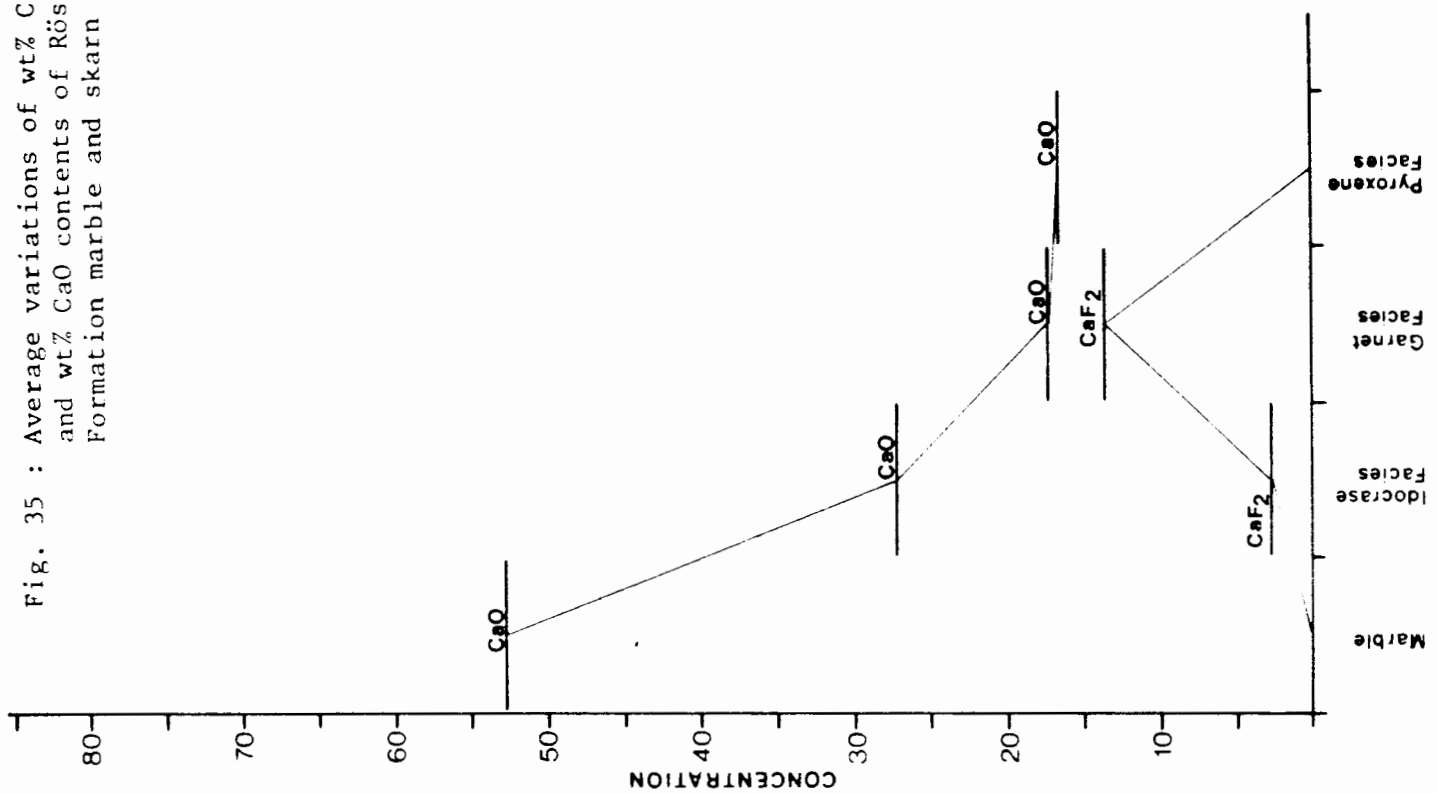

Fig. 35 : Average variations of wt% CaF_2 and wt% CaO contents of Rössing Formation marble and skarn facies

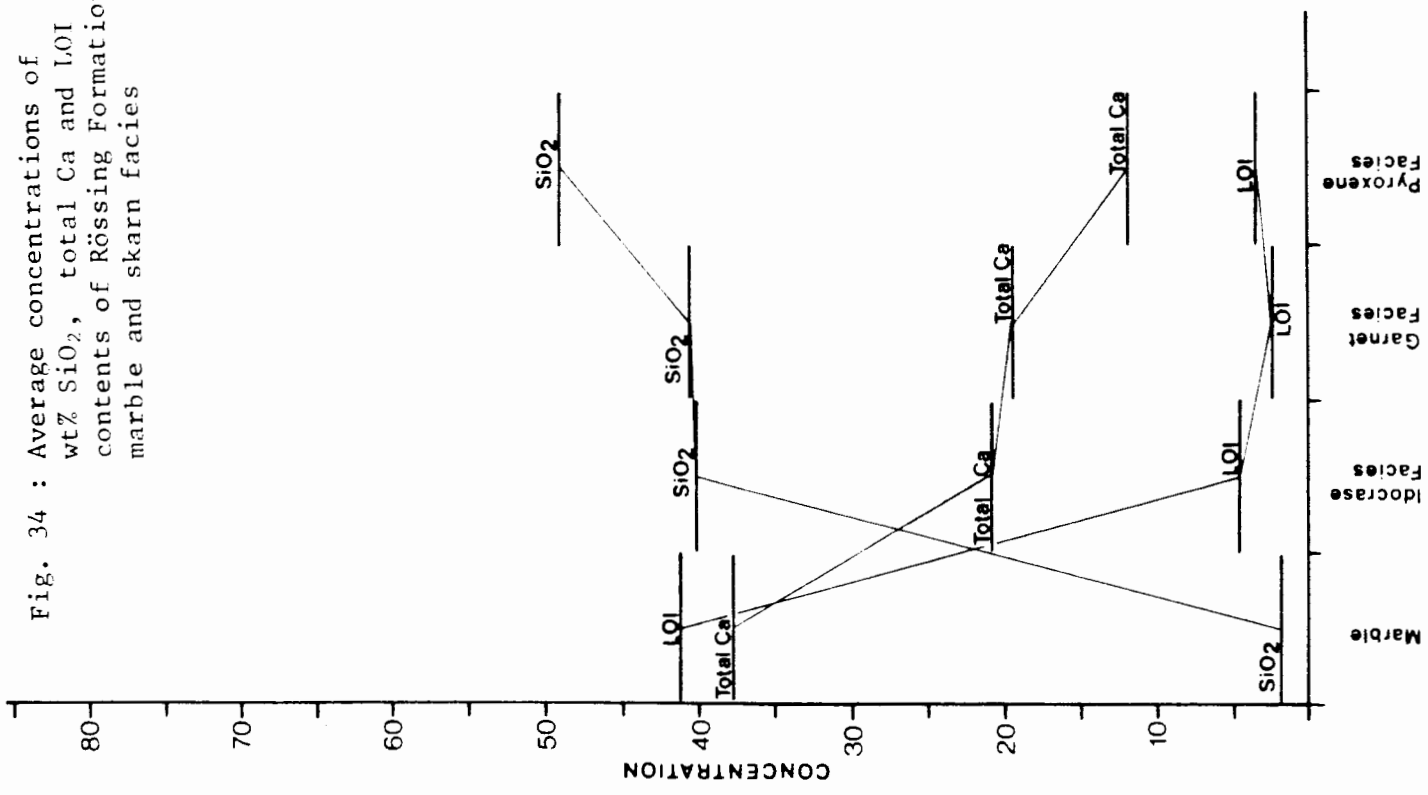

Fig. 34 : Average concentrations of wt% SiO_2, total Ca and LOI contents of Rössing Formation marble and skarn facies

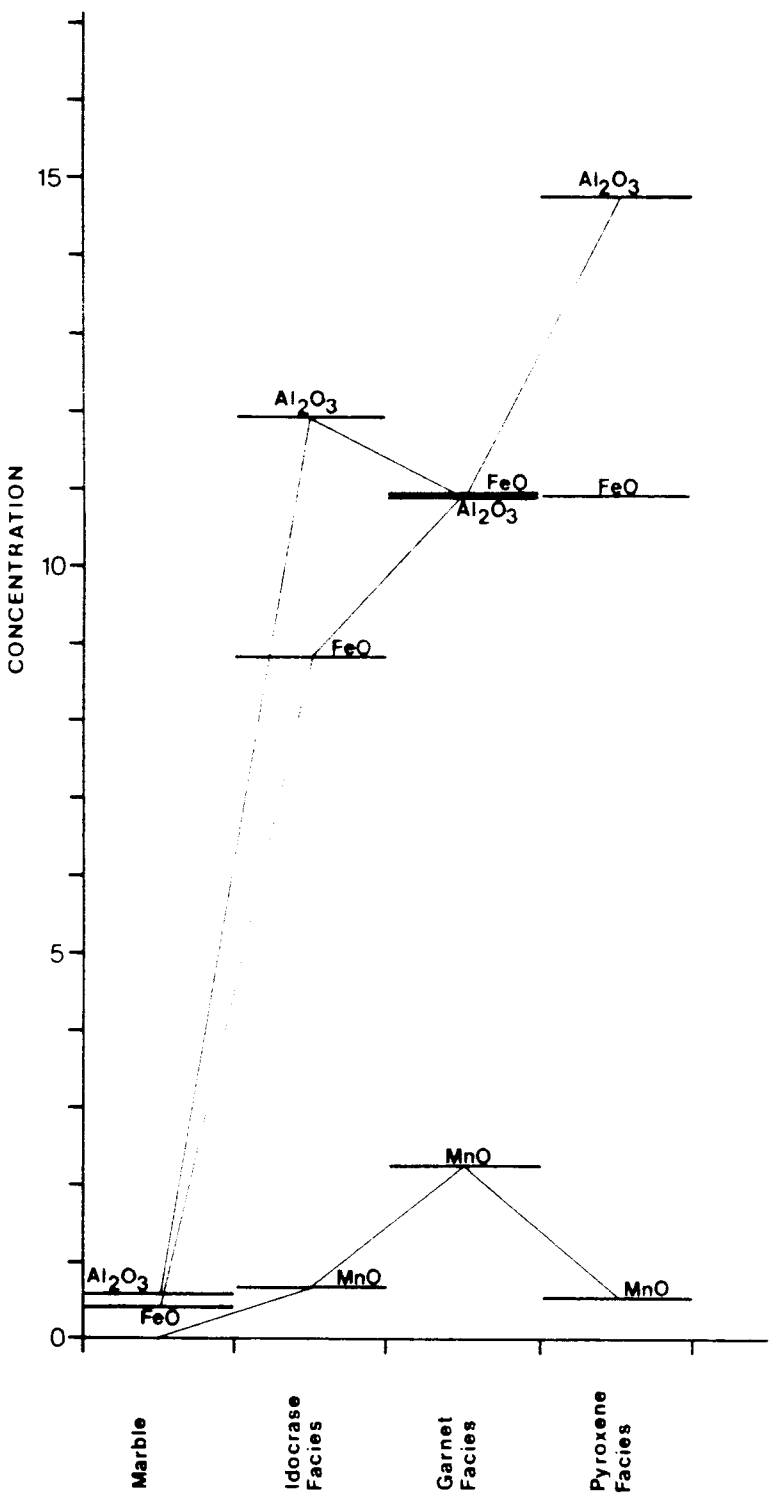

Fig. 36 : Average variations of wt% Al_2O_3, wt% FeO and wt% MnO contents of Rössing Formation marble and skarn facies. (All iron expressed as FeO)

Fig. 37 : Average variations of wt% MgO and TiO_2 contents of Rössing Formation marble and skarn facies

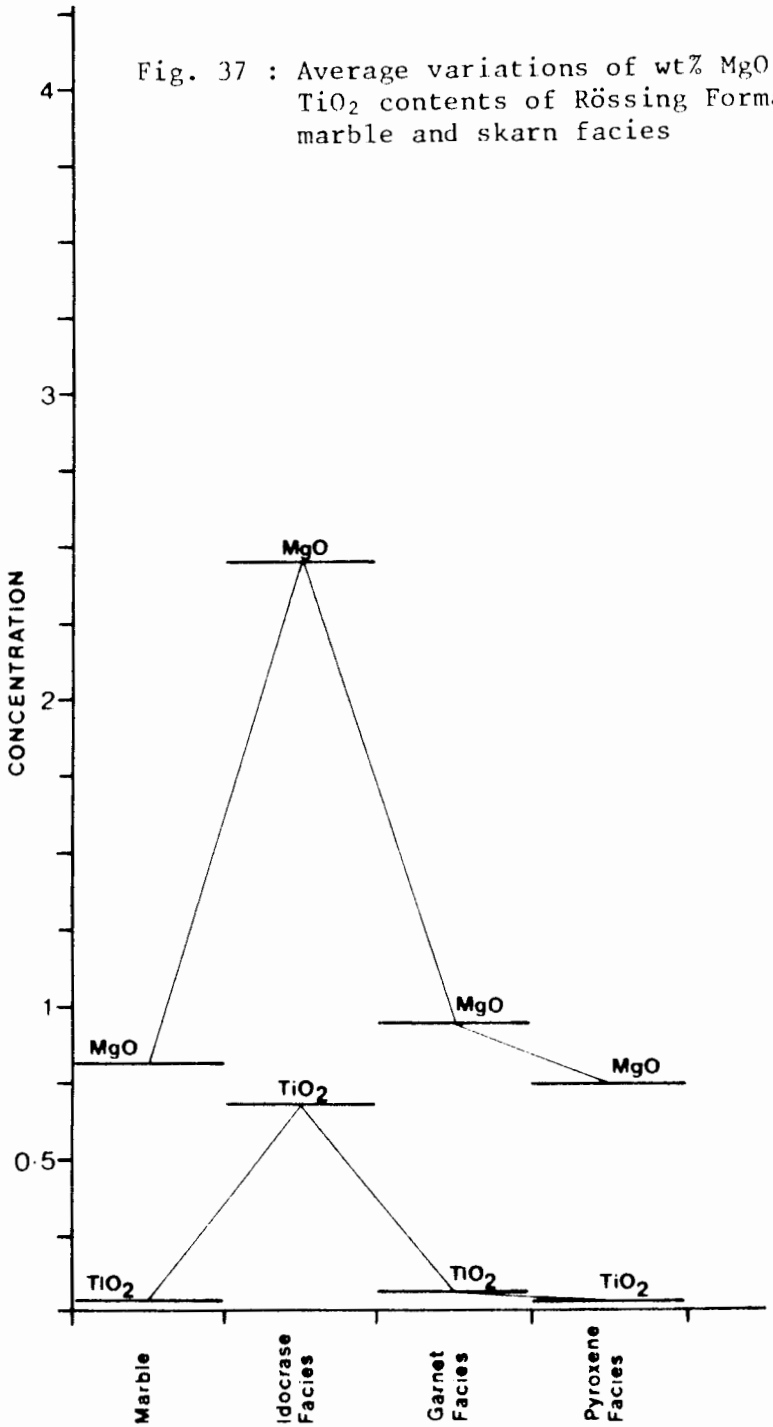

Fig. 38 : Average variations of wt% Na_2O and wt% K_2O contents of Rössing Formation marble and skarn facies

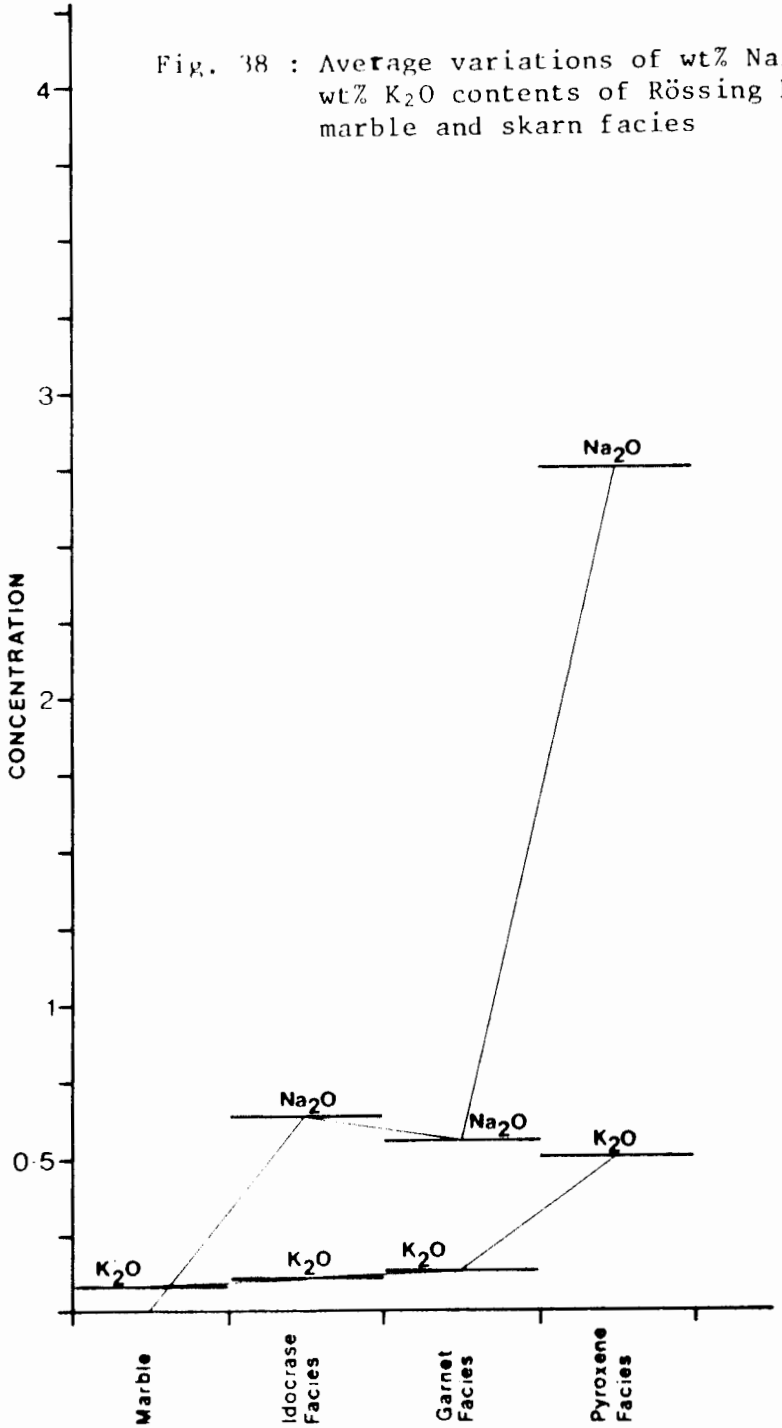

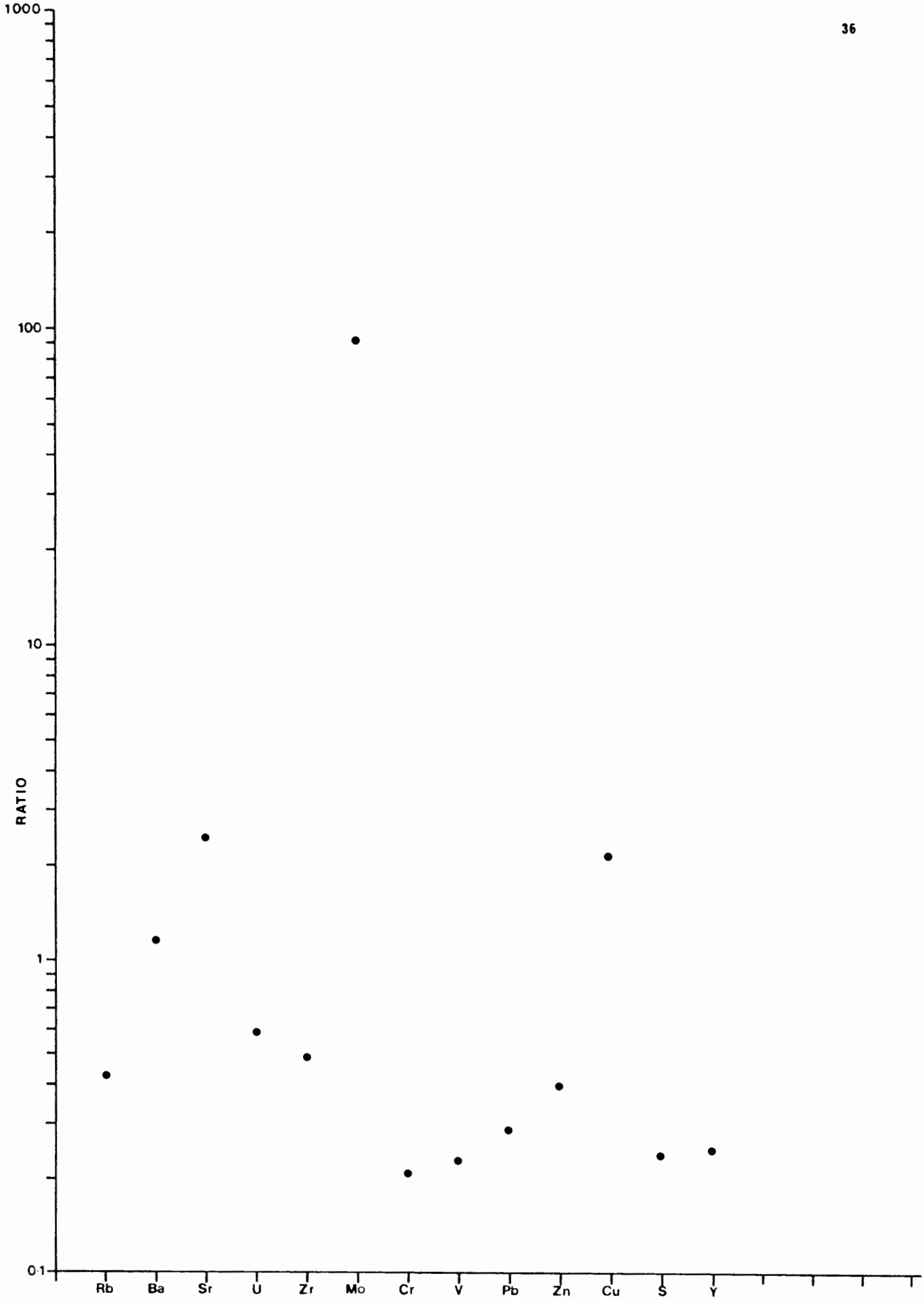

Fig. 39 : Average carbonate-normalised trace element pattern for Rössing Formation (ratio = ppm Rössing Formation/ppm average carbonate)

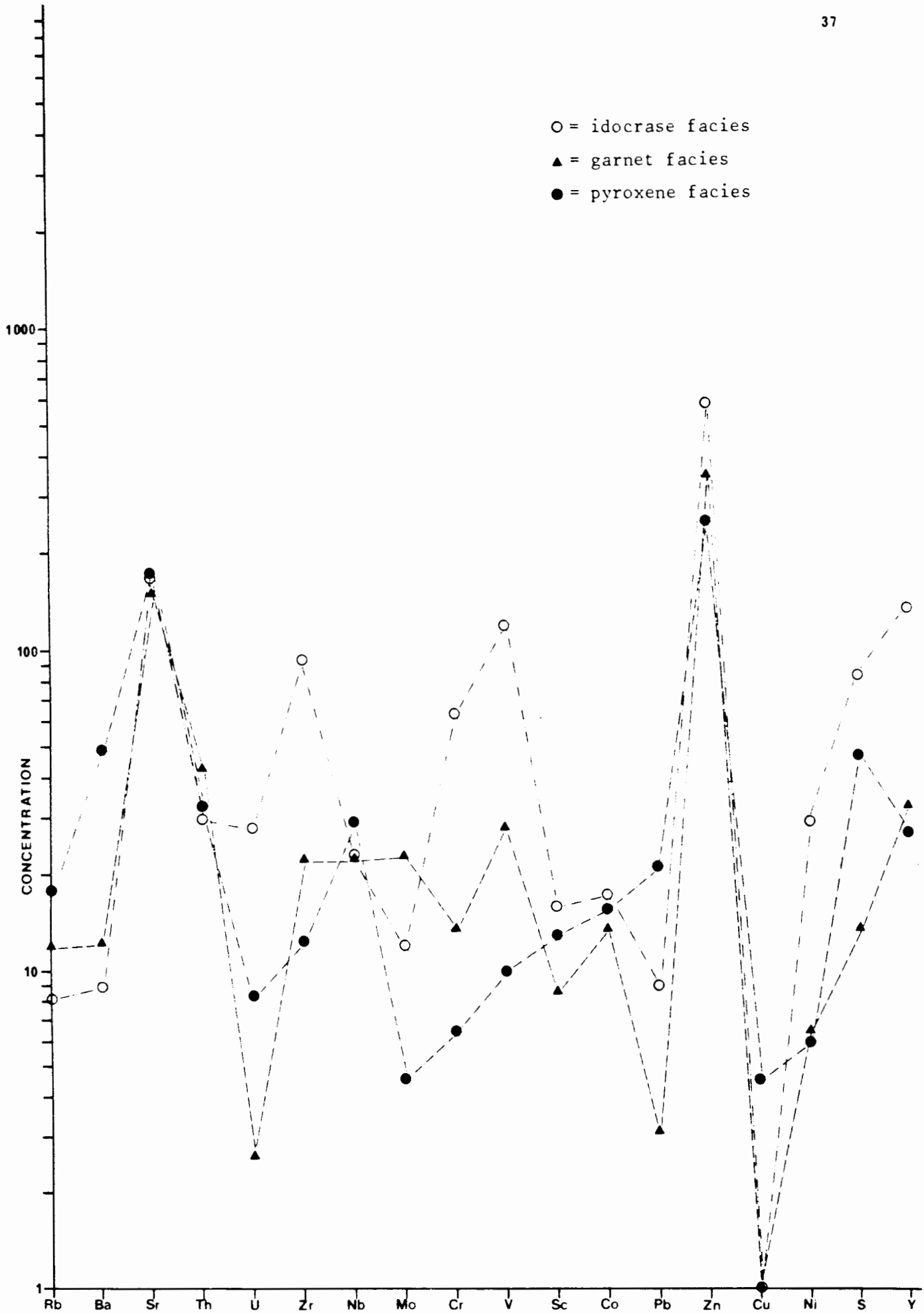

Fig. 40 : Average trace element concentrations (in ppm) of skarn facies hosted by the Rössing Formation marble

Fig. 41 : Average concentrations (in ppm) of Co, Cr, V, Ni, Zn, Zr and Y in skarn facies, intrusives and metasediments

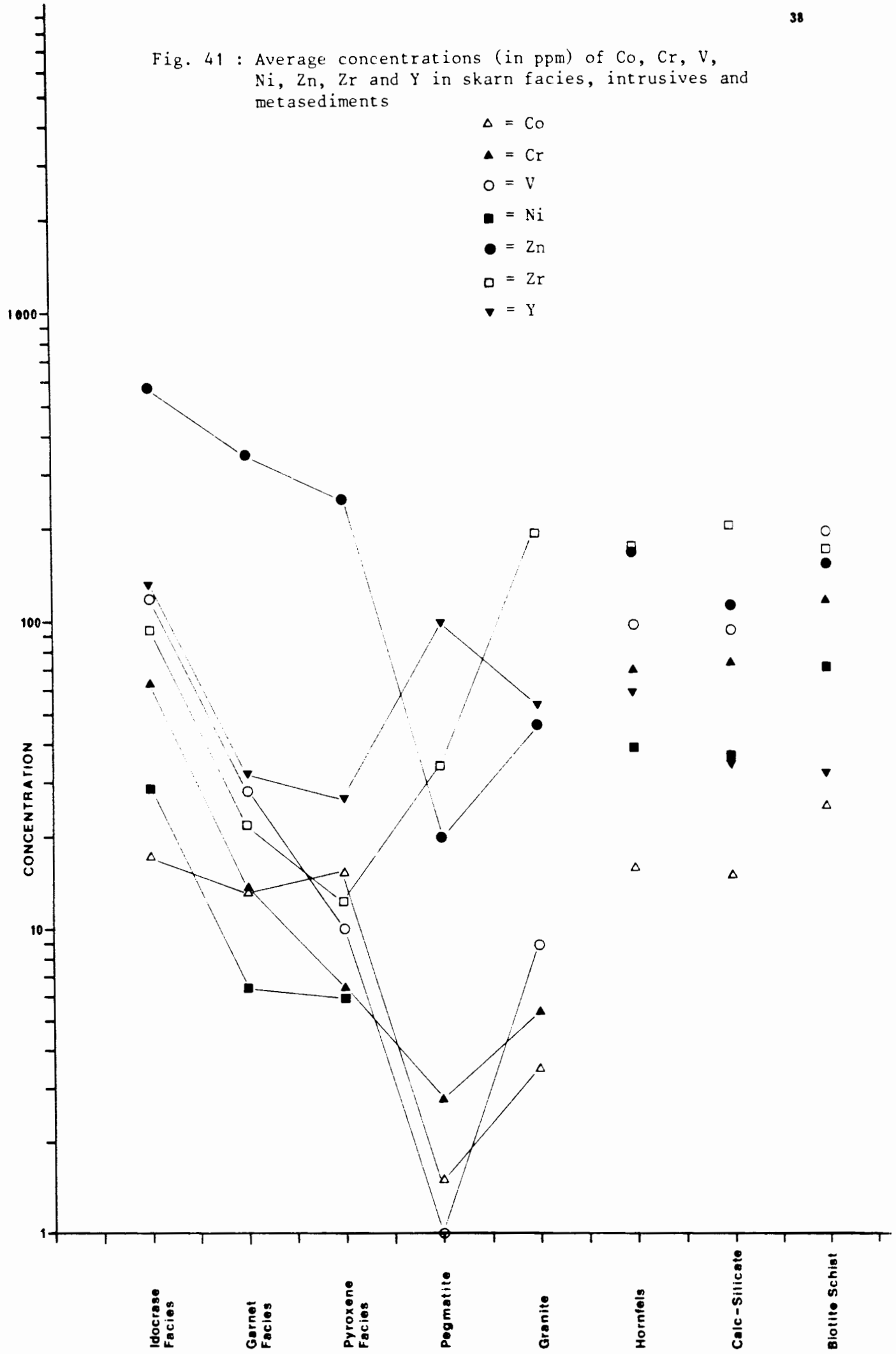

Fig. 42 : Average concentrations (in ppm) of Ba, Rb, Pb and Sr in skarn facies, intrusives and metasediments

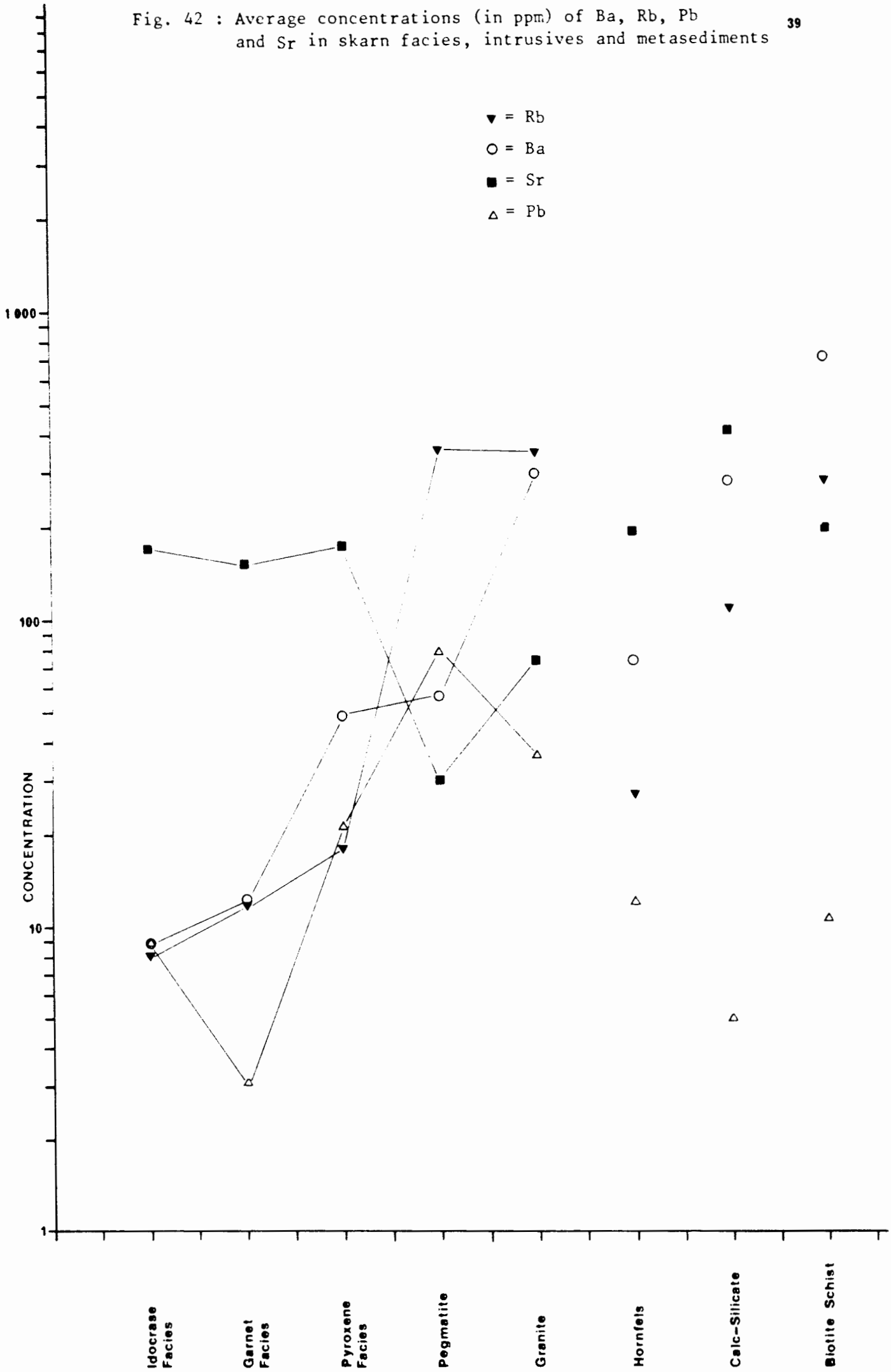

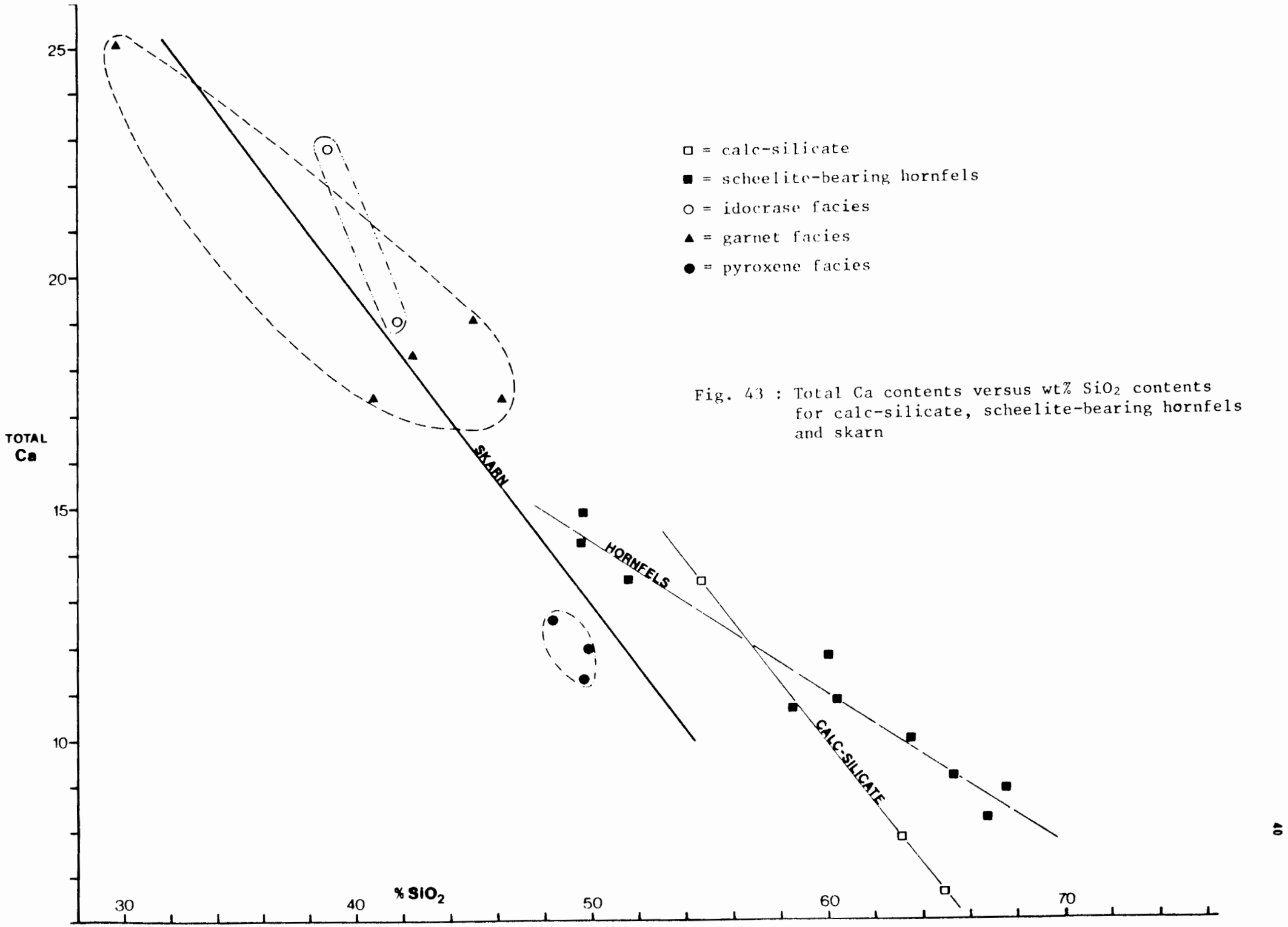

Fig. 43 : Total Ca contents versus wt% SiO_2 contents for calc-silicate, scheelite-bearing hornfels and skarn

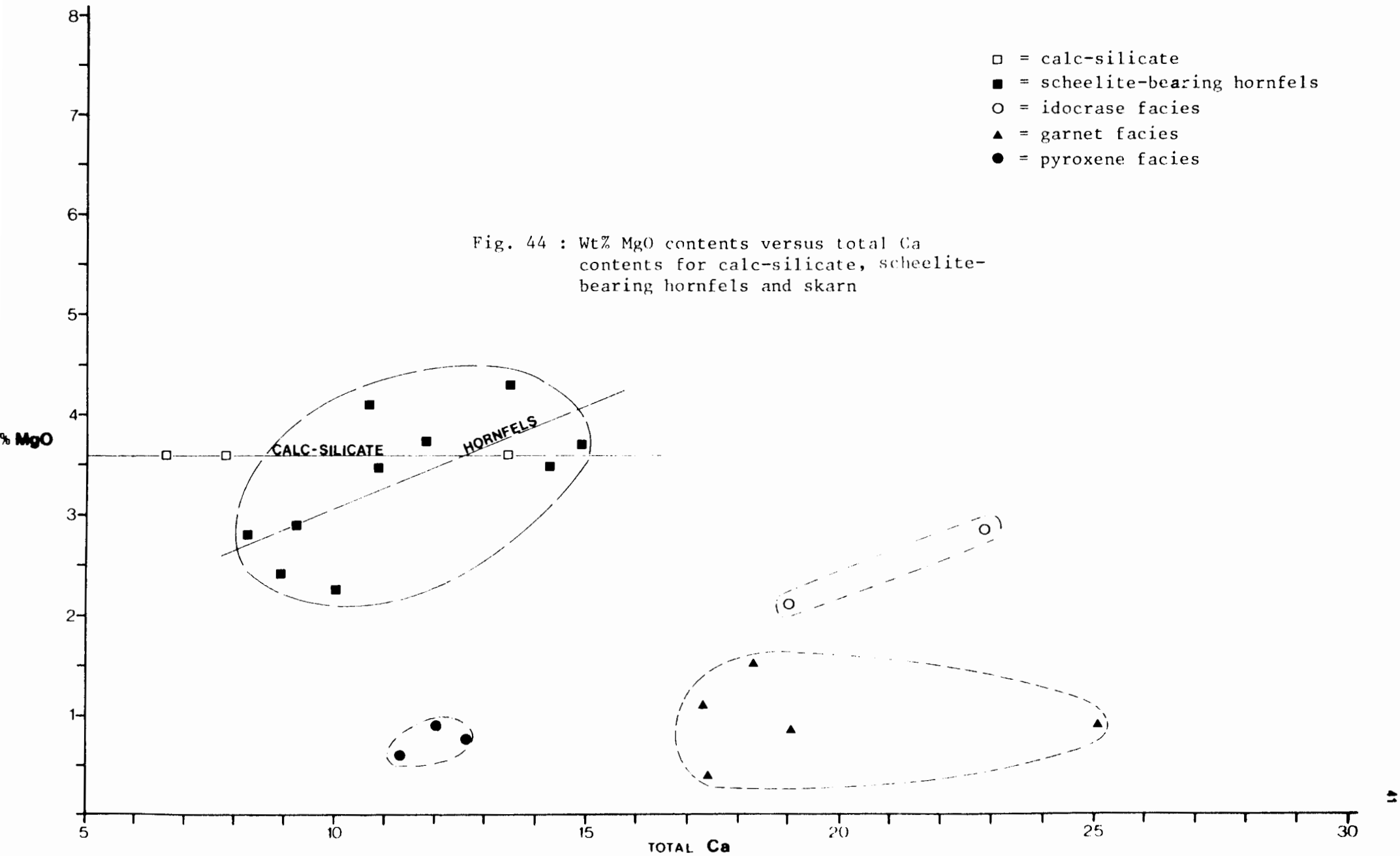

Fig. 44 : Wt% MgO contents versus total Ca contents for calc-silicate, scheelite-bearing hornfels and skarn

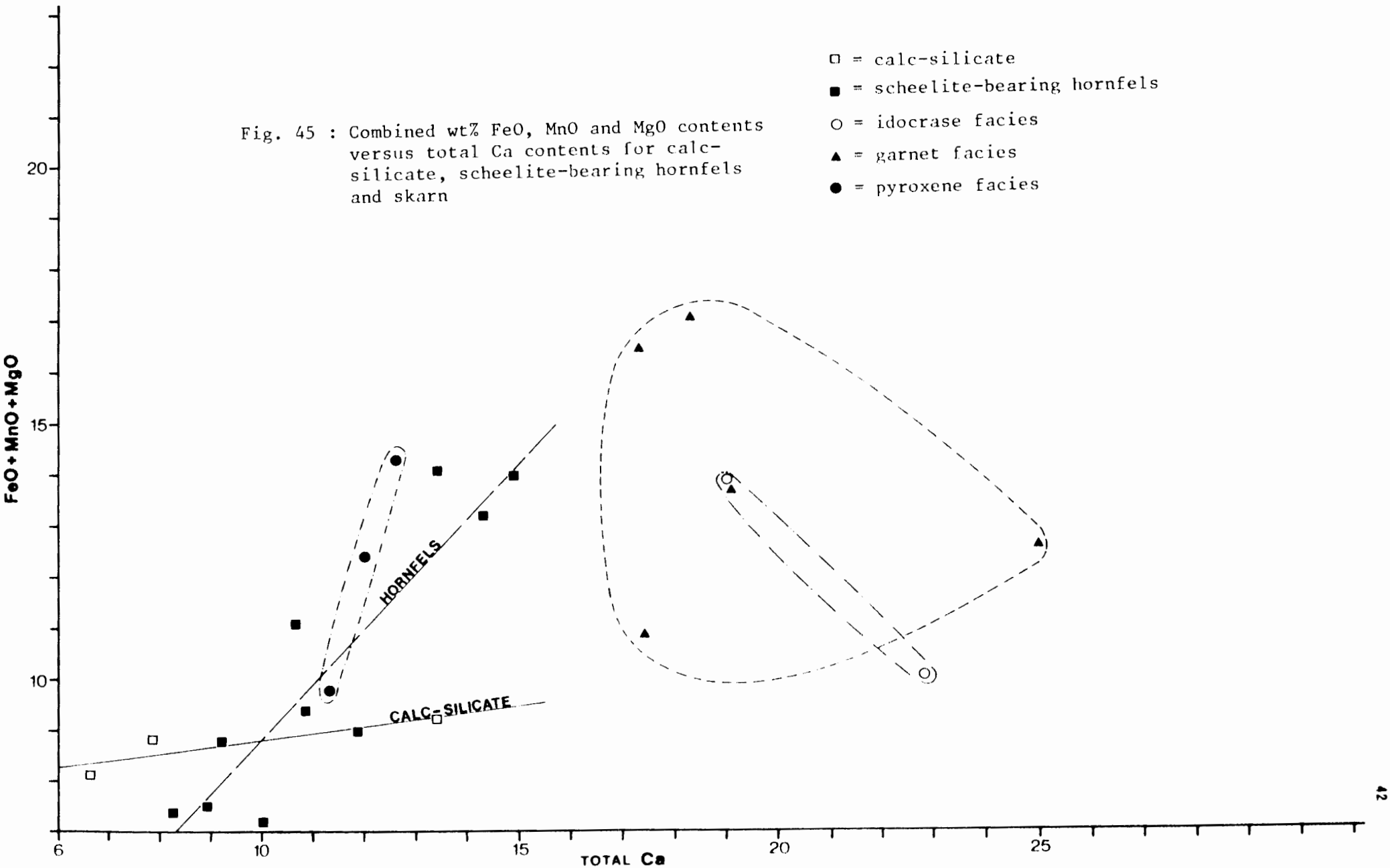

Fig. 45 : Combined wt% FeO, MnO and MgO contents versus total Ca contents for calc-silicate, scheelite-bearing hornfels and skarn

Fig. 46 : Total Ca contents versus wt% TiO_2 contents for calc-silicate, scheelite-bearing hornfels and skarn

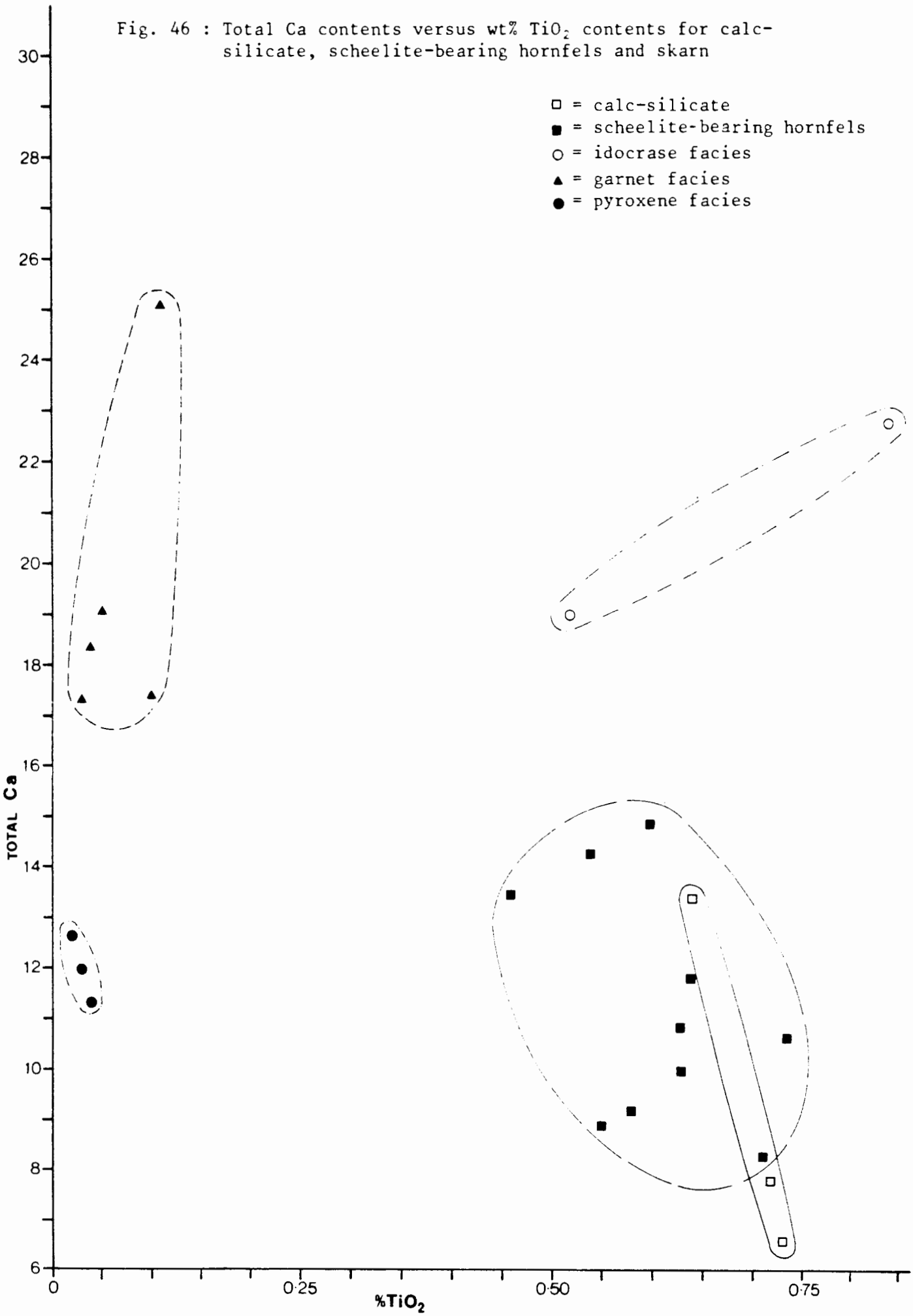

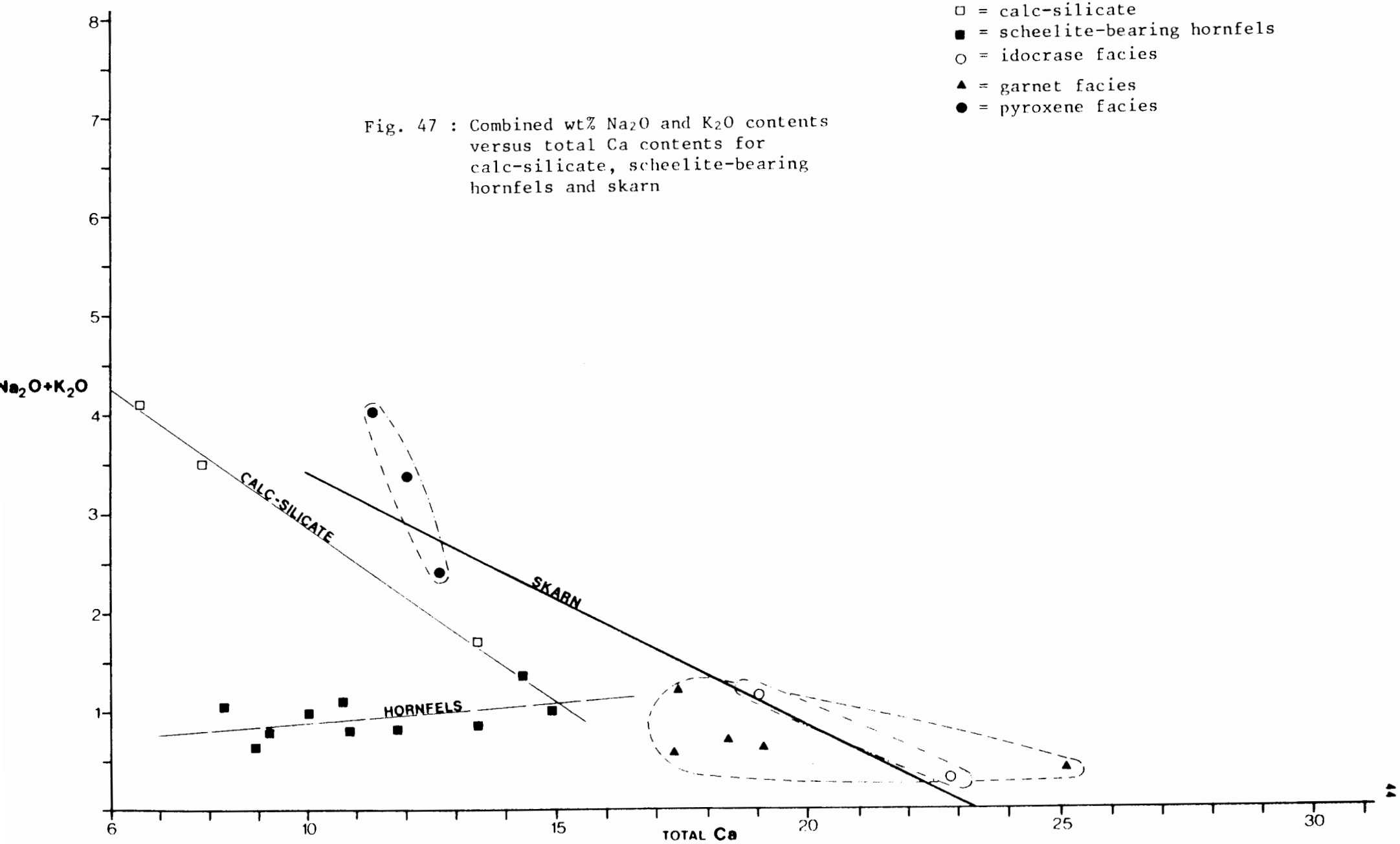

Fig. 47 : Combined wt% Na_2O and K_2O contents versus total Ca contents for calc-silicate, scheelite-bearing hornfels and skarn

Fig. 48 : Wt% K_2O content versus wt% Na_2O content for intrusives in the vicinity of the Otjua prospect

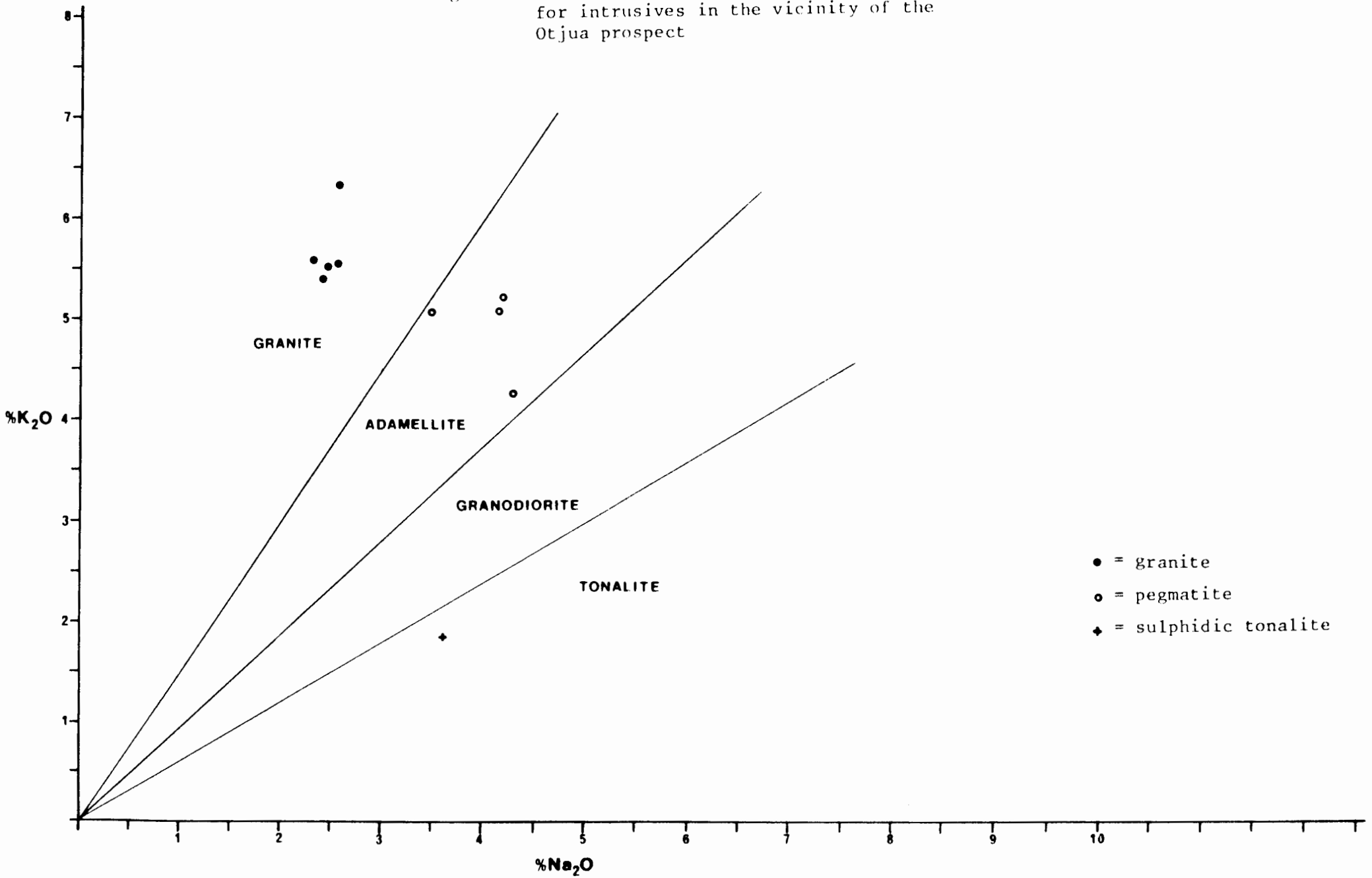

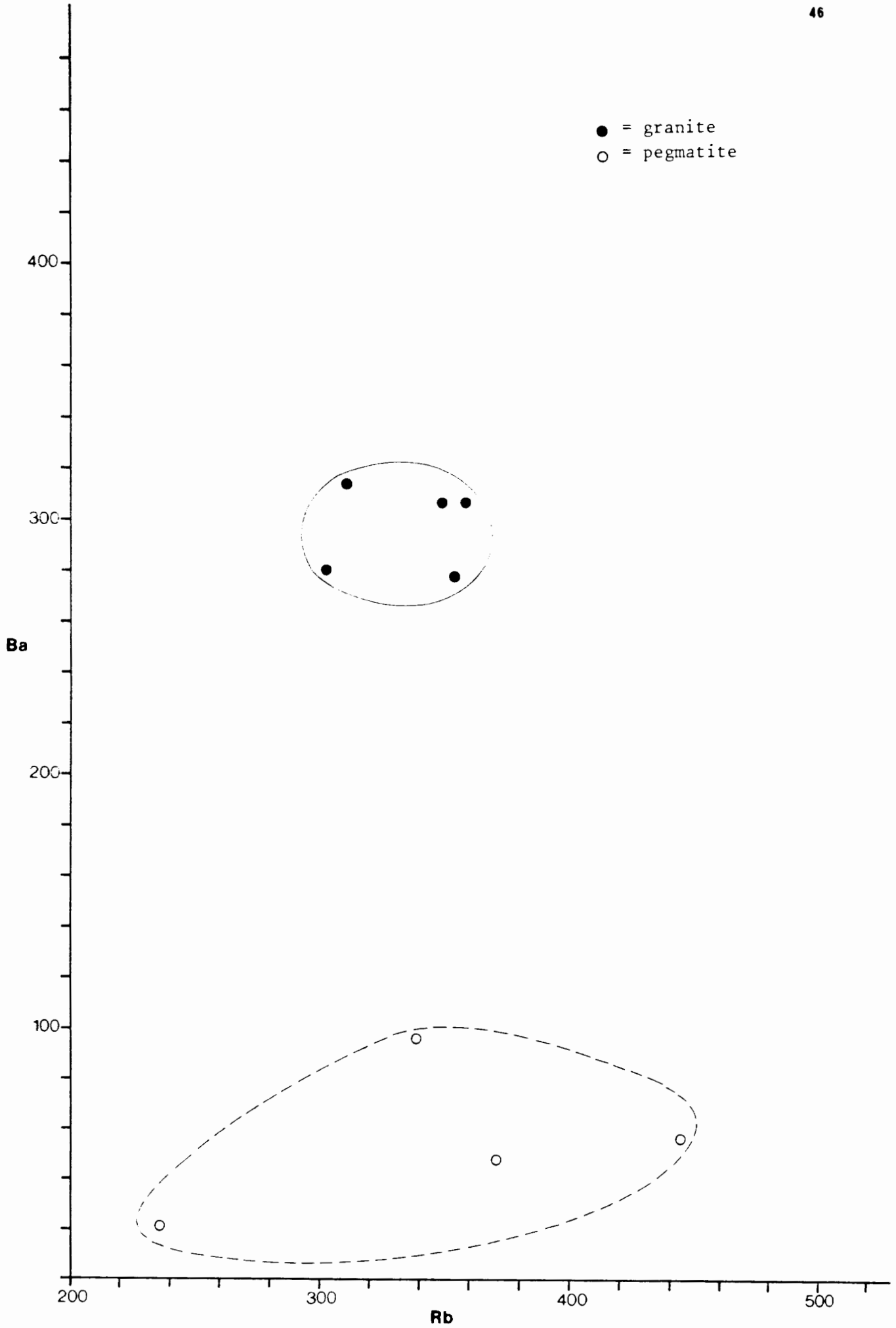

Fig. 49 : Ba concentration (in ppm) versus Rb concentration (in ppm) for intrusives in the vicinity of the Otjua prospect

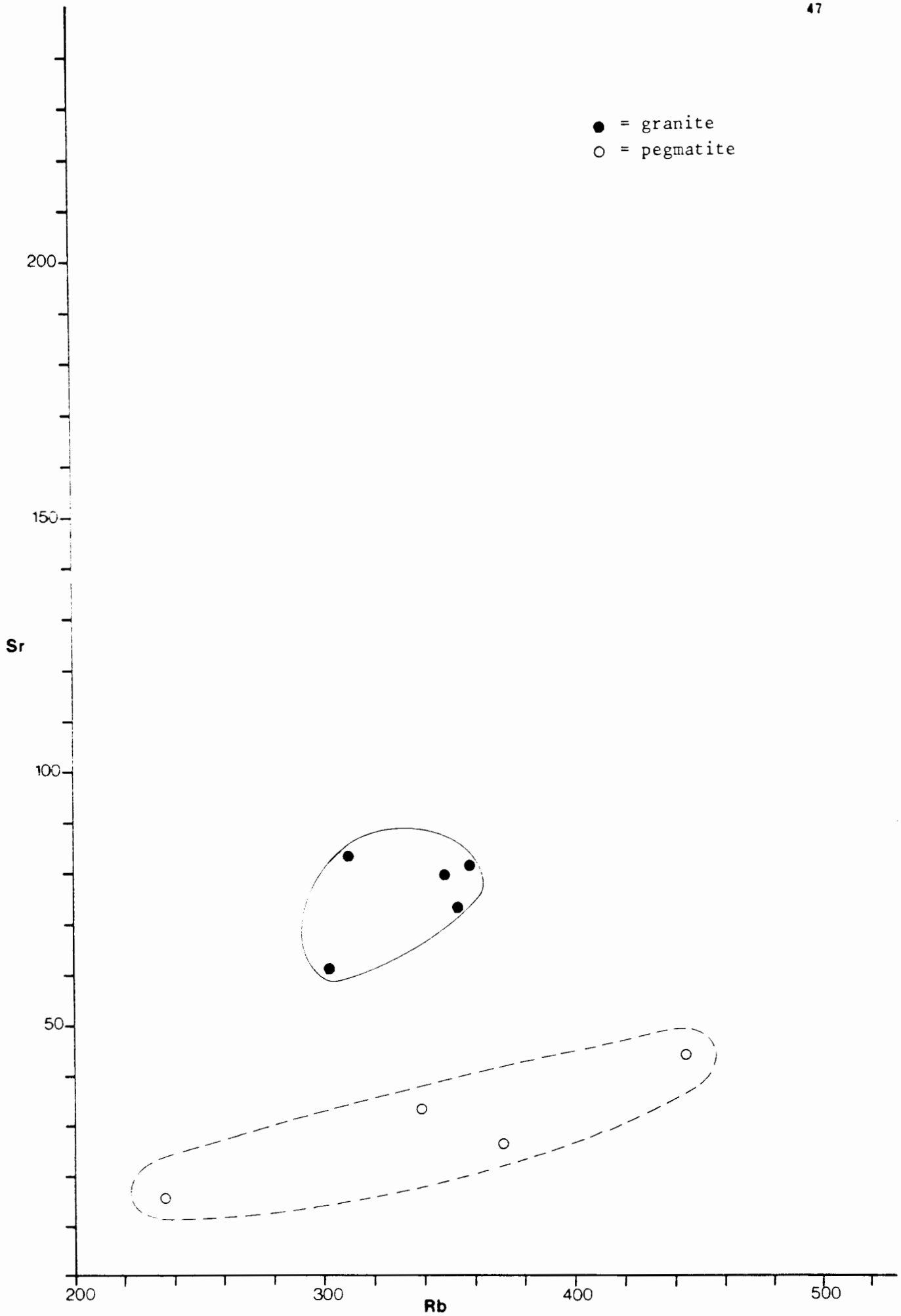

Fig. 50 : Sr concentration (in ppm) versus Rb concentration (in ppm) for intrusives in the vicinity of the Otjua prospect

Fig. 51 : Ternary plot Rb-Ba-Sr for granites
in the vicinity of the Otjua prospect

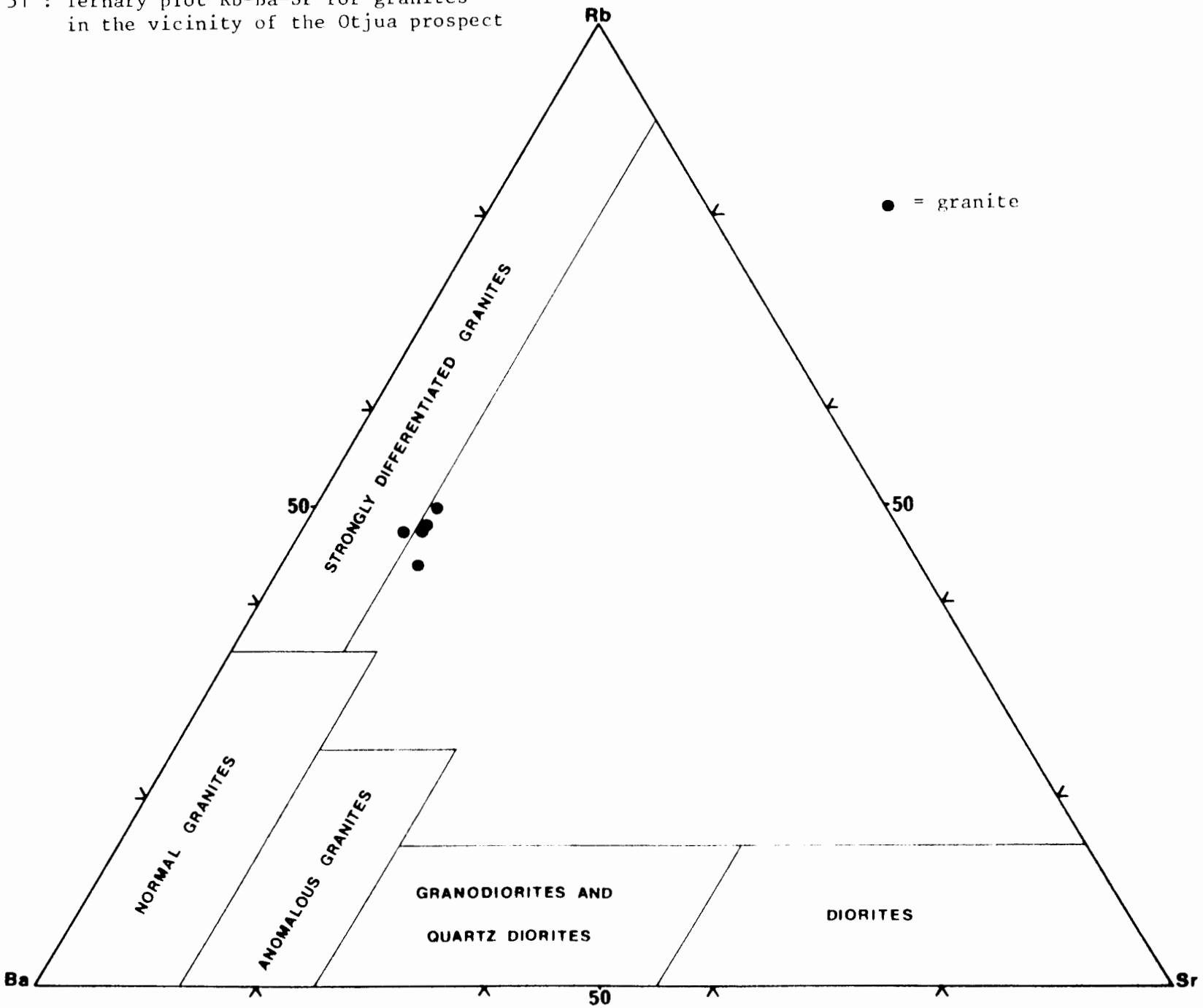

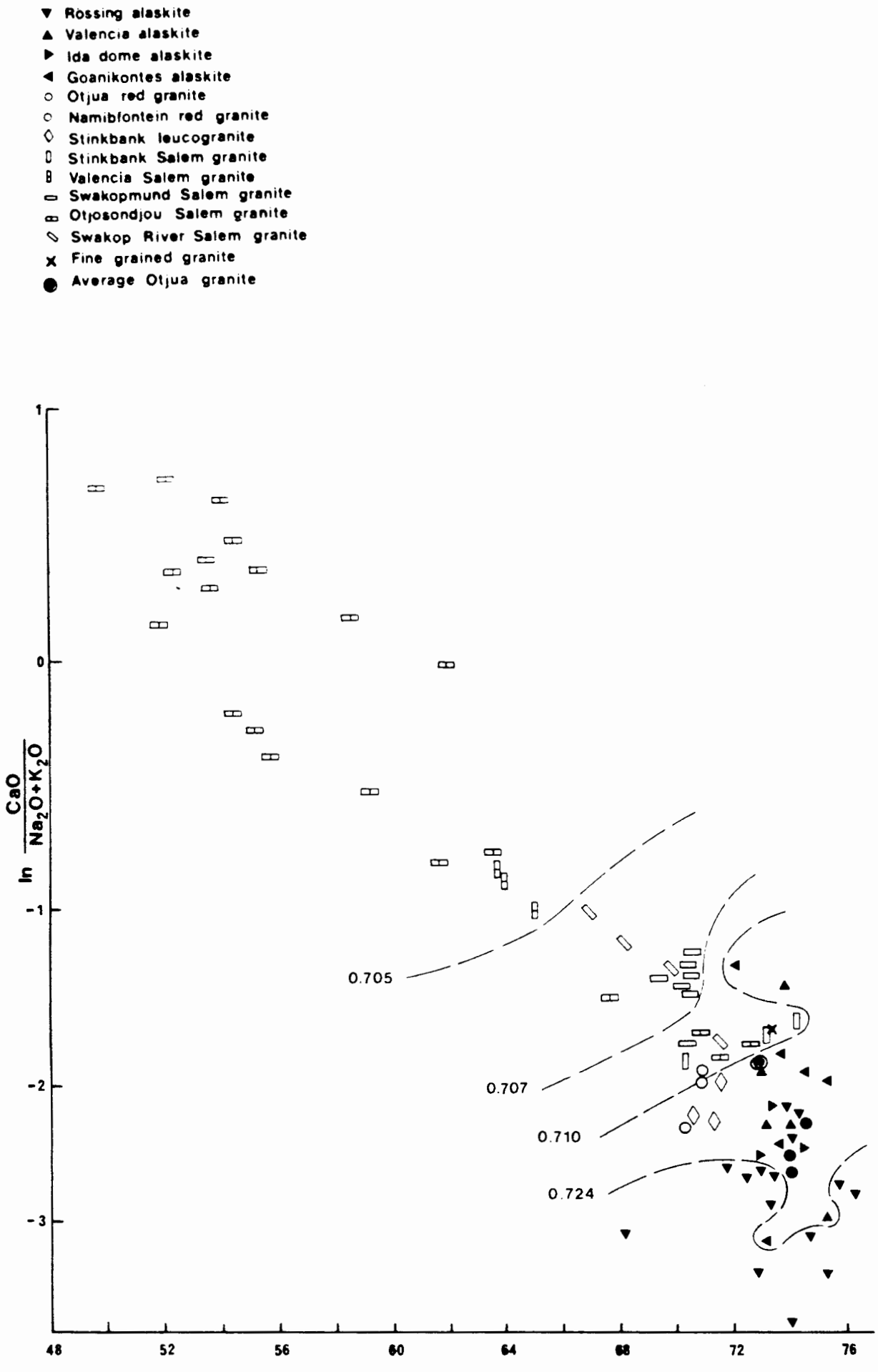

Fig. 52 : ln $CaO/(Na_2O+K_2O)$ versus wt% SiO_2 for some Damaran intrusives (after Marlow, 1981)
Dashed lines represent contours of $(^{87}Sr/^{86}Sr)_I$

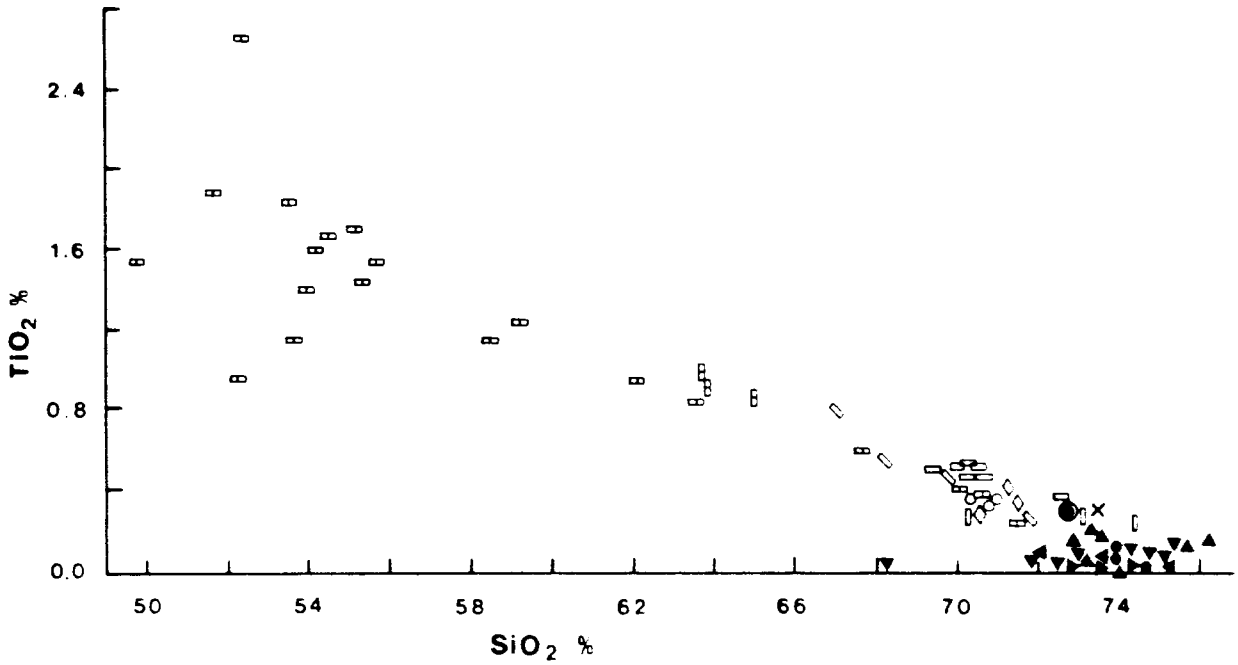

Fig. 53 : Wt% TiO_2 versus wt% SiO_2 for some Damaran intrusives (after Marlow, 1981)

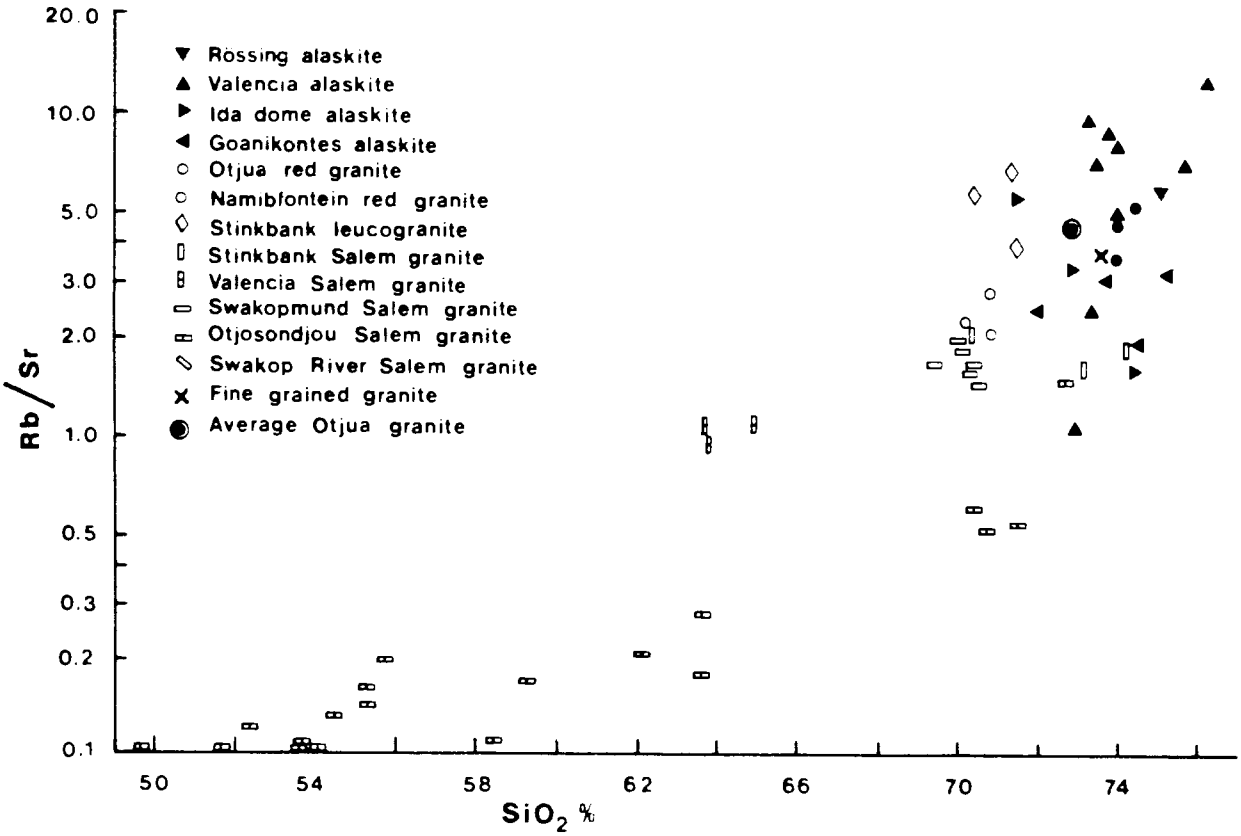

Fig. 54 : Rb/Sr (log scale) versus wt% SiO_2 for some Damaran intrusives (after Marlow, 1981)

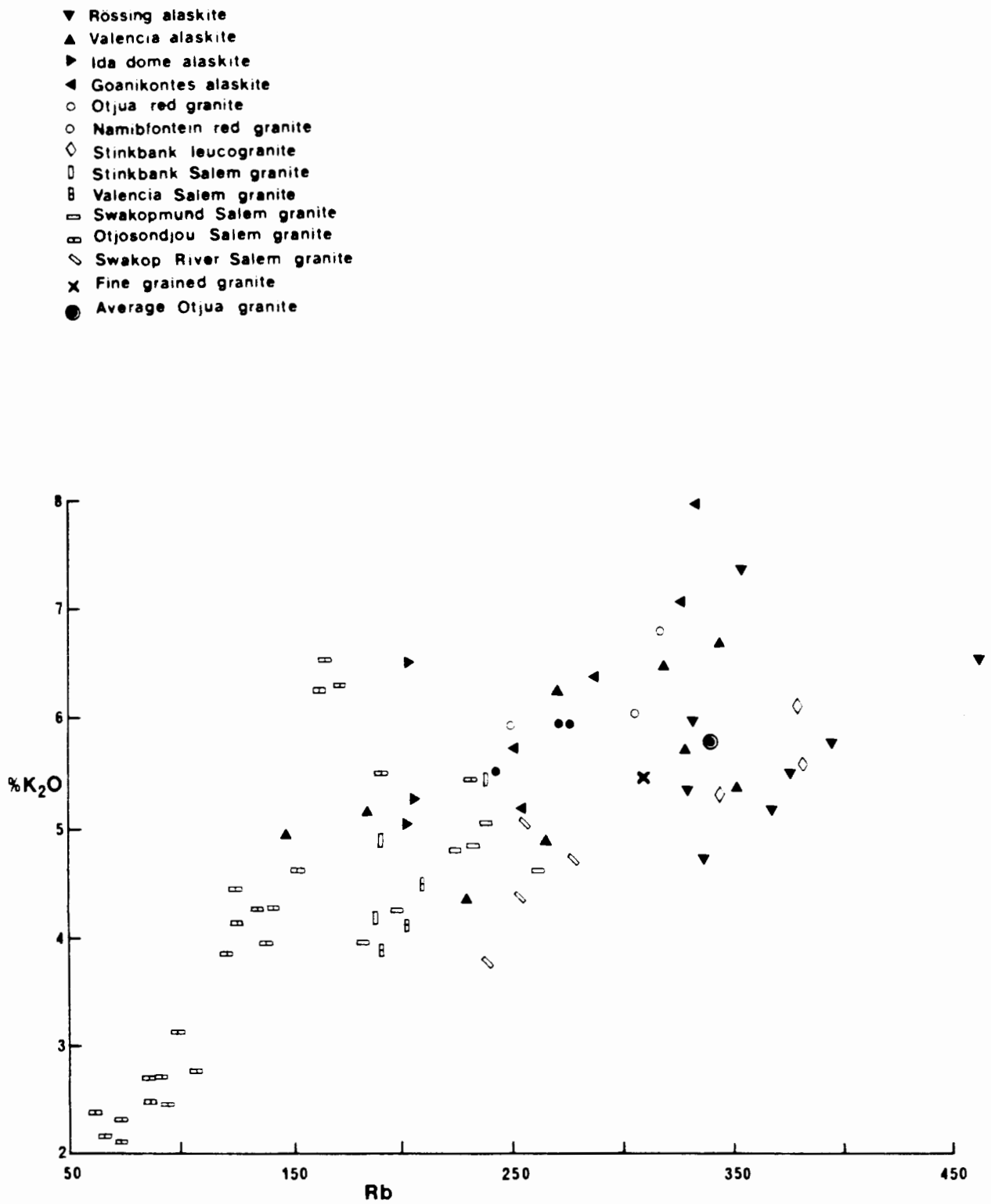

Fig. 55 : Wt%K_2O versus Rb for some Damaran intrusives (after Marlow, 1981)

Fig. 56 : AFM plot for intrusives from the vicinity of the Otjua prospect

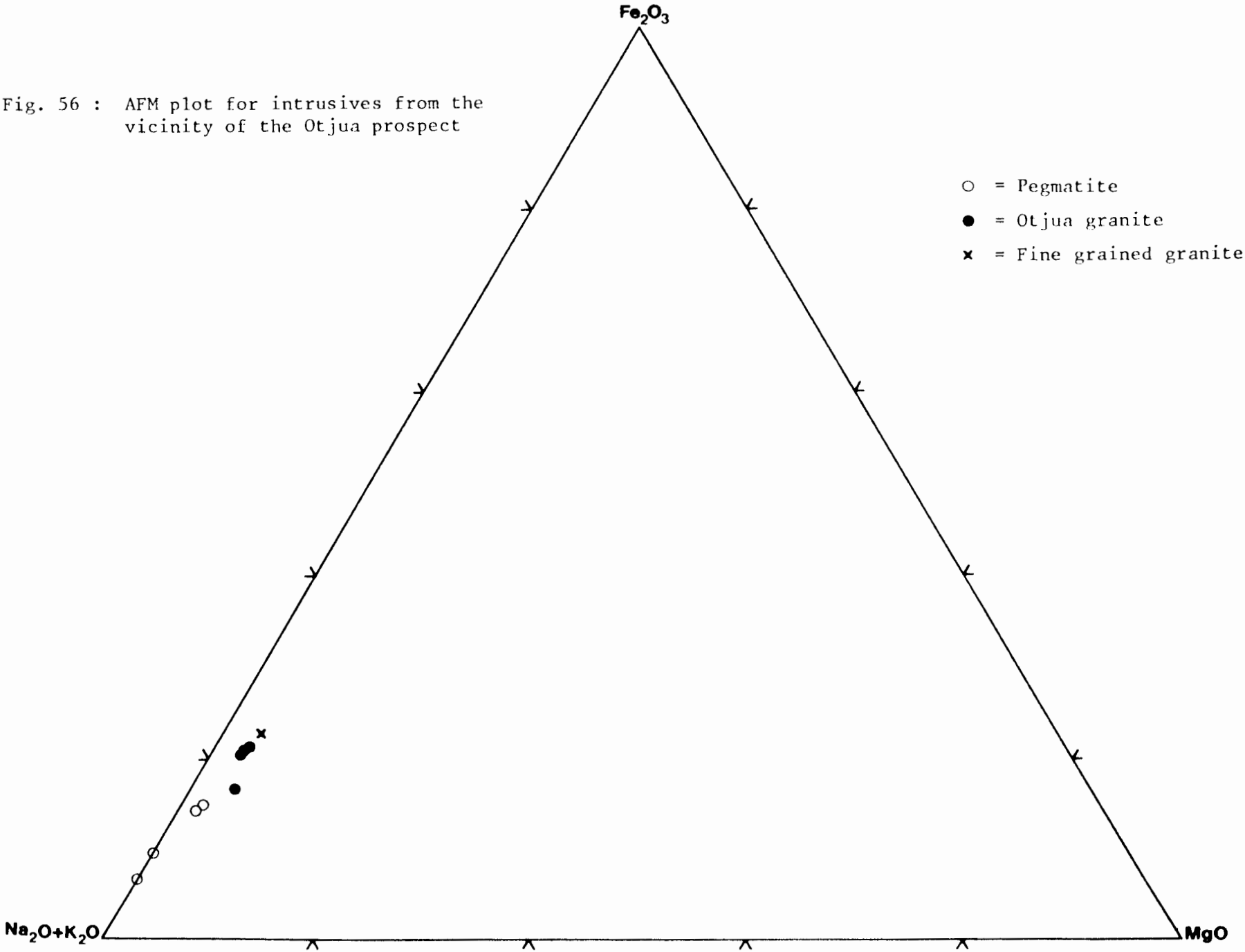

Fig. 57 : $(SiO_2 + Na_2O + K_2O)/(CaO + Al_2O_3)$ versus wt% CaO for all skarn scapolite analyses

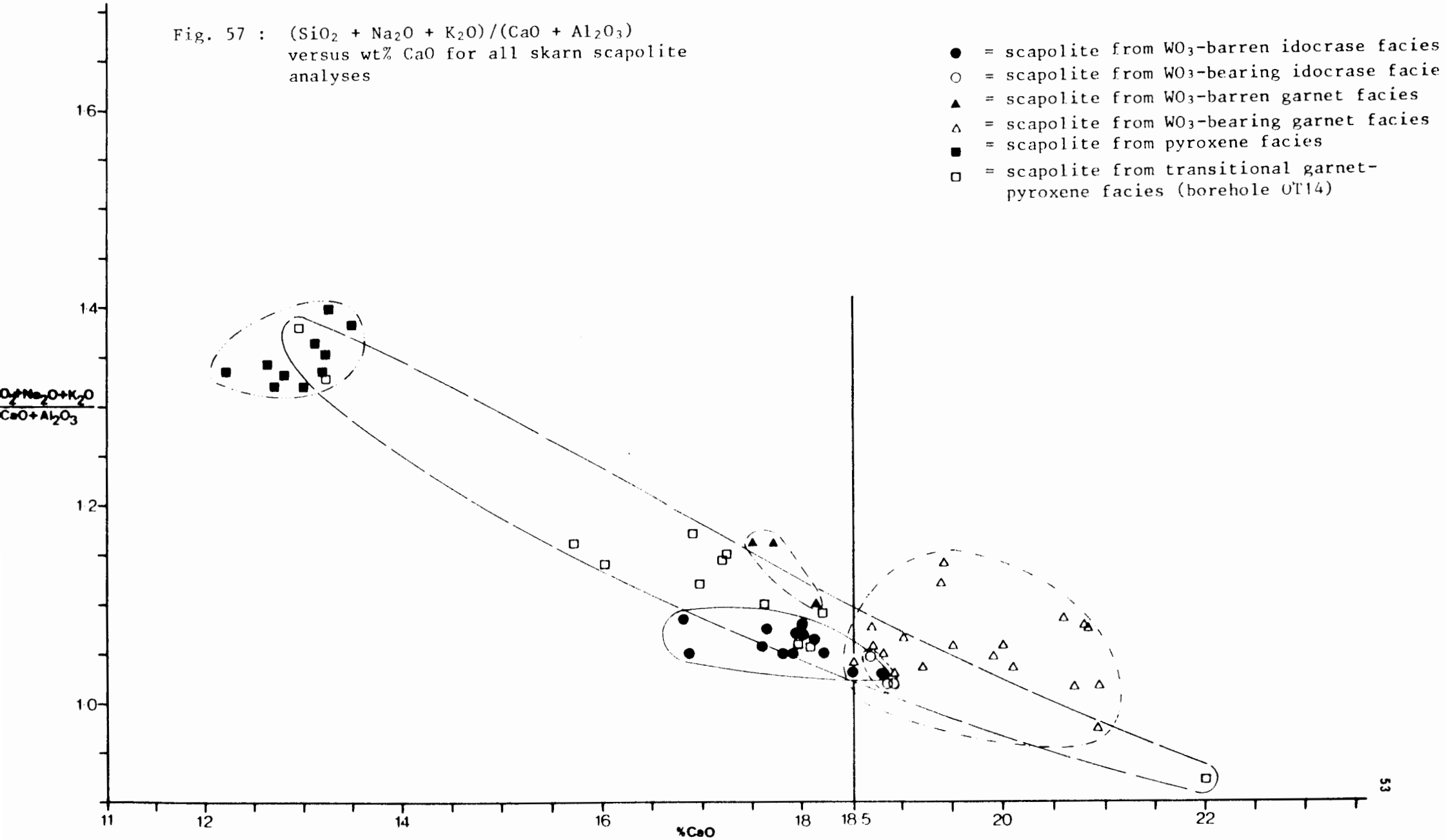

Fig. 58 : Average wt% CaO content of all scapolite analyses in a thin section versus wt% WO_3 content of skarn from which thin section was cut

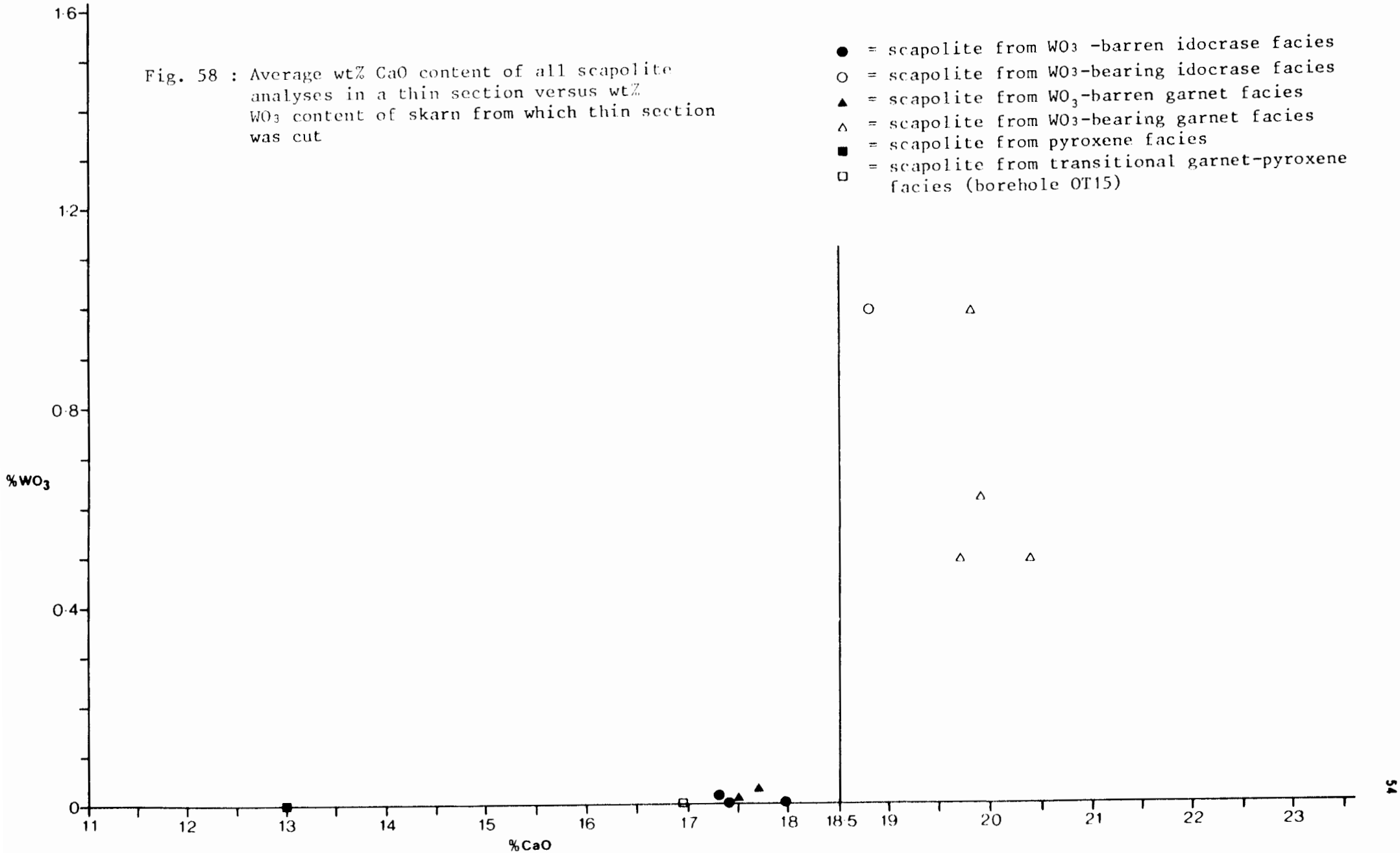

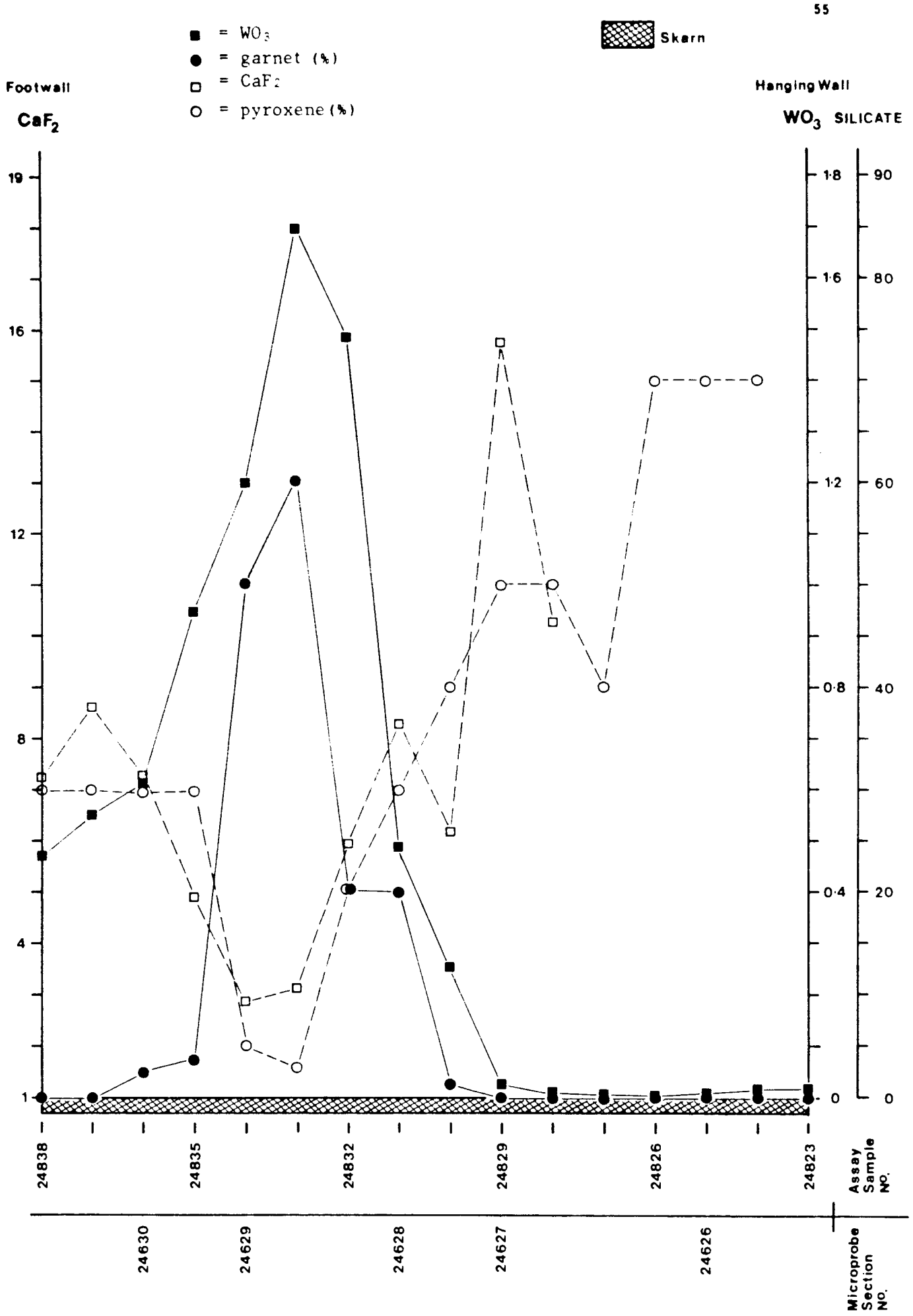

Fig. 59 : Garnet, pyroxene, wt% WO_3 and wt% CaF_2 distribution in the OT5 borehole intersection of the Rössing Formation skarn

Fig. 60 : $(SiO_2 + Na_2O + K_2O)/(CaO + Al_2O_3)$ versus wt% CaO for scapolites from the OT5 borehole intersection of the Rössing Formation skarn

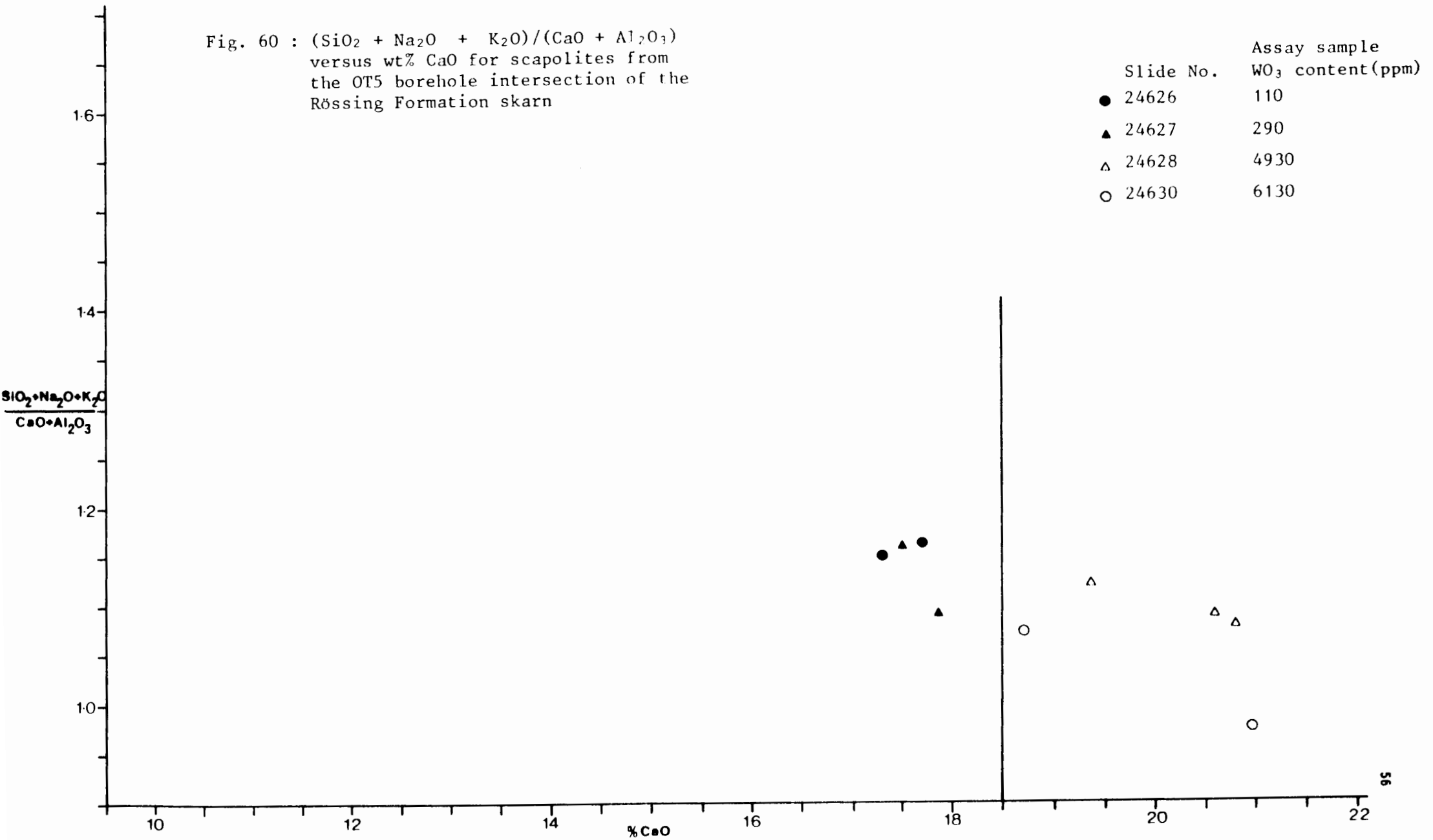

Fig. 61 : Compositions of pyroxene in skarn facies expressed as mole proportions of diopside (Di), johannsenite (Jo) and hedenbergite (Hd)

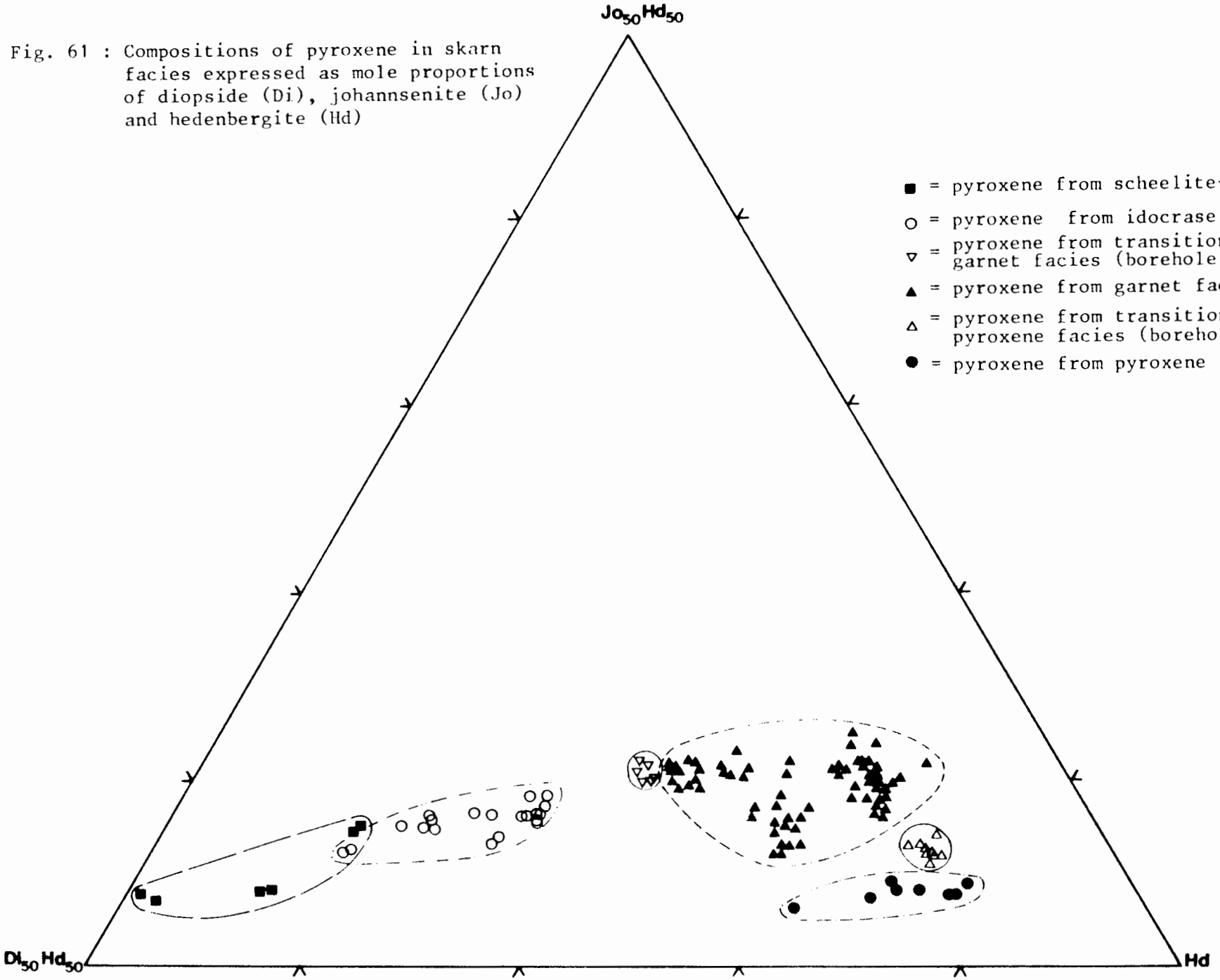

Fig. 62 : Representative analyses of pyroxene from skarn facies, scheelite-bearing hornfels and calc-silicate expressed as mole proportions of enstatite, wollastonite and ferrosilite

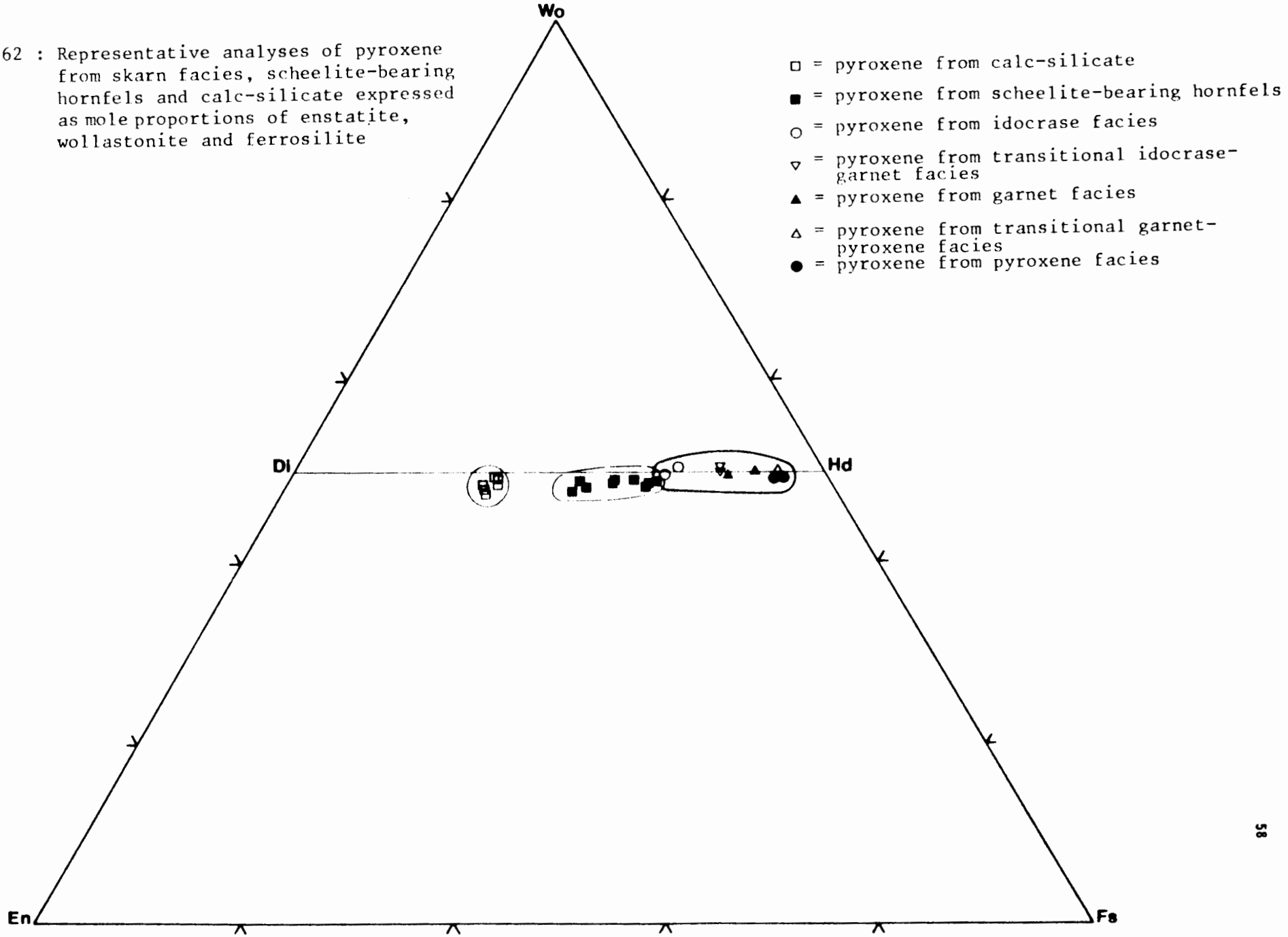

Fig. 63 : Garnet, pyroxene, wt% WO_3 and wt% CaF_2 distribution in the OT17 borehole intersection of the Rössing Formation marble/skarn

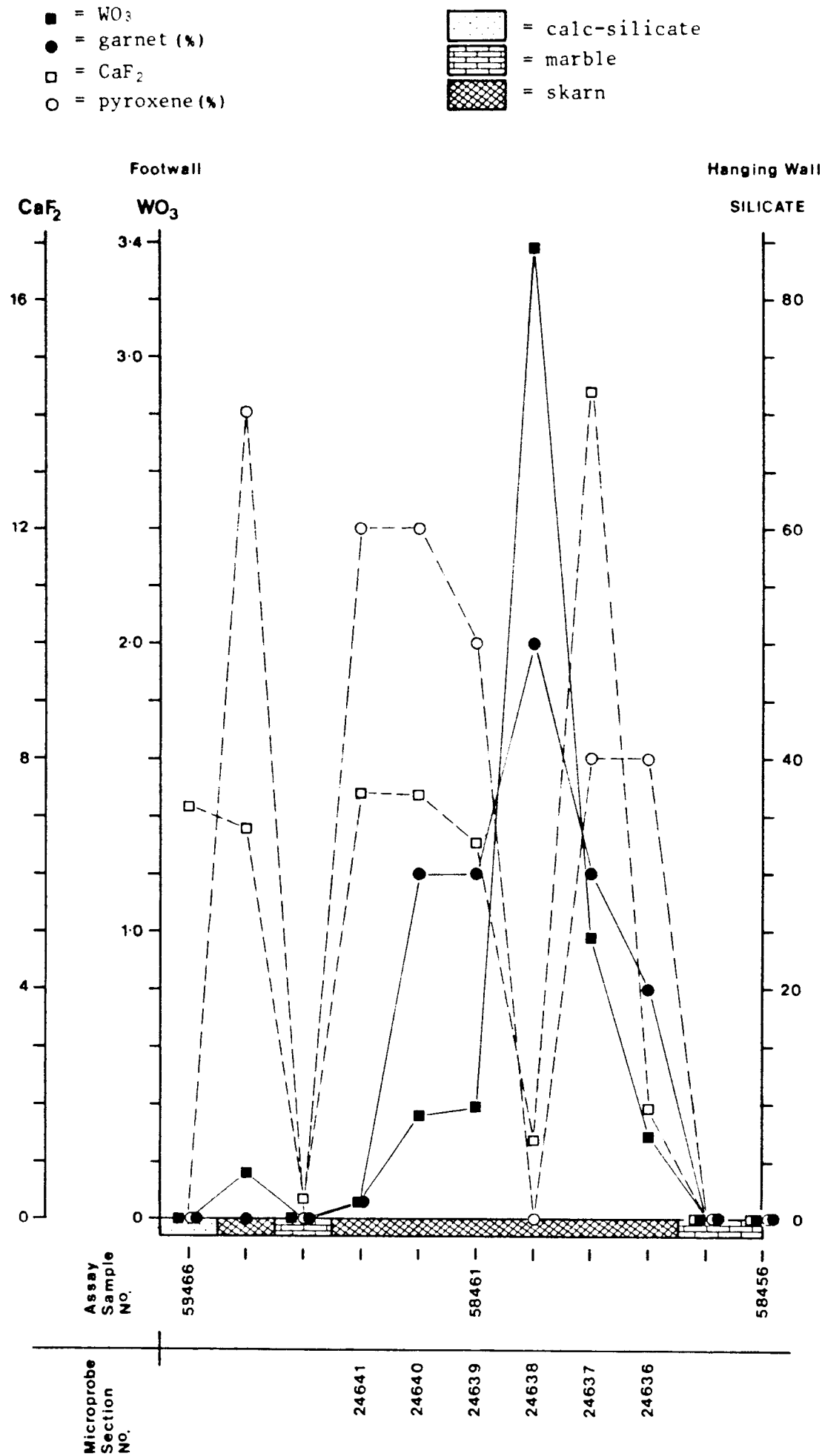

Fig. 64 : Compositions of pyroxene from the OT5 borehole intersection of the Rössing Formation skarn expressed as mole proportions of diopside (Di), johannsenite (Jo) and hedenbergite (Hd)

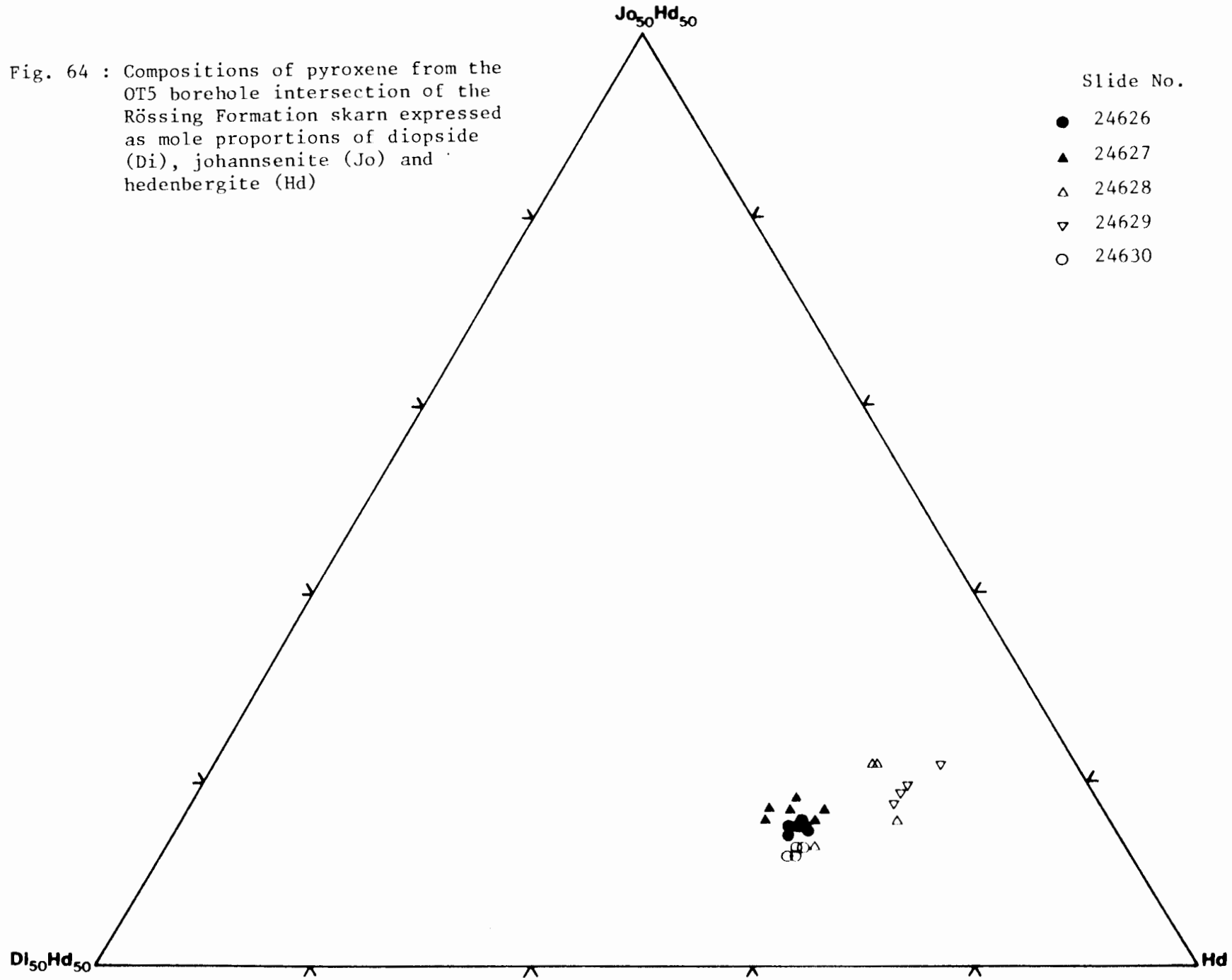

Fig. 65 : Compositions of pyroxene from the OT17 borehole intersection of the Rössing Formation skarn expressed as mole proportions of diopside (Di), johannsenite (Jo) and hedenbergite (Hd)

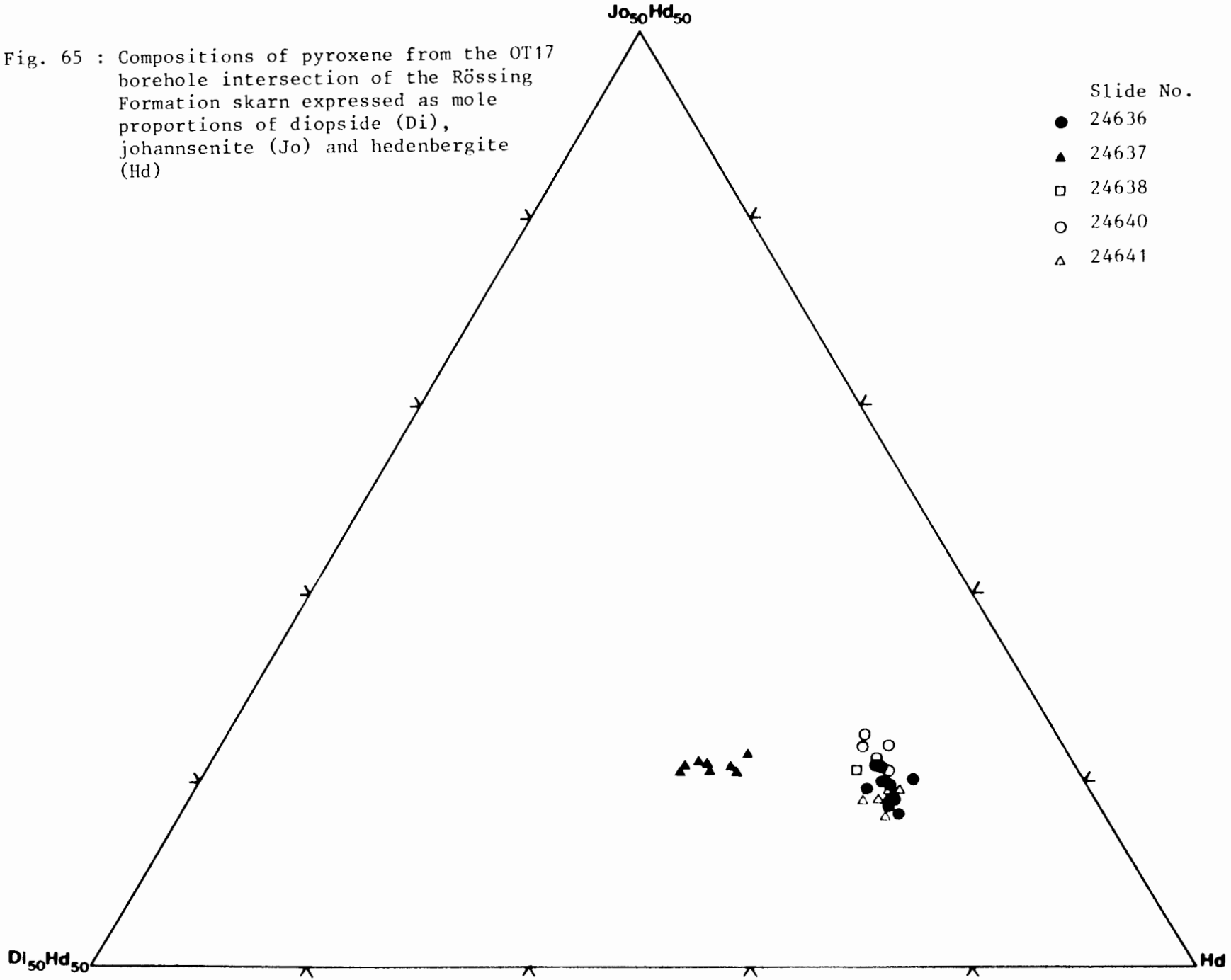

Fig. 66 : Ternary plot (Al + Ti)-(Al + Ti)$_{50}$Mg$_{50}$-(Al + Ti)$_{50}$ Fe$_{50}$ for idocrase analyses from boreholes OT6, OT24 and OT25 with Pine Creek fields (from Newberry, 1982)

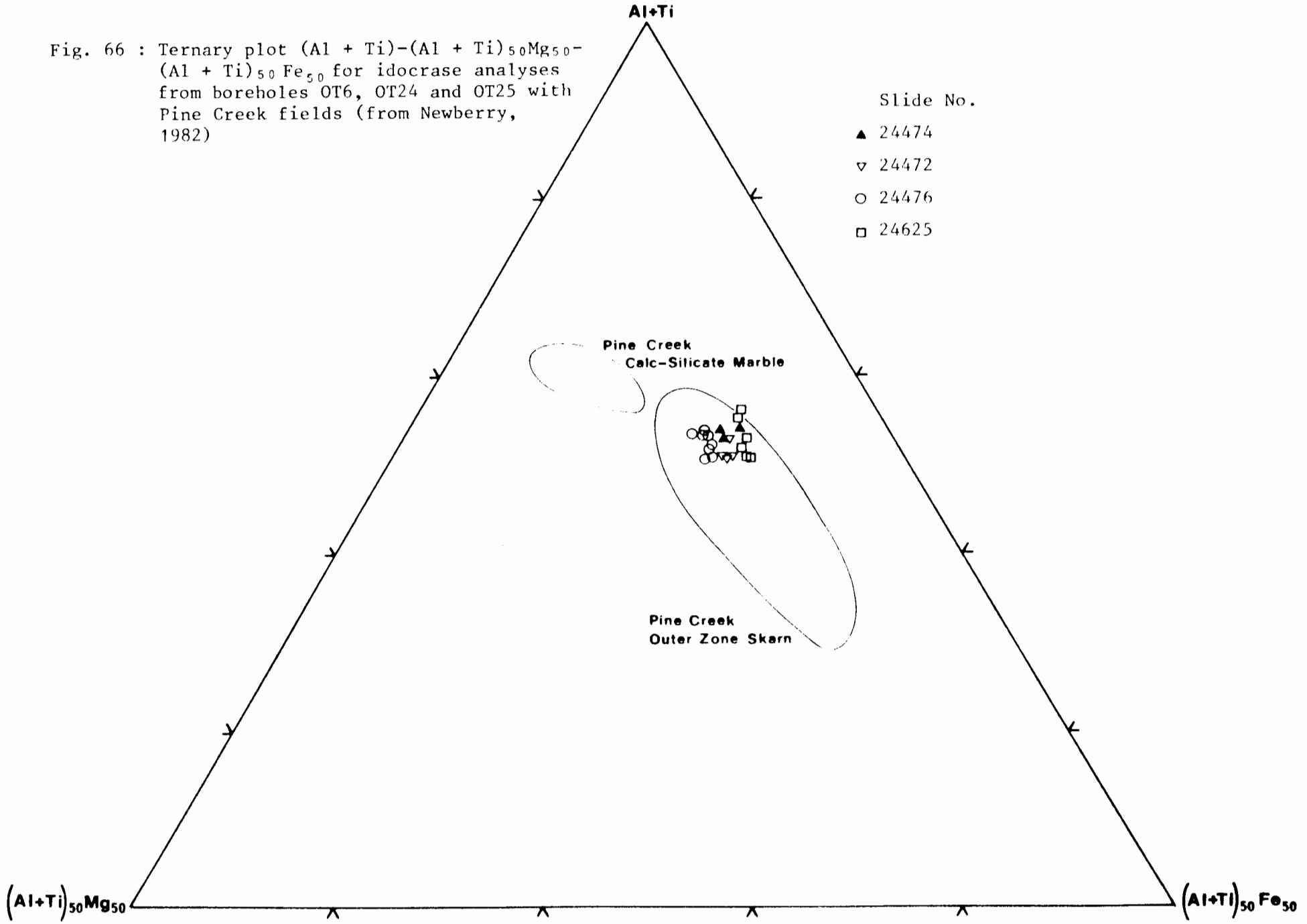

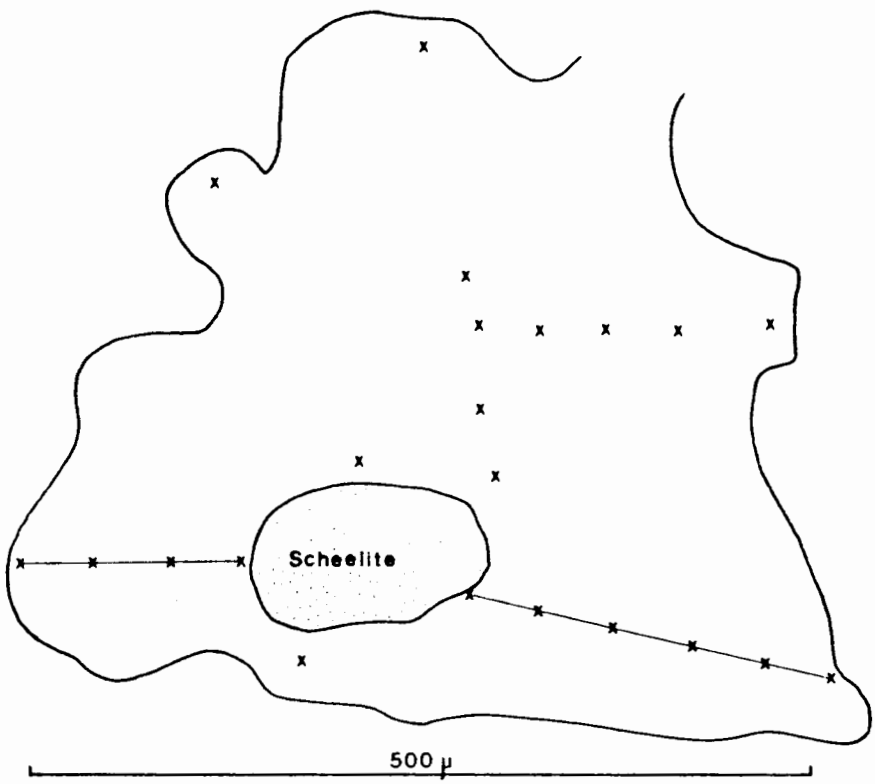

Fig. 67 : Plan showing electron microprobe sampling positions in poikiloblastic garnet from slide 24659

Fig. 68 : Ternary plot CaMn-Ca-CaFe showing variation in garnet composition within a single grain from slide No. 24659 (see Fig. 67)

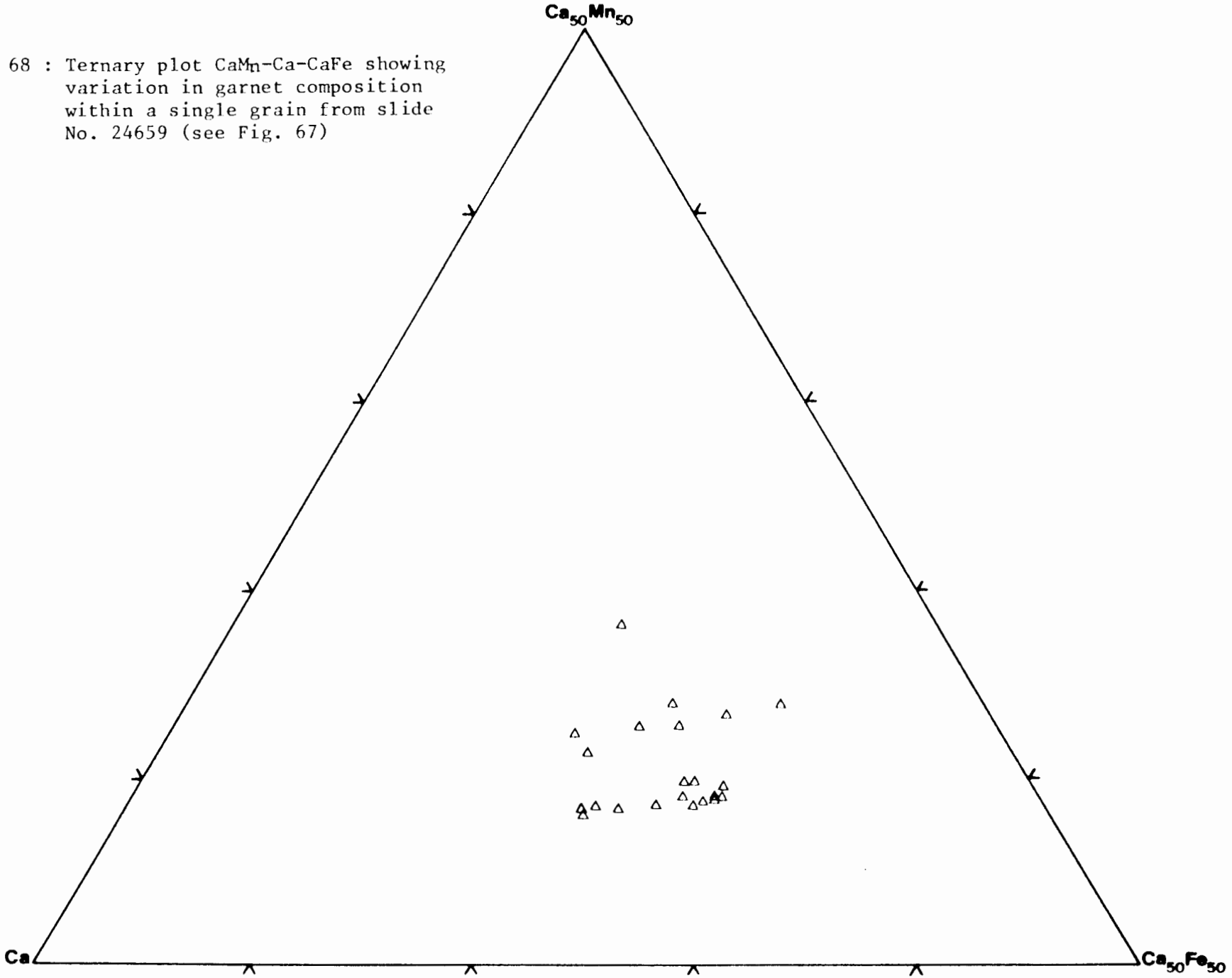

Fig. 69 : Ternary plot CaMn-Ca-CaFe summarising garnet compositions within the skarn system

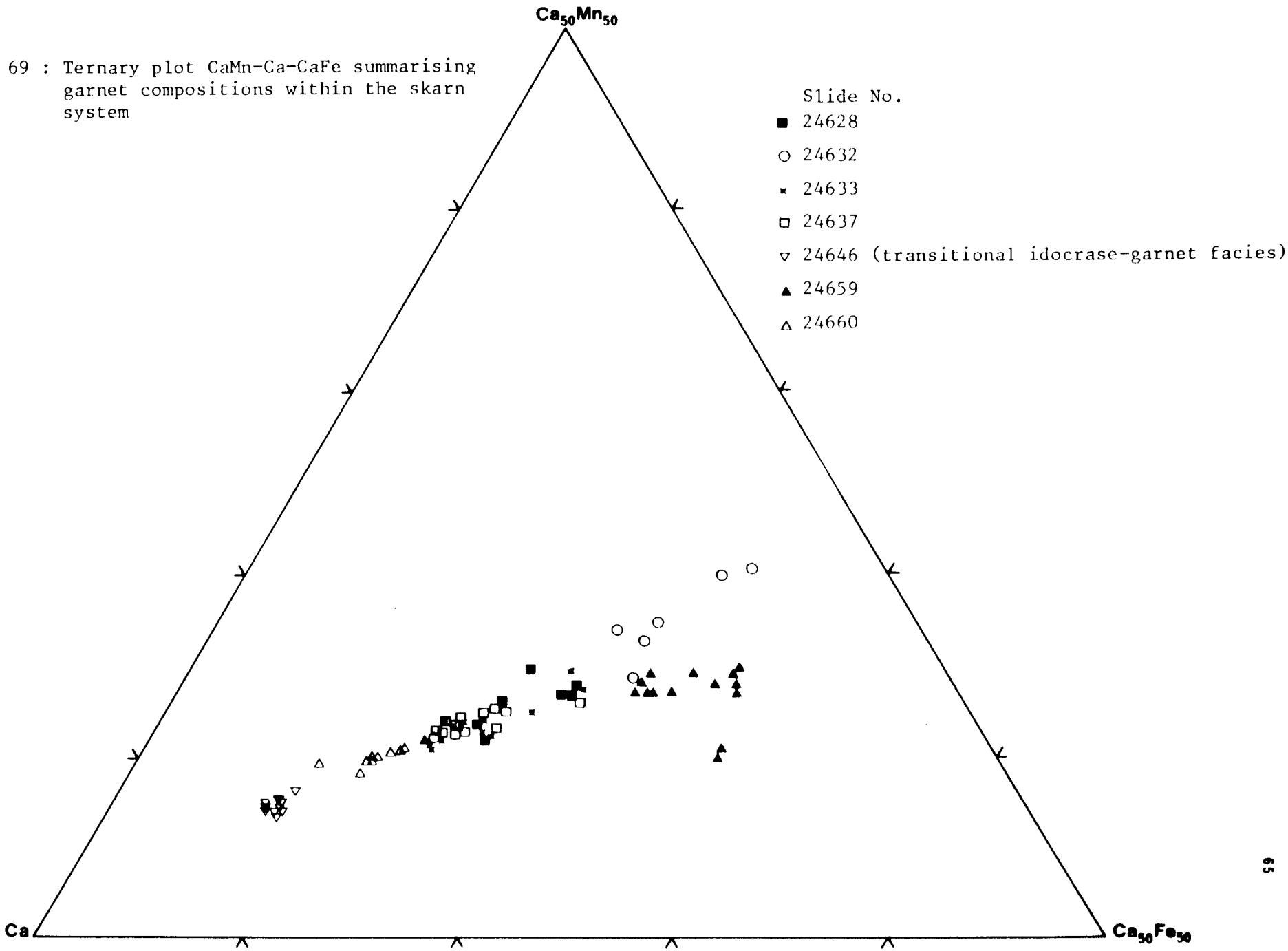

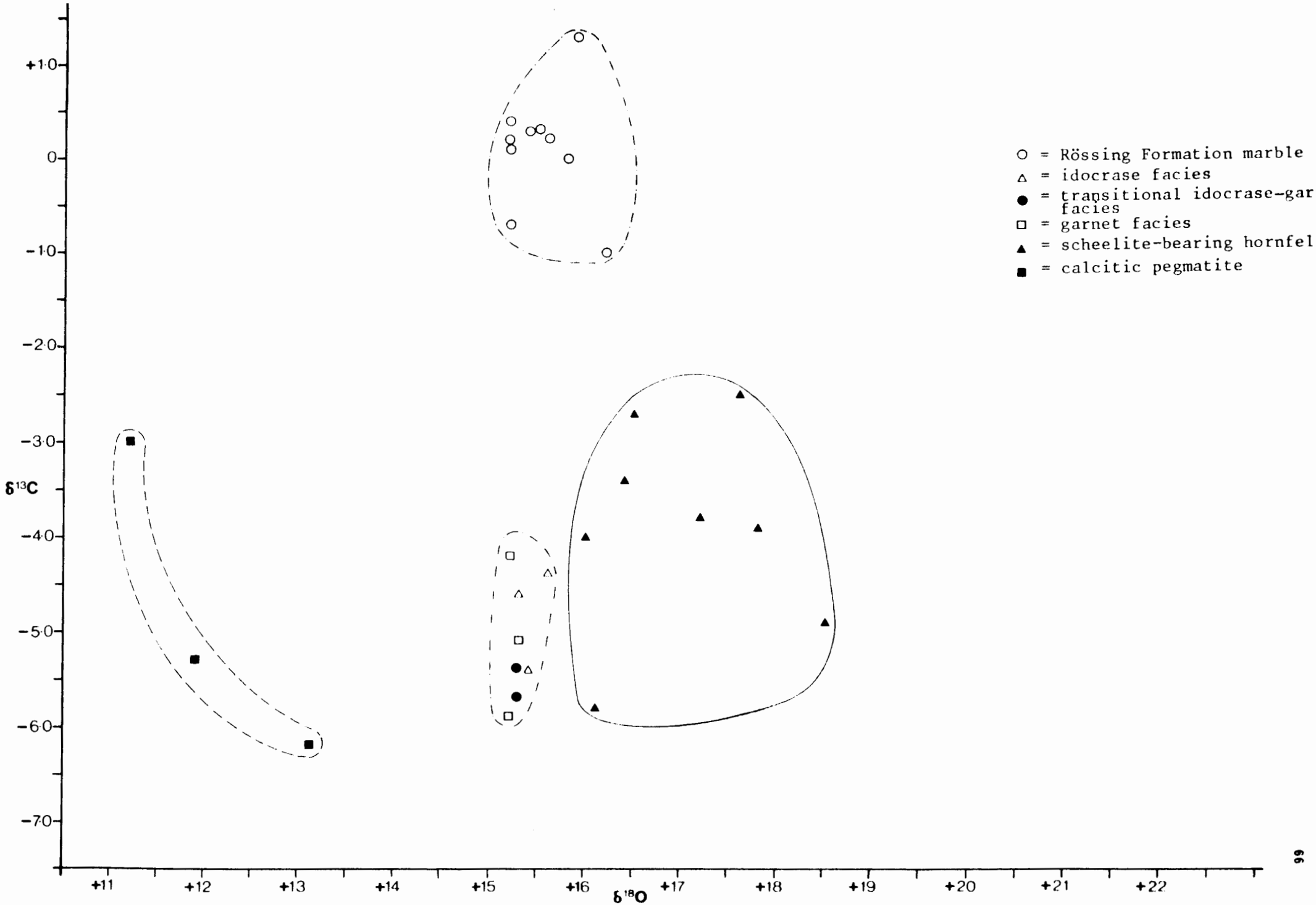

Fig. 70 : $\delta^{13}C$ versus $\delta^{18}O$ for calcite from the Rössing Formation marble, skarn calcite, calcite from hornfels and calcitic pegmatite

Fig. 71 : $\delta^{13}C$ versus % calcite remaining : plot showing progressive depletions in $\delta^{13}C$ value with volatilisation of calcite in a closed system at various temperatures

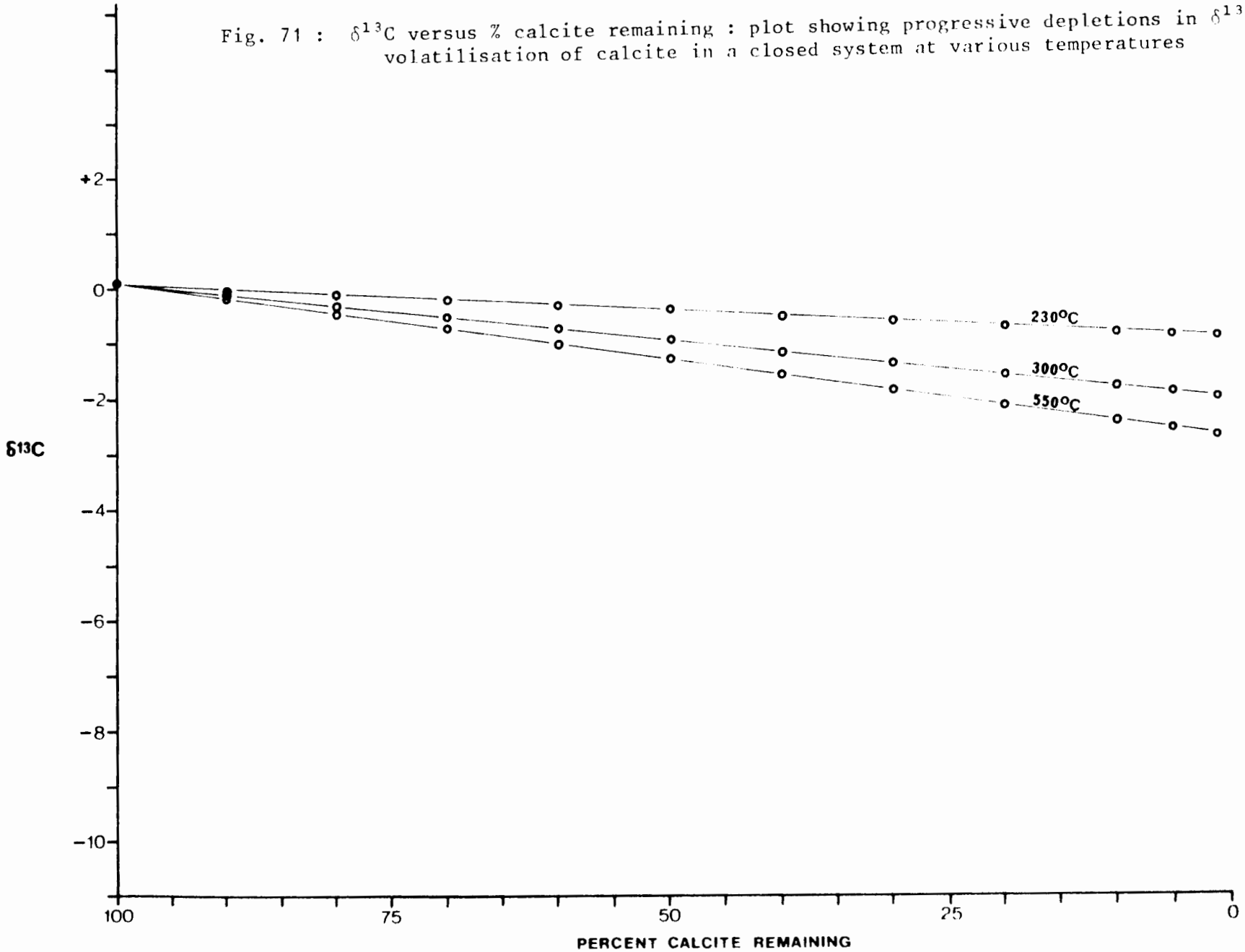

Fig. 72 : Plot showing progressive depletions in $\delta^{13}C$ with volatilisation of calcite in an open system at various temperatures

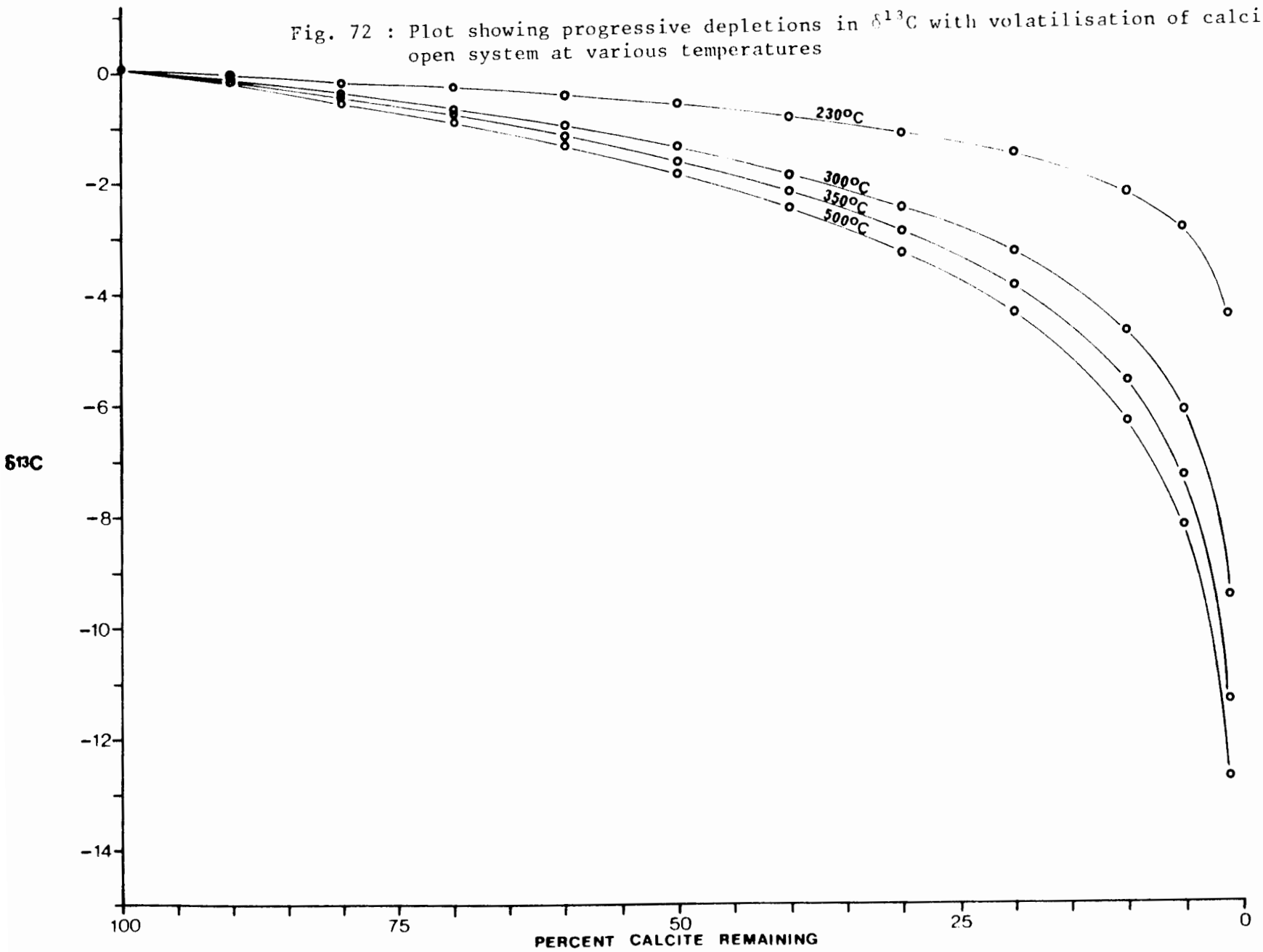

Fig. 73 : Modified ACF plot for marble and skarn analyses

A = molecular proportions of Al_2O_3

C = molecular proportions of CaO and CaF_2

F = molecular proportions of FeO, Fe_2O_3, MnO and MgO

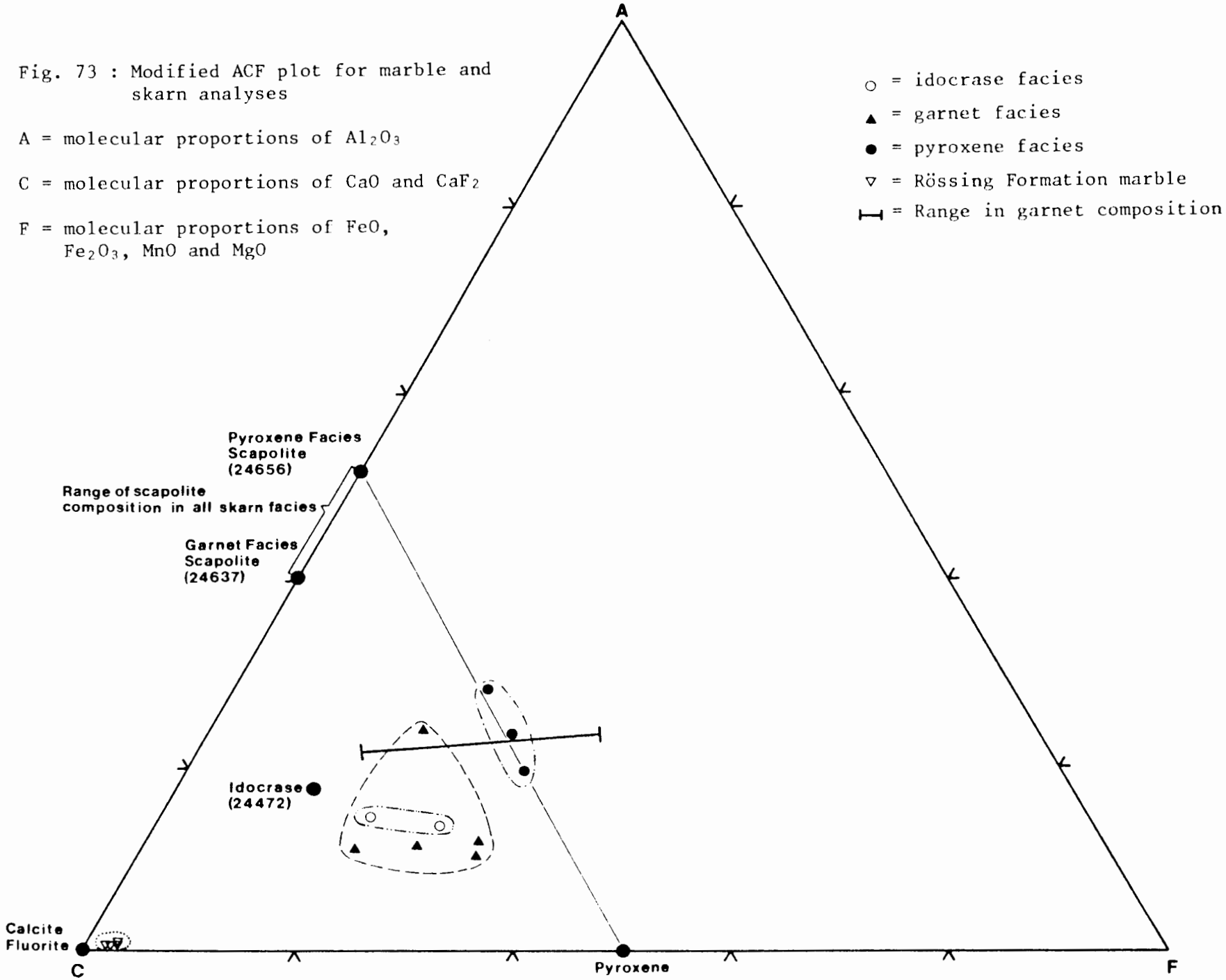

Fig. 74 : Si-SiAl-SiFe plot for skarn analyses

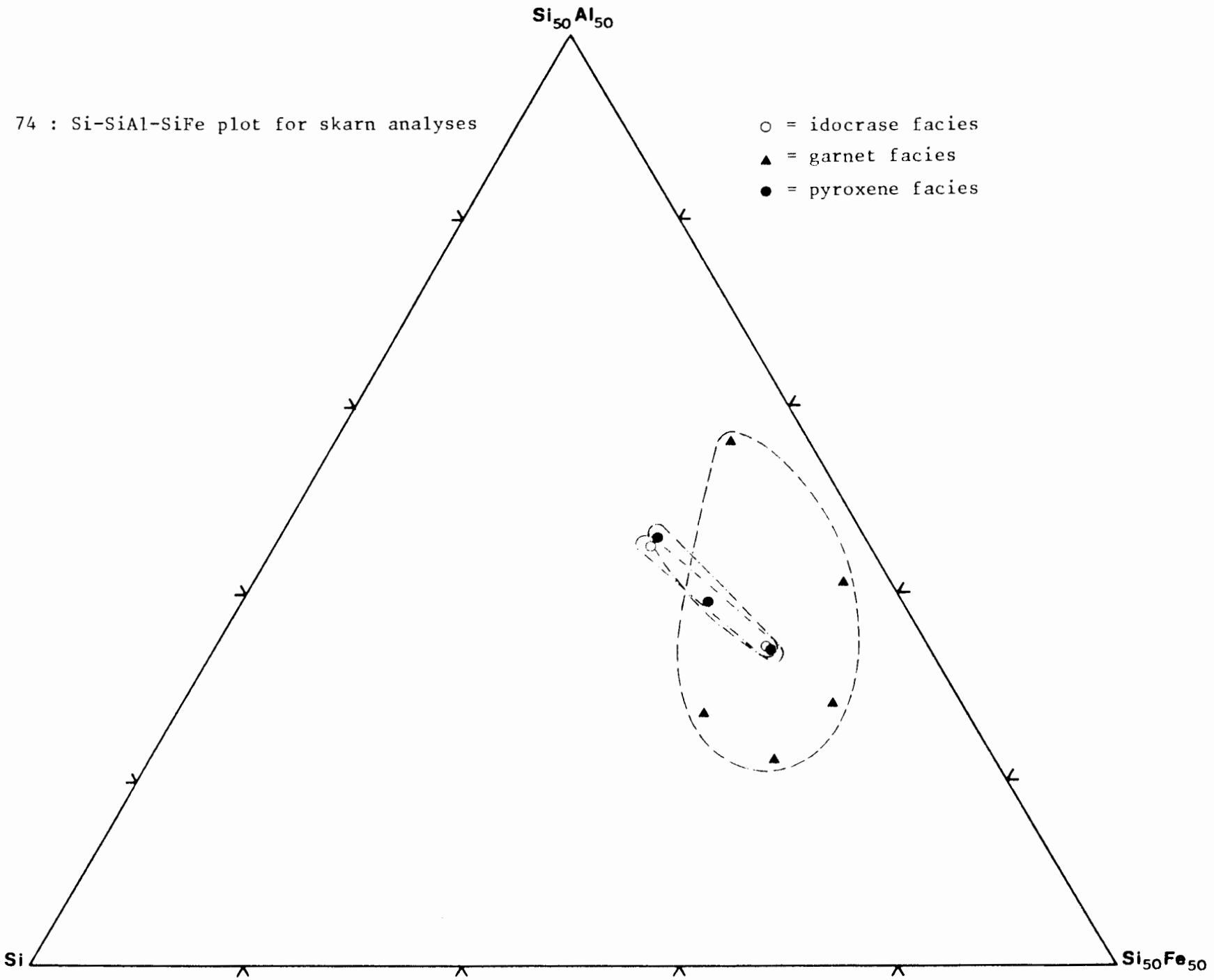

Fig. 75 : Ti + Mg-Mn-Na + K plot for skarn analyses

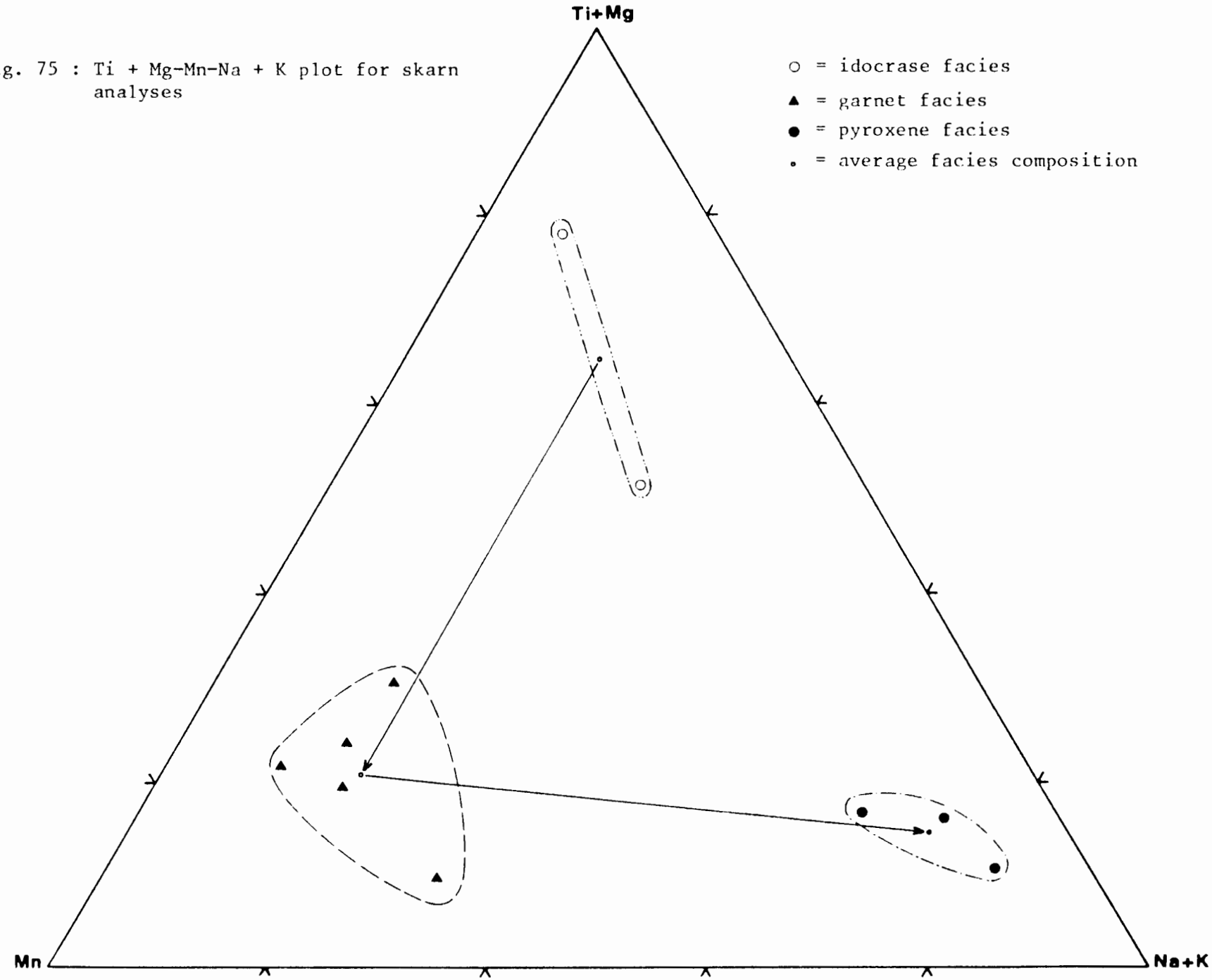

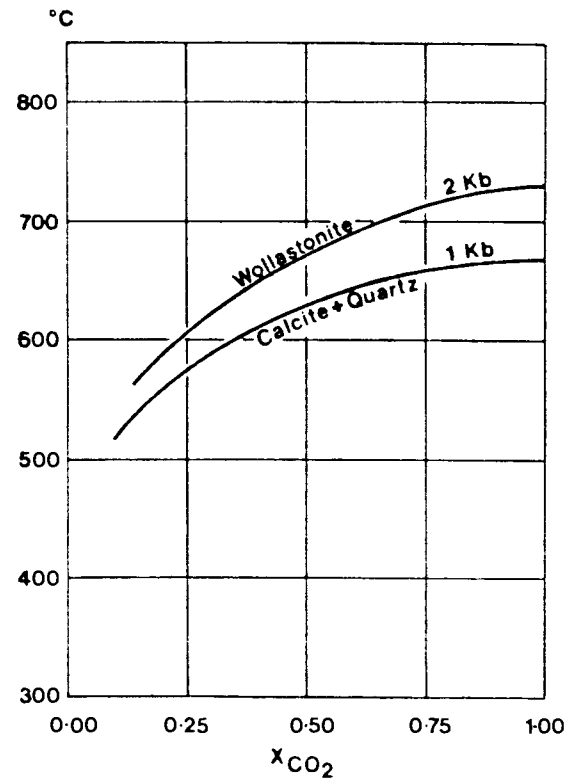

Fig. 76 : Isobaric curves for the reaction calcite + quartz $\rightleftharpoons$ wollastonite (after Winkler, 1976)

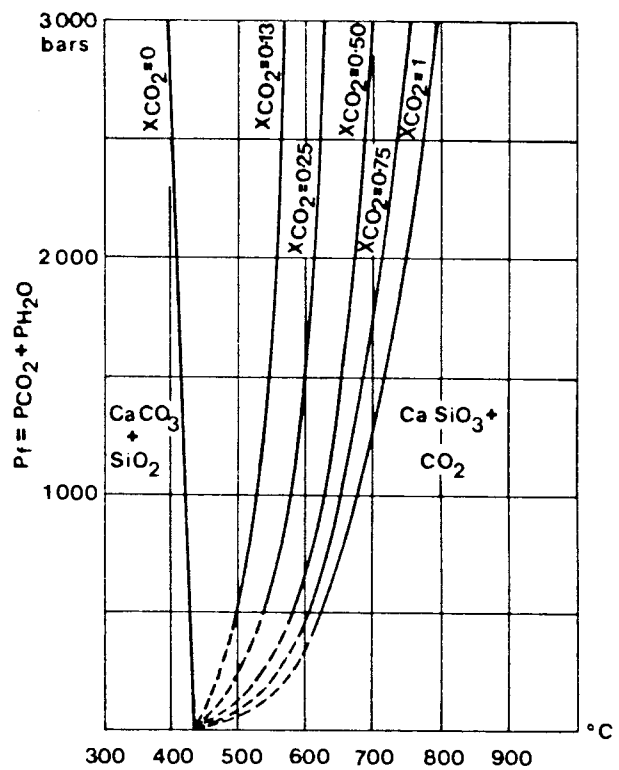

Fig. 77 : Diagram showing the dependence of equilibrium temperatures for the reaction calcite + quartz $\rightleftharpoons$ wollastonite on fluid pressure at various, fixed X_{CO_2} values (after Winkler, 1976)

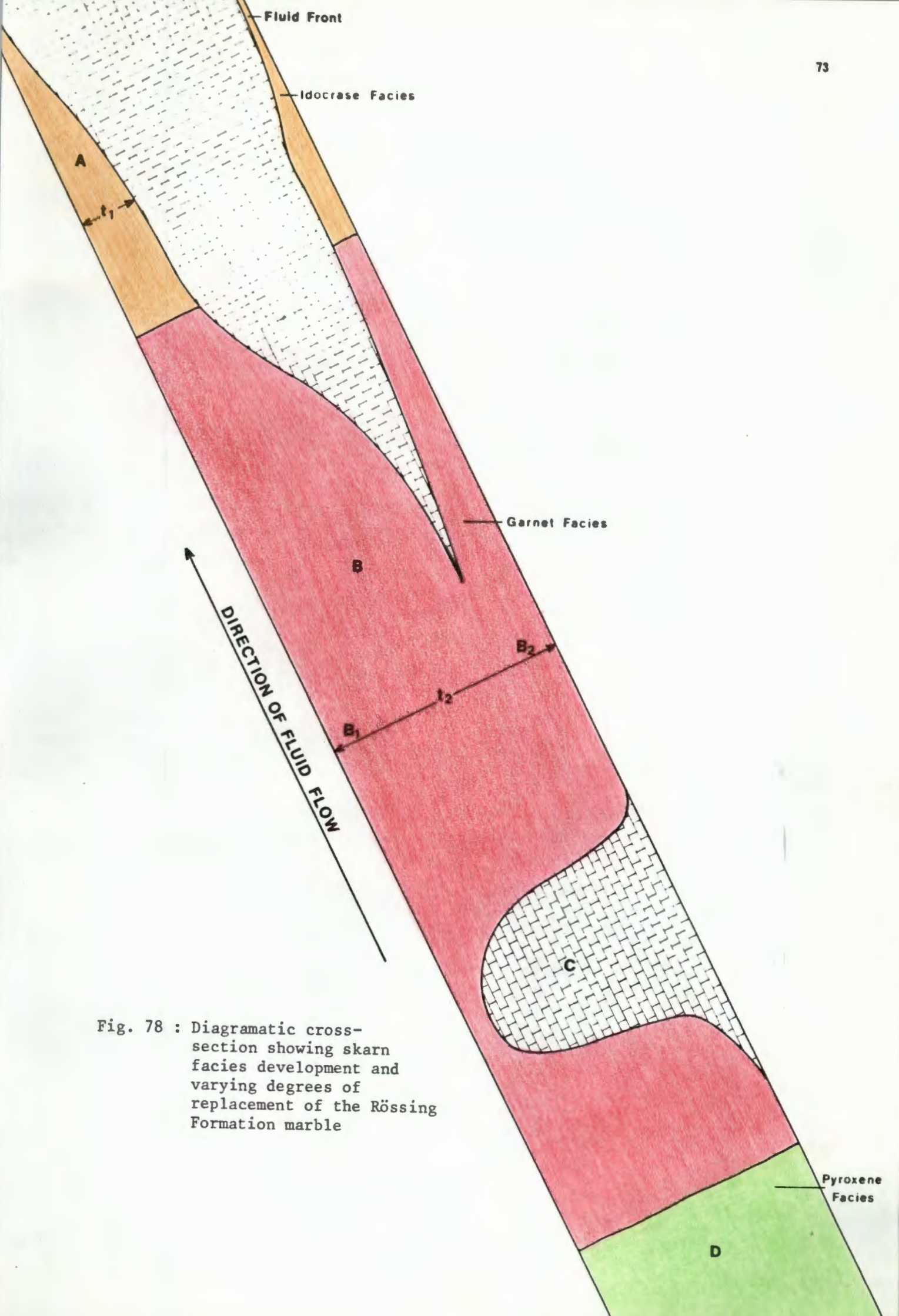

Fig. 78 : Diagramatic cross-section showing skarn facies development and varying degrees of replacement of the Rössing Formation marble

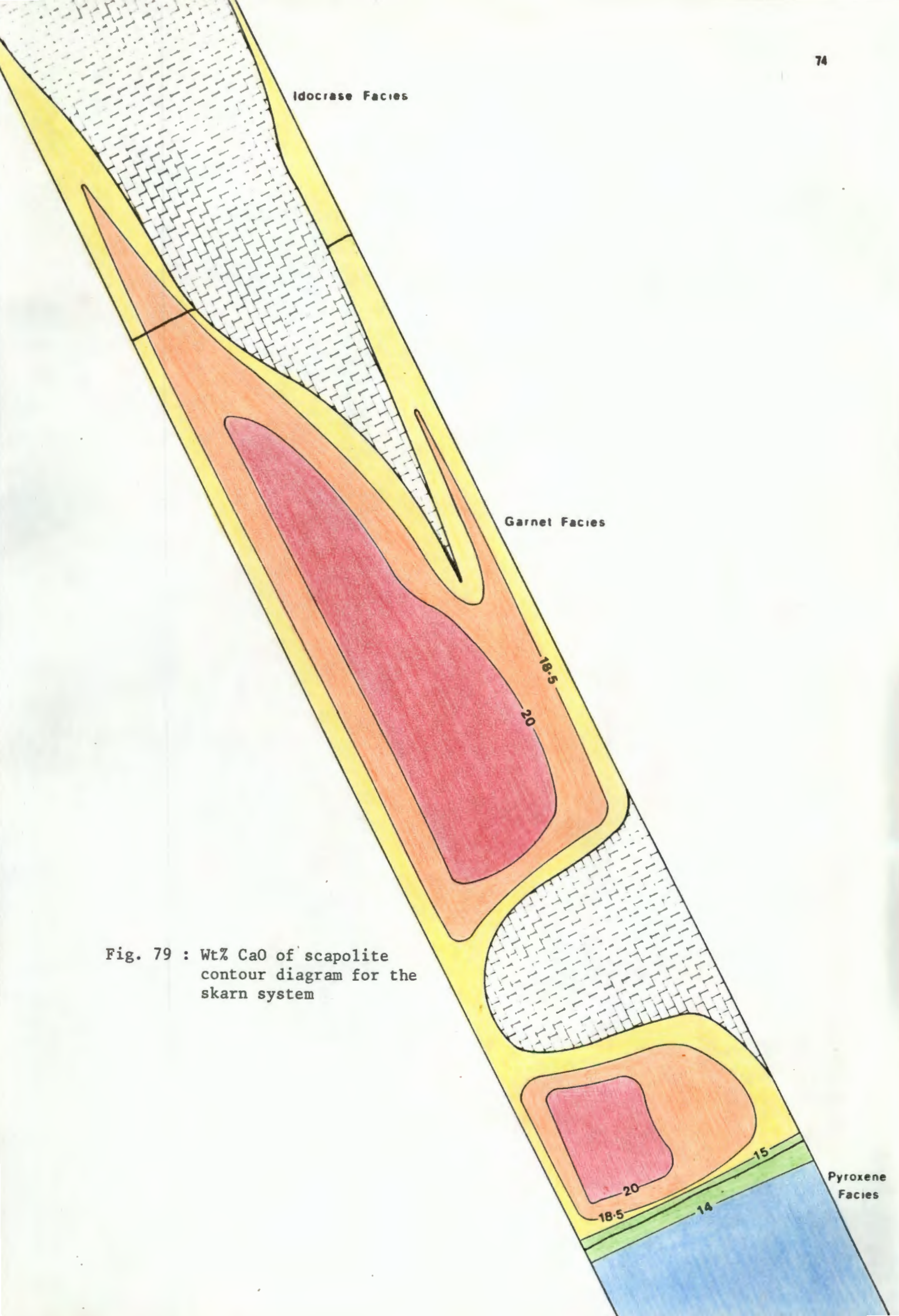

Fig. 79 : Wt% CaO of scapolite contour diagram for the skarn system

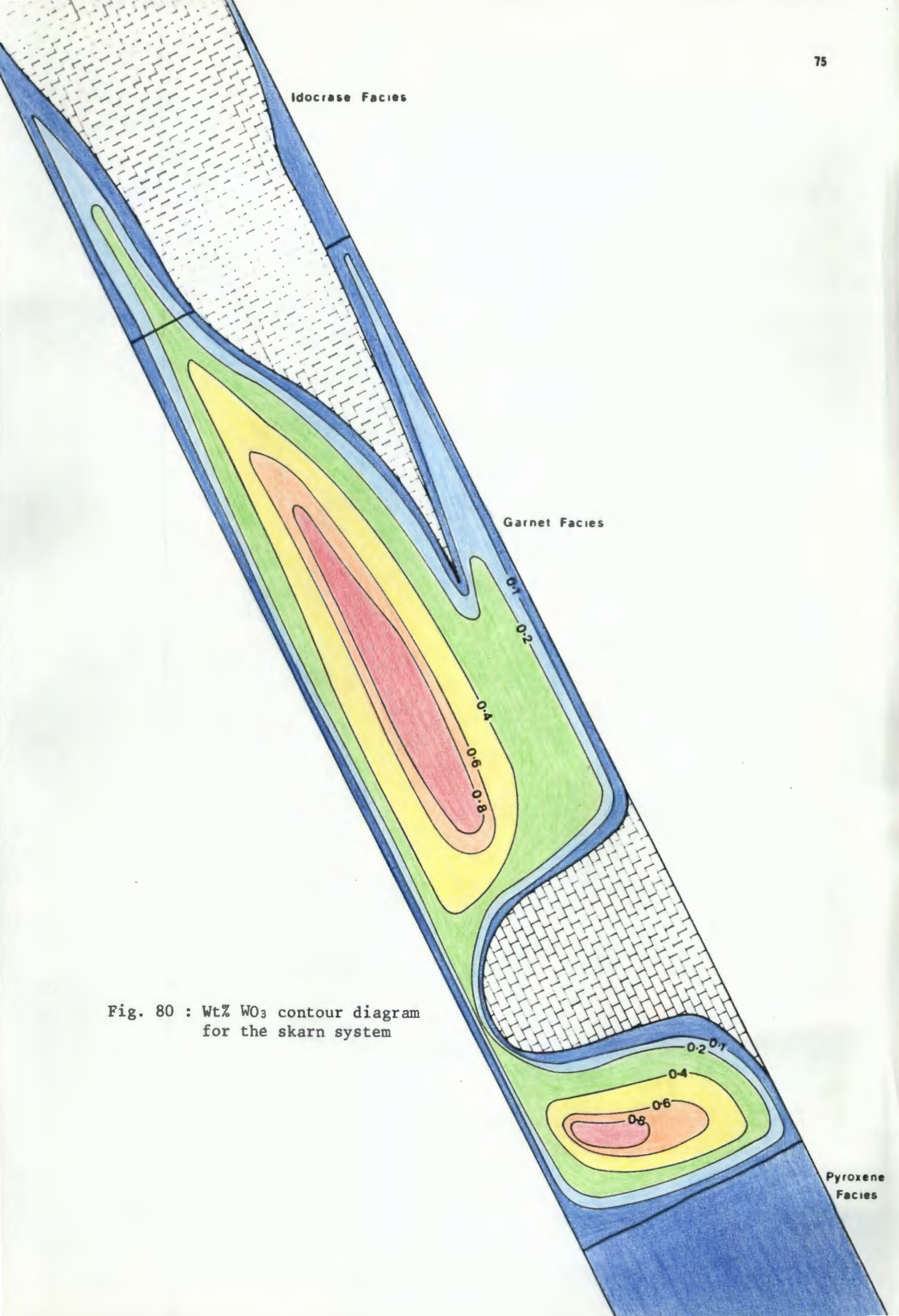

Fig. 80 : Wt% WO_3 contour diagram
for the skarn system

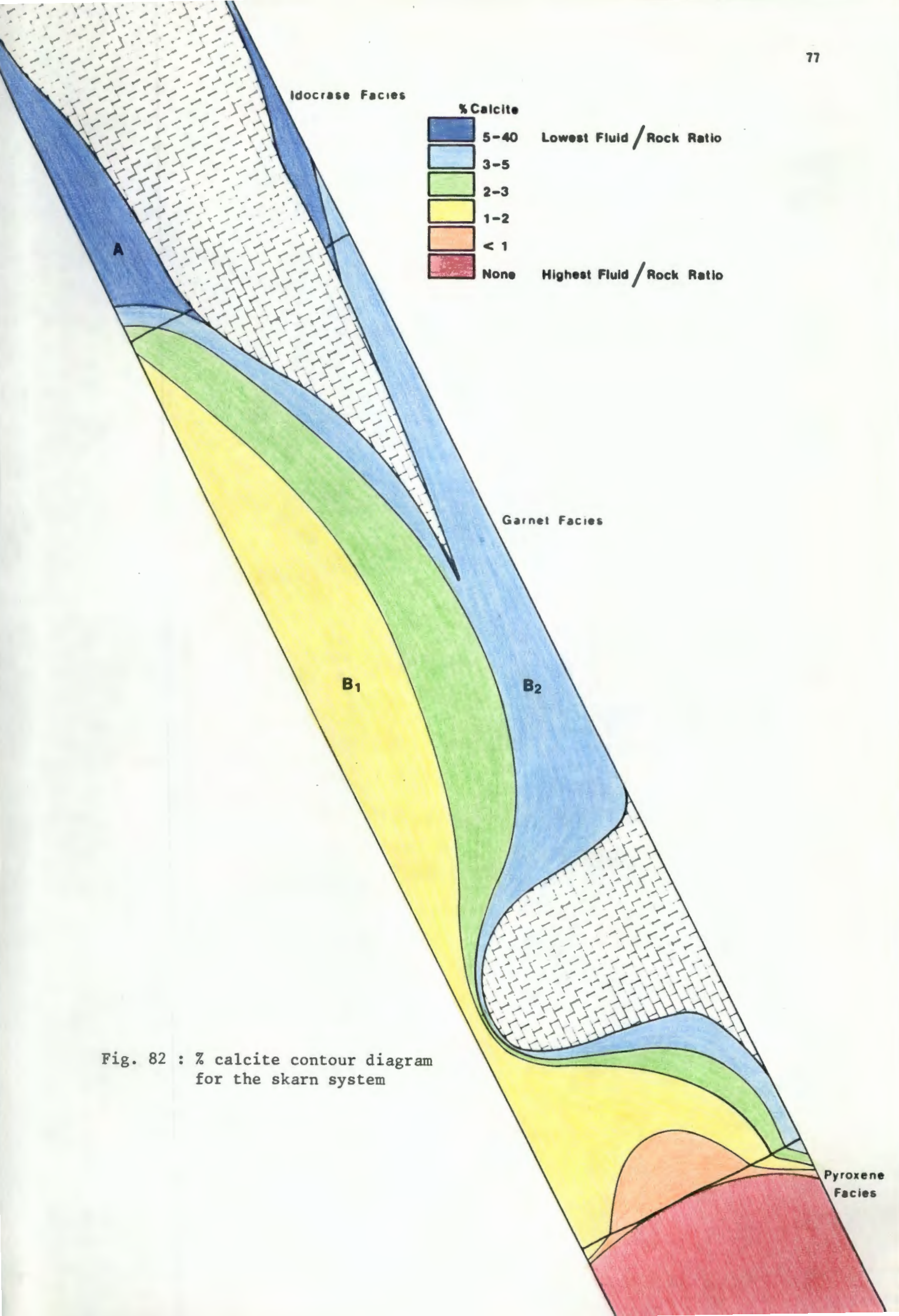

Fig. 82 : % calcite contour diagram for the skarn system

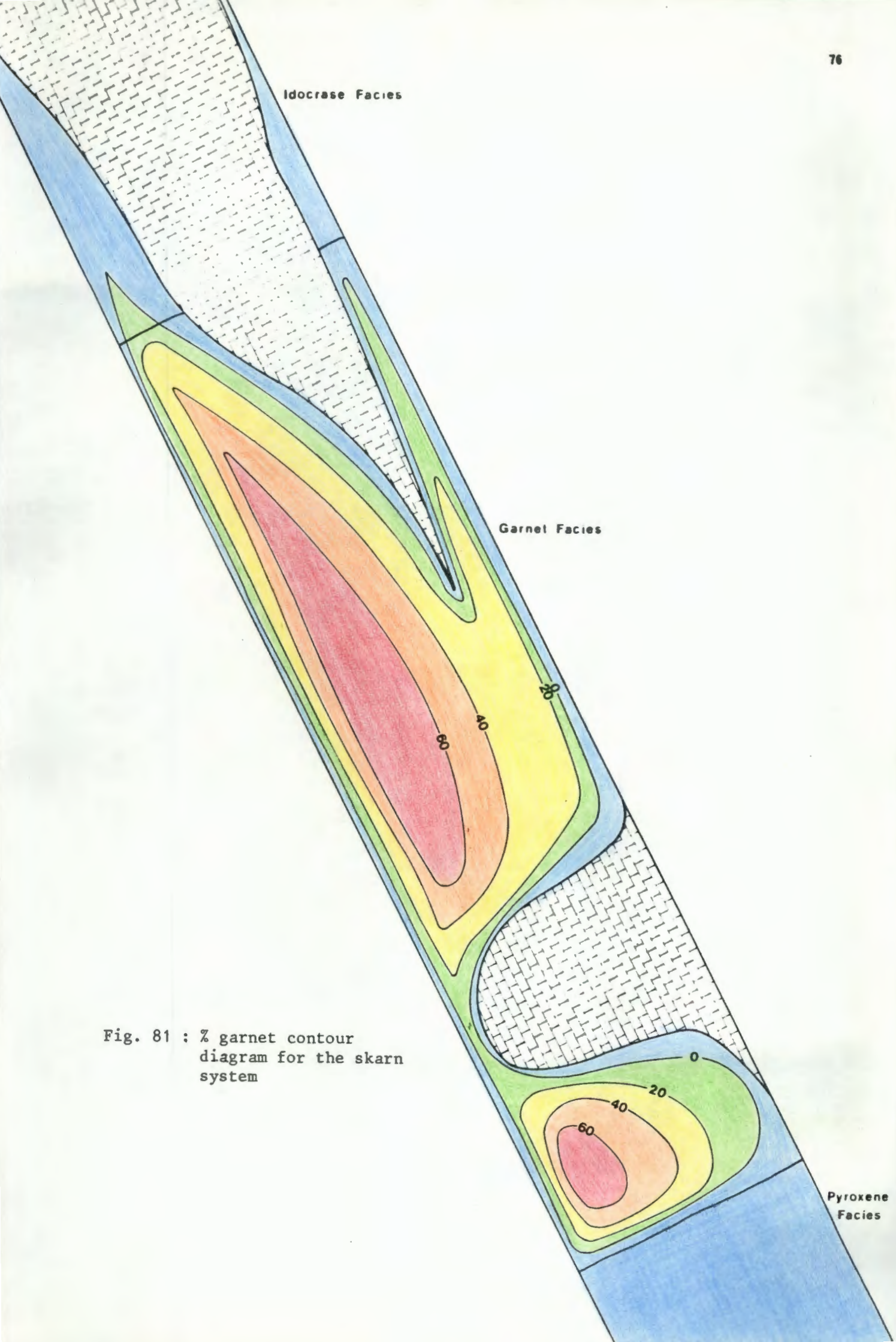

Fig. 81 : % garnet contour diagram for the skarn system

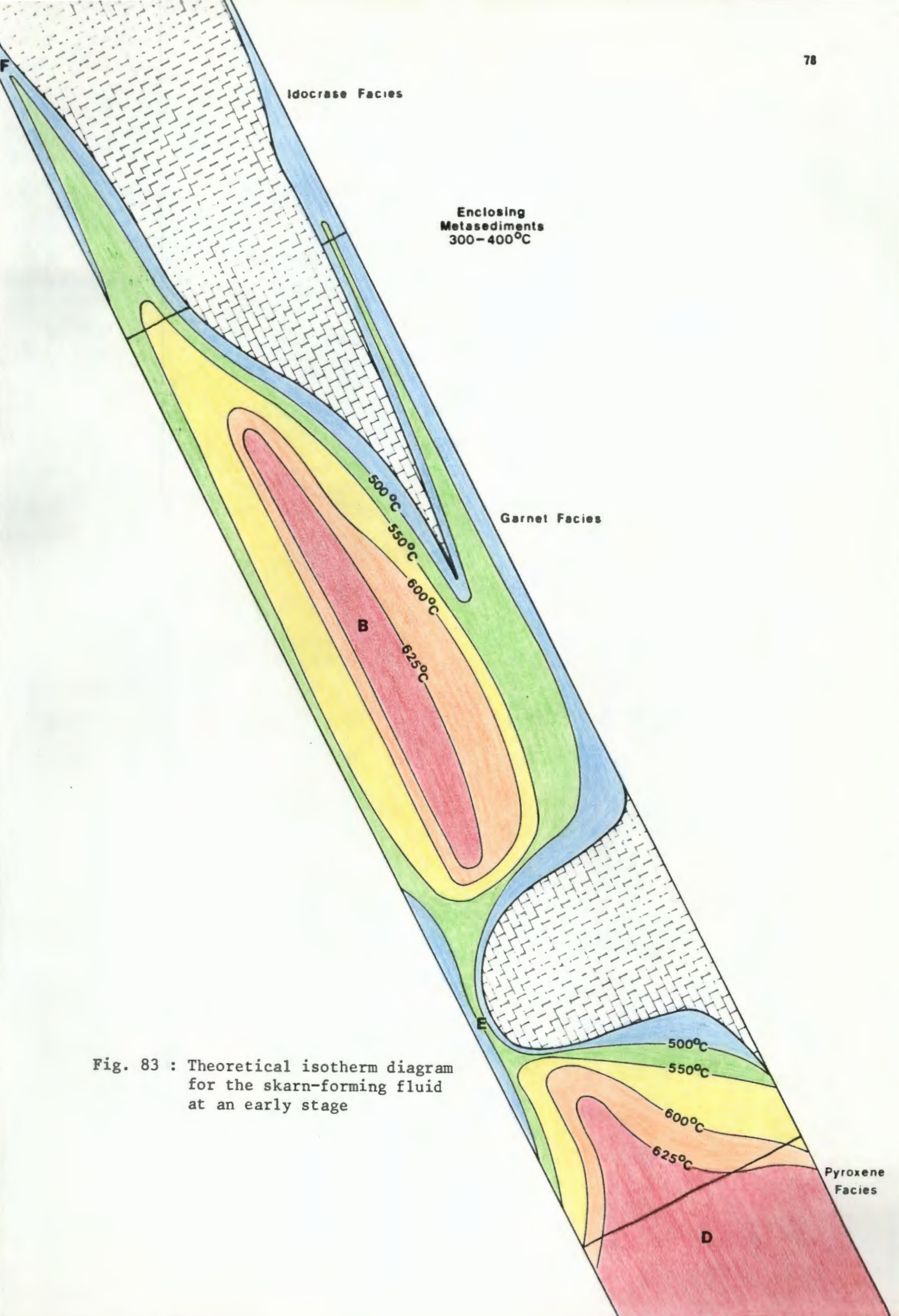

Fig. 83 : Theoretical isotherm diagram for the skarn-forming fluid at an early stage

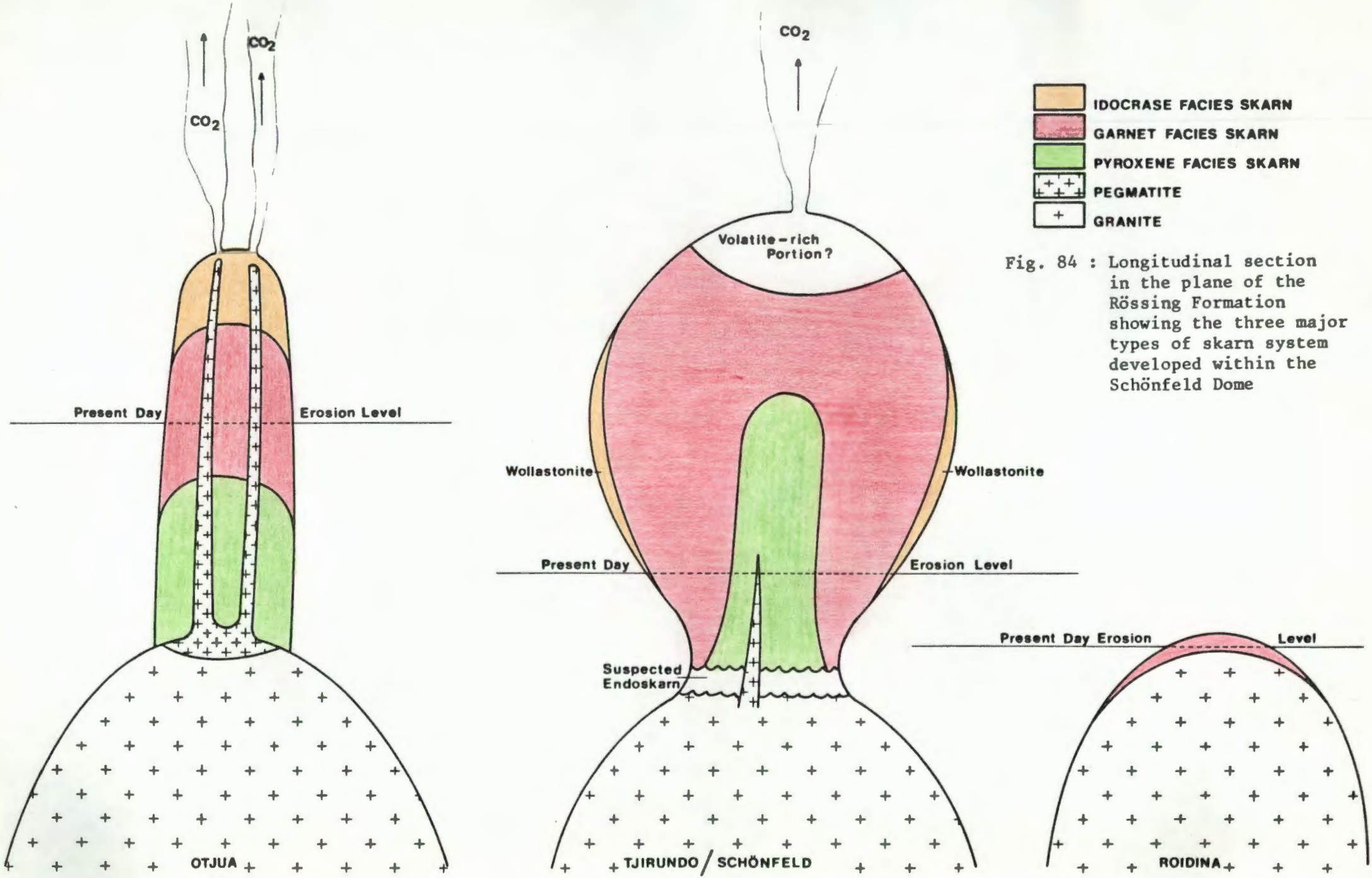

Fig. 84 : Longitudinal section in the plane of the Rössing Formation showing the three major types of skarn system developed within the Schönfeld Dome

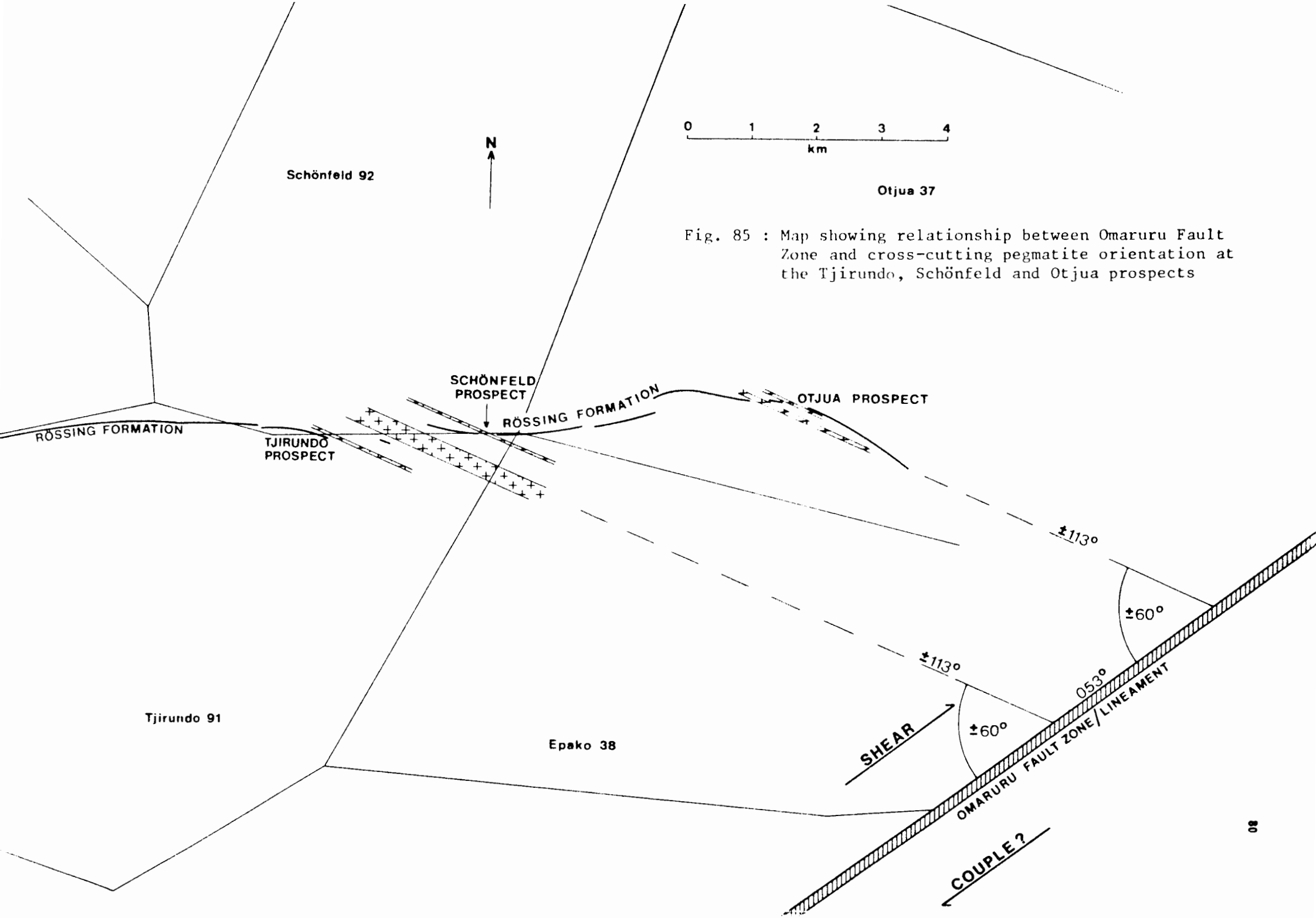

Fig. 85 : Map showing relationship between Omaruru Fault Zone and cross-cutting pegmatite orientation at the Tjirundo, Schönfeld and Otjua prospects

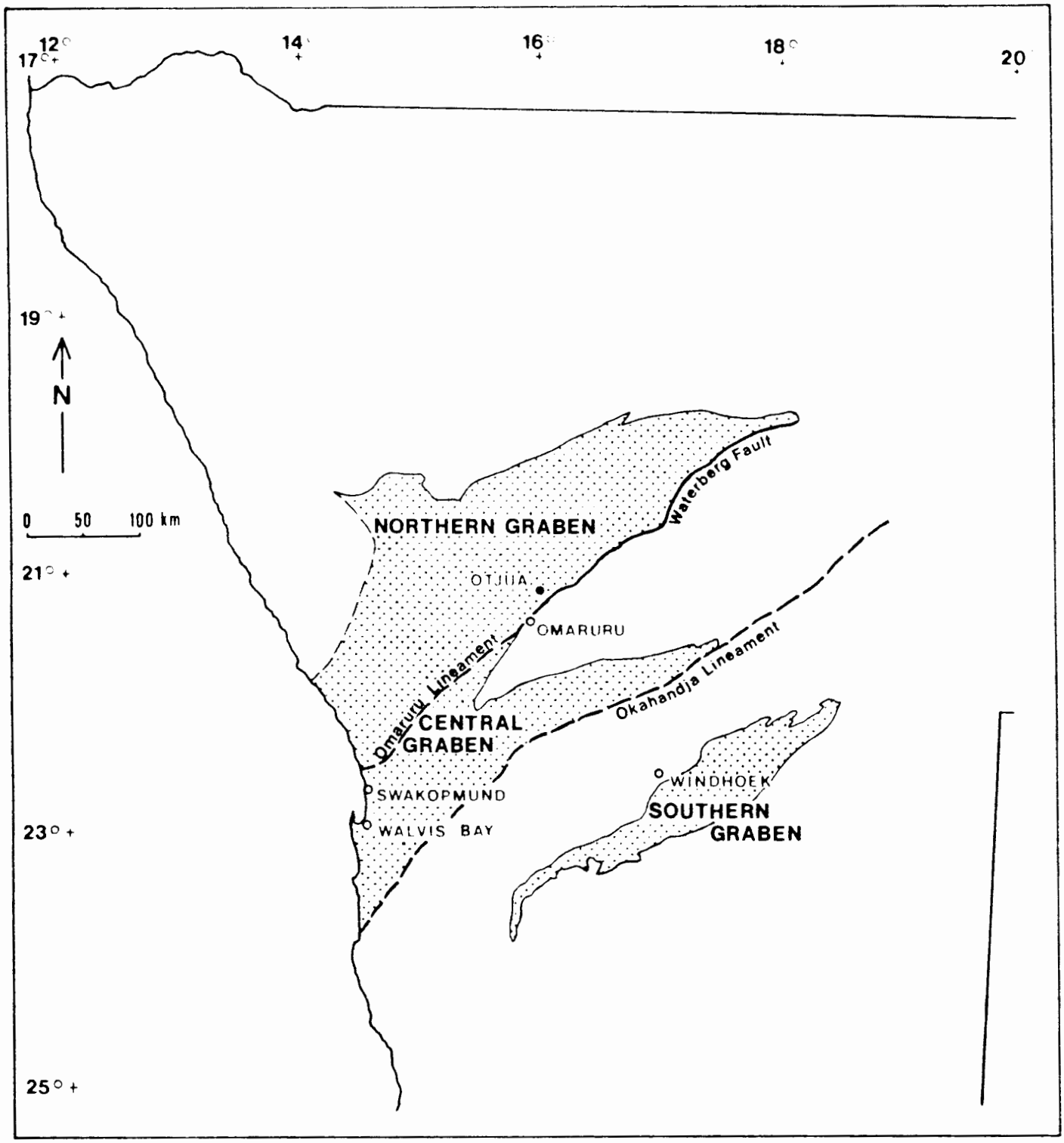

Fig. 86 : Location of northern, central and southern Nosib grabens (after Miller, 1983a)

Fig. 87 : Lineament zones in central SWA/Namibia (after Corner, 1981) showing important uranium occurrences, sediment-hosted scheelite occurrences (W_s) and skarn-hosted scheelite mineralisation (W_g)

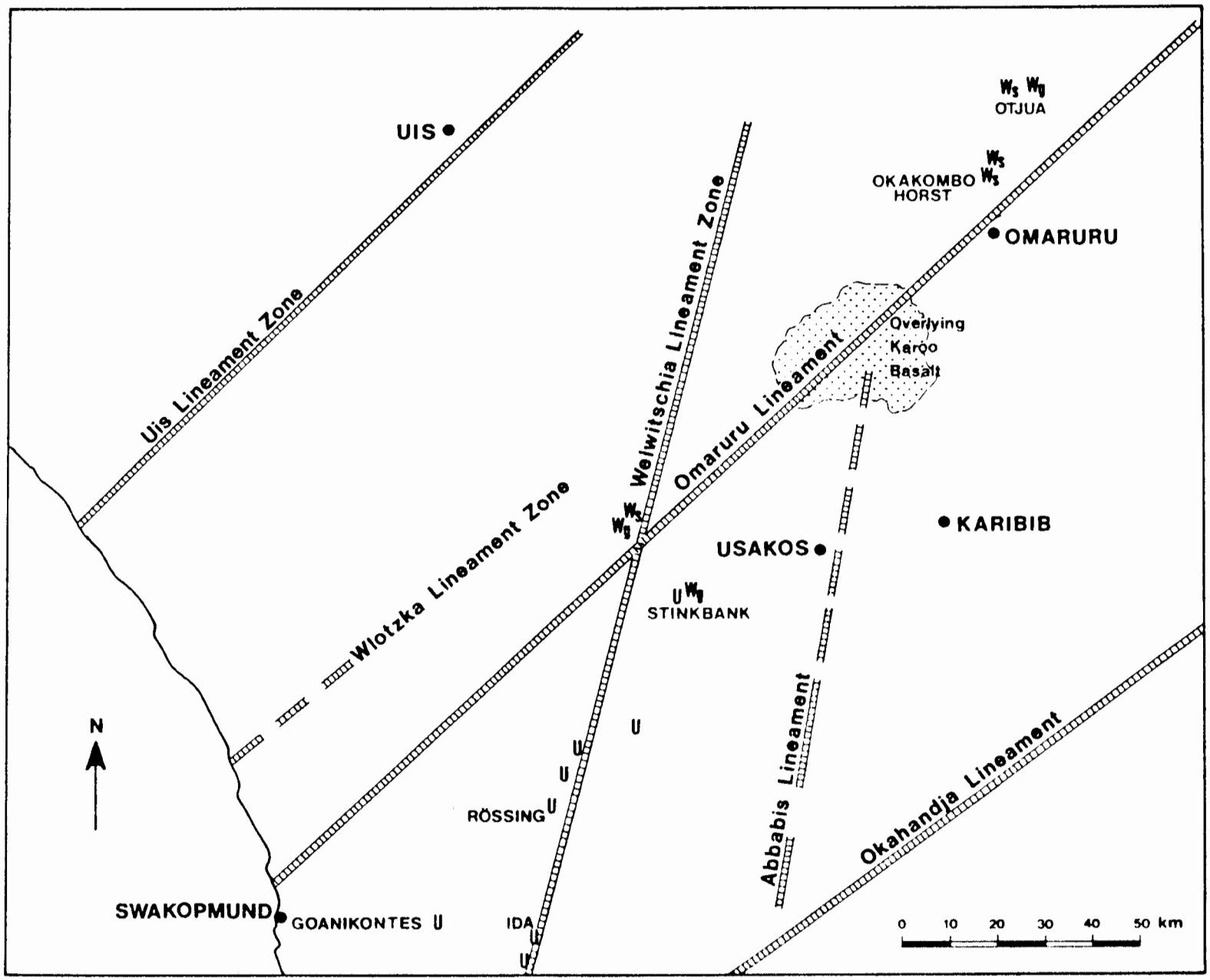

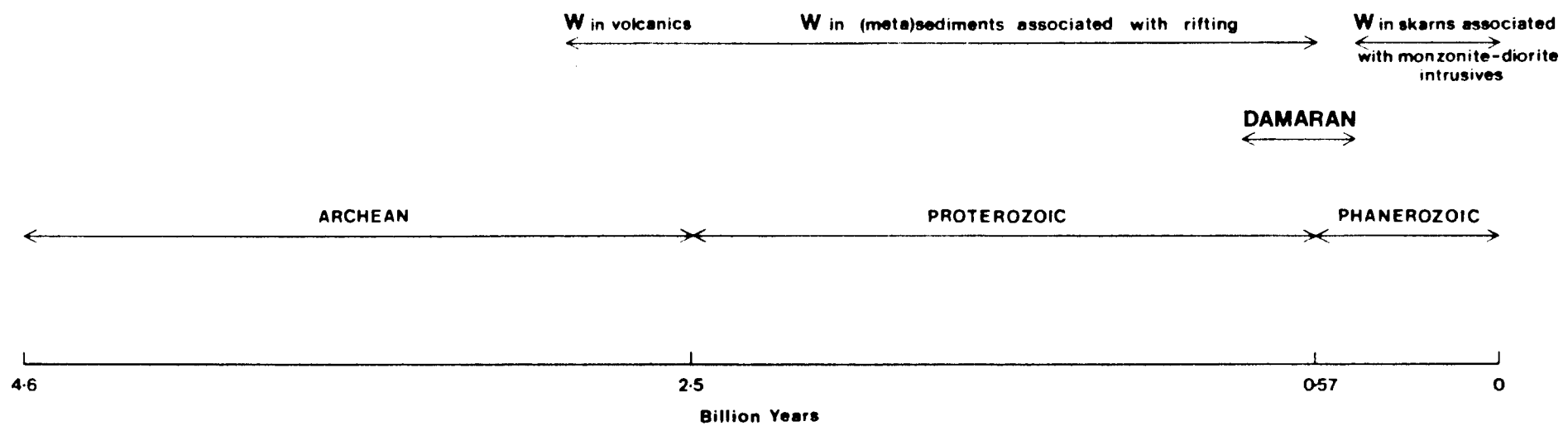

Fig. 88 : Styles of tungsten mineralisation throughout earth history

TABLES

TABLE 1 : Summary of the essential petrographic differences between skarns and scheelite-bearing hornfels

	Skarn	Scheelite-bearing hornfels
Grain Size	Up to several centimetres	<1.5 millimetre
Overall Texture	Locally granoblastic, locally chaotic; garnet and idocrase subidioblastic, commonly poikiloblastic	Xenoblastic-granoblastic; very locally poikiloblastic and chaotic
Major Minerals	Garnet, Idocrase, Pyroxene, Scapolite, Fluorite	Quartz, pyroxene, scapolite and plagioclase
Major Minerals exhibiting piokiloblastic nature	Garnet, Idocrase, Fluorite; locally scapolite	Pyroxene; very locally scapolite and plagioclase
Habit of Calcite	1) Inclusions within garnet and idocrase 2) Anhedral Interstitial	Anhedral interstitial

TABLE 2 : Whole Rock Sample Localities

Sample Number	Sample Description	Sample Locality
OT101	Rössing Formation Marble	Otjua 1A Grid Line 49W/137S
OT102	Idocrase Facies Skarn	Otjua 1A Grid Line 41W/38S
OT103	Idocrase Facies Skarn	Otjua 1A Grid Line 31W/10N
OT104	Garnet Facies Skarn	Otjua 1A Grid Line 26W/27-30N
OT105	Garnet Facies Skarn	Otjua 1A Grid Line 27W/29-33N (trench)
OT106	Garnet Facies Skarn	Otjua 1A Grid Line 24W/28-29N (10m east of line)
OT107	Garnet Facies Skarn	Otjua 1A Grid Line 22W/22-24N
OT108	Garnet Facies Skarn	Otjua 1A Grid Line 17W/35-36N (5m east of line)
OT109	Pyroxene Facies Skarn	Otjua 1A Grid Line 12W/52-55N (5m east of line)
OT110	Pyroxene Facies Skarn	Otjua 1A Grid Line 12W/51-55N
OT111	Pyroxene Facies Skarn	Otjua 1A Grid Line 13W/50-52N
OT112	Otjua Granite	OM6 Survey Beacon (See Map 1)
OT113	Otjua Granite	OM6 Survey Beacon (See Map 1)
OT114	Pegmatite (probably conformable)	Borehole OT23 129.60-133.30m
OT115	Pegmatite (possibly crosscutting)	Borehole OT23 185.08-188.77m
OT116	Pegmatite (possibly crosscutting)	Borehole OT20 153.27-157.10m
OT117	Quartz-biotite Schist	Borehole OT23 118.84-120.50m
OT118	Calc-silicate with minor biotite	Borehole OT23 66.05-67.54m
OT119	Pegmatite (probably conformable)	Borehole OT23 37.05-38.78m

TABLE 2 : Whole Rock Sample Localities (contd.)

Sample Number	Sample Description	Sample Locality
OT120	Sulphidic Tonalite	Borehole OT14 181.12-184.16m
OT121	Orbicular and slightly biotitic Calc-silicate	Borehole OT20 167.40-168.83m
OT122	Orbicular and slightly biotitic Calc-silicate	Borehole OT20 172.95-174.55m
OT123	Quartz-biotite Schist	Borehole OT20 79.07-80.03m
OT124	Rössing Formation Marble	Borehole OT1 66.11-67.60m
OT125	Rössing Formation Marble	Borehole OT20 164.03-165.86m
OT126	Rössing Formation Marble	Borehole OT8 54.00-57.02m
OT127	Otjua Granite	Otjua Granite 1.2km east of Otjua Prospect (see Map 1)
OT128	Otjua Granite	Otjua Granite 200m west of Tar Road (see Map 1)
OT129	Fine grained Granite	Epako-Otjua Boundary Fence (see Map 1)
OT130	Scheelite-bearing Hornfels	Otjua : Borehole OT16 Assay Sample No. 43316
OT131	Scheelite-bearing Hornfels	Otjua : Borehole OT16 Assay Sample No. 43322
OT132	Scheelite-bearing Hornfels	Otjua : Borehole OT22 Assay Sample No. 24191
OT133	Scheelite-bearing Hornfels	Otjua : Borehole OT22 Assay Sample No. 24192
OT134	Scheelite-bearing Hornfels	Otjua : Borehole OT22 Assay Sample No. 24219
OT135	Scheelite-bearing Hornfels	Farm Tjirundo Süd : Surface Sample (see Map 1)
OT136	Scheelite-bearing Hornfels	Farm Tjirundo Süd : Surface Sample (see Map 1)

TABLE 2 : Whole Rock Sample Localities (contd.)

Sample Number	Sample Description	Sample Locality
OT137	Scheelite-bearing Hornfels	Farm Tjirundo Süd : Surface Sample (see Map 1)
OT138	Scheelite-bearing Hornfels	Farm Tjirundo Süd : Surface Sample (see Map 1)
OT139	Scheelite-bearing Hornfels	Farm Tjirundo Süd : Surface Sample (see Map 1)

TABLE 3-1 : Metasediments and Metaintrusive

	Biotite Schist		Calc-Silicate			Sulphidic Tonalite
	OT117	OT123	OT118	OT121	OT122	OT120
			very minor biotite	slightly biotitic	slightly biotitic	
SiO_2	56.70	54.66	54.74	65.20	63.28	75.67
TiO_2	.79	.85	.64	.73	.72	.01
Al_2O_3	16.86	17.76	11.23	11.17	11.21	13.74
Fe_2O_3	7.87	8.34	-	-	-	.94
FeO	-	-	5.37	4.36	5.03	-
MnO	.08	.07	.28	.15	.22	N.D.
MgO	5.00	4.89	3.58	3.62	3.61	N.D.
CaO	4.56	4.31	18.73	9.23	10.97	3.50
Na_2O	1.79	2.17	1.09	2.43	1.67	3.65
K_2O	3.79	4.28	.60	1.71	1.83	1.85
P_2O_5	.20	.20	.21	.24	.22	.02
H_2O	.10	.18	.10	.09	.16	.06
LOI	1.20	1.08	3.61	1.24	1.01	.58
Total	98.94	98.79	100.18	100.17	99.93	100.02
N.B.	All iron expressed as Fe_2O_3		All iron expressed as FeO			All iron expressed as Fe_2O_3
W	15	10	21	10	17	17
F	2200	1070	535	1508	973	N.D.
Rb	340	210	36	137	152	143
Ba	630	740	189	288	346	97
Sr	183	198	343	411	448	254
Th	10.6	10.8	32	7.8	9.9	34
U	N.D.	6.4	6.0	N.D.	N.D.	15.2
Zr	165	171	151	226	229	109
Nb	13.8	15.1	11.2	12.0	13.1	37
Mo	2.5	N.D.	3.3	N.D.	2.6	1.6
Cr	111	121	66	74	76	2.5
V	183	198	94	91	91	N.D.
Sc	21	24	14.3	13.0	14.1	1.6
Co	26	24	16.7	12.4	14.9	2.0
Pb	12.6	8.2	N.D.	7.3	7.8	11.5
Zn	146	151	146	76	110	12.3
Cu	40	64	N.D.	N.D.	N.D.	140
Ni	66	73	36	34	37	N.D.
S	193	546	8.2	N.D.	N.D.	1992
Y	31	33	35	36	35	16.0
Na_2O/K_2O	.4723	.5070				
Na_2O+K_2O	5.58	6.45				
$(Al_2O_3+K_2O)/Na_2O$	11.54	10.16				
$(Al_2O_3+K_2O)/(MgO+CaO+Na_2O)$	1.82	1.94				

TABLE 3-2 : Scheelite-bearing Hornfels

	OT130	OT131	OT132	OT133	OT134	OT135	OT136	OT137	OT138	OT139
SiO_2	60.45	51.58	58.63	49.59	49.70	60.07	67.61	65.35	66.77	63.56
TiO_2	0.63	0.46	0.73	0.54	0.60	0.64	0.55	0.58	0.71	0.63
Al_2O_3	11.80	12.83	12.16	13.07	12.04	9.44	9.60	9.51	10.54	9.56
FeO	5.78	9.15	6.52	9.16	9.69	5.12	4.94	5.57	4.47	4.78
MnO	0.20	0.57	0.43	0.55	0.63	0.15	0.20	0.25	0.12	0.17
MgO	3.45	4.32	4.11	3.48	3.72	3.73	2.38	2.93	2.78	2.26
CaO	15.18	18.81	14.91	19.94	20.83	16.56	12.41	12.84	11.53	14.02
Na_2O	0.66	0.72	0.48	0.77	0.83	0.69	0.31	0.20	0.60	0.67
K_2O	0.14	0.14	0.62	0.57	0.18	0.13	0.32	0.57	0.46	0.30
P_2O_5	0.17	0.14	0.24	0.15	0.19	0.22	0.19	0.16	0.24	0.19
H_2O^-	0.13	0.10	0.13	0.08	0.09	0.10	0.09	0.11	0.04	0.07
LOI	1.28	1.03	1.24	1.60	1.10	2.95	1.43	2.15	1.99	2.71
Total	99.87	99.85	100.20	99.50	99.60	99.80	100.03	100.22	100.25	98.92

N.B. All iron expressed as FeO

W	879	2258	2078	14274	2009	34	86	525	25	2406
F	N.D	1071	827	N.D.	N.D.	150	140	150	220	170
Rb	18.7	12.3	54.9	49	22	8.8	17.8	31	34	20
Ba	18.9	14.6	84	69	14.5	44	73	276	100	30
Sr	190	184	116	226	225	286	186	183	138	160
Th	N.D.	23	15.3	11.6	9.4	14.2	N.D.	8.4	N.D.	N.D.
U	N.D.	6.7	8.1	N.D.	N.D.	N.D.	N.D.	N.D.	N.D.	N.D.
Zr	158	98	240	114	147	279	168	175	183	185
Nb	11.8	37	38	38	38	25	11.3	11.6	19.1	67
Mo	2.5	6.0	5.3	7.9	5.8	4.9	2.9	3.6	4.5	9.0
Cr	67	63	80	70	68	64	62	63	79	72
V	88	119	112	107	106	79	72	89	103	82
Sc	13.0	16.5	17.8	18.9	17.0	12.0	10.9	13.2	13.8	10.7
Co	17.2	19.7	24	16.4	20	11.7	11.9	13.3	12.3	11.8
Pb	14.1	18.6	17.9	9.0	16.4	16.1	N.D.	9.2	9.1	8.4
Zn	140	198	128	200	274	278	112	123	62	169
Cu	3.6	N.D.	N.D.	N.D.	N.D.	29	14.6	33	47	7.4
Ni	37	47	47	40	43	57	29	37	21	33
S	14.4	N.D.	8.5	N.D.	N.D.	28	1636	343	825	29
Y	47	78	88	64	52	92	37	36	60	40

TABLE 3-3 : Marble - Rössing Formation

	OT101	OT124	OT125	OT126
SiO_2	2.85	3.77	3.01	4.67
TiO_2	.03	.01	.02	.05
Al_2O_3	.61	.38	.42	.84
FeO	.45	.37	.25	.51
MnO	.10	N.D.	N.D.	N.D.
MgO	.89	.77	.71	.92
CaO	53.28	53.14	53.58	51.58
Na_2O	N.D.	N.D.	N.D.	N.D.
K_2O	.07	.08	.03	.12
P_2O_5	.16	.10	.09	.10
H_2O^-	.06	.21	.11	.23
LOI	42.09	41.57	41.32	40.58
Total	100.59	100.40	99.54	99.60

N.B. All iron expressed as FeO

W	N.D.	N.D.	N.D.	N.D.
F	N.D.	N.D.	N.D.	N.D.
Rb	N.D.	N.D.	N.D.	5.1
Ba	7.8	8.6	12.7	17.6
Sr	1616	1541	1446	1355
Th	N.D.	N.D.	N.D.	N.D.
U	N.D.	N.D.	N.D.	5.2
Zr	9.0	5.7	9.7	12.8
Nb	N.D.	N.D.	N.D.	N.D.
Mo	14.2	13.6	87	30
Cr	N.D.	2.9	N.D.	6.2
V	N.D.	4.3	4.4	9.1
Sc	N.D.	N.D.	N.D.	N.D.
Co	N.D.	N.D.	N.D.	N.D.
Pb	10.3	N.D.	N.D.	N.D.
Zn	4.1	4.0	12.4	11.4
Cu	N.D.	N.D.	10.5	24
Ni	N.D.	N.D.	N.D.	N.D.
S	97	25	377	637
Y	N.D.	N.D.	3.2	3.2

TABLE 3-4 : Tjirundo Prospect Marble - Rössing Formation

	TJM1	TJM2	TJM3
SiO_2	1.96	2.04	6.00
TiO_2	.02	.01	.06
Al_2O_3	.15	.24	.85
FeO	.22	.25	.34
MnO	N.D.	.04	N.D.
MgO	.53	.60	.67
CaO	54.68	53.91	51.54
Na_2O	N.D.	N.D.	N.D.
K_2O	N.D.	.03	.16
P_2O_5	.06	.04	.04
H_2O^-+LOI	43.52	43.33	40.79
Total	101.14	100.49	100.45

N.B. All iron expressed as FeO

TABLE 3-5 : Skarns

	Idocrase Facies		Garnet Facies					Pyroxene Facies		
	OT102	OT103	OT104	OT105	OT106	OT107	OT108	OT109	OT110	OT111
SiO_2	38.77	41.84	46.20	45.10	40.66	42.42	29.50	49.68	48.37	49.94
TiO_2	.84	.52	.03	.05	.10	.04	.11	.04	.02	.03
Al_2O_3	12.79	11.06	7.53	8.64	18.67	9.48	10.18	16.91	12.57	14.75
Fe_2O_3	.89	1.45	1.75	1.40	1.10	1.78	1.22			
FeO	5.92	9.65	11.67	9.31	7.30	11.89	8.12	8.75	12.93	11.06
MnO	.52	.81	2.17	2.29	2.26	2.12	2.49	.42	.64	.47
MgO	2.84	2.10	1.07	.84	.38	1.51	.89	.61	.75	.90
CaO	29.65	25.05	16.09	14.88	22.99	20.76	12.14	15.82	17.68	16.75
Na_2O	.29	.96	.47	.45	1.02	.55	.30	3.42	1.99	2.86
K_2O	.01	.19	.09	.18	.17	.12	.09	.60	.41	.51
P_2O_5	.22	.15	.09	.07	.11	.12	.08	.17	.15	.10
H_2O^-	0.06	.07	.09	.10	.03	.01	.11	.04	.14	.05
LOI	4.64	4.35	1.82	1.89	3.19	2.19	2.01	3.58	3.63	3.87
CaF_2	3.1	2.1	11.3	16.4	1.9	6.8	32.0	-	-	-
Total	100.54	100.30	100.37	101.60	99.88	99.79	99.24	100.04	99.28	101.29

Fe_2O_3: FeO ratio for idocrase and garnet facies skarn selected as 0.15 on basis of estimation of Fe^{3+} in idocrase and garnet. All iron expressed as FeO for pyroxene facies skarn.

W	722	3783	2835	444	6526	5511	5416	23	21	29
F	←———	Expressed as CaF_2					———→	584	N.D.	N.D.
Rb	N.D.	16.3	7.5	20	10.4	7.7	14.3	18.9	14.2	21
Ba	7.2	10.7	7.4	9.9	6.9	23	14.0	77	37	34
Sr	182	159	128	161	158	157	158	189	168	167
Th	30	29	30	25	N.D.	N.D.	159	N.D.	N.D.	100
U	12.7	44	N.D.	6.2	N.D.	6.6	N.D.	9.5	N.D.	7.4
Zr	126	62	19.3	25	21	19.4	25	15.3	10.6	11.5
Nb	17.2	29	27	26	23	4.3	34	42	19.2	25
Mo	8.2	15.8	56	14.1	13.0	12.7	17.6	4.0	5.9	3.9
Cr	75	51	15.1	15.0	11.3	12.2	15.1	6.0	8.0	5.6
V	137	101	8.6	12.3	51	39	28	8.0	9.5	12.4
Sc	14.7	17.0	8.8	7.8	14.2	7.6	4.8	19.9	7.9	11.0
Co	16.8	17.7	14.4	14.0	8.3	18.2	12.0	11.1	19.9	15.9
Pb	8.4	9.6	N.D.	N.D.	8.2	N.D.	7.4	29	11.3	23
Zn	480	677	375	391	260	538	169	232	247	272
Cu	N.D.	N.D.	N.D.	N.D.	N.D.	N.D.	3.9	1.9	6.8	5.0
Ni	36	22	5.8	8.1	N.D.	13.2	5.6	4.2	7.9	5.9
S	122	42	56	N.D.	N.D.	N.D.	12.8	N.D.	141	N.D.
Y	71	194	8.2	9.2	85	17.9	38	31	26	25

TABLE 3-6 : Granites

	Otjua Granite				Fine grained Granite
	OT112	OT113	OT127	OT128	OT129
SiO_2	72.80	73.17	73.44	71.66	73.44
TiO_2	.25	.25	.26	.35	.28
Al_2O_3	13.49	13.41	13.84	14.80	13.46
Fe_2O_3	2.25	2.19	2.24	1.89	2.49
MnO	N.D.	N.D.	N.D.	N.D.	N.D.
MgO	.34	.30	.34	.47	.39
CaO	1.54	1.54	1.32	.82	1.49
Na_2O	2.49	2.53	2.36	2.60	2.44
K_2O	5.52	5.56	5.66	6.36	5.47
P_2O_5	.10	.07	.08	.41	.07
H_2O^-	.04	.09	.14	.20	.17
LOI	.44	.54	.58	.90	.60
Total	99.26	99.65	100.26	100.46	100.30
W	14	8	8	N.D.	9
F	487	730	N.D.	N.D.	N.D.
Rb	353	358	348	302	310
Ba	278	307	306	280	314
Sr	73	81	79	61	83
Th	41	70	40	19.4	46
U	7.5	8.7	4.8	7.1	6.4
Zr	207	195	208	162	223
Nb	38	35	39	10.8	38
Mo	N.D.	N.D.	N.D.	N.D.	N.D.
Cr	8.4	4.9	4.3	4.1	5.9
V	9.3	9.4	10.3	6.6	9.9
Sc	6.3	5.2	4.9	1.1	6.1
Co	3.2	3.7	3.9	3.3	3.9
Pb	32	34	30	46	38
Zn	31	28	32	91	29
Cu	N.D.	N.D.	N.D.	N.D.	N.D.
Ni	N.D.	N.D.	N.D.	N.D.	N.D.
S	99	N.D.	N.D.	11.6	N.D.
Y	63	85	57	5.7	52
Rb/Sr	4.84	4.42	4.41	4.95	3.73
K/Rb	130	129	135	175	146
K/Ba	165	150	154	189	145
Ba/Rb	0.79	0.86	0.88	0.93	1.01
Ca/Sr	151	136	119	96	128
Ba/Sr	3.8	3.8	3.9	4.6	3.8

All iron expressed as Fe_2O_3

TABLE 3-7 : Average Otjua Granite, Average Granite and Average Low-calcium Granite

	Average Otjua Granite	Average Granite (Taylor, 1968)	Average low-calcium Granite (Turekian and Wedepohl, 1961)
SiO_2	72.77	71.20	74.20
TiO_2	.28	0.40	0.20
Al_2O_3	13.89	14.70	13.60
Fe_2O_3	2.14	FeO 3.24	FeO 1.83
MnO	N.D.	0.05	0.05
MgO	.36	0.55	0.27
CaO	1.31	2.00	0.71
Na_2O	2.50	3.54	3.48
K_2O	5.78	4.18	5.05
P_2O_5	.17	0.16	0.14
H_2O^-	.12	-	-
LOI	.62	-	-
Total	99.94		
Rb/Sr	4.66		
K/Rb	142		
K/Ba	165		
Ba/Rb	.87		
Ca/Sr	126		
Ba/Sr	4.03		

TABLE 3-8 : Pegmatite

	OT114	OT115	OT116	OT119	Average Otjua Pegmatite
SiO_2	72.66	75.54	73.99	74.23	74.11
TiO_2	.07	N.D.	.07	N.D.	0.04
Al_2O_3	15.04	13.58	13.52	14.25	14.10
Fe_2O_3	1.68	.92	1.45	.67	1.18
MnO	N.D.	.04	N.D.	.06	0.03
MgO	.22	N.D.	.18	N.D.	0.10
CaO	1.19	1.01	1.09	.84	1.03
Na_2O	4.16	4.32	3.50	4.18	4.04
K_2O	5.11	4.28	5.10	5.26	4.94
P_2O_5	.05	N.D.	.06	N.D.	0.03
H_2O^-	.04	.11	.04	.02	0.05
LOI	.38	.40	.44	.15	0.34
Total	100.60	100.20	99.44	99.66	
W	13	8	16	17	
F	N.D.	N.D.	N.D.	N.D.	
Rb	371	236	444	339	
Ba	48	21	57	96	
Sr	26	15.3	44	33	
Th	57	4.5	28.0	N.D.	
U	19.9	4.0	21	4.4	
Zr	39	22	47	27	
Nb	70	10.3	127	88	
Mo	N.D.	N.D.	N.D.	N.D.	
Cr	2.1	2.2	3.3	3.5	
V	1.8	N.D.	N.D.	N.D.	
Sc	6.1	6.3	7.6	5.5	
Co	2.7	1.4	2.0	N.D.	
Pb	98	83	69	66	
Zn	31	4.0	31	13.6	
Cu	N.D.	N.D.	N.D.	N.D.	
Ni	N.D.	N.D.	N.D.	N.D.	
S	N.D.	N.D.	N.D.	N.D.	
Y	221	46	109	19.5	
Rb/Sr	14.3	15.4	10.1	10.3	
K/Rb	114	151	95	129	
K/Ba	884	1692	743	455	
Ba/Rb	0.13	0.09	0.13	0.28	
Ca/Sr	327	472	177	182	
Ba/Sr	1.8	1.4	1.3	2.9	

All iron expressed as Fe_2O_3

TABLE 4 : Scheelite-bearing Hornfels : Correlation Coefficient between W Concentration and Major Oxide Contents

(ppm)		(wt.%)	Correlation Coefficient
W	versus	SiO_2	-0.61
W	versus	TiO_2	-0.32
W	versus	Al_2O_3	+0.58
W	versus	FeO	+0.57
W	versus	MnO	+0.53
W	versus	MgO	+0.16
W	versus	CaO	+0.56
W	versus	Total Alkalis	+0.76
W	versus	P_2O_5	-0.43

TABLE 5 : Regression Line Curves for Figures 43-47

	x-axis		y-axis	R^2	a	b	Rock Type
Fig. 43	wt%SiO_2	vs	Tot.Ca	1.0	48.87	-0.65	Calc-Silicate
Fig. 43	wt%SiO_2	vs	Tot.Ca	0.95	30.71	-0.33	W-Hornfels
Fig. 43	wt%SiO_2	vs	Tot.Ca	0.84	46.53	-0.67	Skarn
Fig. 44	Tot.Ca	vs	wt%MgO	1.00	3.66	-0.01	Calc-Silicate
Fig. 44	Tot.Ca	vs	wt%MgO	0.45	1.04	0.20	W-Hornfels
Fig. 45	Tot.Ca	vs	wt%FeO+ MnO+MgO	0.74	7.51	0.13	Calc-Silicate
Fig. 45	Tot.Ca	vs	wt%FeO+ MnO+MgO	0.83	-1.90	1.07	W-Hornfels
Fig. 47	Tot.Ca	vs	wt%Na_2O+ K_2O	1.00	6.39	-0.35	Calc-Silicate
Fig.47	Tot.Ca	vs	wt%Na_2O+ K_2O	0.19	0.50	0.04	W-Hornfels
Fig.47	Tot.Ca	vs	wt%Na_2O+ K_2O	0.77	5.98	-0.26	Skarn

R^2 = Coefficient of Determination
ZLIN Linear Regression Equation : y = a + bx

TABLE 6-1 : Slide Localities of Skarn hosted by the Rössing Formation

Slide No.	Sample Description	Sample Locality	Assay No.
24472	Idocrase + pyroxene + calcite skarn	Borehole OT24	24413
24474	Idocrase + pyroxene + calcite skarn	Borehole OT24	24412
24475	Pyroxene + scapolite skarn	Borehole OT25	24392
24476	Idocrase + calcite + pyroxene skarn	Borehole OT25	24393
24477	Garnet + pyroxene + scapolite + scheelite + fluorite skarn	Borehole OT26	0009
24625	Idocrase + pyroxene skarn	Borehole OT6	58452
* 24626	Pyroxene + scapolite + scheelite skarn	Borehole OT5 : structural hanging wall	24825
* 24627	Pyroxene + scapolite + scheelite + fluorite skarn	Borehole OT5	24829
* 24628	Garnet + pyroxene + scapolite + fluorite + scheelite skarn	Borehole OT5	24831
* 24629	Garnet + scapolite + fluorite + pyroxene skarn	Borehole OT5	24834
* 24630	Pyroxene + scapolite + fluorite + scheelite skarn	Borehole OT5 structural footwall	24836
24632	Garnet + pyroxene + scapolite + fluorite + scheelite skarn	Borehole OT12	24712
24633	Garnet + pyroxene + fluorite + scheelite skarn	Borehole OT2	108881
** 24636	Pyroxene + scapolite + fluorite + scheelite skarn	Borehole OT17 structural hanging wall	58458
** 24637	Garnet + pyroxene + scapolite + fluorite + scheelite skarn	Borehole OT17	58459
** 24638	Garnet + scapolite + fluorite + scheelite skarn	Borehole OT17	58460
** 24639	Garnet + pyroxene + scapolite + scheelite + fluorite skarn	Borehole OT17	58461
** 24640	Garnet + pyroxene + scapolite + fluorite + scheelite skarn	Borehole OT17	58462
** 24641	Pyroxene + fluorite + scheelite skarn	Borehole OT17 structural footwall	58463
24646	Idocrase + garnet + pyroxene + calcite skarn	Borehole OT15	58668
24649	Pyroxene + scapolite skarn	Borehole OT14	58605

* Traverse across intersection (see Fig. 59)

** Traverse across intersection (see Fig. 63)

TABLE 6-1 : Slide Localities of Skarn hosted by the Rössing Formation (contd.)

Slide No.	Sample Description	Sample Locality	Assay No.
24655	Pyroxene + scapolite skarn	Surface sample: 12 West trench WRAOT110	-
24656	Pyroxene + scapolite skarn	Surface sample: 12 West trench WRAOT110	-
24659	Garnet + pyroxene + fluorite + scheelite skarn	Surface sample: 26 West o/crop WRAOT104	-
24660	Garnet + pyroxene + scapolite + fluorite + scheelite skarn	Surface sample: 27 West trench WRAOT105	-

TABLE 6-2 : Slide Localities of Calc-silicate and Scheelite-bearing Hornfels

Slide No.	Sample Description	Sample Locality	Assay No.
24478	Scheelite-bearing hornfels	Borehole OT26	24565
24479	Calc-silicate	Borehole OT25 258.50 metres	-
24481	Calc-silicate	Borehole OT16 125.35 metres	-
43312	Scheelite-bearing hornfels	Borehole OT16 86.93 metres	43312
43323	Scheelite-bearing hornfels	Borehole OT16 102.88 metres	43323

TABLE 7-1 Scapolite : Representative Analyses

	Idocrase Facies			
Analysis No.	1	2	3	4
Slide No.	24476	24476	24476	24475
SiO_2	47.41	46.61	44.94	45.61
TiO_2	.03	ND	ND	.02
Al_2O_3	25.74	26.14	26.44	26.61
FeO	.08	.07	.09	.12
MnO	ND	ND	.01	.03
MgO	.03	.01	.02	.01
CaO	16.84	17.20	18.30	17.00
Na_2O	3.43	3.24	2.79	3.39
K_2O	.70	.64	.47	.62
Total	94.26	93.91	93.06	93.41
Atomic Proportions on basis of 12.0 (Si+Al)				
Si	7.318	7.225	7.086	7.111
Al	4.682	4.775	4.914	4.880
Ti	.004	-	-	.002
Fe	.010	.009	.012	.016
Mn	-	-	.001	.004
Mg	.007	.002	.005	.002
Ca	2.785	2.857	3.092	2.840
Na	1.027	.974	.853	1.025
K	.138	.127	.095	.123
	3.971	3.969	4.058	4.012
% Me	70.7	72.3	76.6	71.4

$$\% \text{ Me} = \frac{(Ca+Mg+Fe+Mn+Ti)}{(Na+K+Ca+Mg+Fe+Mn+Ti)}$$

TABLE 7-1 : Scapolite : Representative Analyses (continued)

	Idocrase Facies		Transitional Idocrase-Garnet Facies B/Hole OT15			Garnet Facies					
Analysis No.	5	6	7	8	9	10	11	12	13	14	15
Slide No.	24472	24472	24646	24646	24646	24637	24637	24626	24626	24630	24630
SiO_2	44.97	45.83	45.75	45.14	45.30	45.52	45.63	46.49	46.78	44.57	45.70
TiO_2	N.D.	N.D.	.03	N.D.	.02	N.D.	N.D.	N.D.	.01	.01	N.D.
Al_2O_3	27.40	27.35	27.81	27.82	28.22	25.65	25.80	26.62	26.02	26.29	25.85
FeO	.10	.10	.04	.15	.12	.19	.15	.10	.07	.12	.18
MnO	N.D.	.01	.06	N.D.	.01	.03	.05	N.D.	.01	.03	.03
MgO	.01	.03	.01	.01	N.D.	.01	N.D.	.01	.02	.01	.02
CaO	18.91	18.68	17.96	17.62	17.79	20.90	19.45	17.30	17.72	20.99	18.76
Na_2O	1.84	1.97	3.11	2.79	2.77	1.60	2.00	3.65	3.61	1.37	1.84
K_2O	.38	.38	.33	.29	.26	.17	.31	.50	.47	.18	.38
Total	93.61	94.35	95.10	93.82	94.49	94.07	93.39	94.67	94.71	93.57	92.76
										Core	Rim
Si	6.984	7.045	6.991	6.951	6.920	7.211	7.201	7.165	7.248	7.079	7.200
Al	5.016	4.955	5.009	5.049	5.080	4.789	4.799	4.835	4.752	4.921	4.800
Ti	-	-	.003	-	.002	-	-	-	.001	.001	-
Fe	.013	.013	.005	.019	.015	.025	.020	.013	.009	.016	.024
Mn	-	.001	.008	-	.001	.004	.007	-	.001	.004	.004
Mg	.002	.007	.002	.002	-	.002	-	.002	.005	.002	.005
Ca	3.147	3.077	2.941	2.907	2.912	3.547	3.289	2.857	2.942	3.572	3.167
Na	.554	.587	.922	.833	.820	.491	.612	1.091	1.085	.422	.562
K	.075	.075	.064	.057	.051	.034	.062	.098	.093	.037	.076
Total	3.791	3.760	3.945	3.818	3.801	4.103	3.990	4.061	4.136	4.054	3.838
%Me	83.33	82.30	74.89	76.56	76.97	87.09	82.98	70.61	71.42	88.63	83.22

TABLE 7-1 : Scapolite : Representative Analyses (continued)

	Transitional Garnet-Pyroxene Facies (Borehole OT14)			Pyroxene Facies	
Analysis No.	16	17	18	19	20
Slide No.	24649	24649	24649	24656	24656
SiO_2	43.71	45.59	46.91	48.46	51.10
TiO_2	.03	.11	.03	.01	.02
Al_2O_3	27.49	26.88	26.73	25.78	27.46
FeO	.08	.17	.19	.08	.02
MnO	.02	.03	.02	N.D.	.03
MgO	N.D.	N.D.	.01	N.D.	N.D.
CaO	18.35	17.60	16.92	13.25	13.47
Na_2O	2.91	3.07	3.45	5.67	5.05
K_2O	.47	.42	.60	.53	.52
Total	93.06	93.87	94.86	93.78	97.67
	Core	Rim		Core	Rim
Si	6.892	7.080	7.179	7.376	7.347
Al	5.108	4.920	4.821	4.624	4.653
Ti	.004	.013	.004	.001	.002
Fe	.011	.022	.024	.010	.002
Mn	.003	.004	.003	-	.004
Mg	-	-	.002	-	-
Ca	3.100	2.929	2.774	2.161	2.075
Na	.890	.924	1.024	1.673	1.408
K	.095	.083	.117	.103	.095
Total	4.103	3.975	3.948	3.948	3.586
%Me	75.90	74.40	70.86	54.88	58.1

TABLE 7-1 : Scapolite : Representative Analyses (continued)

	Scheelite-bearing Hornfels				
Analysis No.	21	22	23	24	25
Slide No.	43312	43312	43312	43312	43312
SiO_2	47.46	45.91	47.57	46.83	47.35
TiO_2	.03	.02	N.D.	N.D.	N.D.
Al_2O_3	22.83	24.20	22.89	23.92	23.98
FeO	.10	.12	.18	.06	.08
MnO	.02	N.D.	.03	.01	.06
MgO	.01	0.02	N.D.	N.D.	.01
CaO	19.14	18.56	19.23	18.48	18.52
Na_2O	2.15	2.28	2.09	2.41	2.34
K_2O	.21	.25	.24	.30	.25
Total	91.95	91.36	92.23	92.01	92.59
	Atomic Proportions on basis of 12.0 (Si + Al)				
Si	7.658	7.402	7.657	7.491	7.515
Al	4.342	4.598	4.343	4.509	4.485
Ti	.004	.002	-	-	-
Fe	.014	.016	.024	.008	.011
Mn	.003	-	.004	.001	.008
Mg	.002	.005	-	-	.002
Ca	3.309	3.206	3.317	3.167	3.149
Na	.673	.713	.652	.747	.720
K	.043	.051	.049	.061	.051
Total	4.048	3.993	4.046	3.984	3.941
%Me	82.3	80.9	82.7	79.7	80.4

TABLE 7-2 : Pyroxene : Representative Analyses

	Idocrase Facies					Transitional Idocrase-Garnet Facies				
Slide No.	24625	24625	24625	24625	24625	24646	24646	24646	24646	24646
SiO_2	48.60	48.92	49.24	48.81	48.70	48.45	48.38	48.46	49.19	48.43
TiO_2	N.D.	N.D.	N.D.	N.D.	N.D.	N.D.	0.06	N.D.	N.D.	N.D.
Al_2O_3	0.32	0.40	0.29	0.37	0.34	0.34	0.68	0.32	0.28	0.40
Cr_2O_3	N.D.	N.D.	N.D.	N.D.	N.D.	0.04	0.05	N.D.	N.D.	0.08
FeO	19.95	19.17	18.43	18.68	20.10	21.16	21.30	21.28	21.45	20.91
MnO	2.09	2.47	2.26	2.32	2.77	3.26	2.96	2.93	2.98	3.25
MgO	4.68	4.72	5.42	5.27	4.27	3.33	3.21	3.31	3.25	3.19
CaO	23.95	23.58	23.93	24.20	24.00	23.52	23.45	23.48	23.44	23.67
Na_2O	0.12	0.07	0.11	0.11	0.08	0.08	0.11	0.07	0.07	0.08
K_2O	N.D.	N.D.	N.D.	N.D.	N.D.	N.D.	N.D.	N.D.	N.D.	N.D.
Total	99.71	99.33	99.68	99.76	100.26	100.18	100.20	99.85	100.66	100.01
	Cation proportions based on 6 oxygens									
Si	1.957	1.969	1.967	1.955	1.957	1.960	1.955	1.965	1.975	1.962
Ti	-	-	-	-	-	-	0.002	-	-	-
Al	0.015	0.019	0.014	0.017	0.016	0.016	0.032	0.015	0.013	0.019
Cr	-	-	-	-	-	0.001	0.002	-	-	0.003
Fe	0.672	0.645	0.616	0.626	0.675	0.716	0.720	0.722	0.720	0.708
Mn	0.071	0.084	0.076	0.079	0.094	0.112	0.101	0.101	0.101	0.112
Mg	0.281	0.283	0.323	0.315	0.256	0.201	0.193	0.200	0.194	0.193
Ca	1.033	1.017	1.024	1.039	1.033	1.020	1.016	1.020	1.009	1.027
Na	0.009	0.005	0.009	0.009	0.006	0.006	0.009	0.006	0.005	0.006
K	-	-	-	-	-	-	-	-	-	-
Sum	4.038	4.022	4.029	4.040	4.037	4.032	4.030	4.029	4.017	4.030

TABLE 7-2 : Pyroxene : Representative Analyses (continued)

	Garnet Facies					Transitional Garnet-Pyroxene Facies				
Slide No.	24637	24637	24660	24660	24632	24649	24649	24649	24649	24649
SiO_2	49.42	48.88	48.58	47.97	47.75	47.06	46.74	47.74	47.40	47.75
TiO_2	N.D.	N.D.	N.D.	N.D.	0.08	N.D.	N.D.	N.D.	N.D.	0.04
Al_2O_3	0.45	0.46	0.40	0.30	0.70	0.28	0.07	0.33	0.30	0.29
Cr_2O_3	N.D.	N.D.	N.D.	N.D.	N.D.	N.D.	N.D.	N.D.	N.D.	N.D.
FeO	21.75	21.98	22.61	22.61	22.03	25.43	25.81	25.28	25.36	25.13
MnO	3.13	3.35	3.17	2.96	2.82	1.79	2.10	1.87	1.81	1.90
MgO	3.07	2.84	2.04	2.14	2.90	1.39	1.28	1.43	1.37	1.54
CaO	22.31	22.31	22.89	23.04	22.77	23.10	23.08	23.17	23.16	23.02
Na_2O	.07	.06	0.05	.05	0.09	0.08	0.04	0.11	0.11	0.11
K_2O	N.D.	N.D.	N.D.	N.D.	N.D.	N.D.	N.D.	N.D.	N.D.	N.D.
Total	100.10	99.88	99.74	99.07	99.14	99.13	99.12	99.93	99.51	99.78
	Cation proportions based on 6 oxygens									
Si	1.989	1.981	1.982	1.973	1.956	1.957	1.952	1.964	1.960	1.965
Ti	-	-	-	-	0.002	-	-	-	-	0.001
Al	0.021	0.022	0.019	0.015	0.034	0.014	0.003	0.016	0.015	0.014
Cr	-	-	-	-	-	-	-	-	-	-
Fe	0.732	0.745	0.771	0.778	0.755	0.884	0.902	0.870	0.877	0.865
Mn	0.107	0.115	0.110	0.103	0.098	0.063	0.074	0.065	0.063	0.066
Mg	0.184	0.172	0.124	0.131	0.177	0.086	0.080	0.088	0.084	0.094
Ca	0.962	0.969	1.001	1.015	0.999	1.029	1.033	1.021	1.026	1.015
Na	0.005	0.005	0.004	0.004	0.007	0.006	0.003	0.009	0.009	0.009
K	-	-	-	-	-	-	-	-	-	-
Sum	4.000	4.009	4.011	4.019	4.028	4.039	4.047	4.033	4.034	4.029

TABLE 7-2 : Pyroxene : Representative Analyses (continued)

	Pyroxene Facies				
Slide No.	24655	24655	24655	24655	24655
SiO_2	47.60	49.61	48.23	48.21	48.34
TiO_2	N.D.	N.D.	N.D.	0.06	N.D.
Al_2O_3	0.29	0.16	0.28	0.26	0.12
Cr_2O_3	N.D.	N.D.	N.D.	N.D.	N.D.
FeO	26.58	24.84	25.83	26.40	25.90
MnO	1.18	1.35	1.18	1.12	1.24
MgO	1.45	1.75	1.86	1.43	1.64
CaO	23.18	22.80	22.75	22.91	22.89
Na_2O	0.09	0.05	0.09	0.11	0.08
K_2O	N.D.	N.D.	N.D.	N.D.	N.D.
Total	100.37	100.56	100.22	100.50	100.21
	Cation proportions based on 6 oxygens				
Si	1.955	2.004	1.971	1.971	1.977
Ti	N.D.	N.D.	N.D.	0.002	N.D.
Al	0.014	0.008	0.013	0.013	0.006
Cr	-	-	-	-	-
Fe	0.913	0.839	0.883	0.903	0.886
Mn	0.041	0.046	0.041	0.039	0.043
Mg	0.089	0.105	0.113	0.087	0.101
Ca	1.020	0.987	0.996	1.003	1.003
Na	0.007	0.004	0.007	0.009	0.006
K	-	-	-	-	-
Sum	4.039	3.993	4.024	4.027	4.022

TABLE 7-2 : Pyroxene : Representative Analyses (continued)

	Scheelite-bearing Hornfels					Calc-silicate				
Slide No.	43323	43323	43312	43312	24478	24479	24479	24481	24481	24481
SiO_2	51.23	51.78	50.50	50.44	50.34	52.64	52.50	51.88	51.78	51.61
TiO_2	.03	.01	.04	.05	.04	.05	.05	.04	.04	.01
Al_2O_3	.41	.22	.41	.46	.58	.45	.42	.37	.54	.41
Cr_2O_3	.05	.02	N.D.	N.D.	N.D.	N.D.	.03	.04	.05	.04
FeO	16.22	15.79	18.38	17.99	17.61	11.11	11.18	11.70	11.82	11.94
MnO	1.06	1.17	2.26	2.20	1.24	.58	.66	.51	.57	.51
MgO	7.95	8.00	5.75	5.82	7.02	11.75	11.62	10.94	11.00	11.13
CaO	22.77	23.16	22.81	22.86	22.95	23.81	23.88	24.08	23.64	23.98
Na_2O	.12	.06	0.07	.09	.14	.16	.13	.12	.14	.14
Total	99.84	100.21	100.22	99.91	99.92	100.55	100.47	99.68	99.58	99.77
	Cation proportions based on 6 oxygens									
Si	1.995	2.005	1.991	1.992	1.977	1.985	1.984	1.983	1.981	1.974
Ti	.001	-	.001	.002	.001	.002	.001	.001	.001	-
Al	.019	.010	.019	.021	.027	.020	.019	.017	.024	.018
Cr	.002	.001	-	-	-	-	0.001	.001	.002	.001
Fe	.528	.511	.606	.594	.578	.350	.353	.374	.378	.382
Mn	.035	.038	.076	.074	.041	.019	.021	.017	.018	.016
Mg	.461	.461	.338	.343	.411	.661	.655	.623	.627	.635
Ca	.950	.961	.964	.967	.966	.962	.967	.986	.969	.983
Na	.009	.004	.006	.007	.011	.012	.010	.009	.011	.011
Sum	4.000	3.991	4.001	4.000	4.012	4.011	4.011	4.011	4.011	4.020

TABLE 7-3 : Idocrase : Representative Analyses

Analysis No.	1	2	3	4	5	6
Slide No.	24476	24476	24472	24472	24625	24625
SiO_2	36.36	35.64	36.09	36.18	36.44	36.57
TiO_2	1.03	.91	1.20	1.15	1.09	1.73
Al_2O_3	16.30	16.83	16.34	15.90	16.58	15.49
Cr_2O_3	N.D.	.01	.04	N.D.	N.D.	.02
FeO	4.51	4.58	4.95	5.23	4.95	5.32
MnO	.63	.58	.66	.65	.68	.67
MgO	1.54	1.58	1.37	1.47	1.17	1.27
CaO	35.67	35.86	35.45	35.53	35.12	35.06
Na_2O	.03	.04	.02	.04	.07	.08
K_2O	N.D.	N.D.	N.D.	N.D.	.01	N.D.
Total	96.07	96.03	96.12	96.15	96.11	96.21

Cation proportions calculated on the basis of 78 oxygens

Anal. No.	1		2		3		4		5		6	
Si	17.957	18.0	17.644	18.0	17.854	18.0	17.926	18.0	17.990	18.0	18.087	
Al	.043		.356		.146		.074		.010			
Al	9.445		9.464		9.381		9.211		9.637		9.029	
Ti	.383		.339		.446		.429		.405		.643	
Cr	-	12.825	.004	12.869	.016	12.901	-	12.893	-	12.947	.008	12.817
Fe	1.863		1.896		2.048		2.167		2.044		2.201	
Mg	1.134		1.166		1.010		1.086		.861		.936	
Mn	.264		.243		.277		.273		.284		.281	
Ca	18.874	19.167	19.021	19.302	18.790	19.086	18.861	19.172	18.576	18.933	18.579	18.937
Na	.029		.038		.019		.038		.067		.077	
K	-		-		-		-		.006		-	
OH	9.883		9.907		9.900		9.915		9.879		9.897	

Cation proportions calculated assuming H_2O contents of 3wt%

TABLE 7-4 : Garnet : Representative Analyses

Analysis No.	1	2	3	4	5	6
Slide No.	24659	24659	24659	24646	24632	24632
SiO_2	37.65	37.87	37.81	38.73	37.40	38.03
TiO_2	.17	N.D.	.08	.12	.05	.14
Al_2O_3	19.56	20.39	19.98	20.23	20.74	20.17
Cr_2O_3	N.D.	N.D.	N.D.	N.D.	N.D.	N.D.
FeO	9.24	12.44	12.08	6.41	13.83	10.70
MnO	4.54	6.64	6.58	3.40	8.38	7.77
MgO	N.D.	.04	.04	.04	.16	.09
CaO	27.89	22.18	23.00	31.11	19.61	23.28
Total	99.05	99.56	99.57	100.04	100.17	100.18
Atomic proportions calculated on the basis of 12 oxygens						
Si	2.979	2.996	2.996	2.998	2.963	2.992
Ti	.010	-	.005	.007	.003	.008
Al	1.824	1.901	1.866	1.846	1.937	1.870
Cr	-	-	-	-	-	-
Fe^{3+}	.176	.099	.134	.154	.063	.130
Fe^{2+}	.436	.724	.667	.261	.853	.574
Mn	.304	.445	.442	.223	.562	.518
Mg	-	.005	.005	.005	.019	.011
Ca	2.365	1.880	1.953	2.580	1.665	1.962
Sum	8.094	8.050	8.068	8.074	8.065	8.065
Mol% of end members (see Shimazaki, 1977)						

TABLE 8 : Rössing Formation: Isotopic Composition of Marble Calcite

	Sample No.	Sample Locality	$\delta^{18}O$	$\delta^{13}C$	Number of Analyses
a)	OTS-00-P103	Surface : line 49 West	+15.4	+0.3	2
	OTS-01-P104	Borehole OT1	+15.2	+0.1	2
	OTS-20-125	Borehole OT20	+15.5	+0.3	3
	OTS-15-58665	Borehole OT15	+15.2	+0.2	2
	OTS-26-0008	Borehole OT26	+15.6	+0.2	3
b)	OTS-00-01	2km east of Line 12 West	+15.2	+0.4	2
	OTS-00-02	375m east of Line 12 West	+16.2	-1.0	1
	OTS-00-03	500m west of Line 49 West	+15.8	0.0	2
	OTS-00-04	800m west of Line 49 West	+15.9	+1.3	2
c)	OTS-00-05	TSM1 marble - Tjirundo Süd (see Map 1)	+15.4	+0.3	2
	OTS-00-06	TSM2 marble - Tjirundo Süd (see Map 1)	+15.2	-0.7	2
		n	11	11	
		$\bar{x}$	15.5	0.1	
		S. Dev.	0.3	0.6	
		Max. Value	16.2	1.3	
		Min. Value	15.2	-0.7	

a) Samples from Otjua prospect

b) Samples from vicinity of Otjua prospect

c) Samples from Okakombo horst

TABLE 9 : Rössing Formation : Isotopic Composition of Skarn Calcite

Sample No.	Locality	Skarn Facies	$\delta^{18}O$	$\delta^{13}C$
OTS-06-58452A	Borehole OT6	Idocrase	15.4	-5.4
OTS-24-24409	Borehole OT24	Idocrase	15.6	-4.4
OTS-24-24472	Borehole OT24	Idocrase	15.3	-4.6
OTS-15-58666-1	Borehole OT15	Idocrase-Garnet (Transitional Facies)	15.3	-5.7
OTS-15-24643	Borehole OT15	Idocrase-Garnet (Transitional Facies)	15.3	-5.4
OTS-22-24253	Borehole OT22	Garnet	15.2	-4.2
OTS-10-94495	Borehole OT10	Garnet	15.2	-5.9
OTS-17-24636	Borehole OT17	Garnet	15.3	-5.1
		n	8	8
		$\bar{x}$	+15.3	-5.1
		S. Dev.	0.1	0.6
		Max. Value	+15.6	-4.2
		Min. Value	+15.2	-5.9

TABLE 10 : Closed System Fractionation : $\delta^{13}C$ values of the residual calcite at various temperatures

Percent Calcite Remaining	230°C(α=1.001)	300°C(α=1.0021)	550°C(α=1.0027)
100	0.1	0.1	0.1
90	0	-0.11	-0.17
80	-0.1	-0.32	-0.44
70	-0.2	-0.53	-0.71
60	-0.3	-0.74	-0.98
50	-0.4	-0.95	-1.25
40	-0.5	-1.16	-1.52
30	-0.6	-1.37	-1.79
20	-0.7	-1.58	-2.06
10	-0.8	-1.79	-2.33
5	-0.85	-1.90	-2.47
1	-0.89	-1.98	-2.57

Fractionation Factors from Bottinga (1968)

TABLE 11 : Open System : Rayleigh Fractionation : $\delta^{13}C$ values of the residual calcite at various temperatures

Percent Calcite Remaining	230°C(α=1.001)	300°C(α=1.0021)	350°C(α=1.0025)	500°C(α=1.0028)
100	0.1	0.1	0.1	0.1
90	-0.01	-0.12	-0.16	-0.20
80	-0.12	-0.37	-0.46	-0.52
70	-0.26	-0.65	-0.79	-0.90
60	-0.41	-0.97	-1.18	-1.33
50	-0.59	-1.35	-1.63	-1.84
40	-0.82	-1.82	-2.19	-2.46
30	-1.10	-2.43	-2.91	-3.27
20	-1.51	-3.27	-3.92	-4.40
10	-2.20	-4.72	-5.64	-6.33
5	-2.89	-6.17	-7.36	-8.25
1	-4.50	-9.53	-11.35	-12.71

Fractionation Factors from Bottinga (1968)

TABLE 12 : Isotopic Composition of Interstitial Calcite from Scheelite-bearing Hornfels

Sample No.	Sample Locality	$\delta^{18}O$	$\delta^{13}C$
OT130	Otjua - Whole Rock Analysis OT130	18.5	-4.9
OT132	Otjua - Whole Rock Analysis OT132	17.6	-2.5
OT133	Otjua - Whole Rock Analysis OT133	16.0	-4.0
OT134	Otjua - Whole Rock Analysis OT134	16.1	-5.8
OT137	Tjirundo Süd - Whole Rock Analysis OT137	17.8	-3.9
OT139	Tjirundo Süd - Whole Rock Analysis OT139	17.2	-3.8
TS27	Tjirundo Süd	16.4	-3.4
TS41	Tjirundo Süd	16.5	-2.7
	n	8	8
	$\bar{x}$	17.0	-3.9
	S. Dev.	0.8	-1.0
	Max. Value	18.5	-2.5
	Min. Value	16.0	-5.8

TABLE 13 : Isotopic Composition of coexisting Graphite and Calcite from the Rössing Formation

Graphite	Sample No.	Sample Locality	$\delta^{13}C$
	TSM1	Tjirundo Süd	-4.0
	TSM2	Tjirundo Süd	-4.8
	OTS-00-03	500m west of Otjua skarn	-4.0
	OTS-00-04	800m west of Otjua skarn	-3.5

Calcite	Sample No.	$\delta^{13}C$	$\delta^{18}O$
	TSM1	+0.3	15.4
	TSM2	-0.7	15.2
	OTS-00-03	0.0	15.8
	OTS-00-04	+1.3	15.9

	Δ(Cc-Gr)	Equilibration Temperature (°C)
TSM1	4.3	586
TSM2	4.1	612
OTS-00-03	4.0	626
OTS-00-04	4.8	519

(Temperatures obtained from : $\Delta^{13}C(Cc\text{-}Gr) = -0.00748T + 8.68$ (T in°C) (from Valley and O'Neil, 1981)

TABLE 14 : $\delta^{18}O$ Values for Quartz and Feldspar from Pegmatite

Sample No.	Sample Locality	Quartz	K-feldspar	Δ(Quartz-K-feldspar)	Temperature (°C)
WRAOT114	See Table 2	16.7	14.8	+1.9	290
WRAOT115	See Table 2	16.4	14.0	+2.4	240
WRAOT116	See Table 2	16.1	14.3	+1.8	300
Average		16.4	14.4	+2.0	280

Crystallisation Temperatures calculated from:

$$1000 \ln\alpha_{\text{Quartz-K-feldspar}} = (0.74)10^6 T^{-2} - 0.43 \quad (T \text{ in kelvin})$$

(from Matsuhisa et al., 1979)

TABLE 15 : Isotopic Composition of Calcite from vuggy Calcite-bearing Pegmatite

Sample No.	Sample Locality	$\delta^{13}C$	$\delta^{18}O$	Temperature °C
OTS-26-37650	Borehole OT26	-6.2	13.1	
OTS-26-38190	Borehole OT26	-5.3	11.9	237
OTS-25-14490	Borehole OT25	-3.0	11.2	
Average		-4.8	12.1	

Temperatures calculated from Quartz-calcite fractionation curve (Friedman and O'Neil, 1977) using average $\delta^{18}O$ value of 16.4 for pegmatite quartz

TABLE 16 : Average Inter-element Ratios for the Skarn Facies

	Idocrase Facies	Garnet Facies	Pyroxene Facies
Ca/Si	1.1087 100%	1.0203 92%	0.5194 46.9%
Ca/Al	3.3085 100%	3.3714 101.9%	1.5351 46.4%
Ca/Fe	3.0378 100%	2.2809 75.1%	1.4108 46.4%
Ca/Si+Al+Fe	0.6521 100%	0.5831 89.4%	0.3044 46.7%
Ca/Mn	40.24 100%	11.06 27.5%	30.31 75.3%
Ca/Mg	14.02 100%	34.29 244.6%	26.46 188.7%
Ca/Mg+Fe+Mn	2.35 100%	1.79 76.2%	1.28 54.5%
Ca/Mn+Mg	10.39 100%	8.36 80.5%	14.13 136%
Ca/Na+K	37.94 100%	37.14 97.9%	4.84 12.8%

TABLE A : 19 Boreholes drilled into Garnet Facies Skarn

Borehole No.	Thickness of Skarn (metres)	Combined Marble/Skarn Thickness (metres)	% Skarnification	$\%WO_3$	$\%CaF_2$
OT1	0.16	2.45	6.5	0.42	1.71
2	2.35	2.64	89	0.40	4.79
3	2.92	2.92	100	0.49	10.77
4	1.07	1.07	100	0.30	22.70
5	2.30	2.30	100	0.43	N/A
9	0.14	2.23	6.3	0	0
10	1.63	2.38	68.5	0.59	N/A
11	1.09	2.58	42.2	0.57	N/A
12	2.01	3.02	66.6	0.50	9.26
13	0.06	1.37	4.4	0	0.1
16	2.86	2.86	100	0.58	10.37
17	1.14	1.97	57.9	0.73	6.75
18	0.97	0.97	100	0.48	3.51
19	0.71	0.71	100	0.45	7.61
20	0.31	1.99	15.6	0.22	3.70
21	0.11	1.96	5.6	0.27	8.00
22	0.2	1.36	14.7	0	0
23	0.74	1.88	39.4	0.36	5.36
26	0.14	1.37	10.2	0.52	10.30

Fig.22 Correlation coefficient between Degree of Skarnification (assuming Constant Volume Replacement) and WO_3 content of Skarn = +0.54

Fig.22 Correlation coefficient between Degree of Skarnification (assuming Constant Volume Replacement) and CaF_2 content of Skarn = +0.56

Fig.21 Correlation coefficient between Thickness of Skarn and WO_3 Content of Skarn = +0.55

Fig.21 Correlation coefficient between Thickness of Skarn and CaF_2 Content of Skarn = +0.41

Fig.23 Correlation coefficient between Combined Marble and Skarn Thickness and Degree of Skarnification = +0.07

Correlation coefficient between Combined Marble and Skarn Thickness and WO_3 content of skarn = +0.31

Correlation coefficient between Combined Marble and Skarn Thickness and CaF_2 content of skarn = -0.03

Fig.20 Correlation coefficient between CaF_2 and WO_3 contents of Skarn = +0.44

N/A = Not Available

TABLE A (continued)

Boreholes drilled into Idocrase Facies Skarn

Borehole No.	Thickness of Skarn (metres)	Combined Marble/Skarn Thickness (metres)	% Skarnification	$\%WO_3$	$\%CaF_2$
OT6	0.61	3.09	19.7	0	
OT24	1.49	2.91	51.2	0.19	
OT25	0.57	3.11	18.3	0	
Borehole drilled into Transitional Idocrase-Garnet Skarn					
OT15	1.17	2.46	47.5	0.90	
Borehole drilled into Transitional Garnet-Pyroxene Skarn					
OT14	1.27	1.27	100	0.02	

PHOTOGRAPHS

Photo 1 : View of the Otjua prospect from the OM6 survey beacon (sample site OT112) : prominent outcrops are pegmatite. Note Otjua granite in foreground

Photo 2 : Two examples of scheelite-bearing hornfels enclosed by biotite schist : note amphibole reaction skarn on contact between hornfels and schist in sample No. 24191. Sample No. 24191 is whole rock analysis OT132. Sample No. 24192 is whole rock analysis OT133 (see Table 2)

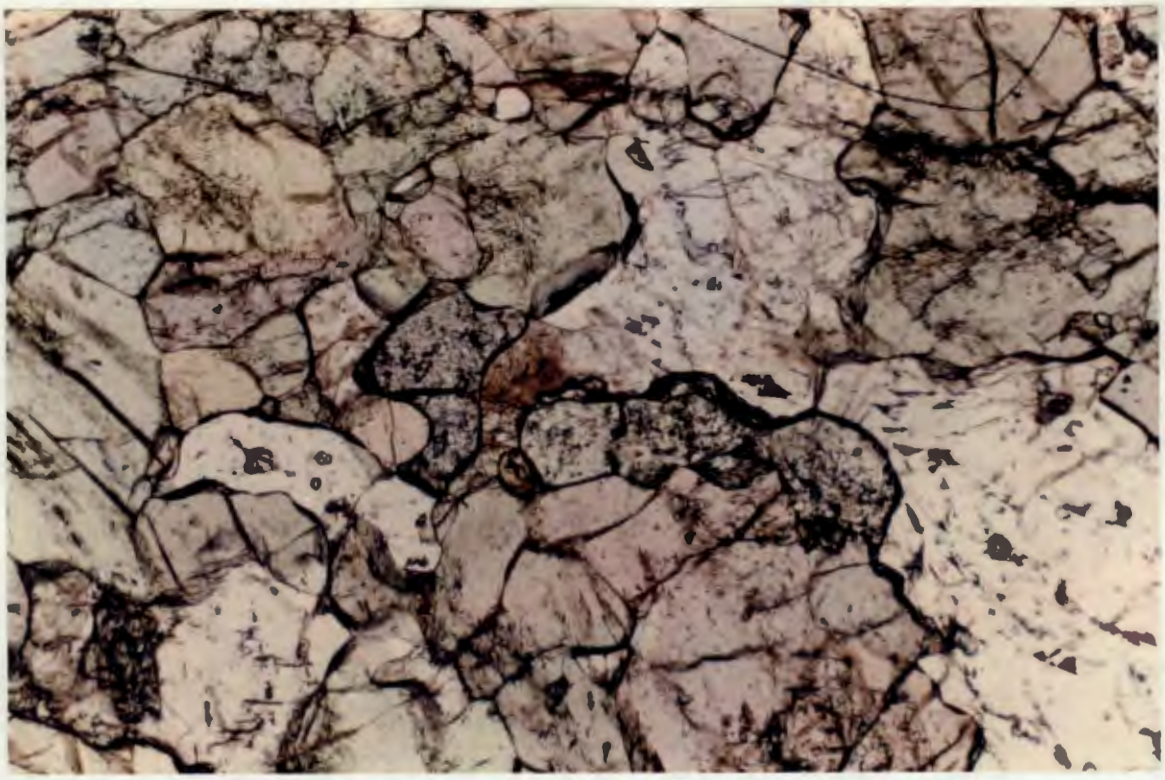

Photo 3 : Scheelite-bearing hornfels (photomicrograph, plane polarized light, slide No. OT133) : note high relief of scheelite in centre of picture, sphene crystal between the two scheelite crystals; pyroxene and scapolite and minor quartz comprise remainder of slide; triple point junctions. Field of view is 2.5mm

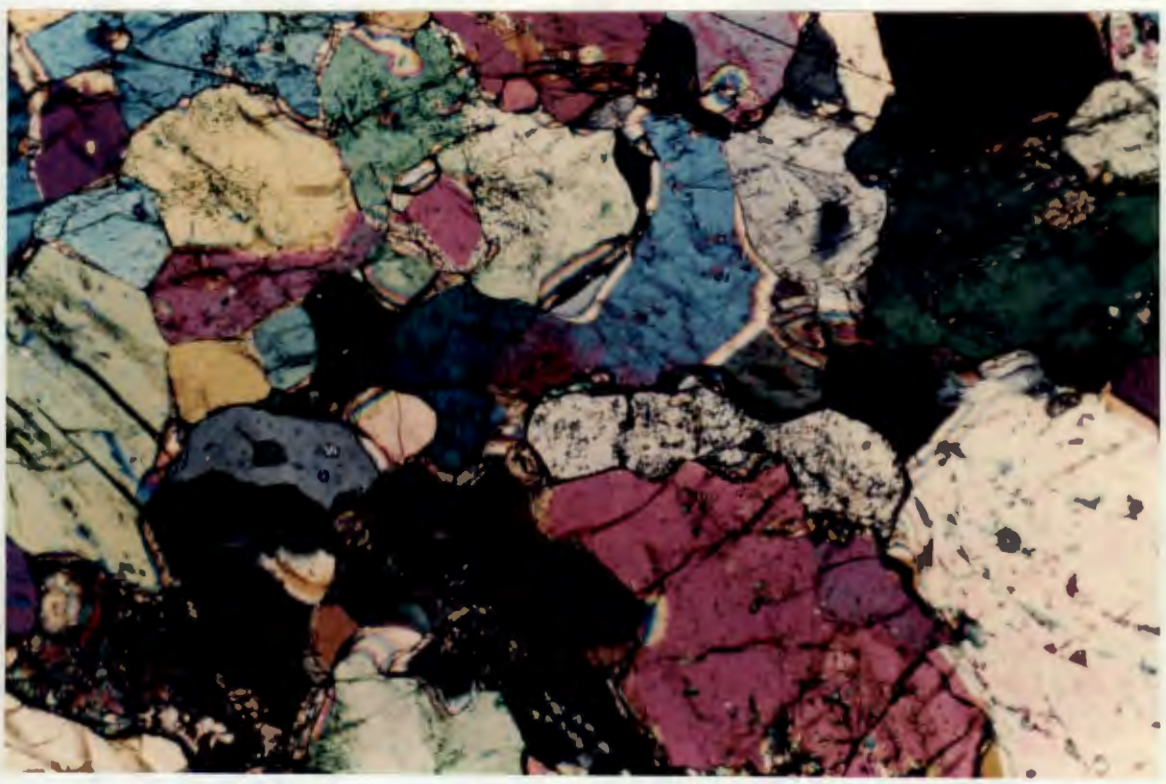

Photo 4 : Scheelite-bearing hornfels (photomicrograph, crossed polars slide No. OT133, same view as photo 3): note highly birefringent scapolite and second order colours of scheelite, dark grey mineral is quartz. Field of view is 2.5mm

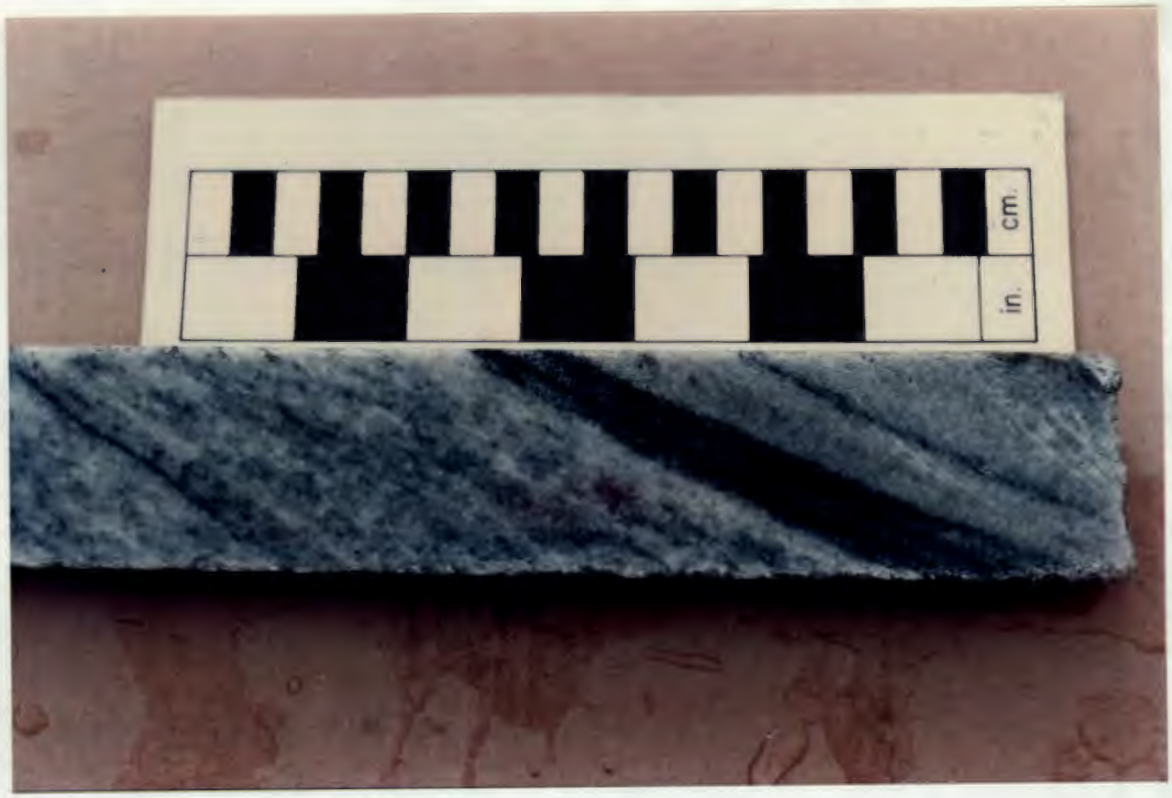

Photo 5 : Rössing Formation marble (borehole OT26) : note graphite-rich bands

Photo 6 : Rössing Formation marble (photomicrograph, crossed polars, slide No. P103) : note triple junctions; light grey crystal is a plagioclase feldspar. Field of view is 2.5mm

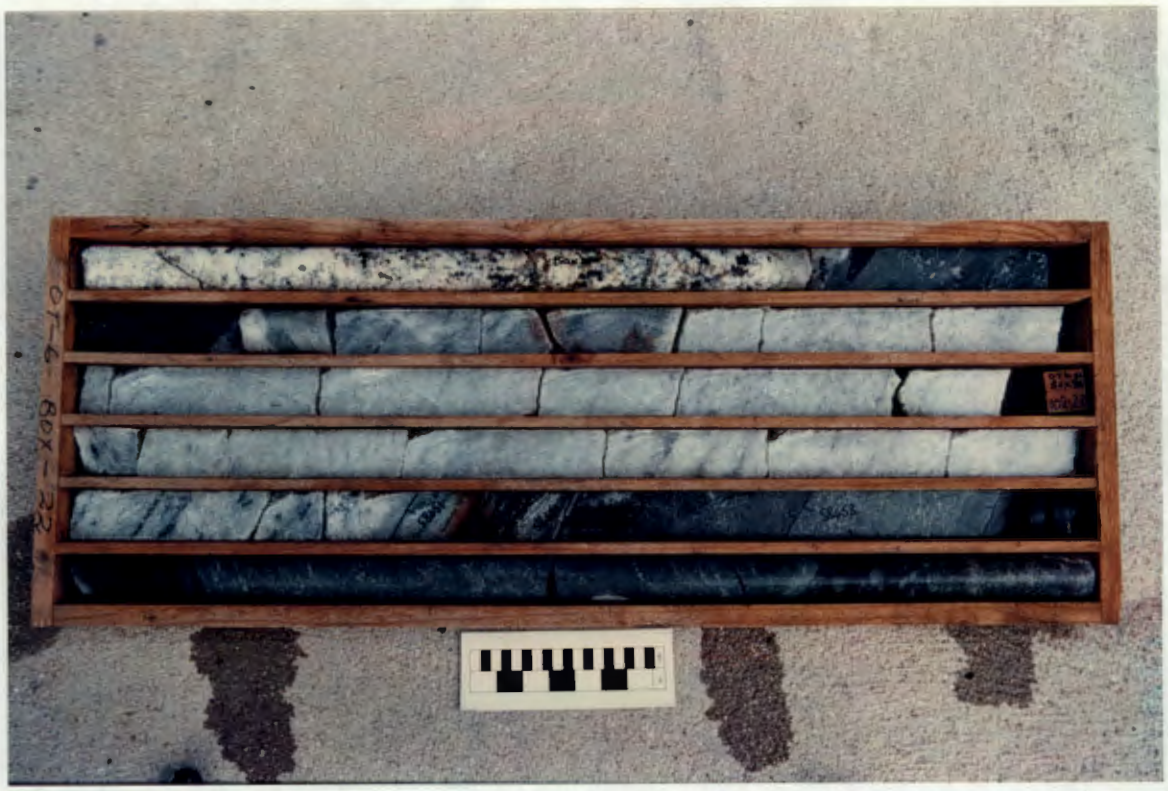

Photo 7 : OT6 borehole intersection : partial replacement of Rössing Formation marble by idocrase facies skarn. Note development of skarn on (structural) footwall of marble only

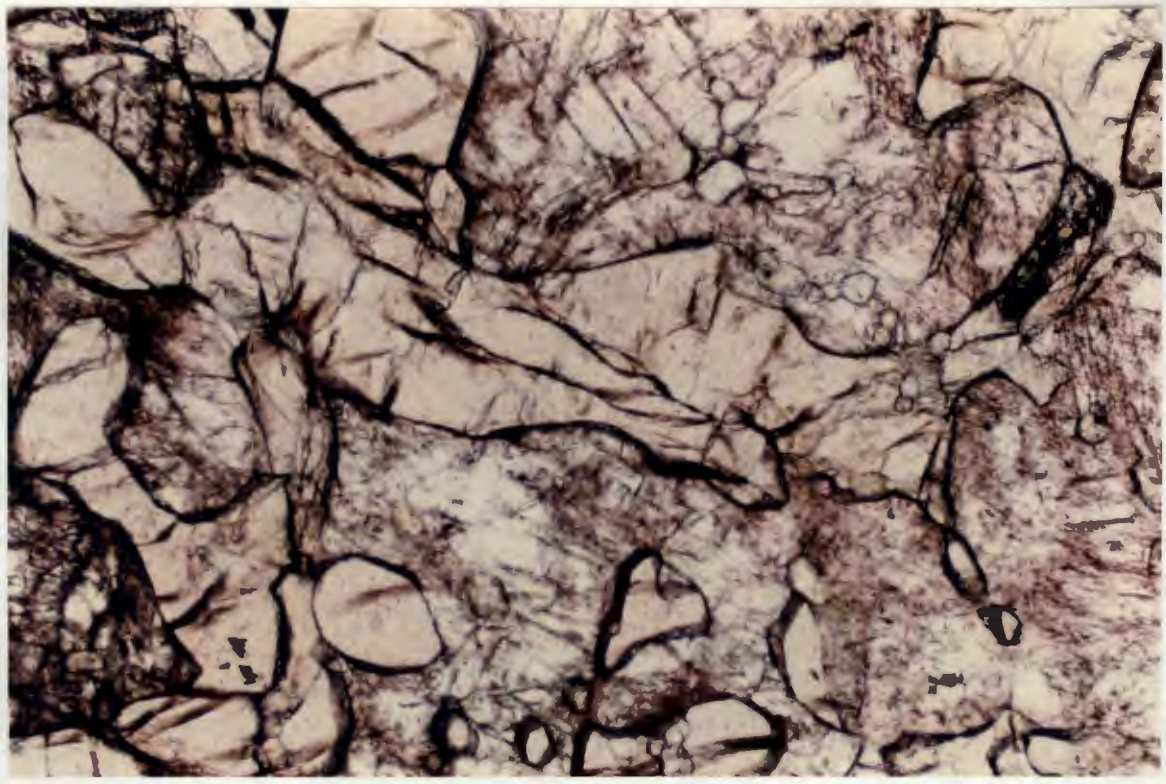

Photo 8 : Idocrase facies skarn (photomicrograph, plane polarized light, slide No. 24472) : idocrase basal (high relief) overgrowing scapolite (pale pink). Top idocrase crystal is a basal section, note prominent cleavages (yellow interference colours in photo 9). Field of view is 2.5mm

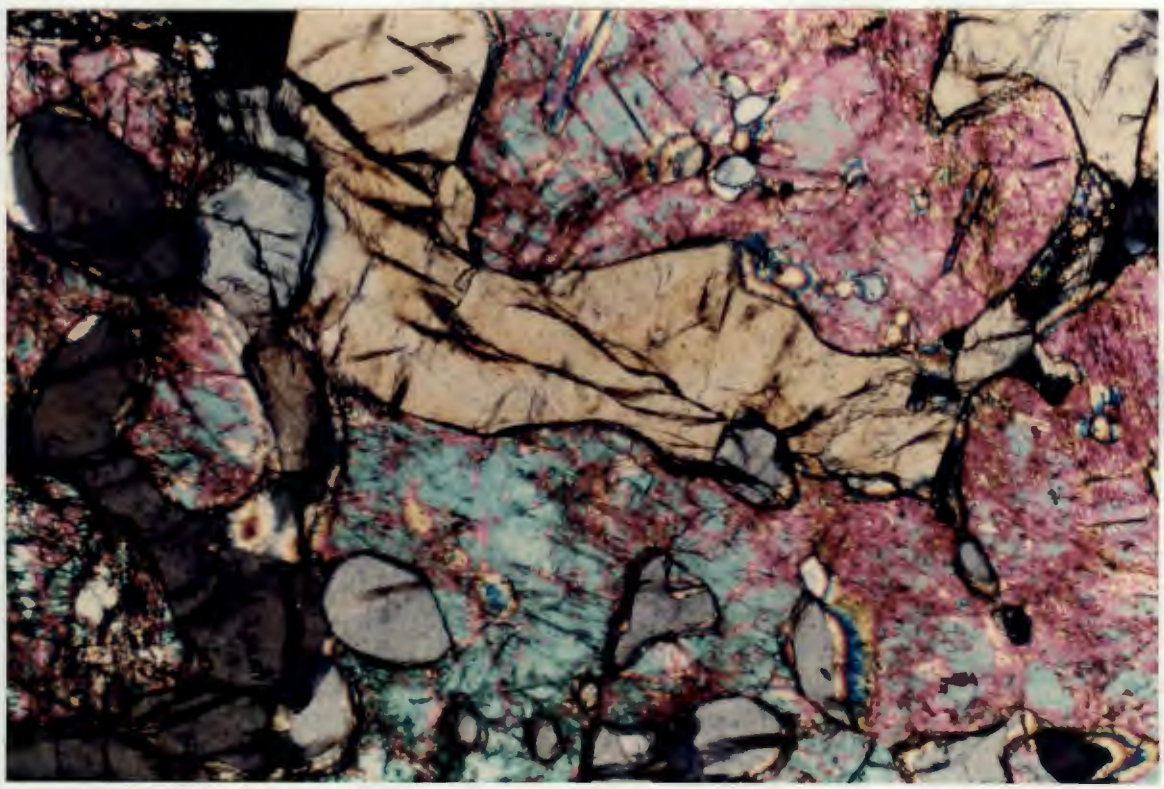

Photo 9 : Idocrase facies skarn (photomicrograph, crossed polars, slide No. 24472, same view as photo 8). Note first order colours of idocrase and highly birefringent scapolite. Field of view is 2.5mm

Photo 10 : OT17 borehole intersection : partial replacement of Rössing Formation marble by garnet facies skarn (see Fig. 63 for details of mineralogy). Note development of skarn on (structural) footwall side of marble and garnet-rich core zone.

Photo 11 : OT16 borehole intersection : complete replacement of the Rössing Formation marble by garnet facies skarn

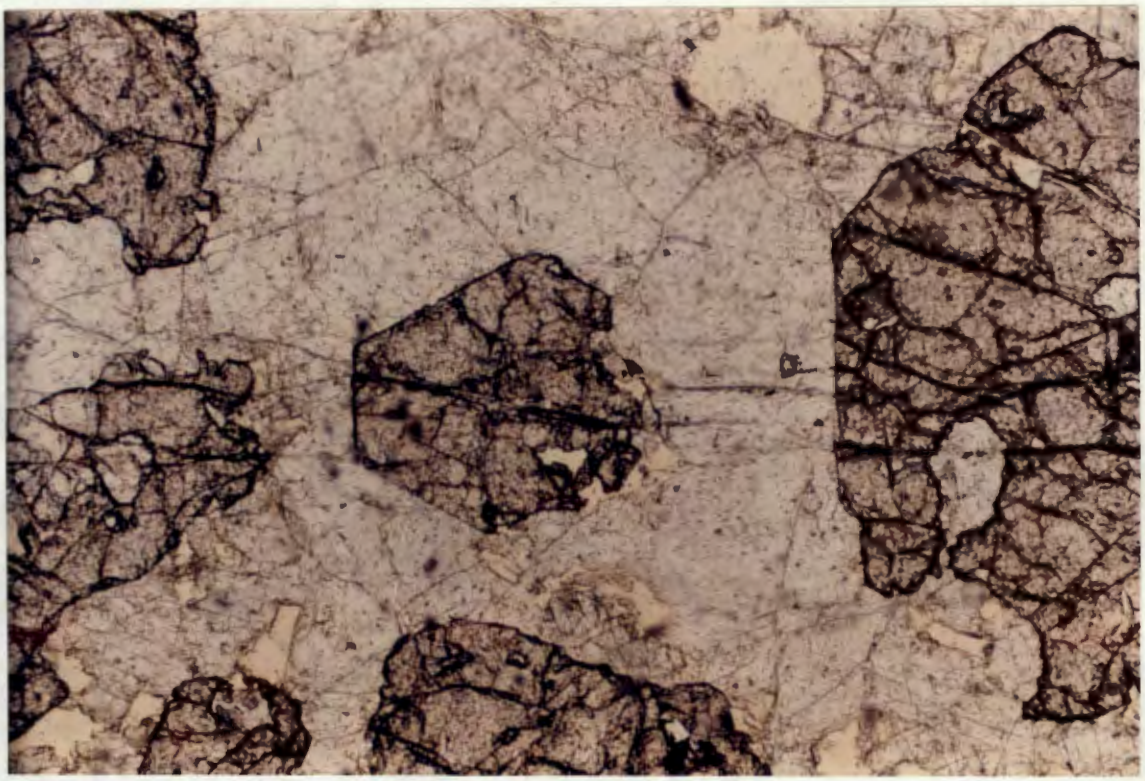

Photo 12 : Garnet facies skarn (photomicrograph, plane polarized light, slide No. 38995) : sub-idioblastic garnet in fluorite. Field of view is 2.5mm

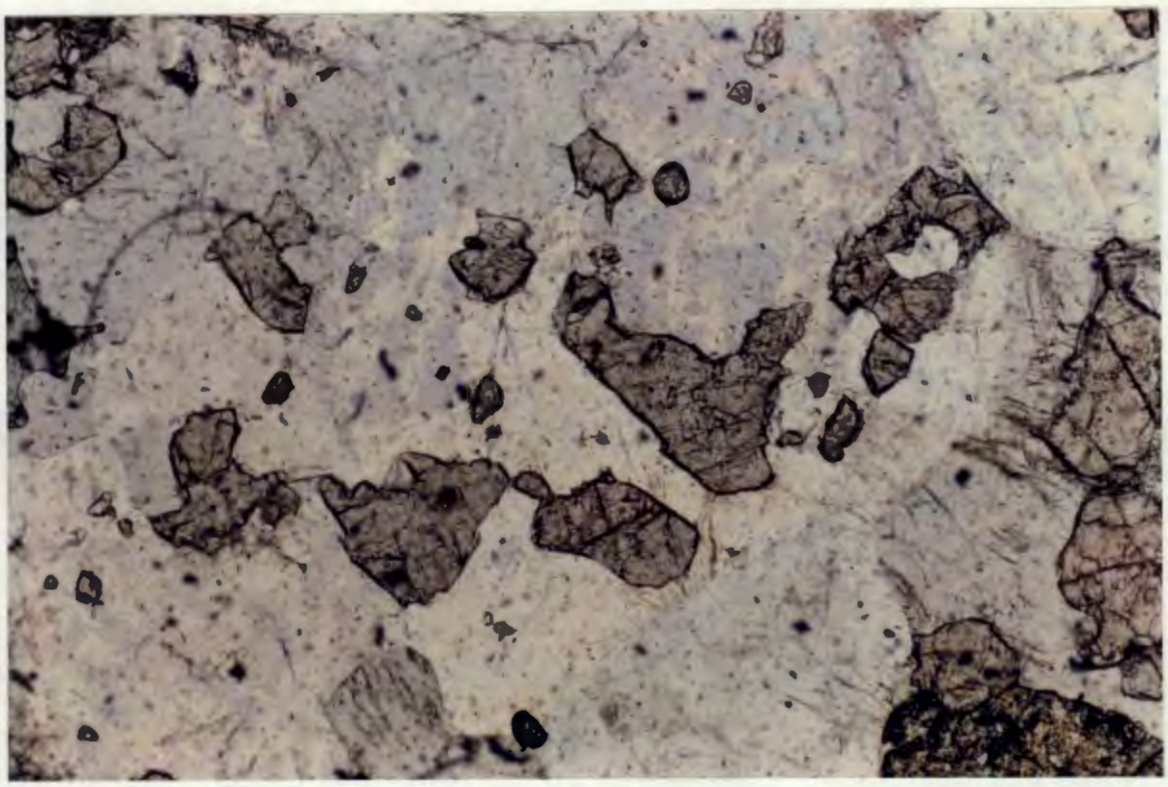

Photo 13 : Garnet facies skarn (photomicrograph, plane polarized light, slide No. 38988) : xenoblastic garnet and scapolite. Note edge of scheelite crystal at bottom right corner. Field of view is 2.5mm

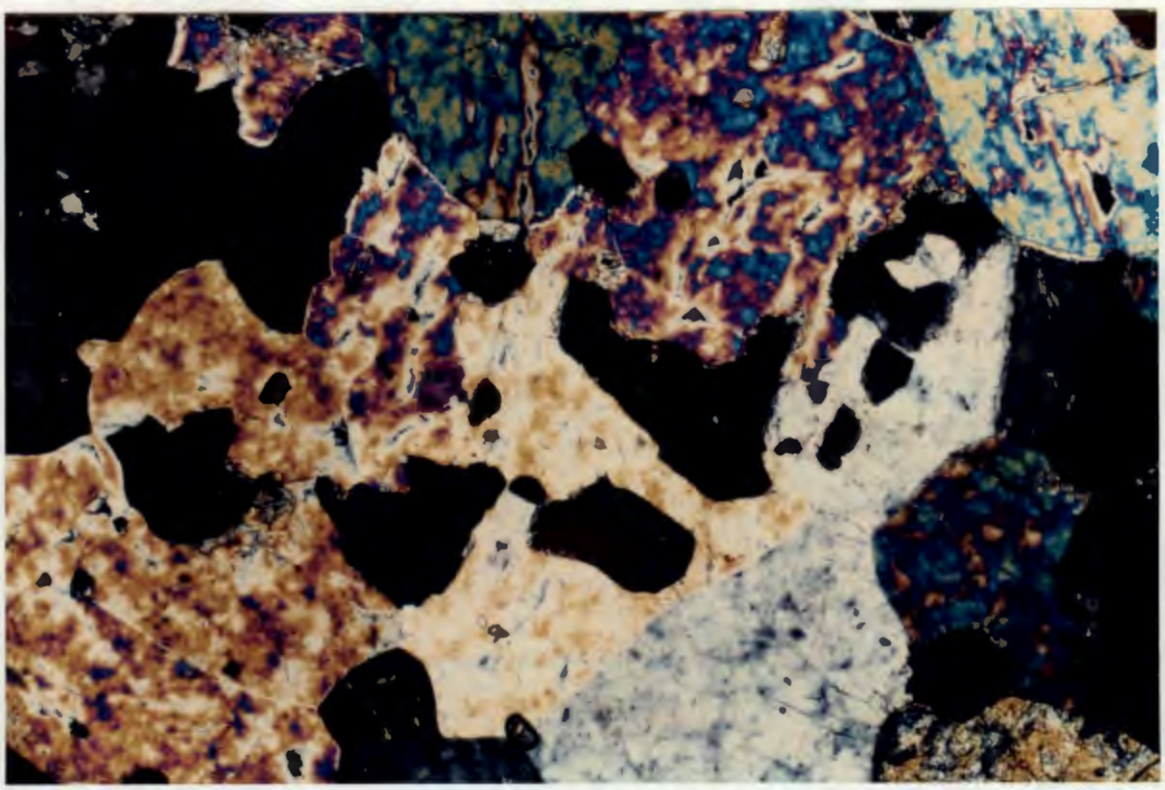

Photo 14 : Garnet facies skarn (photomicrograph, crossed polars, slide No. 38988, same view as photo 13) : note highly birefringent scapolite, first order colours of scheelite. Field of view is 2.5mm

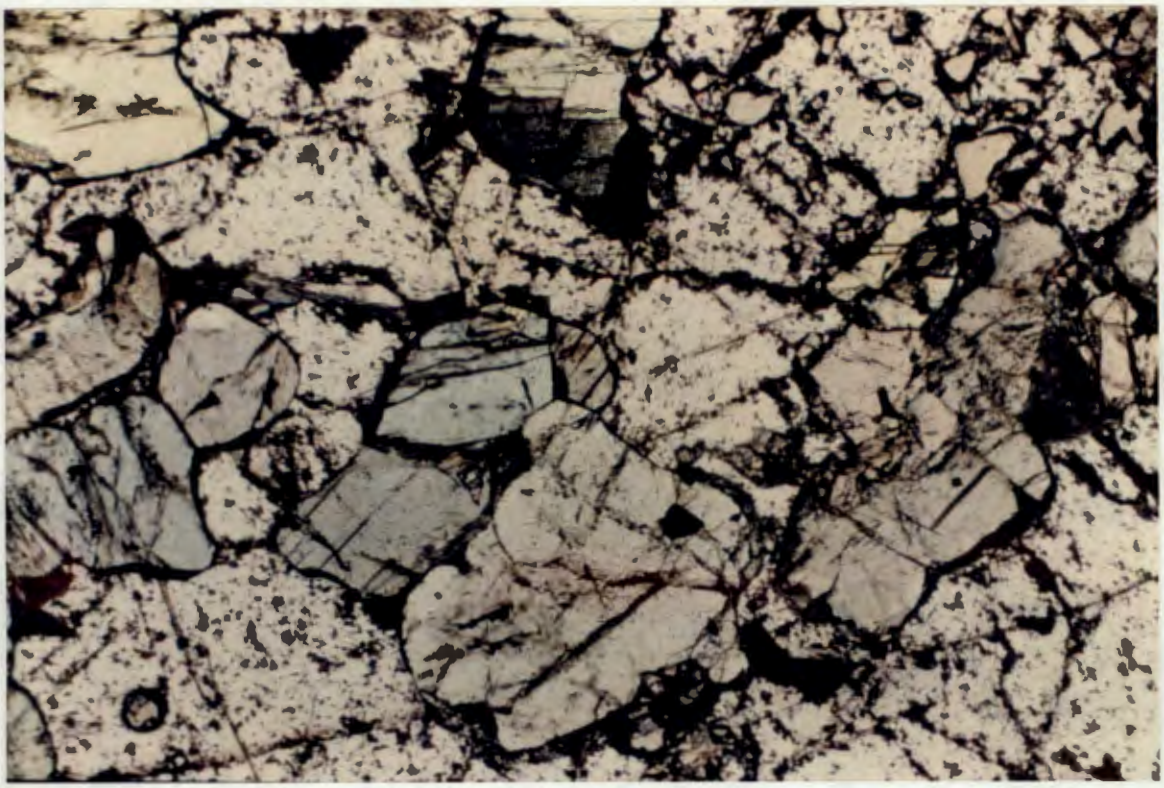

Photo 15 : Garnet facies skarn (photomicrograph, plane polarized light, slide No. 24632) : pyroxene crystals in a groundmass of fluorite

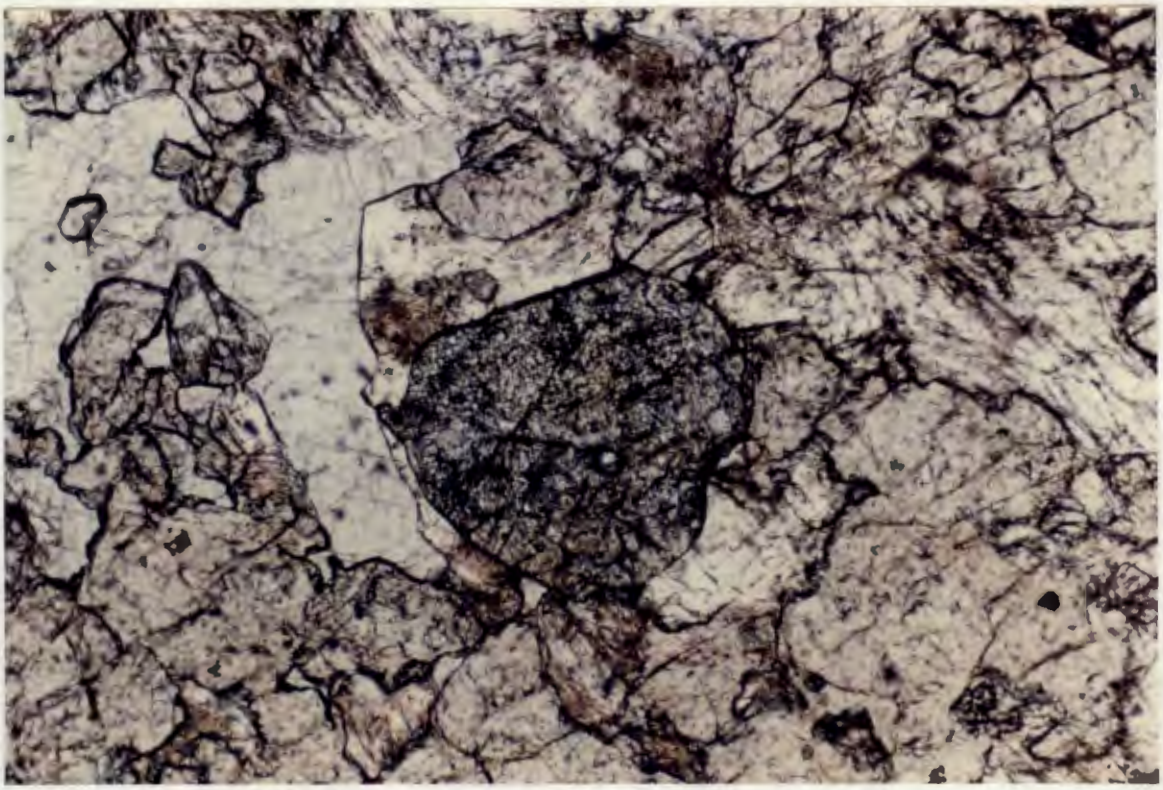

Photo 16 : Garnet facies skarn (photomicrograph, plane polarized light, slide No. 38988) : scheelite crystal (centre, high relief) surrounded by scapolite (low relief) and xenoblastic garnet. Note anhedral fluorite (light grey, low relief, prominent cleavage, top left). Field of view is 2.5mm

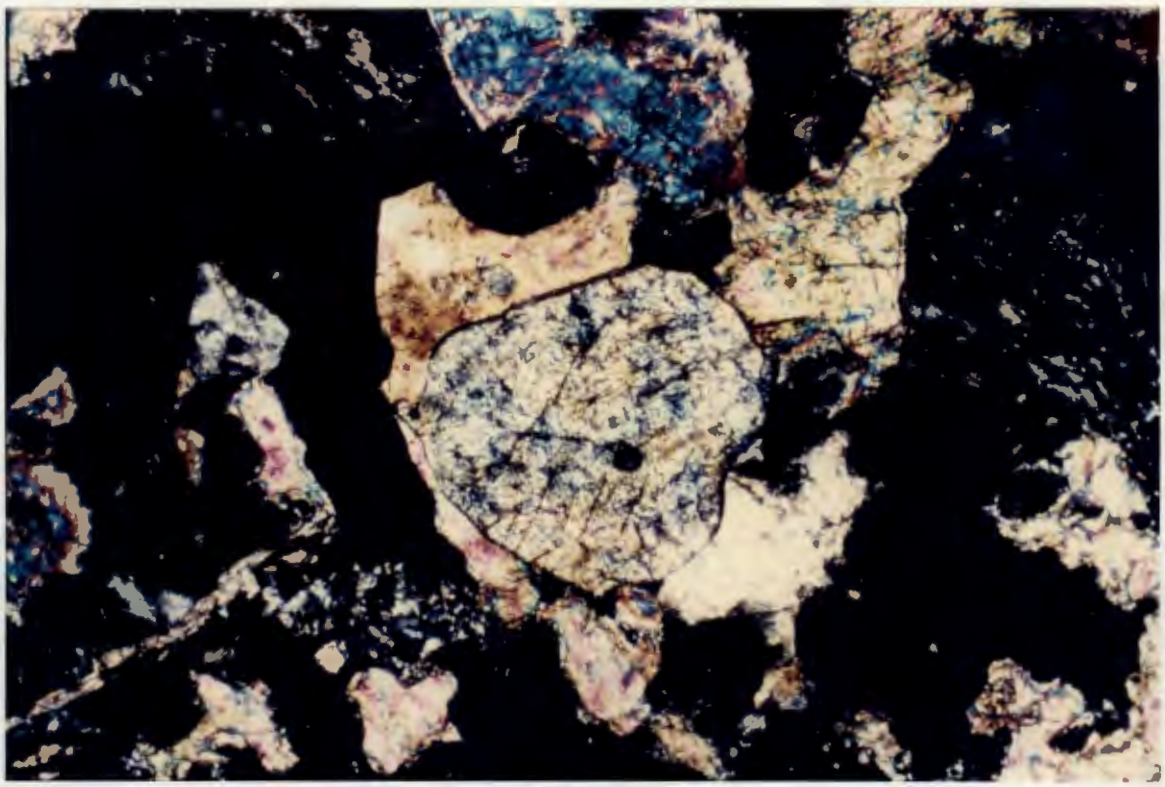

Photo 17 : Garnet facies skarn (photomicrograph, crossed polars, slide No. 38988, same view as photo 16) : note high birefringence of scapolite. Field of view is 2.5mm

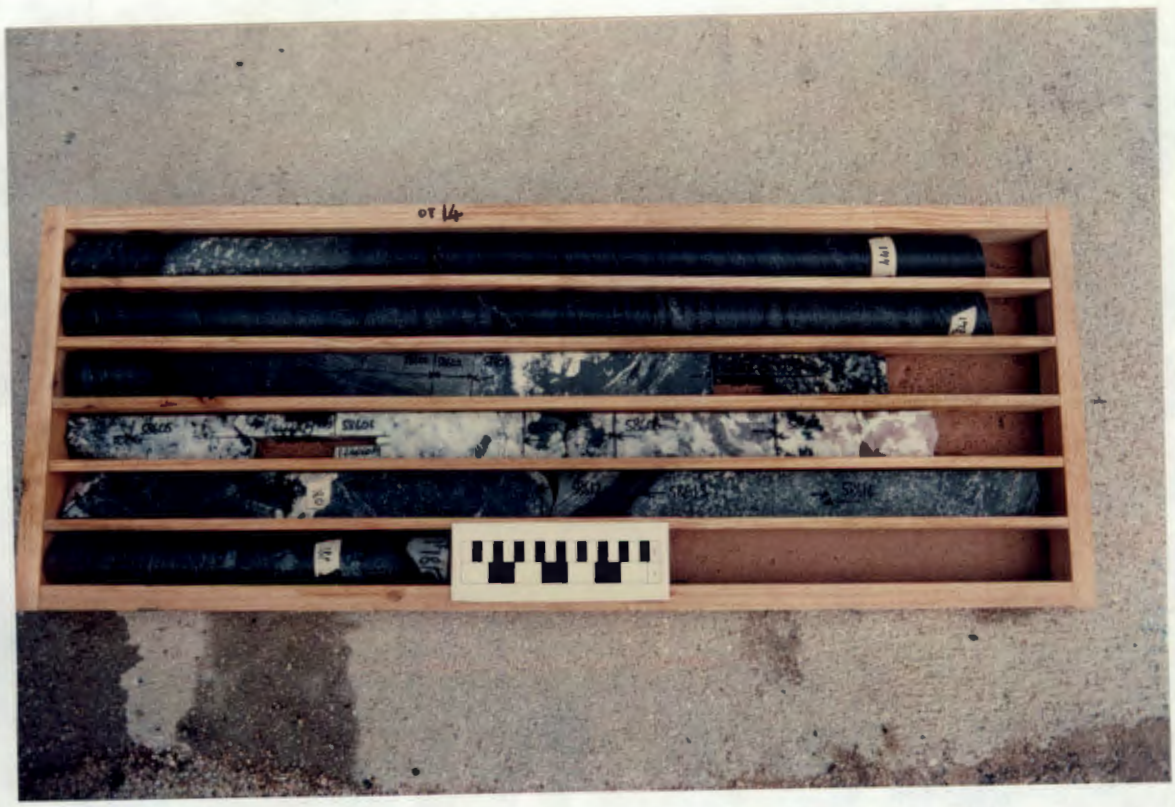

Photo 18 : OT14 borehole intersection : transitional garnet-pyroxene facies skarn. Note complete replacement of Rössing Formation marble. The pink mineral is fluorite

Photo 19 : Otjua granite (sample locality OT112). Quartz-tourmaline nest

Photo 20 : Otjua granite (photomicrograph, crossed polars, slide No. T200) : myrmekite texture developed on edge of plagioclase feldspar (in extinction) where in contact with microcline feldspar. Field of view is 2.5mm

Photo 21 : Fine-grained granite (photomicrograph, crossed polars, slide No. T204) : randomly oriented needle-shaped crystals in quartz. Field of view is 1mm

Photo 22 : Tourmaline pegmatite-biotite schist contact : note how contact is parallel to the schistosity of the schist and absence of baking of the schist

Photo 23 : Pegmatite : prominent banding and shorl-rich zones

Photo 24 : Pegmatite : micrographic texture

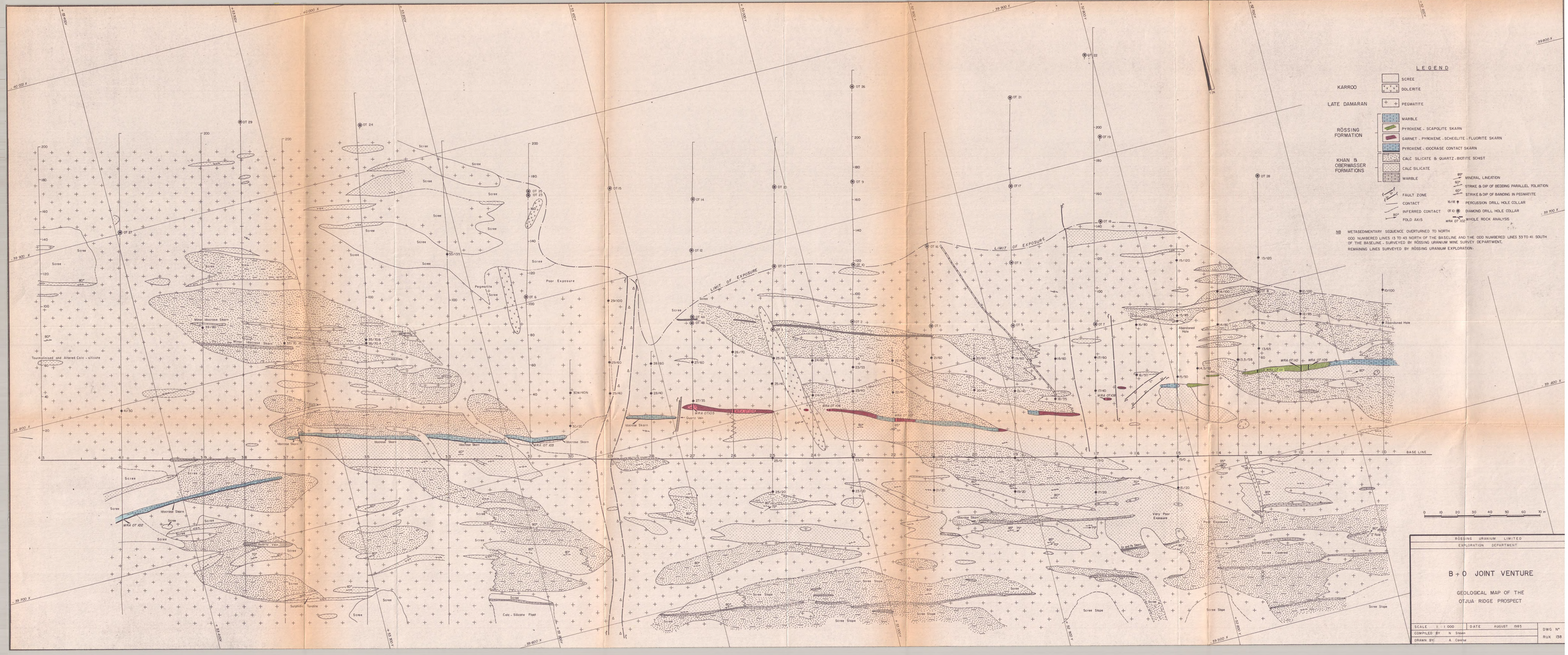
LEGEND
KARROO
SCREE
DOLERITE
LATE DAMARAN
PEGMATITE
RÖSSING FORMATION
MARBLE
PYROXENE - SCAPOLITE SKARN
GARNET - PYROXENE - SCHEELITE - FLUORITE SKARN
PYROXENE - IDOCRASE CONTACT SKARN
KHAN & OBERWASSER FORMATIONS
CALC SILICATE & QUARTZ - BIOTITE SCHIST
CALC SILICATE
MARBLE
MINERAL LINEATION
STRIKE & DIP OF BEDDING PARALLEL FOLIATION
STRIKE & DIP OF BANDING IN PEGMATITE
FAULT ZONE
CONTACT
INFERRED CONTACT
FOLD AXIS
PERCUSSION DRILL HOLE COLLAR
DIAMOND DRILL HOLE COLLAR
WHOLE ROCK ANALYSIS
NB METASEDIMENTARY SEQUENCE OVERTURNED TO NORTH
ODD NUMBERED LINES 13 TO 43 NORTH OF THE BASELINE AND THE ODD NUMBERED LINES 33 TO 41 SOUTH OF THE BASELINE - SURVEYED BY RÖSSING URANIUM MINE SURVEY DEPARTMENT.
REMAINING LINES SURVEYED BY RÖSSING URANIUM EXPLORATION.
LIMIT OF EXPOSURE
BASE LINE
Idocrase Skarn
Tourmalinised and Altered Calc - silicate
Scree
Pegmatite
Poor Exposure
Very Poor Exposure
Abandoned Hole
Quartz Vein
Scree Slope
Scree Covered
Calc - Silicate Float
Surphitic Tonalite
WRA 07103
WRA 07102
WRA 07106
WRA 07109
WRA 07110
WRA 07111
WRA 07112
WRA 07113
WRA 07114
WRA 07115
WRA 07116
WRA 07117
WRA 07118
WRA 07119
WRA 07120
WRA 07121
WRA 07122
WRA 07123
WRA 07124
WRA 07125
WRA 07126
WRA 07127
WRA 07128
WRA

DAMARALAND

T N.

EAUSIRO NORD 108

EAUSIRO WEST 109

OTJUMUE NORD 108

OTJUMUE 109

OTJUMUE SÜD 110

OTJUMUE OST 111

MOLKENHOF 102

ETENDERO 85

ETENDERO 103

OHERE OOS 152

OHERE 104

EHUIRO 120

OKAKONGO 93

OKONGUA 94

SCHÖNFELD 92

KLEIN OTUWAPA 36

OTJUA 37

OTJUA GRANITE

RADIOMETRICALLY ANOMALOUS

TJIRUNDO 91

TJIRUNDO

SCHÖNFELD

EPAKO 38

RÖDINA 4

RÖDINA

OKARUMUTI 147

KOMPANENO 154

CLAIM 1972 BROCKMAN

RADIOMETRICALLY ANOMALOUS LATE GRANITE

GROSS OKANDJOU 187

TJIRUNDO SÜD 149

OKAKOMBO HORST

EPAKO SÜD 39

KASSANDARA 40

OKORONYAMA 41

KOMPANENO SÜD 59

KAKOMBO 90

LINDHOLM 63

OKARUNDU NORD 121

RADIOMETRICALLY ANOMALOUS LATE GRANITE

NEU OKANDJOU 181

PLAAS 188

PROBABLY KUISEB SCHIST OR EARLY PRE D'SALEM GRANITE

OMARURU TOWN AND TOWNLANDS

GAME RESERVE (NO ACCESS)

AIRFIELD (NO ACCESS)

OMARURU

OVIMBARRA 127

OTJOMPAUE 125

TRIANGLE 126

OTJOMPAUE WEST 134

THIS AREA PROBABLY CONTAINS NUMEROUS W-BEARING PEGMATITES: B+O ANOMALY

OMARURU RIVER

EAUSIRO RIVER

KUISEB RIVER

KHAN RIVER

FELDIC DYKE

F3

Rb-Sr age 478 +/- 4 Ma; $(^{87}Sr/^{86}Sr)_I$ = 0·7196; $\delta^{18}O$ = 15·1

Haack et al (1983)

STRIKE AND DIP OF FOLIATION
STRIKE AND VERTICAL DIP OF FOLIATION
STRIKE AND DIP OF BEDDING
FELDSPAR ORIENTATION
LINEATION
FOLD AXIS
ANTICLINE
SYNCLINE
FAULT (BLOCK ON DOWNTHROWN SIDE)
SKARN
T3 A4 TUNGSTEN OCCURRENCE
* OT129 WHOLE ROCK SAMPLE SITE

0 1 2 3 4 5 6 7 8 9 10 km

LEGEND

SEDIMENTS

GROUP	SUB GROUP	FORMATION	MEMBER
SWAKOP	KHOMAS	KUISEB	
		KARIBIB	ARISES
			OT.JONGEAMA HARMONIE
		OBERWASSER	
		RÖSSING	
		KHAN	

ALLUVIUM

PREDOMINANTLY WEST OF OMARURU FAULT ZONE: Quartzites and pelitic schist locally garnetiferous with minor calc silicate tourmalinite (*,+) and siliceous skarn / exhalite? (cc?) greywackes and chemical sediments.

EAST OF OMARURU FAULT ZONE 1. Nodular very mafic cordierite (?) schist 2. Aluminous schist (local sillimanite)

COARSE GRAINED GRAPHITE AND CALCITE PURE CALCITIC MARBLE WITH MINOR CALC-SILICATE

MARBLE AND CALC-SILICATE

QUARTZ BIOTITE SCHIST AND MINOR CALC-SILICATE (LATTER BEST DEVELOPED TOWARDS BASE OF FORMATION)

PURE CALCITIC MARBLE (<20m THICK)

QUARTZ BIOTITE SCHIST AND MINOR CALC-SILICATES LATTER BEST DEVELOPED TOWARDS TOP OF FORMATION

INTRUSIVES

POST KARROO: RING DYKE AND QUARTZ - FELDSPAR PORPHYRIES

KARROO: DOLERITE

DAMARAN:

- (COARSE GRAINED TOURMALINE, GARNET, BIOTITE, TRACE MUSCOVITE PEGMATITE — STRATIGRAPHIC LEVEL INTO WHICH GRANITE NORMALLY INTRUDES
- NON-PORPHYRITIC NON-FOLIATED GRANITE OR LEUCOGRANITE, QUARTZ-TOURMALINE NESTS: — KARIBIB MARBLE AND BELOW
- SALEM-TYPE PORPHYRITIC K-FELDSPAR BIOTITE XENOLITHS FELDSPAR ALIGNMENT PROBABLY OF IGNEOUS ORIGIN, LATEST PHASE IS RADIOMETRICALLY ANOMALOUS AND HAS MINOR TOURMALINE COMPOSITION GRANITE-GRANODIORITE-GRANITE — KUISEB WEST OF OMARURU FAULT ZONE
- WHITE COARSE GRAINED LEUCOPEGMATITE (+/-) MAFICS <5% OR MEDIUM GRAINED LEUCOGRANITE (+/-) NON PORPHYRITIC, MAYBE FOLIATED — KUISEB
- GARNETIFEROUS NON PORPHYRITIC LOCALLY FOLIATED LEUCOGRANITE (MEDIUM GRAINED MAFICS <5%) — KUISEB
- SALEM-TYPE FOLIATED PORPHYRITE-PORPHYROBLASTIC K-FELDSPAR — KUISEB

OMARURU GEOCHRONOLOGY (EX-GEOLOGICAL SURVEY, WINDHOEK)

AGE (Ma)	ACID INTRUSIVES AND DEFORMATION PHASES	SYMBOL
480	1) SYN D3-POST TECTONIC SALEM GRANITE 2) D3 DEFORMATION	+ + + + + + + + + + + +
510	D3 DEFORMATION	
520	LEUCOGRANITES	+ + + + + + + + + + + +
550	PRE- AND SYN D3 TECTONIC SALEM SUITE	+ + + + + + + + + + + +
570	D2 DEFORMATION	

RÖSSING URANIUM LIMITED
EXPLORATION DEPARTMENT

B+O JOINT VENTURE
WESTERN PERIPHERAL AREA
RECONNAISSANCE MAP
GEOLOGY

SCALE 1:100000 | DATE MAY 1985 | DWG N° RUX 437

GEOLOGY BY N. STEVEN and I. L. KUYPER

DRAWN BY D. C. PRETORIUS

WEST

EAST

1500m A.M.S.L

41 39 37 35 33 31 30 29 28 27 26 25 24 23 22 21 20 19 18 17 16 15 14 13 12

43/30 39/80 37/70 35/75 29/100 33/135 29/40 28/40 29/60 28/60 27/35 27/60 26/70 25/40 25/60 24/40 24/60 23/40 23/60 22/40 22/60 21/60 20/40 20/60 19/40 19/60 18/35 18/60 17/40 17/60 16/50 15/50 15/85 15/120 13/65 13/120 12/85 12/100

OT 6 OT 23 OT 15 OT 24 OT 25 OT 27 OT 14 OT 17 OT 13 OT 20 OT 3 OT 2 OT 1 OT 16 OT 10 OT 9 OT 26 OT 21 OT 22 OT 5 OT 11 OT 17 OT 18 OT 19 OT 7 OT 8 OT 29

1400m
1300m
1200m
1100m

0 10 20 30 40 50 60 70 80m

MARBLE
IDOCRASE FACIES
GARNET FACIES
PYROXENE FACIES

ROSSING URANIUM LIMITED
EXPLORATION DEPARTMENT

B+O OMARURU JOINT VENTURE

OTJUA RIDGE PROSPECT

VERTICAL LONGITUDINAL PROJECTION

SCALE 1:1000 | DATE JUNE 1984 | DWG N°
COMPILED BY N. STEVEN | RUX 148
DRAWN BY D. C. PRETORIUS

PLAN

SECTION LINE 21

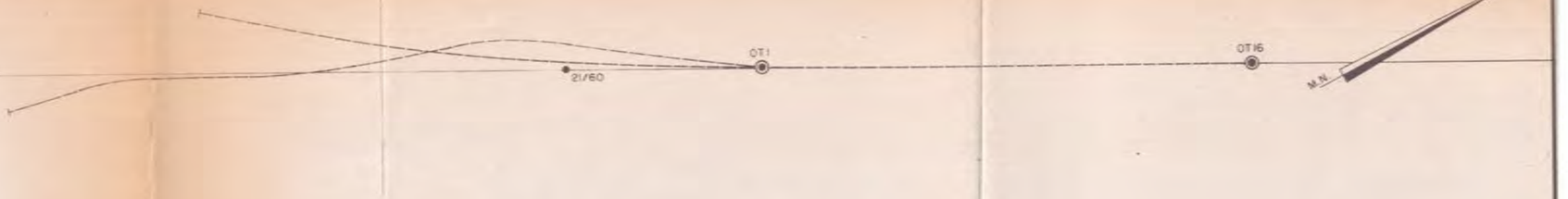

SECTION

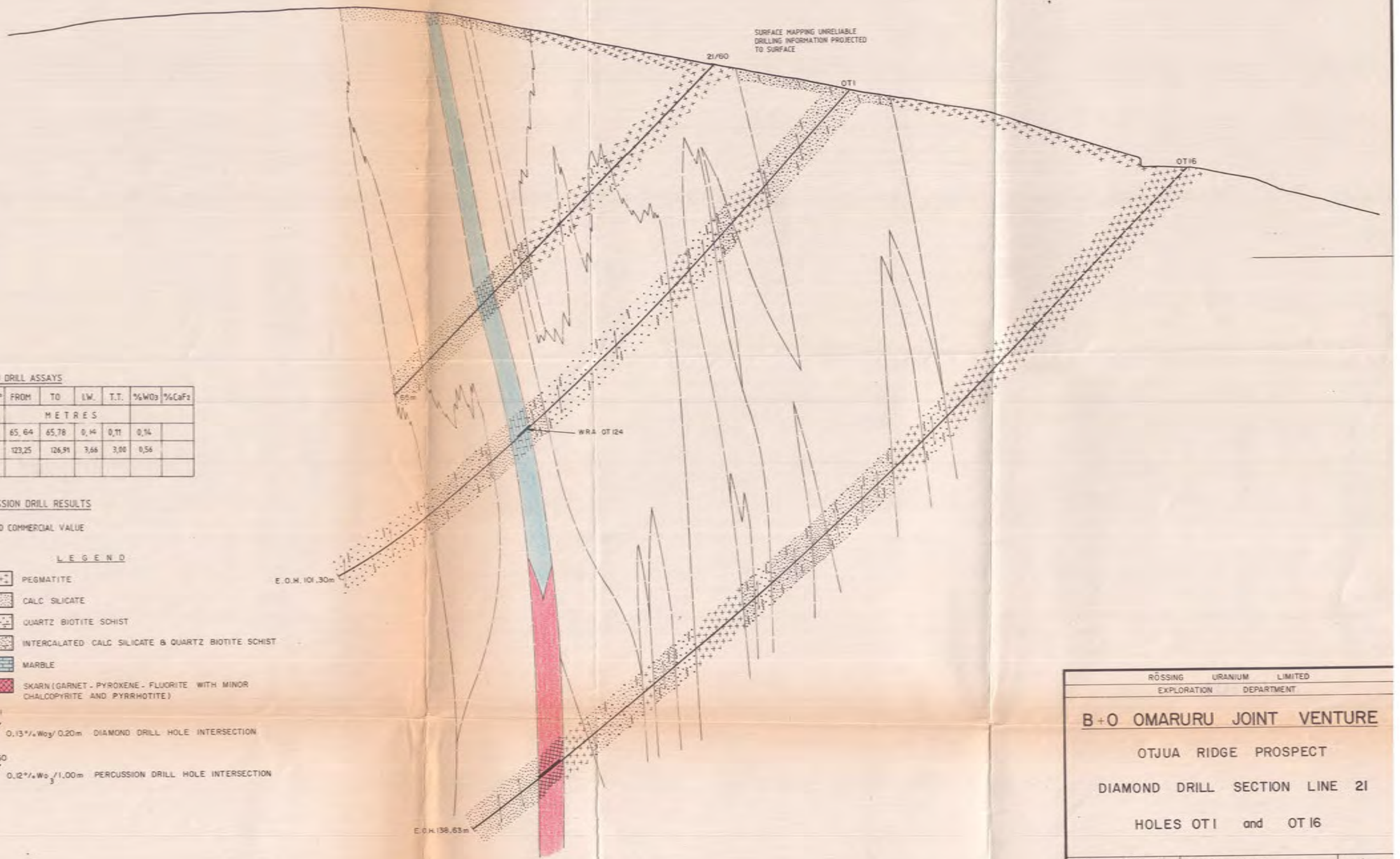

DIAMOND DRILL ASSAYS

HOLE N°	FROM	TO	I.W.	T.T.	%WO3	%CaF2
	METRES					
OT1	65.64	65.78	0.14	0.11	0.14	
OT16	123.25	126.91	3.66	3.00	0.56	

PERCUSSION DRILL RESULTS

21/60 NO COMMERCIAL VALUE

LEGEND

- PEGMATITE
- CALC SILICATE
- QUARTZ BIOTITE SCHIST
- INTERCALATED CALC SILICATE & QUARTZ BIOTITE SCHIST
- MARBLE
- SKARN (GARNET - PYROXENE - FLUORITE WITH MINOR CHALCOPYRITE AND PYRRHOTITE)

OT 1

0.13 %$_{e}$Wo$_{3}$/ 0.20m DIAMOND DRILL HOLE INTERSECTION

21/60

0.12 %$_{e}$Wo$_{3}$/1.00m PERCUSSION DRILL HOLE INTERSECTION

RÖSSING URANIUM LIMITED
EXPLORATION DEPARTMENT

B+O OMARURU JOINT VENTURE

OTJUA RIDGE PROSPECT

DIAMOND DRILL SECTION LINE 21

HOLES OT1 and OT16

SCALE 1:500	DATE JUNE 1983	DWG. N°:
GEOLOGY BY N STEVEN		RUX. 162
DRAWN BY D C PRETORIUS		

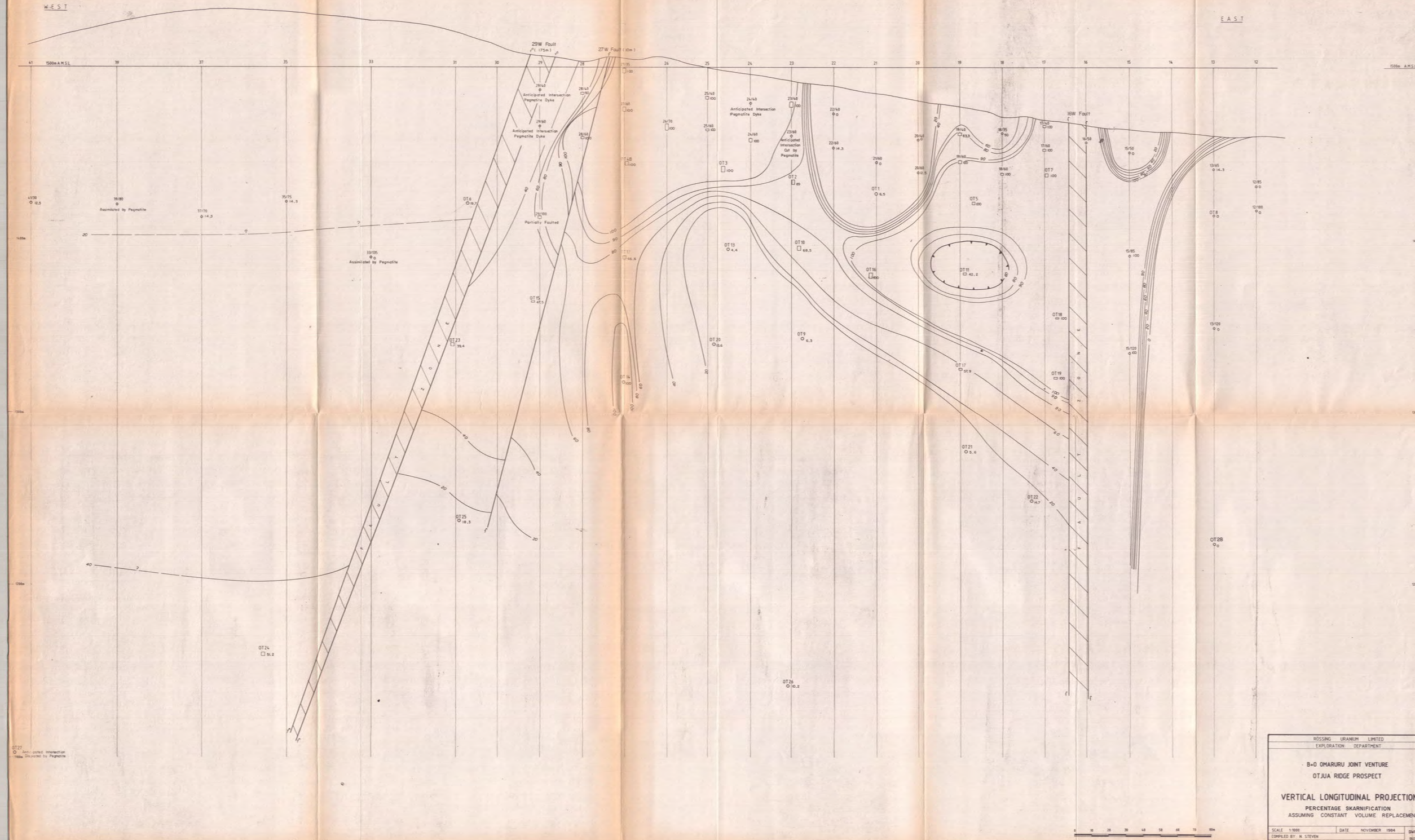

ROSSING URANIUM LIMITED
EXPLORATION DEPARTMENT

B+O OMARURU JOINT VENTURE

OTJUA RIDGE PROSPECT

VERTICAL LONGITUDINAL PROJECTION

PERCENTAGE SKARNIFICATION
ASSUMING CONSTANT VOLUME REPLACEMENT

SCALE 1:1000	DATE NOVEMBER 1984	DWG Nº
COMPILED BY N. STEVEN		RIDX 407
DRAWN BY A. Correia		

WEST

EAST

1500m A.M.S.L.

29W Fault (±175m)

27W Fault (±30m)

19W Fault

41/30 0

39/88 Anticipated Intersection Pegmatite Dyke

37/78 0.06

35/75 0.25

33/135 0

29/40 Anticipated Intersection

28/40 0.28

29/60 Anticipated Intersection

28/60 0.16

29/100 0.29

27/80 0.54

27/35 0.24

25/40 0.23

24/40 Anticipated Intersection

23/40 0.29

24/70 0.28

25/60 0.26

24/60 0.39

23/60 Anticipated Intersection

22/40 0

22/60 0.05

28/40 0

29/60 0

28/60 0

18/40 0.24

19/60 0.33

18/60 0.16

18/35 0

17/40 0.13

17/60 0.10

16/50 0

15/50 0

15/85 0.05

15/120 0

13/65 0.23

13/120 0

12/85 0

12/100 0

OT1 0.42

OT2 0.40

OT3 0.49

OT4B 0.30

OT5 0.43

OT6 0

OT7 0.45

OT8 0

OT9 0

OT10 0.59

OT11 0.57

OT12 0.5

OT13 0

OT14 0.02

OT15 0.90

OT16 0.58

OT17 0.73

OT18 0.48

OT19 0.45

OT20 0.22

OT21 0.27

OT22 0

OT23 0.36

OT24 0.19

OT25 0

OT26 0.52

OT28 0

OT27 Displaced by Pegmatite

Anticipated Intersection

0 10 20 30 40 50 60 70 80m

ROSSING URANIUM LIMITED
EXPLORATION DEPARTMENT

B+O OMARURU JOINT VENTURE

OTJUA RIDGE PROSPECT

VERTICAL LONGITUDINAL PROJECTION

GRADE IN $\%WO_3$ FOR IA SKARN

(N.B. H.W. Contact Skarn Included Where Possible)

SCALE 1:1000	DATE NOVEMBER 1984	DWG N° RUX 405
COMPILED BY N. STEVEN		
DRAWN BY A. Carelse		

WEST

EAST

1500m A.M.S.L.

20W Fault (175m)

27W Fault (10m)

16W Fault

Anticipated Intersection Assimilated by Pegmatite

Anticipated Intersection

Anticipated Intersection Displaced by Pegmatite

Partial Assimilation by Pegmatite

OT1 0.16
OT2 2.35
OT3 2.92
OT4 1.07
OT5 2.3
OT6 0.6
OT7 0.25 coreless
OT8 0
OT9 0.14
OT10 1.63
OT11 1.09
OT12 2.01
OT13 0.04
OT14 1.27
OT15 1.17
OT16 2.88
OT17 1.14
OT18 0.97
OT19 0.71
OT20 0.3
OT21 0.14
OT22 0.2
OT23 0.74
OT24 1.49
OT25 0.57
OT26 0.14
OT27 Anticipated Intersection Displaced by Pegmatite
OT28 0

0 10 20 30 40 50 60 70 80m

ROSSING URANIUM LIMITED
EXPLORATION DEPARTMENT

B+O OMARURU JOINT VENTURE

OTJUA RIDGE PROSPECT

VERTICAL LONGITUDINAL PROJECTION

True Width of Skarn in metres (H.Wand F.W combined)
Diamond holes - calculated from intersection angle, Percussion Measured from section

SCALE 1:1000	DATE NOVEMBER 1984	DWG N° RUX 402
COMPILED BY K. STEVEN		
DRAWN BY A. Coetsee		

WEST

EAST

1500m AMSL

29W Fault
(175m)

27W Fault
10m)

16W Fault

41 39 37 35 33 31 30 29 28 27 26 25 24 23 22 21 20 19 18 17 16 15 14 13 12

39/80
Marble Displaced by Pegmatite

33/135
Partial Assimilation by Pegmatite

29/40
Assimilated by Pegmatite

29/60
Partial Assimilation

29/80
Partially Faulted

25/40
Disruption by Dolerite

25/60
Disruption by Dolerite

24/40
Anticipated Intersection Displaced by Pegmatite

23/60
Anticipated Intersection Assimilated by Pegmatite

OT 1 2.45
OT 2 2.64
OT 3 2.92
OT 4 3.09
OT 5 2.3
OT 6 3.09
OT 7 0.25 Careless
OT 8 1.74
OT 9 2.23
OT 10 2.38
OT 11 2.59
OT 12 3.02
OT 13 1.37
OT 14 1.27
OT 15 2.46
OT 16 2.86
OT 17 1.97
OT 18 0.97
OT 19 0.71
OT 20 1.96
OT 21 1.96
OT 22 1.36
OT 23 1.88
OT 24 2.14
OT 25 3.0
OT 26 1.37
OT 28 < 1.0

OT27
Anticipated Intersection
Displaced by Pegmatite

0 10 20 30 40 50 60 70 80m

RÖSSING URANIUM LIMITED
EXPLORATION DEPARTMENT

B+O OMARURU JOINT VENTURE

OTJUA RIDGE PROSPECT

VERTICAL LONGITUDINAL PROJECTION

COMBINED SKARN & MARBLE TRUE THICKNESSES IN 'm'
Diamond - Calculated From Intersection Angle
Percussion - Measured From The Section

SCALE 1:1000	DATE NOVEMBER 1984	DWG Nº RUX 406
COMPILED BY N. STEVEN		
DRAWN BY A. Coetzee		